Università
Ca'Foscari
Venezia

Scuola Dottorale di Ateneo
Graduate School

Dottorato di ricerca
in Scienze Ambientali
Ciclo 29°
Anno di discussione 2017

Modelling of climate change effects on nutrients

SETTORE SCIENTIFICO DISCIPLINARE DI AFFERENZA: CHIM/12
Tesi di Dottorato di Marco Pesce, matricola 811050

Coordinatore del Dottorato	**Supervisore del Dottorando**
Prof. Gabriele Capodaglio	**Prof. Antonio Marcomini**

Doctoral thesis in Environmental Sciences, XXIX cycle

Department of Environmental Sciences, Informatics and Statistics, Ca' Foscari University of Venice

Academic Year 2016/2017

Advisor: Prof. Antonio Marcomini

Department of Environmental Sciences, Informatics and Statistics

Ca' Foscari University of Venice

Venice, Italy

Co-Advisor: Prof. Andrea Critto

Department of Environmental Sciences, Informatics and Statistics

Ca' Foscari University of Venice

Venice, Italy

Ca' Foscari University of Venice

Venice, Italy

2017

TABLE OF CONTENTS

LIST OF FIGURES

LIST OF TABLES

LIST OF ACRONYMS

AOGCM – Atmosphere-Ocean General Circulation Model
ARPAV – Regional Environmental Protection Agency
AR4 – Fourth Assessment Report
AR5 – Fifth Assessment Report
CDO – Climate Data Operators
CFCs – Chlorofluorocarbons
Chl-a – Chlorophyll-a
CMCC – Centro Euro-Mediterraneo sui Cambiamenti Climatici
CO_2 – Carbon dioxide
CH_4 – Methane
DIC – Dissolved Inorganic Carbon
DIN – Total Inorganic Nitrogen
DIP – Total Inorganic Phosphorus
DEM – Digital Elevation Model
DO – Dissolved Oxygen
EBM – Energy balance model
EMS – Earth System Model
GAPs – Good Agricultural Practices
GCM – General Circulation Model
GHGs – Greenhouse gases
HAB – Harmful Algal Blooms
HRU – Hydrologic Response Unit
INM – Integrated Nutrient Management
IPCC – Intergovernmental Panel on Climate Change
MAV – Magistrato alle Acque di Venezia
NetCDF - Network Common Data Format
NSE – Nash-Sutcliffe Performance Indicator
N_2O – Nitrous oxide
R^2 – Coefficient of determination
RCM – Regional Climate Model
RCP – Representative Concentration Pathway
SRES – Special Report on Emission Scenarios
SAMANET – Continuous Monitoring Network of the Lagoon of Venice
SWAT – Soil and Water Assessment Tool
TAR – Third Assessment Report (IPCC)
VLW – Venice Lagoon Watershed

ABSTRACT

It has been recognized that the increase of atmospheric greenhouse gases (GHG) due to anthropogenic activities is causing changes in Earth's climate. Coastal waterbodies such as estuaries, bays and lagoons together with the ecological and socio-economic services they provide, could be among those most affected by the ongoing changes on climate. Because of their position at the land-sea interface, they are subjected to the combined changes in the physico-chemical processes of atmosphere, upstream land and coastal waters.

Particularly, climate change is expected to alter phytoplankton communities by changing their climate and environmental drivers, such as temperature, precipitation, wind, solar radiation and nutrient loadings, and to exacerbate the symptoms of eutrophication events, such as hypoxia, harmful algal blooms (HAB) and loss of habitat.

A better understanding of the links between climate-related drivers and phytoplankton is therefore necessary for predicting climate change impacts on aquatic ecosystems. In this context, the integration of climate scenarios and environmental models can become a valuable tool for the investigation and prediction of phytoplankton ecosystem dynamics under climate change conditions.

Here we present the case study of the Zero river basin in Italy, one of the main contributors of freshwater and nutrients loadings to the salt-marsh Palude di Cona, a waterbody belonging to the lagoon of Venice. To predict the effects of climate change on nutrient loadings and their effects on the phytoplankton community of the receiving waterbody, we applied an integrated modelling approach made of an ensemble of GCM-RCM climate projections, the hydrological model SWAT and the ecological model AQUATOX.

Climate scenarios point out an increase of precipitations in the winter period and a decrease in the summer months, while temperature shows a significant increase over the whole year.

Water discharge and nutrient load simulate by SWAT show a tendency to increase in the winter period, and a reduction during the summer months. AQUATOX predicted changes in the concentration of nutrients in the salt-marsh Palude di Cona, and variations in the biomass and species of the phytoplankton community.

1 GENERAL INTRODUCTION

1.1 The science of climate change: current and future changes in the climate system

In its Fifth Assessment Report, the Intergovernmental Panel on Climate Change (IPCC 2013) identified human activities as the dominant cause of the observed warming since the mid-20th century. According to several independent studies, this position is shared by 90%-100% of publishing climate scientists (Cook et al. 2016).

Human activities are altering the energy budget of the Earth by increasing the emissions and the resulting atmospheric concentrations of greenhouse gases (GHGs), and by reshaping the land surface at a global scale. Anthropogenic GHGs such as carbon dioxide (CO_2), methane (CH_4), nitrous oxide (N_2O), and chlorofluorocarbons (CFCs) in the atmosphere have continuously increased since the pre-industrial era (Fig. 1.1). Land-use practices, by affecting both the surface-energy budget and the carbon cycle, play an equally important role in climate change (Ludwig and Asseng 2006) (Pielke Sr. 2005). Since 1850, about 35% of GHGs emissions directly resulted from changes in land use, such as urbanization and agriculture (Foley et al. 2005).

As a result of these pressures, the overall climate system is undergoing an unequivocal and continuous warming (Fig. 1.2), with global surface mean temperatures that have been increasingly warmer in the last three decades, showing a warming trend of 0.85 ± 0.2 °C over the period 1880-2012 (IPCC 2013). To date, 15 of the 16 warmest years on record have occurred during the 21st century, with 2015 being the warmest year since record keeping began in 1880 (NOAA 2016).

Multiple lines of evidence support this rapid increase in temperatures: on average, global sea level rose about 17 ± 3 cm in the last century, and the rate nearly doubled in the 21st century (Church and White 2006); Greenland and Antarctic ice sheets have lost mass (Bintanja et al. 2013; Khan et al. 2014); Arctic sea ice has declined over the last decades (Maslowski et al. 2012; Parkinson and Comiso 2013); extreme heat events are becoming more common (Herring et al. 2015);

It must be highlighted that, even though global warming and climate change are considered a global threat, they do not manifest geographic homogeneity. For example, regions like Western Europe and the Arctic are warming faster than the global average (van Oldenborgh et al. 2009; Zhang 2005). Thus, the resulting impacts of climate change can differ geographically.

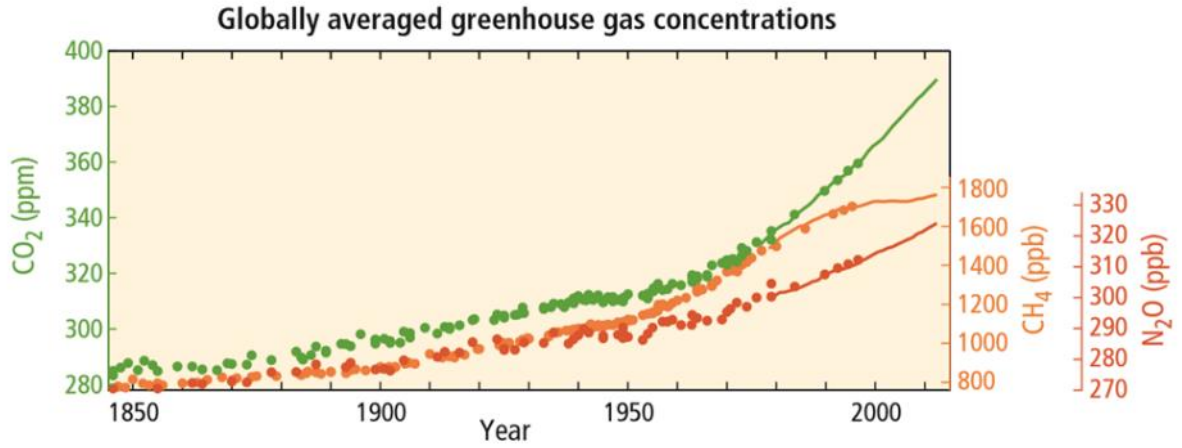

Fig. 1.1 – Atmospheric concentration of GHGs: Carbon dioxide, CO_2 (green); Methane, CH_4 (orange); Nitrous Oxide, N_2O (red) (Hartmann, Tank, and Rusticucci 2013).

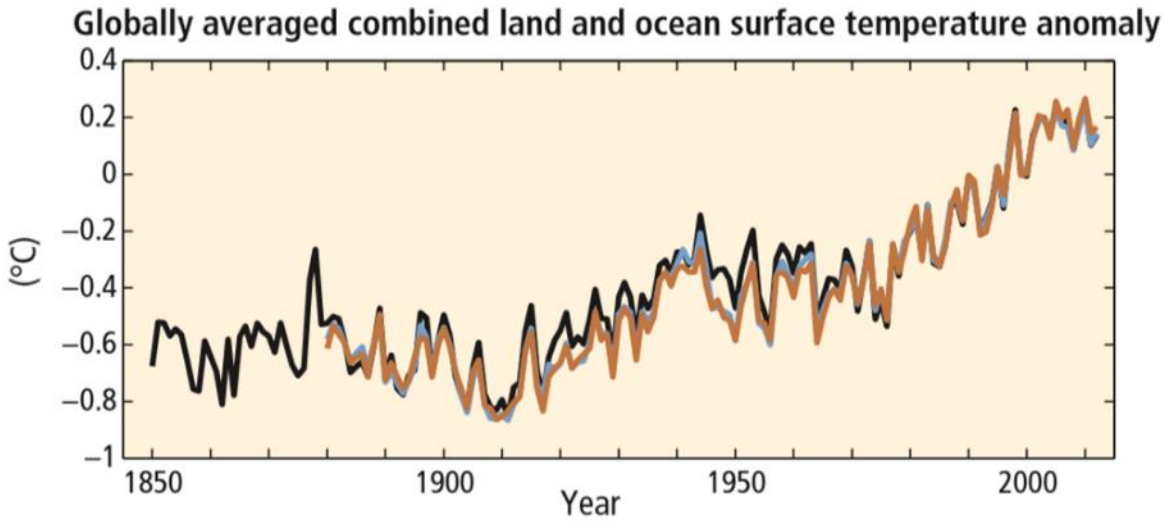

Fig. 1.2 – Averaged global surface (land and ocean) temperature change. Colors indicate different datasets (IPCC 2013).

Continued emissions of GHGs will sustain the rising trend of surface temperature over the 21st century (Fig. 1.3a), forcing climate change to continue for centuries (Karl 2003). Projected global average surface warming for the end of the century (2081-2100) relative to the average

over the period 1986-2015 are projected to be in the ranges of 0.3°C to 4.8°C (IPCC 2013), as shown in Fig. 1.3b.

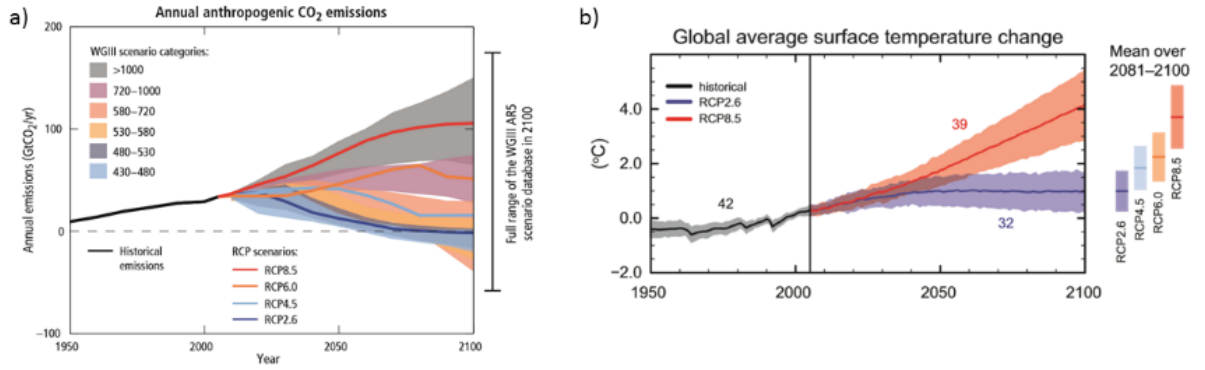

Fig. 1.3 – a) Past emissions of carbon dioxide (black), and future Representative Concentration Pathways (RCPs) (colored lines) and associated scenario categories of emissions, which summarize the wide range of emission scenarios published in the scientific literature. b) Global average surface temperature from 1950 to 2100 as determined by the simulations run for the IPCC AR5. Temperature trajectories are shown only for RCP 2.6 (blue line and area) and RCP 8.5 (red line and area) (IPCC 2013).

Climate projections are plausible representations of future climate conditions and can be generated adopting a variety of approaches (Moss et al. 2010): incremental techniques, where climatic variables (e.g. temperature, precipitation) are changed by plausible amounts (Garg et al. 2013); spatial and temporal analogues in which monitored climate variables can be used as example of future conditions in another region or period (Ford et al. 2010); and climate system models (Fowler et al. 2007; Graham et al. 2007; Xu 1999). Climate models are powerful tools based on well-known physical processes that are used to simulate and explain the transfer of energy and material through the climate system, and the responses of the climate system to natural and anthropogenic forcing. Climate models are mainly used for making climate projections over the coming centuries and beyond (Cooney 2012; Ferguson 2010), indicating areas with higher chances to be warmer or cooler and wetter or drier than the present conditions. Different types of climate models exist. The simplest forms are the Energy Balance Models (EBMs), simple models focusing on the energetics and thermodynamics of the climate system. They attempt to find the balance between the energy input and output of the Earth system (North, Cahalan, and Coakley 1981).

Atmosphere-Ocean General Circulation Models (AOGCMs) simulate the principal dynamics of the physical components of the climate system (atmosphere, ocean, land and ice), and are

used to make projections of the future based on GHG emissions and aerosol concentrations (Mechoso and Arakawa 2015). These models were used in the IPCC Forth Assessment Report (AR4) and are still widely adopted in climate impact studies. General Circulation Models (GCMs) portray the global climate as a three-dimensional grid with a spatial horizontal resolution of between 250 and 600 km. Regional Climate Models (RCMs) add further detail to GCMs (Rummukainen 2010). They increase the spatial resolution of a limited area of interest by capturing the fundamental climatic and morphologic features of that area. RCMs usually have a resolution as fine as 50 or 25 km. Recently, higher resolution RCMs have been developed, adopting spatial grids of 12.5 km to 8 km (Jacob et al. 2014). Earth System Models (EMSs) are the current the state of the art in climate modelling. They expand the potentialities of GCMs by simulating very important climate-related biogeochemical cycles such as the carbon cycle, the ozone cycle, or the sulphur cycle (Flato 2011). Climate models make use of GHGs and aerosol emission scenarios to make projections of possible future climate conditions. Emission scenarios are storylines describing how future populations totals, economic development and land use change might unfold (Arnell et al. 2004). The best known emission scenarios belong to the Special Report on Emission Scenarios (SRES) (Arnell et al. 2004), which were used in the IPCC Third Assessment Report (TAR) and AR4. Each SRES scenario is based on assumptions about future economic and technological development, which in turn influence greenhouse gas emissions, land use and other driving forces of climate change. The SRES scenarios are divided into four scenario families: A1, A2, B1, and B2. A brief description of the scenario families is portrayed in Table 1.1.

Table 1.1 – The four SRES scenario families and the projected global average surface temperature by the end of the 21st century (IPCC 2000).

	Economic Focus	Environmental Focus
Globalization	A1 Rapid economic growth 1.4 – 6.4 °C	B1 Global environmental sustainability 1.1 – 2.9 °C
Regionalization	A2 Regionally oriented economic development 2.0 – 5.4 °C	B2 Local environmental sustainability 1.4 – 3.8 °C

Currently, a new process has been established for developing scenarios. Instead of starting with socio-economic scenarios from which emission projections are generated, as in the SRES scenarios, the new process starts from an emission trajectory and concentration by the year 2100, and the consequent radiative forcing (W m^{-2}), which describes the balance between incoming and outgoing radiation to the atmosphere caused by changes in atmospheric constituents (e.g. carbon dioxide). The central point of this concept is that each radiative forcing pathways can be achieved by various permutations of socio-economic and technological development circumstances (Moss et al. 2010). The new scenarios, defined as Representative Concentration Pathways (RCPs) (van Vuuren et al. 2011), are used in the IPCC AR5. RCPs are scenarios that specify concentrations and corresponding emissions, but do not directly refer to specific socio-economic trajectories like the SRES scenarios. RCPs do not describe fixed scenarios, as many different socio-economic trajectories can lead to the same level of radiative forcing. RCPs differentiate each other by the stabilization value of radiative forcing at the end of the 21st century. The IPCC selected four RCP scenarios from the published literature (Meinshausen et al. 2011): RCP 2.6, RCP 4.5, RCP 6.0, RCP 8.5. A brief description of these RCP scenarios is portrayed in Table 1.2.

Table 1.2 – RCPs global warming increase projections (van Vuuren et al. 2011).

		2046 – 2065	2081 – 2100
Scenario	Radiative Forcing (W m^{-2})	Mean and likely range (°C)	Mean and likely range (°C)
RCP2.6	2.6	1.0 (0.4 to 1.6)	1 (0.3 to 1.7)
RCP4.5	4.5	1.4 (0.9 to 2.0)	1.8 (1.1 to 2.6)
RCP6.0	6.0	1.3 (0.8 to 1.8)	2.2 (1.4 to 3.1)
RCP8.5	8.5	2.0 (1.4 to 2.6)	3.7 (2.6 to 4.8)

It is important to highlight that both climate and emission scenarios cannot be considered as predictions or forecasts but merely as possible future outcomes, as no probability or likelihoods of happening are assigned to them (Nakicenovic and Swart 2000). This feature raised several critiques, as many scientists stated the necessity to have probability estimates to correctly assess climate change risks resulting from different scenarios (Webster et al. 2003).

1.2 The effects of climate change on nutrients and phytoplankton of coastal aquatic ecosystems and modeling methods of assessment

In its last report, the IPCC documented a plethora of effects at the global, regional and local scale. Current climate change and global warming are causing changes in temperature, sea level, precipitation patterns, frequency of droughts and other extreme events, air-water circulation patterns, food security, ecosystem health and species distribution, and human health (IPCC 2014b). The sustained warming of the last decades and the resulting changes in climate will exacerbate existing risks and create new ones by acting both on the magnitude of hazards (e.g. floods, sea level rise, air pollution, pollutant loadings), and on the exposure and vulnerability of targets (humans or ecosystems). In general, the effects of climate change will be mostly disadvantageous, even though some regions of the planet may benefit from these changes (Smith et al. 2009).

Potential impacts of climate change on the hydrology and water availability have received much attention in the last decades (Arnell 1999, 2003; Haddeland et al. 2014; Steele-Dunne et al. 2008). On the other hand, much less focus has being placed on the concomitant changes in water quality (Whitehead et al. 2009). In its previous reports, the IPCC did not cover the topic of water quality with great detail.

Many aquatic ecosystems such as lakes, estuaries and coastal waterbodies (e.g. lagoons, salt-marshes, etc.) are affected by direct anthropogenic pressures (e.g. overloads of nutrients, release of contaminants, etc.) originating mainly from land-based human activities. Until recently, the impacts of climate change and direct anthropogenic pressures on ecosystems have been discussed separately (Schiedek et al. 2007), and the awareness and number of studies on the combined impacts of climate- and non-climate-related drivers increased only in the last decade (Noyes et al. 2009; Schiedek et al. 2007; Stahl et al. 2013; Wakelin et al. 2015). In particular, the combined effects of climate change and nutrient availability may severely affect aquatic ecosystems over the 21st century, especially those of coastal areas. Coastal zones are among the most productive ecosystems on Earth and are providers of a wide range of resources and services for human activities (UNEP 2006). Given their global importance,

coastal aquatic environments became a major concern regarding the potential impacts of climate change (Christopher D. G. Harley et al. 2006).

Phytoplankton is responsible for a large share of photosynthesis and primary production of coastal areas, and plays an essential role in several biogeochemical cycles such as carbon, nutrient and oxygen cycles (Paerl and Justic 2011). Furthermore, it is at the base of every aquatic food web, and changes in its processes, dynamics and composition have repercussions on both the environment and higher trophic levels (Hernandez-Farinas et al. 2014; Schloss et al. 2014).

Nowadays, coastal areas are recognised as being particularly vulnerable to future global climate change. They are already subjected to multiple anthropic pressures such as population growth and land-use alteration (Lloret, Marín, and Marín-Guirao 2008). The rapid urbanization and industrialization, together with the conversion of natural land to agricultural purposes, has increased the loading of nutrients discharging into coastal waters, causing cascading impacts on water quality and ecosystems, and consequent impairments to ecosystem services. Considering this, additional stress from climate change might further exacerbate existing pressures as well as creating new ones, with evident consequences for aquatic ecosystems (Rabalais et al. 2009).

Changes in climate may directly impact on coastal aquatic ecosystems through large scale changes in the chemical and physical conditions, such as temperature, stratification, and acidification (Hoegh-Guldberg and Bruno 2010). For example, the distribution, abundance, and structure of phytoplankton communities as well as their phenology and productivity, are changing in response to warming, acidifying, and stratifying waters (Hunter-Cevera et al. 2016; Lassen et al. 2010; Weisse, Gröschl, and Bergkemper 2016). Sea level rise might have further important consequences on coastal ecosystems, especially in those of shallow waters. For example, shallow lagoons can have well-developed benthic microalgae communities that can contribute to a major portion of the fixed carbon in the system (Parodi and De Cao 2002). In the case of sea level rise, microalgae are expected to capture a smaller proportion of the solar radiation due to the stronger light attenuation in the water column (Brito et al. 2012).

In addition, climate-related changes in the availability of nutrients may also affect coastal primary producers. The nutrient supply, together with solar radiation and temperature, controls phytoplankton dynamics. There is scientific evidence that climate change will affect nutrient availability by altering sources, transport and fate of nutrients, with consequent effects on aquatic ecosystems (Boxall et al. 2009). First, the use of industrial fertilizers may increase in order to cope with an increasing food demand (Tilman et al. 2011), changes in temperature and precipitation (Howden et al. 2007), and harsher environmental conditions (Abberton et al. 2016) such as the decrease in soil organic carbon caused by raising temperatures (Brevik 2013; Follett et al. 2012; Kirschbaum 1995), and the increased leaching and runoff of water and nutrients due to the expected greater occurrence of extreme events (Aydinalp and Cresser 2008; Ludwig and Asseng 2006). On the other hand, factors such as: increased production costs of fertilizers due to high-demand and depletion of nitrogen, phosphorus and potassium reserves (Blanco 2011); application of good agricultural practices (GAPs) and integrated nutrient management (INM) (Moustache 2017); and enhanced nutrient uptake by the plants caused by the CO_2 fertilization effect in some regions of the planet (Kanter et al. 2016) might balance out the increase fertilizer usage.

Second, nutrient loads are expected to increase over the 21st century due to climate change (Bouraoui, Galbiati, and Bidoglio 2002; Huttunen et al. 2015; Jeppesen et al. 2009). Effects of climate change on the hydrologic cycle alter those physical processes (e.g. runoff, leaching, percolation, water retention time, evapotranspiration) that regulate the transport of nutrients from land to water bodies (Alam and Dutta 2013; Culbertson et al. 2016; El-Khoury et al. 2015; Ockenden et al. 2016). Increased temperature can accelerate nutrient mineralization from organic matter in the soil and applied manure (Eghball et al. 2002), thereby increasing the amount of inorganic forms of nitrogen and phosphorus. Decrease in precipitation could reduce river flow and nutrient loadings, but it will simultaneously reduce the dilution of nutrients (Whitehead et al. 2009). In addition, drier summers may lead to long periods of soil moisture deficits, leading to increased hydrophobicity of the soil surface, with increased runoff when the wet season comes (Boxall et al. 2009). Prolonged droughts may also increase the number of soil cracks, which will favor the percolation of water and mobile forms of nutrients (i.e.

nitrates, NO_3^-) through the soil profile, thereby reducing the quality of streams and groundwater (Green et al. 2011). Increased winter precipitation and more frequent and extreme flood events during summer will increase runoff and associated wash-off of organic matter and fertilizers, thereby contributing to the increase of nutrient contamination of water bodies (Jeppesen et al. 2009; Najafi and Moradkhani 2015; Sterk et al. 2016; Whitehead et al. 2009).

Finally, climate change will also impact atmospheric depositions. Volatile forms of nutrients such as ammonia can be transported in the atmosphere through a combination of volatilization and dispersion processes, which are dependent on soil properties, air temperature and wind, all of which are predicted to change over this century (Hole and Engardt 2008). Drier summers could also increase the dry transport of nutrients. Increased drying of the soil could facilitate the transport of fine sediment in the form of dust (Zobeck and Van Pelt 2006).

The sum of these changes can significantly alter the nutrient ratio in coastal waters. Redfield (1934) found a remarkable consistency between the proportion of nutrients in seawater and the chemical composition of marine phytoplankton, which tends towards an average atomic weight C:N:Si:P ratio of 106:16:15:1, known as the “Redfield Ratio”. However, the conditions of coastal water are not constant, and so is the ratio, which is modulated by several factors such as nutrient loading, oceanic inputs and groundwater (Paerl and Justic 2011; Zirino et al. 2016a). In these conditions, the limiting nutrient, defined as the element in least supply relative to the requirements for growth of phytoplankton cells (Davidson, Flynn, and Cunningham 1992), is not well-defined. Although in estuaries and coastal areas nitrogen (N) has been identified as the limiting nutrient (Elmgren and Larsson 2001; Howarth and Marino 2006), “co-limited” or “alternate” conditions of nitrogen N and P are commonly observed (Malone et al. 1996; Paerl et al. 1995). Changing climate conditions and modified nutrient ratios may significantly alter the phytoplankton community and generate the conditions for water quality problems in coastal environments.

In particular, numerous studies predict an increase in eutrophication events (Justić, Rabalais, and Turner 2005; Paerl 2006) and related symptoms, such as elevated biomass (Cadée and

Hegeman 2002), harmful algal blooms (HABs) (Davidson et al. 2014; Paerl and Huisman 2008; Wells et al. 2015), reduced water quality, loss of biodiversity, and hypoxia (Glibert et al. 2014; Paerl and Paul 2012; Rabalais et al. 2009). Eutrophication occurs as a result of complex interactions between numerous factors (Jeppesen et al. 2005). The increased loadings of nutrients from coastal watersheds, combined with higher temperatures, increased rates of biological processes and mineralization (Pörtner and Knust 2007), enhanced stratification (Blanchard et al. 2012), changes in wind regional patterns (Chan et al. 2008), and the decrease of wetlands associated with sea level rise (Blankespoor, Dasgupta, and Laplante 2012) will all contribute to trigger eutrophication events more frequently. Eutrophication poses already a great threat to the integrity of coastal ecosystems and climate change may further escalate its effects in the future decades (Rabalais et al. 2009).

This justifies the interest and necessity for a better understanding of the links between climate-related drivers and primary producers for predicting the effects of climate change on the state and functioning of aquatic ecosystems (Ho and Michalak 2015; Wells et al. 2015). In this context, the integration of climate scenarios and process-based environmental models can become a valuable tool for the investigation and prediction of aquatic ecosystem dynamics under climate change conditions. Supported by empirical studies, these approaches can contribute to better represent the processes and interactions between climate, abiotic and biotic factors regulating phytoplankton dynamics and its community structures. The adoption of model-based methodologies in order to assess environmental responses to climate change has recently become more popular (Guse et al. 2015; Taner, Carleton, and Wellman 2011; Trolle et al. 2011). In the last decades, the adoption of process-based models have become a popular tool for assessing the impacts of climate change on hydrologic and abiotic components of aquatic systems (Vohland et al., 2014). Most modelling studies have analysed the impacts of climate change on single environmental aspects. For example, hydrologic, water quality and rainfall-runoff and sediment transport models are among the preferred and most used tools to assess the likely impacts of climate change on watershed hydrology (Amin et al. 2017; Leta et al. 2016; Trinh et al. 2017), loadings of nutrients (Huttunen et al. 2015) and sediments (Bussi et al. 2016; Samaras & Koutitas 2014), and water quality (Wilby et al. 2006). A number of

hydrologic models have been applied to climate change impacts studies, such as SWAT (Arnold et al. 1998), CE-QUAL-W2 (Cole and Buchak 1995) and BASINS (EPA 2015). These models are selected for a number of specific reasons: physical processes are well understood and simulated; required data are generally limited and easily available; computational requirements are low, even for long-term simulations, allowing the user to implement climate and land use change scenarios; and the majority of available tools and models is open-source and freely available on the internet.

Models are also useful tools to study the potential conditions of ecosystems under different pressures, such as future climate and nutrient loadings. In 2002, IPCC stated that most ecosystem models are not suitable to project changes on biodiversity and ecosystems. However, since that time a number of studies have been submitted to the scientific literature. To date, the number of studies that apply process-based ecosystem models to assess the impacts of global change on biological processes focuses mostly on lakes (Mooij et al. 2010). In the last years more studies on other types of water bodies appeared in the scientific literature (Brito et al. 2012; Bussi, Whitehead, et al. 2016; Guse et al. 2015; Rodrigues et al. 2015; Wakelin et al. 2015). A number of ecosystem models have already been applied to climate change impact assessment studies, such as EwE (Hoover, Pitcher, and Christensen 2013; Watson et al. 2013), AQUATOX (Taner et al. 2011), PCLake (Mooij et al. 2007; Mooij, De Senerpont Domis, and Janse 2009), ECO-SELFE (Rodrigues et al. 2015), DYRESM-CAEDYM (Schlabing et al. 2014), POLCOMS-ERSEM (Wakelin et al. 2015) and PROTBAS (Markensten, Moore, and Persson 2010).

The integration of climate, hydrologic, and ecosystem models provides a means to deal with the complex and interrelated nature of recent global environmental change problems, and help to explain, explore, and predict environmental-system response to natural and human-induced stressors (Laniak et al. 2013). Traditionally, environmental models have been applied to assess the impact of a single pressure in a single environmental medium. Today this approach is no longer considered as sufficient for effective decision-making in environmental matters. It is recognized that a comprehensive approach, able to model the environment and its physico-chemical and biological processes, as well as the exposure to environmental

pressures and the consequent responses of ecosystems, is required to assess and address environmental problems (EPA 2008; Laniak et al. 2013).

EPA (2008, 2009) defines integrated modeling as "a systems analysis-based approach to environmental assessment. It includes a set of interdependent science-based components (models, data, and assessment methods) that together form the basis for constructing an appropriate modeling system. The constructed modeling system is capable of simulating the environmental stressor-response relationships relevant to a well specified problem statement".

The integrated modeling approach is fundamental for describing the complexity of environmental systems and can provide a better understanding of the links among the components that characterise an environmental problem. The adoption of this approach aims to significantly improve the effectiveness of decisions and to provide a comprehensive outcome able to positively impact management actions and policies (EPA 2009). The concepts of the integrated modeling approach are being applied to an increasing number of environmental problems but several challenges that limit their application still exist. In the context of combined impacts of climate change and nutrient loadings in aquatic ecosystems, an integrated modeling approach should adopt tools able to foresee changes in climate variables (i.e. climate models), as well as non-climate-related drivers (e.g. land-use change models), and link them to impact assessment tools such as hydrologic and ecosystem models. Section 1.3 illustrates the “model cascade” approach, an integrated modelling method commonly adopted the field of climate change impact assessment.

1.3 The adoption of the “model cascade” approach to model climate change impacts on nutrients and aquatic ecosystems

Kiesel (2009) defines a “model cascade” as a sequence of combined models where one model provides the input for another model. In climate change impact assessment studies, a model cascade is a top-down approach that usually starts with socioeconomic assumption for the development of global greenhouse gas emission scenarios, continues to the impact of GHGs

and aerosols on the global climate system, up to the impacts of climate change on the abiotic and biotic compartments of the environment. A common representation of a model cascade in shown in Fig. 1.4. The approach is characterized by a number of assumptions and related uncertainties that tend to expand at each step of the process to the extent that information on potential impacts might be unhelpful (Maslin 2013; Wilby and Dessai 2010) as shown in Fig. 1.5.

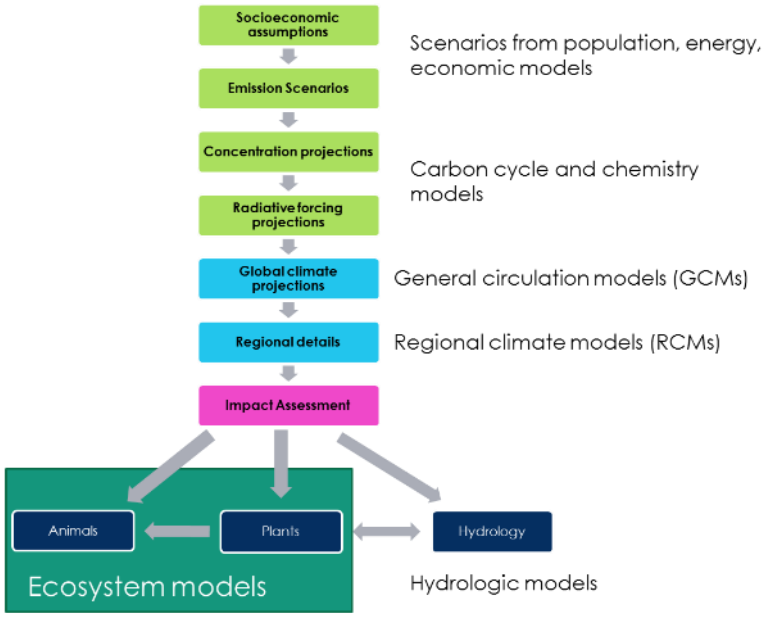

Fig. 1.4 – Conceptual representation of a "model cascade". Socioeconomic, Geochemical, Climate, Hydrologic, and Ecosystem models are involved.

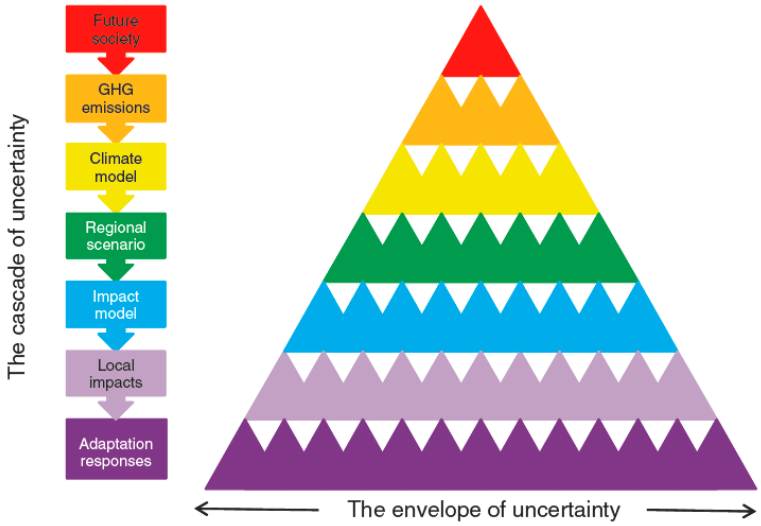

Fig. 1.5 – The cascade of uncertainty in a top-down approach. Every step of the process brings some degrees of uncertainty, from future scenarios to hydrological models (Wilby and Dessai 2010).

A series of considerations and assumptions can be made for each step of the model cascade. The model cascade generally starts from the generation of climate scenarios. Here, uncertainties arise from different sources. First, climate models are based on our best understanding of how the earth-climate system works, and still contain assumptions for processes that are not entirely known, for example cloud formation (Charlson 2001). Second, climate models differ from each other for technical reason, or simulate physical processes in different ways (Wiens et al. 2009). Third, they are based on inadequate resolutions for impact assessment studies. The resolution of GCMs is generally too coarse for most climate impact assessment studies, and information on the future climate on a scale as close as possible to the size of the impact area should be provided (Maslin 2013). Different method to increase the spatial resolution of climate projections exist. Currently, the most used are the nesting of RCMs into GCMs (Wilcke and Bärring 2016) and statistical downscaling (Flint and Flint 2012). Even though RCMs and downscaling can improve the resolution of GCMs, some systematic errors may still exist. Systematic errors in regional climate models are caused by an imperfect conceptualization of the area and can increase the error in impact assessment studies (Villani et al. 2015). In order to reduce the bias, post-process methods can be applied to the output of RCMs. Several bias correction methodologies exist and have been applied in the literature to

solve the problems presented in the output of RCMs (Chen, Brissette, and Lucas-Picher 2015; Haerter et al. 2011).

Hydrological models such as rainfall-runoff water quality models are based on well-known physical processes. However, results from these models are strongly dependent on the availability, quality and resolution of input data and their parameterization (Liu and Gupta 2007). The quality of results is also dependent on the way calibration is performed and on the quality of time-series of monitoring data used in the calibration process.

Finally, ecosystem models are strongly dependent on the input from hydrological models. For example, model-simulated eutrophication events are heavily influenced by nutrient input from hydrological models and weather conditions provided by climate models. Moreover, ecosystems are rarely closed systems, and continuously interact with the surrounding environment. Models struggle with this aspect, as it is impossible to predict all the external factors that may influence an ecosystem over a long period of time (Littell et al. 2011). Finally, in a period of global change, ecosystems are continuously affected by a wide number of stressors and it becomes difficult to identify the correct cause-effect relationship (Stahl et al. 2013).

In conclusion, the adoption of model-based methodologies in climate change impact assessment can provide useful information for adaptation management decisions, even though these studies are still characterised by a high degree of uncertainty. The integration of models can generate knowledge and information that can be used to explain, explore, and predict the behavior of environmental systems in response to human and natural pressures (Laniak et al. 2013). Given model's intrinsic state of not being completely defined and clear, and the impossibility to provide a perfect representation of the phenomena they model, model output should be analysed and included in a wider decision-making context in order to gain useful insight for the management of environmental pressures (Vohland et al. 2014).

1.4 Research aim

This dissertation attempts to develop and apply an integrated modeling approach to study the impacts of climate change on nutrient loadings and the consequent effects on the first trophic level of coastal aquatic ecosystems over the 21st century. The overall aim of this study is to develop an approach for assessing potential long-term effects of climate change on the productivity and community structure of coastal phytoplankton at a catchment scale. The approach can investigate the consecutive impacts of climate change along the land-water continuum, from climate-related impacts on stream flow and nutrient loadings, to direct influence of temperature changes on coastal waters. This approach consists of climate scenarios and tools able to provide climate data suitable for impact assessment studies, and two separate environmental models used to depict the physico-chemical and biological characteristics of a watershed and of the receiving waters of a coastal environment. This study is a further attempt to integrate climate scenarios and tools with environmental models to assess the responses of coastal aquatic ecosystems. The main objective of the study is to present the approach, illustrate its applicability through a local case study, and discuss strengths, limitations and areas of improvement. Specific objectives are:

- To develop and apply an integrated modelling approach that allows for the assessment of the impacts of climate change on the Zero river basin (ZRB) and the salt-mars "Palude di Cona" (PDC), Italy.
- To select an ensemble of future climate scenarios for the 21st century, and optimize their use for hydrological and ecosystem modelling.
- To develop a process-based hydrological model of ZRB, that allows for the assessment of climate change on the hydrology and nutrient loading.
- To implement an ecosystem model for the phytoplankton of PDC.
- To provide an assessment of the projected changes in climate, temperature (T) and precipitation (P) on the study area over the 21st century.
- To assess the impacts of climate change on nutrients and coastal phytoplankton community of the area of study over the 21st century.
- To carry out a variability analysis of the future impacts of climate change on nutrient loadings and coastal phytoplankton communities.

1.5 Outline of the dissertation

The dissertation is organized as follows: Chapter 2 describes the study area. It focuses on climate, morphological and geological aspects, land use and hydrology of the area. Chapter 3 describes the methodological approach and its implementation on the Zero river basin and the receiving waters of Palude di Cona, a salt-marsh located in the northern basin of the Lagoon of Venice. Chapter 4 presents the results of the study. First, it presents the results of calibration of SWAT and AQUATOX. Second, it shows the projected changes for temperature (T) and precipitation (P) on the Zero river basin by the mid (2041-2070) and end of this century (2071-2100). Finally, it presents the projected changes in freshwater discharge, nutrient loadings, and the consequent impacts on the ecosystems. Chapter 5 presents an overall summary of the study and a discussion of the current research findings, acknowledges strengths and limitations of the study, and provides insight for future research in the field.

2 STUDY AREA

2.1 Location and overview

This chapter presents the case study of the Zero river basin (ZRB) and the shallow water area named “Palude di Cona” (PDC), which belong to the land-water continuum of the Venice Lagoon Watershed (VLW), in Italy (Fig. 2.1). The ZRB is located between latitudes 45°28’N and 45°48’N, and longitudes 11°54’E and 12°25’E. It has a surface area of 140 km^2 and its waters flow eastward with an elevation decline from 110 m to 1 m above sea level. The Zero river merges with the Dese river 2 kilometers from the coast before flowing into the lagoon of Venice from different outlets. The two rivers together provide the greatest contribution of freshwater (21% of the total) to the lagoon of Venice (Zuliani et al. 2005). The ZRB is described in Section 2.3. PDC is a shallow water area in the upper-north basin of the lagoon of Venice (latitude of 45°31’N and longitude of 12°24’E) that maintained its original salt-marsh features over the centuries. PDC is described in Section 2.4.

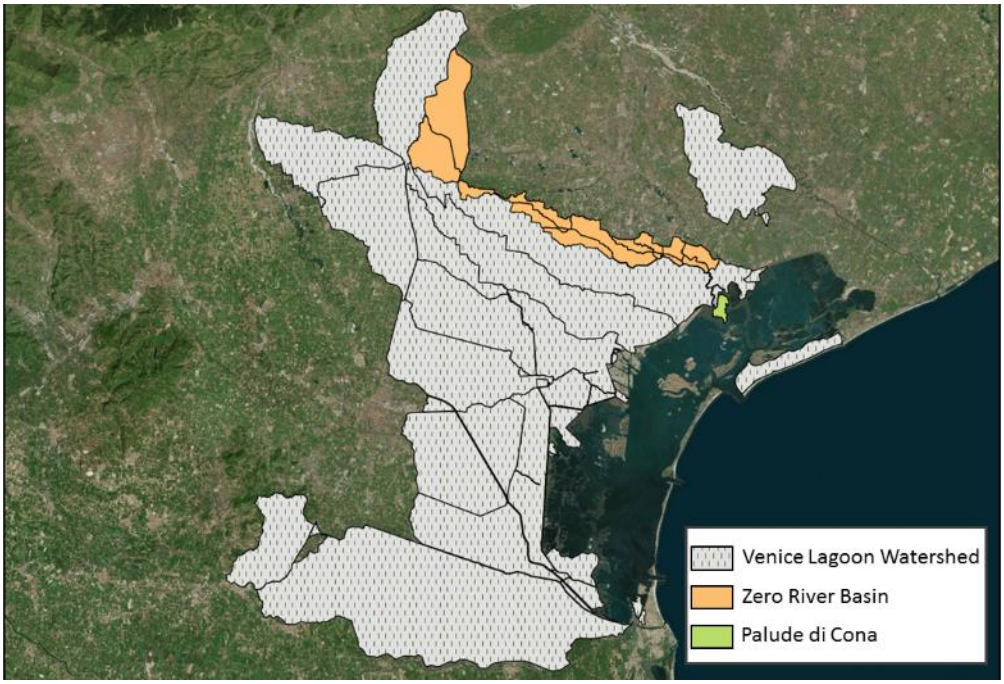

Fig. 2.1 - The study area consists of the Zero river basin (ZRB, orange) and Palude di Cona (PDC, green), a shallow marsh area in the upper-north area of the Venice Lagoon Watershed (VLW).

2.2 Climate

Due to its transitional position and the several climatic influences involved (i.e. the effects of the Mediterranean Sea, the orography of the Alps, the Continental climate of Central Europe, and the Azores High) the area of the VLW features a Mediterranean climate with unique characteristics typical of more Continental climates (Guerzoni and Tagliapietra 2006). Mild winters and dry summers, typical of Mediterranean climates, are replaced by cold winters and summers with frequent storms. The area shows a clear climatic gradient from the watershed to its lagoon. As shown in Fig. 2.2, the climate of the lagoon is characterized, on average, by warmer (+1° C) and drier (-250 mm of rain) conditions. The region of the VLW has a marked inter-annual climate variability, which can originate years climatologically very different from each other.

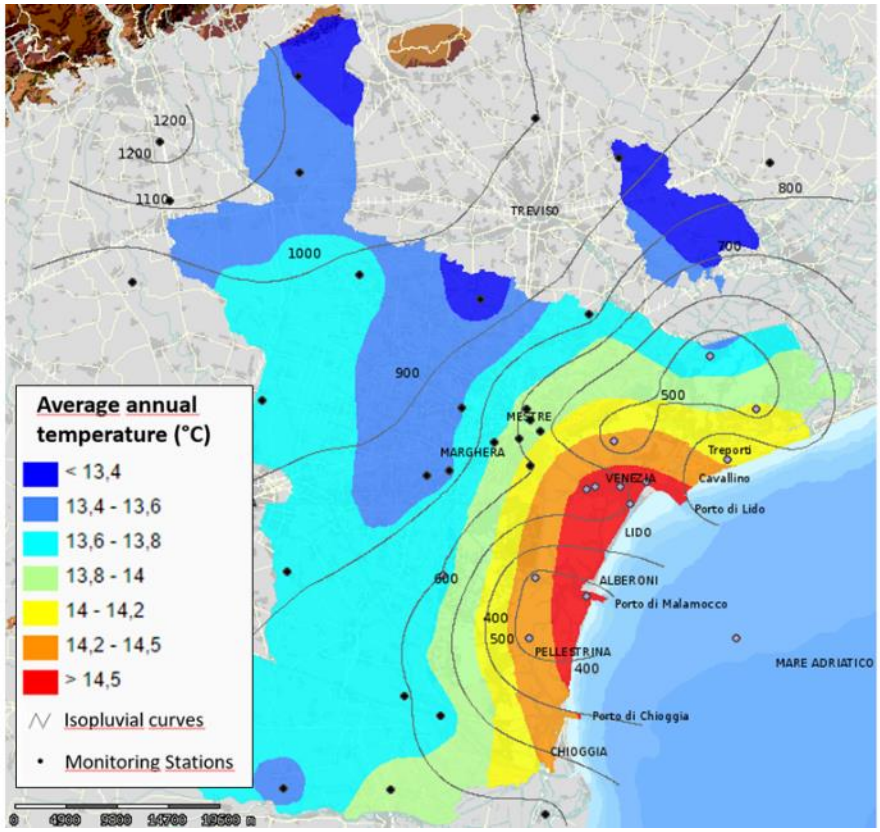

Fig. 2.2 – Average temperatures (°C) and isopluvial curves (mm/year) for the 2001-2003 period in the VLW (Guerzoni and Tagliapietra 2006).

As temperature and precipitation are considered the most important climate variables in climate change studies, they are thoroughly described in sections 2.2.1 and 2.2.2. Sections 2.2.3 and 2.2.4 describe the wind components (i.e. speed and directions) and the solar radiation of PDC, as they are important climate variables for phytoplankton dynamics. The location of the weather stations is shown in Fig. 2.3. In this study, the weather stations "Castelfranco Veneto", "Zero Branco", "Mogliano Veneto" describe the climatic profile of the ZRB, while the weather station "Venezia – Istituto Cavanis" is deemed as representative of the climate of PDC. The selected weather stations belong to and are managed by the meteorological service of the Regional Environmental Protection Agency (ARPAV).

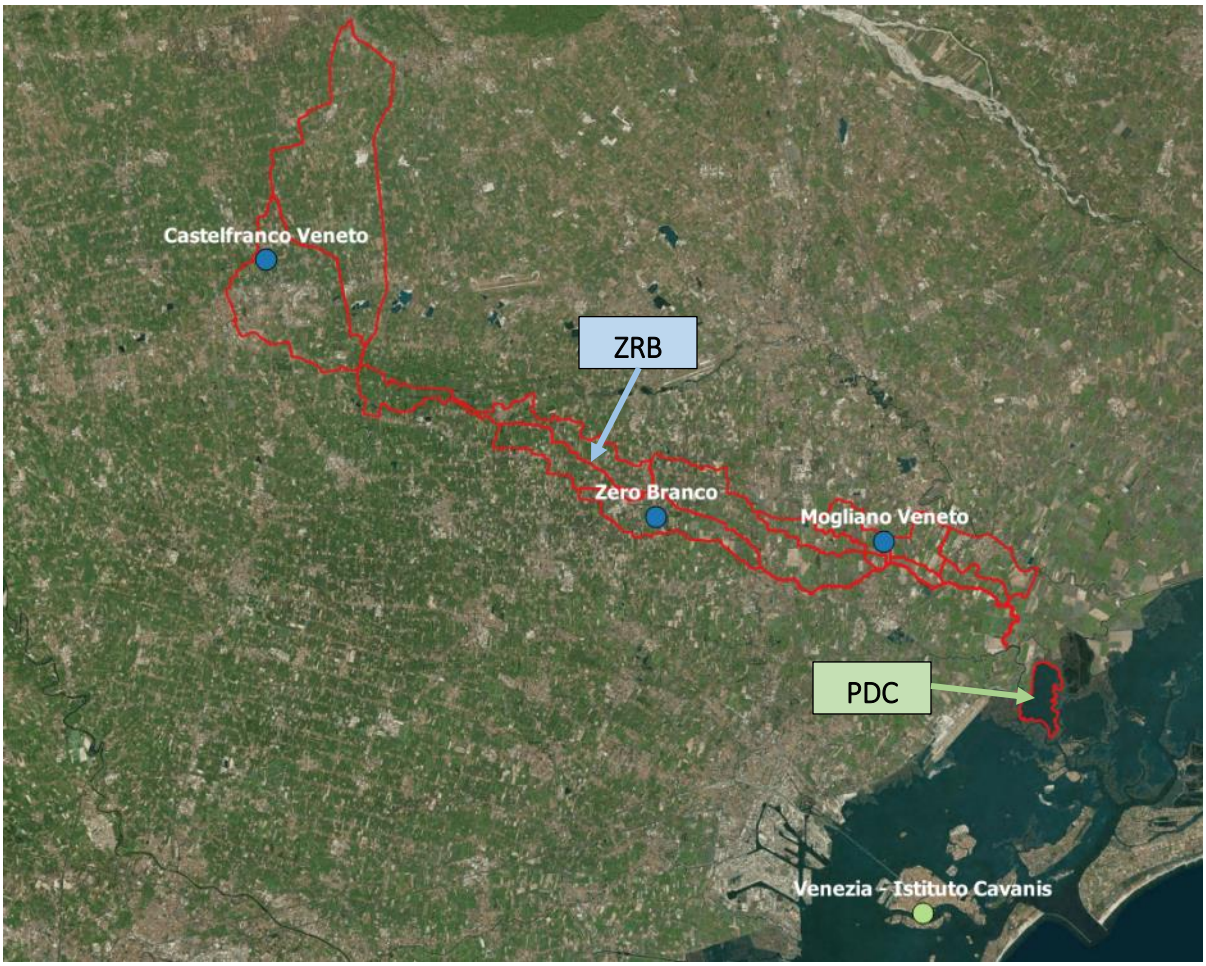

Fig. 2.3 – Position of the weather stations selected for this study. The weather stations "Castelfranco Veneto", "Zero Branco", and "Resana" (blue dots) are used to describe the climate of the ZRB, while the weather station "Venezia – Istituto Cavanis (green dot) are used to describe the climate of PDC.

2.2.1 Temperature

Temperature along the ZRB-PDC land-sea continuum features an annual average of 14 °C in the period 2004-2013, and shows the typical temperature gradient characterizing the VLW, with temperatures increasing of 1 °C from the north-western part of the basin to the coast (Fig. 2.4). The lowest temperatures occur in the months of January and December, with temperatures at an average of 4 to 5 °C, while the warmest months are July and August, with monthly averages around 25 °C (Fig. 2.5). The temperature gradient between the north-western part of the ZRB and PDC is always observed throughout the year, but it appears less marked during the summer period.

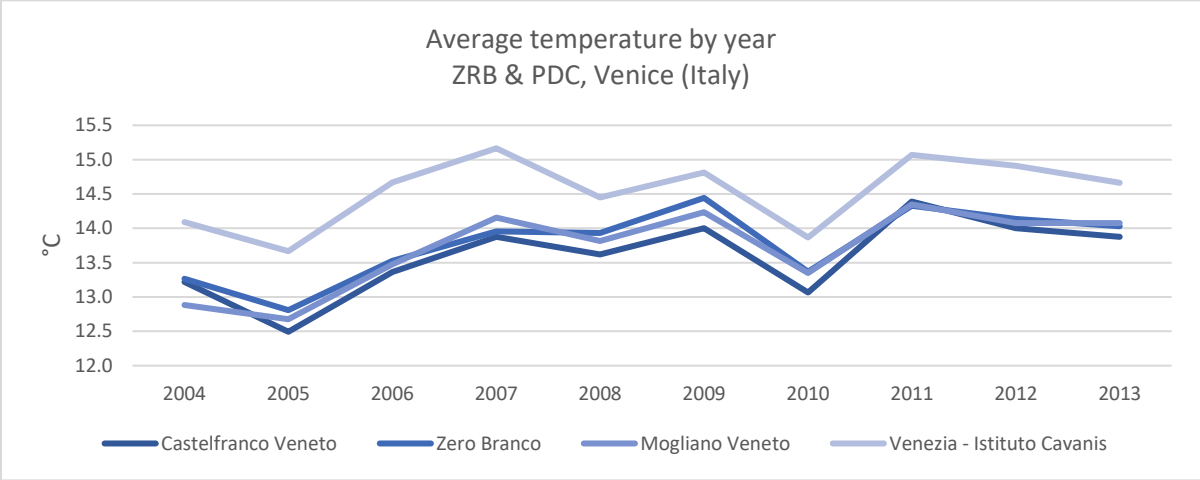

Fig. 2.4 – Average temperature by year (°C) in the decade 2004-2013 for four weather stations considered in the study. Data source: ARPAV – Servizio Meteorologico.

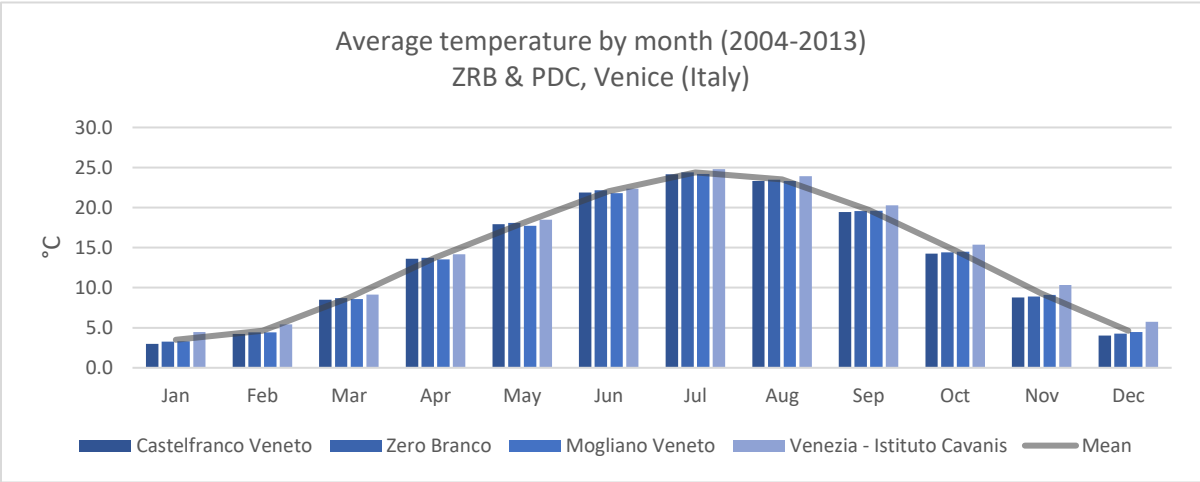

Fig. 2.5 – Average temperature by month (°C) in the decade 2004-2013 for the four weather stations considered in the study. Data source: ARPAV – Servizio Meteorologico.

2.2.2 Precipitation

The precipitation along the ZRB-PDC land-sea continuum features an annual average of 1000 mm for the period 2007-2012. The precipitation shows the climatic gradient of the area, with more precipitation in the north-eastern part of the basin with respect to the lagoon (Fig. 2.6). There is marked variability in precipitation among years, with very wet years (2008, 2010) and dry years (2011, 2012). Precipitations are generally well distributed throughout the year, with peaks in spring and autumn and minimums during the winter and summer periods (Fig. 2.7). Summers are frequently characterized by intense storms of short duration (Guerzoni and Tagliapietra 2006).

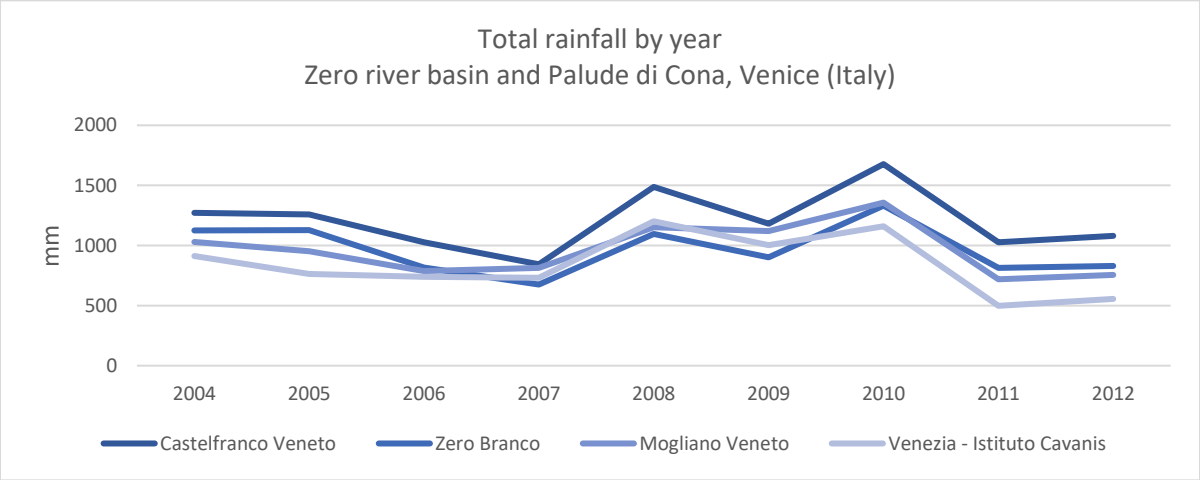

Fig. 2.6 – Total rainfall by year (mm) in the decade 2004-2013 for the four weather stations considered in the study. Data source: ARPAV – Servizio Meteorologico.

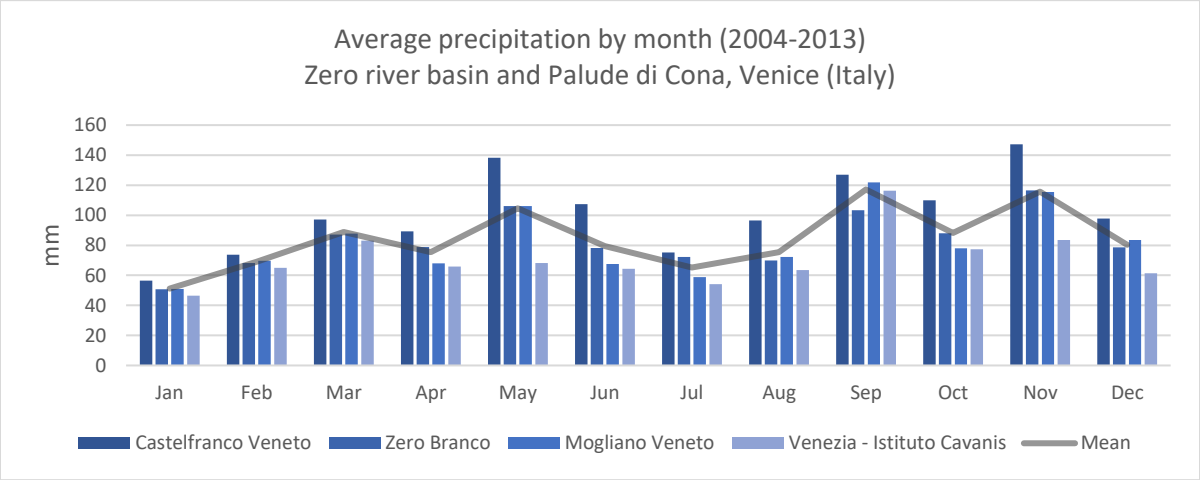

Fig. 2.7 – Average precipitation by month (mm) in the decade 2004-2013 for the four weather stations considered in the study. Data source: ARPAV – Servizio Meteorologico.

2.2.3 Wind speed and direction

Wind speed in the lagoon of Venice has an annual mean that varies between 1.4 to 1.9 m/s (Fig. 2.8) for the decade 2004-2013, and shows a low variability throughout the year (Fig. 2.9). The most common wind direction is from north-east (NE), followed by south, east, north and south-east. Winds from NE are dominant for 7-8 months of the year, from October until May, while winds from SE dominate during summer. The strongest prevailing winds of these two regimes are the Bora (NE) and the Sirocco (SE), which influence the dynamics of the system Adriatic Sea/Lagoon of Venice (Lovato et al. 2010).

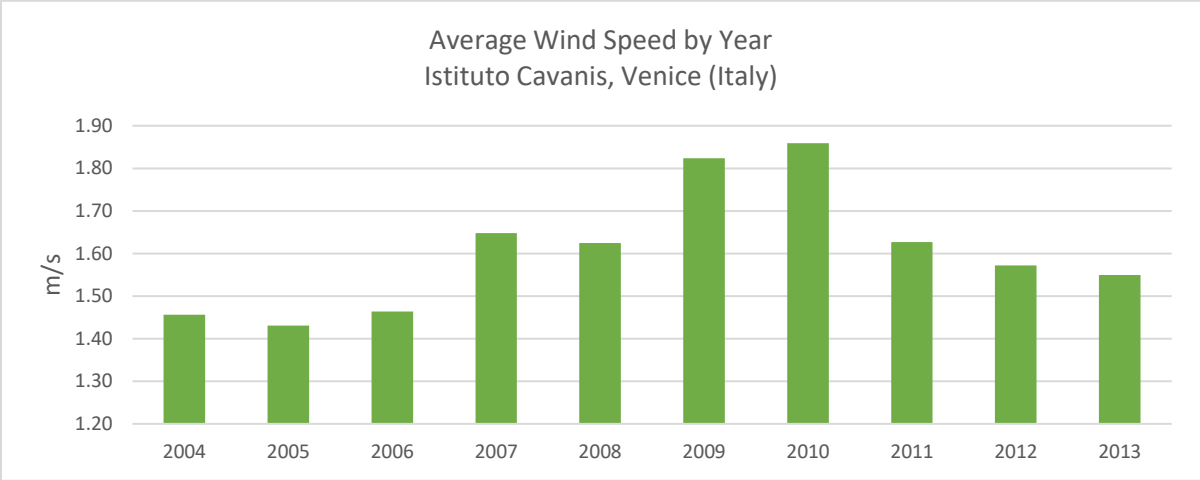

Fig. 2.8 – Average wind speed by year in Palude di Cona. Measures refer to the weather station "Venezia – Istituto Cavanis". Data Source: ARPAV – Servizio Meteorologico.

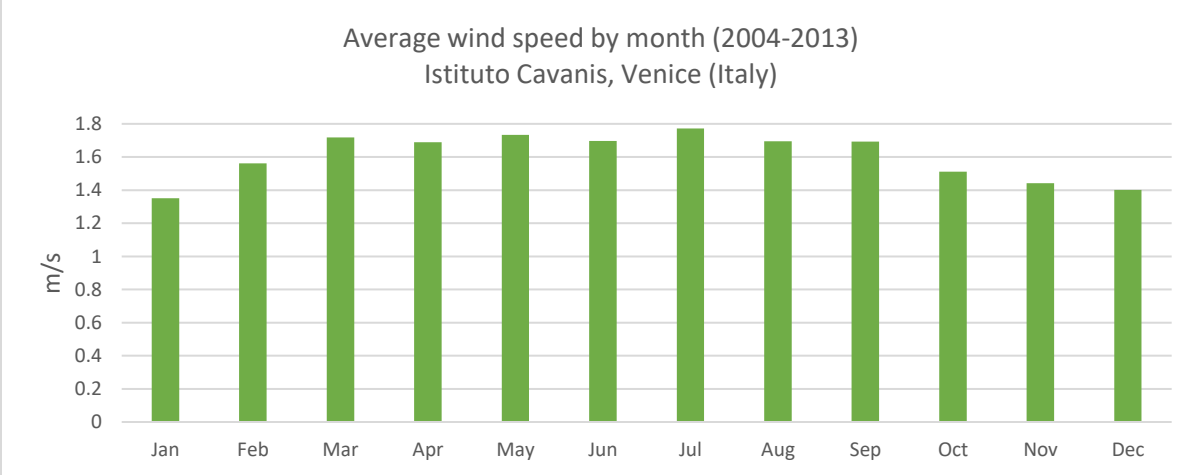

Fig. 2.9 – Average wind speed by month in Palude di Cona. Measures refer to the weather station "Venezia – Istituto Cavanis". Data Source: ARPAV – Servizio Meteorologico.

2.2.4 Solar radiation

Annual average solar radiation in the lagoon of Venice is 14.1 MJ/m^2 over the decade 2004-2013 (Fig. 2.10). Given its latitude (45.3° N), solar radiation reaches its peak of 25 MJ/m^2 in the months of June and July, and lowest of 5 MJ/m^2 in the winter time (Fig. 2.11).

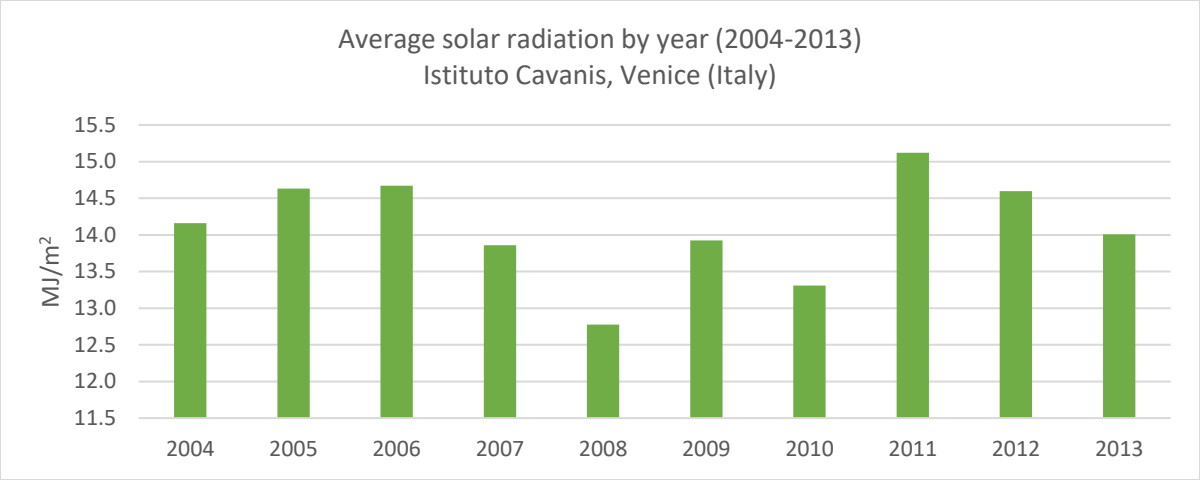

Fig. 2.10 – Average solar radiation by year in Palude di Cona. Measures refer to the weather station "Venezia – Istituto Cavanis". Data Source: ARPAV – Servizio Meteorologico.

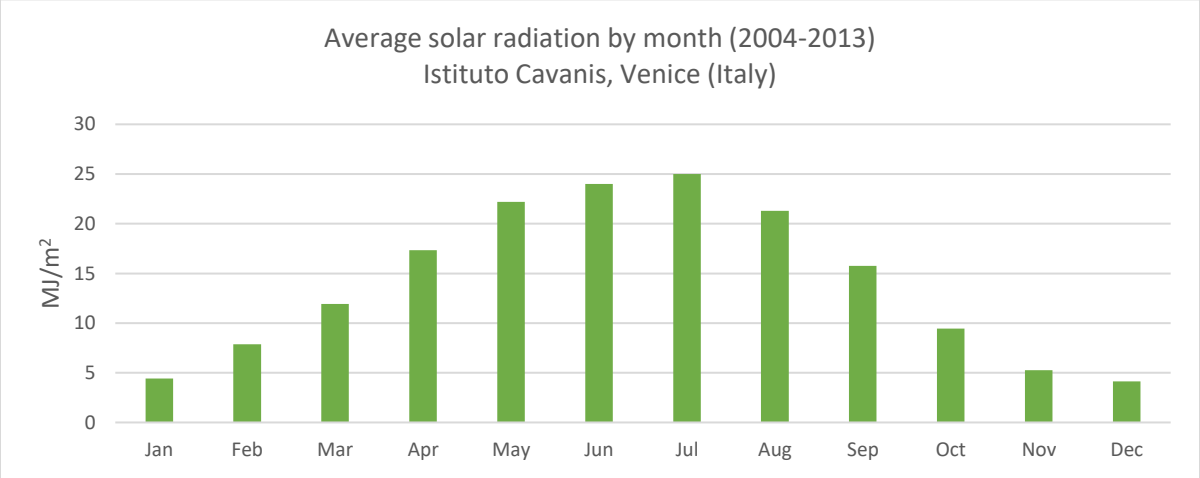

Fig. 2.11 – Average solar radiation by month in Palude di Cona. Measures refer to the weather station "Venezia – Istituto Cavanis". Data Source: ARPAV – Servizio Meteorologico.

2.3 The Zero river basin

2.3.1 Morphological and geological aspects

The region of the ZRB is located in the Venetian floodplain, as represented in Fig. 2.12. This area of the floodplain consists mainly of depositions from the rivers Brenta, Piave and Musone (ARPAV 2001). Sediments are predominantly dominated by carbonates, with differences in percentage depending on the river from which they originate. There is a progressive granulometric differentiation of the sediment from the "high plain" (north-west) to the "low plain" (south-east). The high plain consists mainly of coarse gravel with a sandy matrix. The sections further downstream are progressively characterised by sandy-silty-clay sediments (ARPAV 2004a).

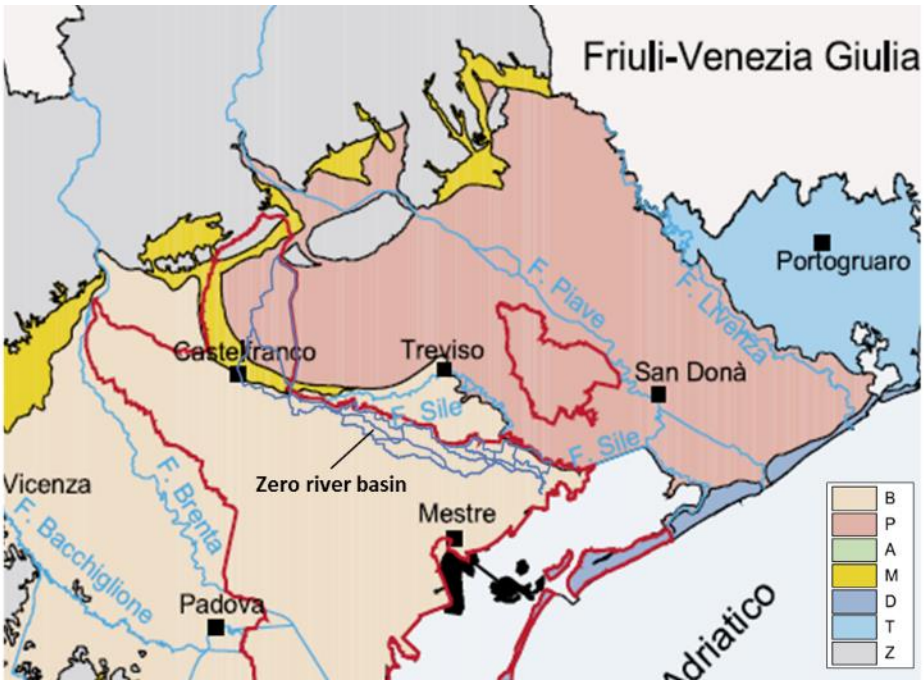

Fig. 2.12 – Depositional systems of the Venetian floodplain. Legend: B – Brenta river floodplain; P – Piave river floodplain; A – Adige river floodplain; M – Musone river floodplain; D – coastal and lagoon plain; T – Tagliamento river floodplain; Z – Alps, Prealps and moraine hills. Source: adapted from (ARPAV 2004b).

The ZRB has a surface area of 140 km^2 and its waters flow eastward with an elevation decline from 110 m to 1 m above sea level (Fig. 2.13). Approximately 93% of its surface has an inclination between 0 and 2%, and only 2% of the surface has an inclination above 5%. This

makes the morphology of the basin mainly flat. The steeper slopes can be found at the feet of the hilly area “Colli di Asolo”, at the head of the basin. The region between the high plain and the low plain, defined as “media Pianura Veneta”, is also characterized by the natural phenomenon of springs, which takes place in the area called “spring belt” (Fig. 2.13). The distance between the water table of the unconfined aquifers and the surface decreases with distance downstream, ranging from 50 m to less than 1 m deep. When the water table intersects the surface, a spring is generated.

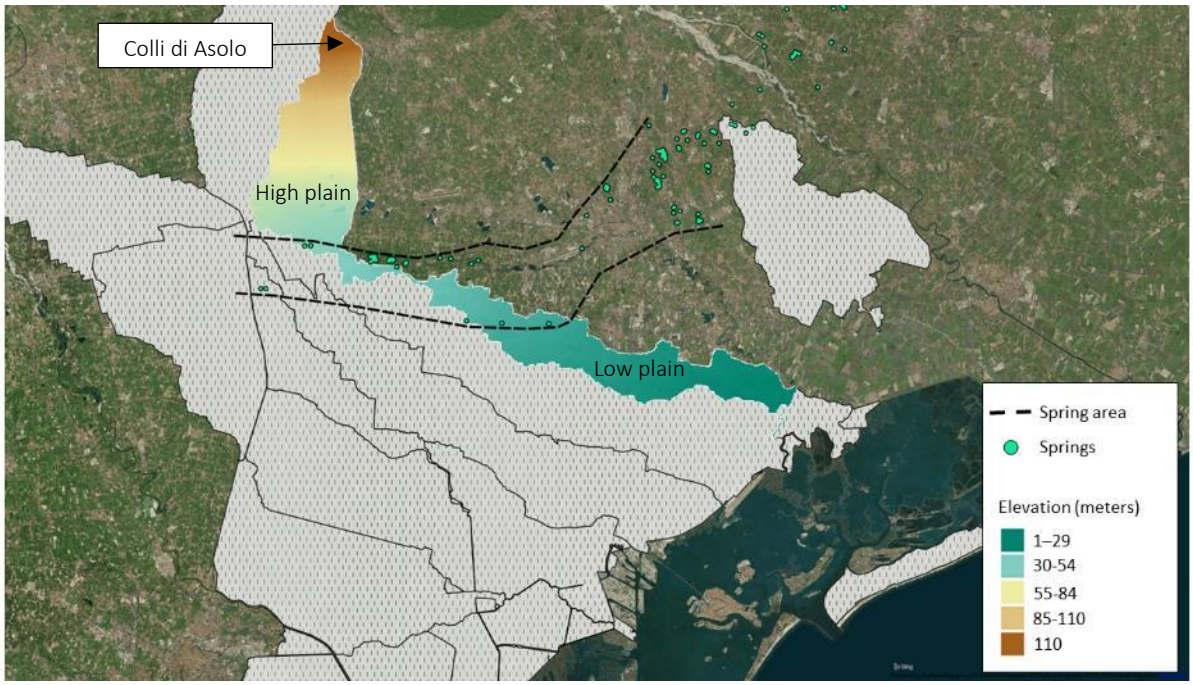

Fig. 2.13 – The Zero river basin is located at an altitude that goes from 110 m to 1 m above sea level. The central area is characterised by a spring zone, which influences the hydrology of the basin.

The morphology and characteristics of the sediment, together with the local climate and human activities, are the main factors in the pedogenesis of the soils of the ZRB. The soils of the VLW are classified in “districts”(ARPAV 2004a), as shown in Fig. 2.14.

The high plain is characterized mainly by soils of the Piave and Musone floodplains, while the remaining surface, the medium and low plain, is made of soil of the Brenta floodplain. The soils of the Piave floodplain are characterized by profiles with well-marked horizons. Superficial horizons are strongly decarbonated due to runoff and leaching. Clay is transported in depth, forming a clear clay horizon. Typical soils of the Musone floodplain show well-marked horizons.

Horizons tend to be decarbonated at the surface, with carbonate concretions (calcic horizon) in the deeper horizons caused by the percolation of carbonate-rich waters. Also, some of these soils feature a coarse texture also in the superficial horizons, due to agricultural management practices (i.e. tillage).

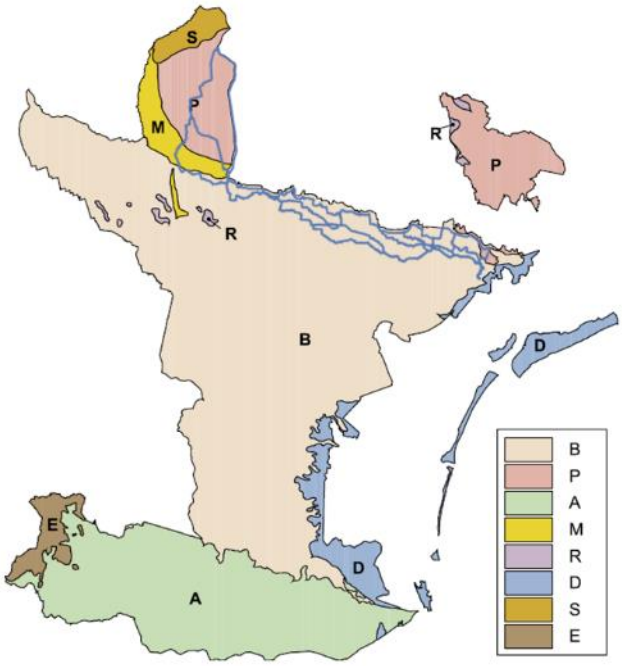

Fig. 2.14 – Subdivision of the Venice lagoon Watershed in soil districts. B – Brenta river floodplain; P – Piave river floodplain; A – Adige river floodplain; M – Musone river floodplain; R – Spring rivers floodplain; D – Coastal area; S – Asolo Hills; E -Euganei Hills. (ARPAV 2004a) .

The soils of the Brenta floodplain belong to the ancient part of the plain. The strong pedogenesis of the area generated soil with decarbonated superficial horizons. Carbonates accumulate in the deeper horizons. Moving downward, texture becomes progressively finer. Soils with loamy textures are characteristic of the northern zone of the floodplain, while loamy textures are common in the central area. Finally, silt-clay-loam textures are typical of soils bordering the lagoon of Venice. Generally, soils of the Brenta floodplain tend to be poorly drained, resulting in a superficial water table, usually within a depth of 150 cm.

2.3.2 Land use in the Zero river basin

The ZRB features distinct suburban traits. The vegetative cover consists mainly of agricultural crops, while forested areas are present only sporadically and in the forms of hedges and tree rows. The land use of the ZRB shows the typical characteristics of the VLW (Fig. 2.15a and b) (ARPAV 2009). Agricultural areas in the ZRB represent 73% of the total surface, while the remaining surface of the basin is covered by artificial (24%), semi-natural[1] and forested areas (4 %) (Fig. 2.15b).

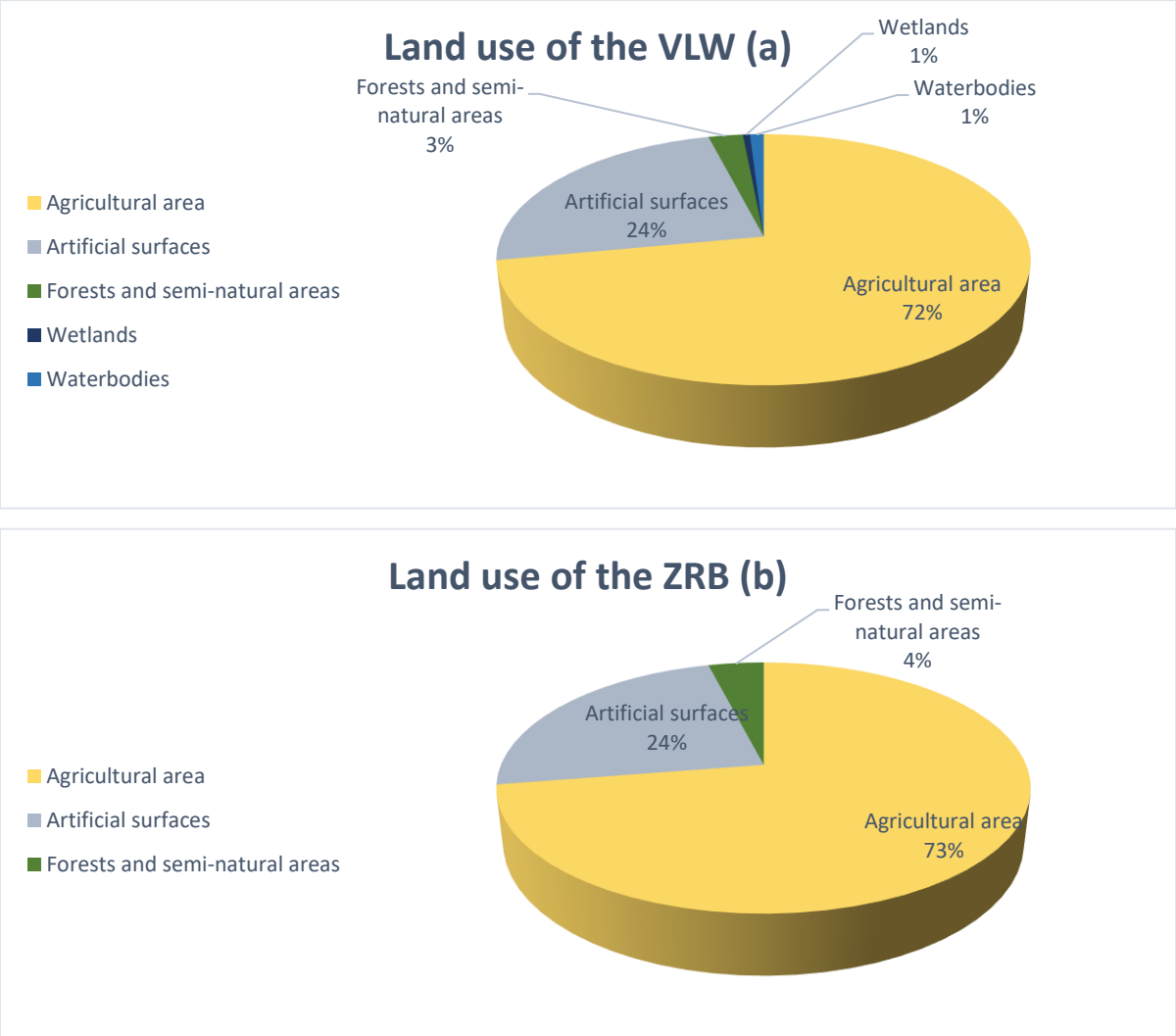

Fig. 2.15 – Comparison between the land uses of the VLW and the ZRB. (a) Main land uses of the VLW. (b) Main land uses of the ZRB (ARPAV 2009).

[1] Any area where human induced changes can be detected or that is human managed, but that still features the characteristics of a natural habitat (EEA 2006).

Agricultural areas are dominated by industrial crops. The most widespread crop is corn (*Zea mays* L.), followed by soy (*Glycine max* L.), and autumn-winter cereals such as winter wheat (*Triticum aestivum* L.) and barley (*Hordeum vulgare* L.). A small percentage of the agricultural land is also used for the cultivation of beets and other permanent horticultural crops. In the north-western part there is a significant presence of livestock farms, with a density of 5 to 10 farms per km^2 (ARPAV 2009). The agricultural activities of the area input a substantial amount of chemical substances such as synthetic fertilizers and pesticides, and organic fertilizer (i.e. manure and urea). For this reason, the region of Veneto has implemented the European Directive on nitrates 1991/676/CEE, which aims at regulating the input of fertilizers, especially nitrogen fertilizers, from agricultural activities.

Artificial surfaces are mainly represented by housing areas (54%), industrial businesses (32%) and transportation and services (14%). The north-western area of the ZRB is also characterized by the presence of surface-mining areas, to the detriment of agricultural land. Table 2.1 illustrates a classification of the main land use categories in the Zero river basin based on the CORINE land-use classification system (EEA 2006).

Table 2.1 – Classification of the main land use categories in the ZRB (ARPAV 2009).

Land Use	Relative %	Absolute %
ARTIFICIAL SURFACES	**100**	
Housing areas	54	13
Industrial businesses	33	8
Transportation and services	13	3
AGRICULTURAL AREAS	**100**	
Corn	62	45
Soy	18	9
Autumn-Winter Cereals	13	13
Pasture	8	6
SEMI-NATURAL AND FORESTED AREAS	**100**	
Semi-natural areas	75	3
Forested areas	25	1

2.3.3 Hydrology of the Zero river basin

The zero river is 47 km long and originates near “San Marco di Resana”, located 32 metres above sea level. Along its way, the river collects the waters of numerous tributaries, the most important being the streams “Brenton del Maglio”, “Scolo Vernise” and “Rio Zermason” (Fig. 2.16). The environment and the hydrology of the ZRB are heavily influenced by human activities and natural phenomena, that has given rise to a complex hydrologic network. Hydrology is influenced not only by climate and hydrologic events happening within its drainage area, but also by those occurring in the neighboring basins. Such a complex and dynamic situation poses a number of difficult challenges to hydrological and water quality modelling, which have been assessed in different studies (Essenfelder, Giove, and Giupponi 2016; Giupponi et al. 2012). The basin is characterised by several hydraulic infrastructures and artificial channels developed to reclaim land for agricultural purposes, and to regulate the flow discharging into the lagoon of Venice (CVN 2006). In case of emergencies, hydraulic nodes can divert a considerable fraction of peak flow outside the basin. Furthermore, spring waters originating in the surrounding areas influence the hydrology of the Zero river. The main contribution comes from the unconfined aquifer system located on the high plain (Servizio Acque Interne 2008). The spring water influx is highly variable along the year, and has a not entirely negligible influence over the hydrology of the Zero river.

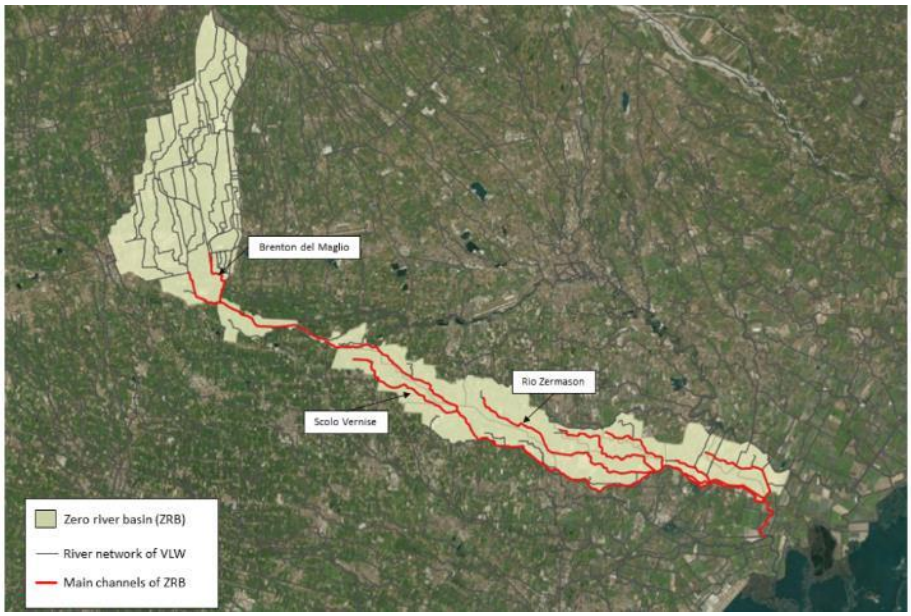

Fig. 2.16 – River network of the ZRB (Adapted from ARPAV 2010*).*

2.4 Palude di Cona

2.4.1 Morphological and geological aspects

Palude di Cona is a shallow water area that preserved its original salt-marsh characteristics, located near the airport of Venice. It borders the ZRB on its north-western side and is surrounded by barene (salt-marshes) and velme (mudflats), typical ecological elements of the lagoon of Venice. A barena is the flat and silty emerged part of a salt-marsh, frequently covered by halophytic plants which are submerged during high tides. A velma is a shallow muddy area emerging during low tides. The complex morphology and hydrodynamic of PDC make it an interesting natural laboratory to study the transfer and accumulation of nutrients and pollutants in the lagoon of Venice. The area is 4 km long, 0.9 km to 1.7 km wide, with a mean depth between 50 and 80 cm (Fig. 2.17). It is surrounded and crisscrossed by navigation channels that affect its hydrology. Surface sediments of PDC, made up of solid materials and fluid that were transported from the VLW to the lagoon, are dominantly of silt texture (Molinaroli 2006). Mud content (the incoherent material that includes all sediment particles less than 63 μm in size) in PDC is above 95% (MAV 1999). This reflects the effects of hydrodynamics on the sediment of the northern part of the lagoon, where small sediment particles are transported toward the landward side of the lagoon thanks to the strong current at the seaward inlets.

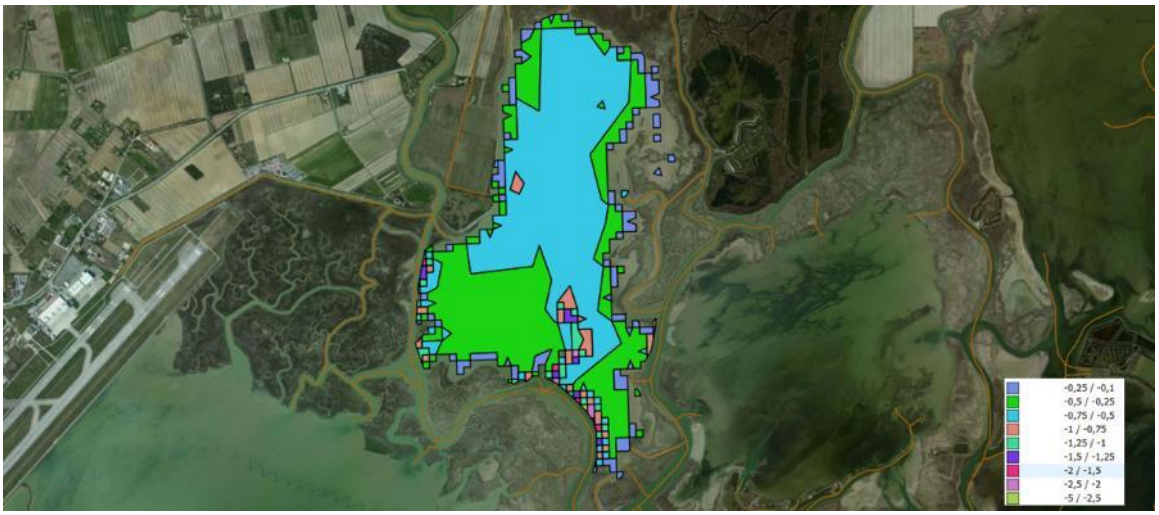

Fig. 2.17 – Palude di Cona, situated in the northern basin of the Venice lagoon, is an ecologically important marsh area. The map shows the bathymetry and the channelization of the area. Colored boxes represent the depth of the bottom surface. Yellow lines indicate the navigation channels of the area (Guerzoni and Tagliapietra 2006).

2.4.2 Physico-chemical characteristics

The physico-chemical characteristics of PDC, as those of the entire lagoon of Venice, are characterized by extreme diurnal fluctuations. However, it is possible to identify clear trends over higher temporal scales. Physico-chemical characteristics are defined by a number of factors, the most important being the freshwater inputs from the VLW, and the Adriatic Sea. The strong influence of freshwaters is observed in the salinity values of PDC, which are lower than the average value of the Lagoon of Venice (Zirino et al. 2014). Salinity values oscillate between 30 and 15 PSU, with an average of 23.5 PSU in the period 2007-2012. In Fig. 2.18 is shown an inverse correlation between salinity and freshwater discharge from the rivers Zero for the time period 2007-2012 (Pearson's coefficient R=-0.77).

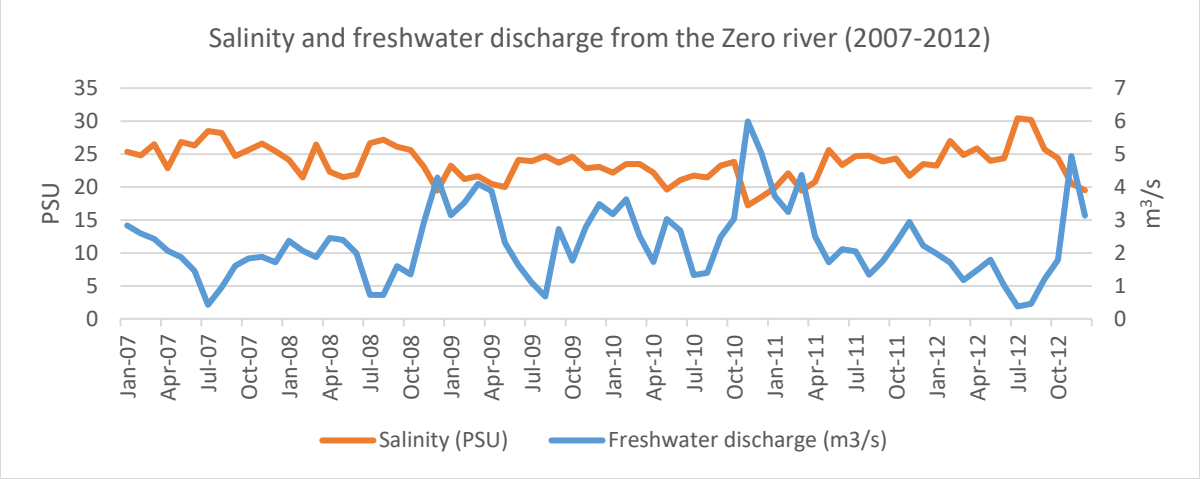

Fig. 2.18 – Salinity and freshwater discharge from the Zero river (2007-2012). There is an evident inverse correlation between the two variables (Pearson's coefficient R=-0.77). Data source: Magistrato alle Acque di Venezia and SAMANET.

Turbidity of the shallow waters in PDC is characterized by high temporal variability and is function of climate conditions, watershed loadings, hydrodynamics of the Venice lagoon, and difficult-to-predict local phenomena such as boat traffic. In Fig. 2.19 is represented the monthly variability of total suspended solids (TSS, mg/l) obtained from data of the station 1B of the MELa1-3 (Monitoraggio Ecologico Lagunare) programme (MAV & CVN 2002) over the period 2001-2009, with the exception of 2006, when no data were collected. Seasonal average turbidity for the period 2001-2009 ranges from 5.44 mg/l to 43.5 mg/l, with peaks reached

during the summer season. Bloom (2004) hypothesizes that higher TSS concentrations in the warmer months represent increased anthropogenic activities during these periods.

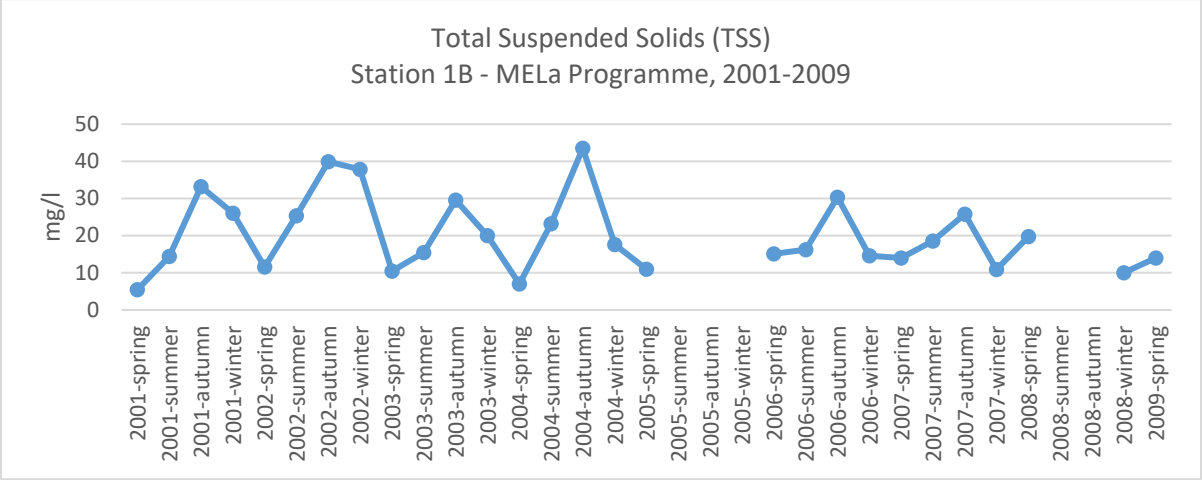

Fig. 2.19 – Seasonal averages of Total Suspended Solids (TSS) in PDC in the light of data provided by station 1B of the MELa monitoring programme (MAV & CVN 2002).

The shallow waters of PDC promote rapid temperature equilibrium between water and air, with water temperature following the seasonal trends of air temperature. The temperature in PDC shows an expected seasonal pattern (Fig. 2.20), with highest values in the summer reaching 26-27 °C, while wintertime lows typically around 5-7 °C, as indicated by data provided by the station 1B of the continuous monitoring network SAMANET (Ferrari, Badetti, and Ciavatta 2004).

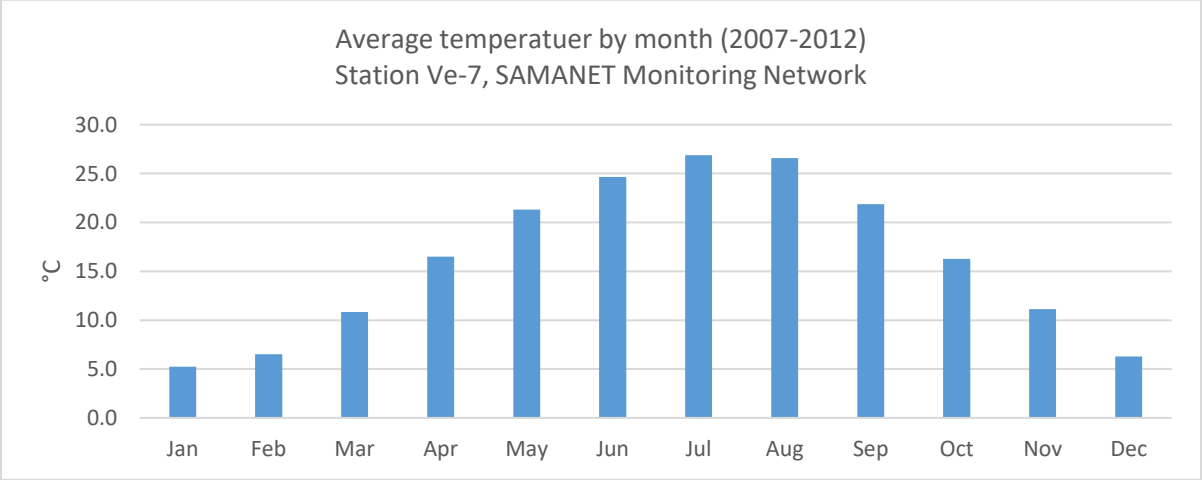

Fig. 2.20 - Average water temperature by month in PDC. Measures refer to the weather station 1B of the continuous monitoring network SAMANET.

Dissolved oxygen (DO) concentrations fluctuate with water temperature seasonally as well as diurnally (daily). Oxygen in water is controlled by temperature, which affects its solubility. In Fig. 2.21 is represented the monthly variability of DO in water (mg/l) for the station Ve-7 of the SAMANET monitoring network over the period 2007-2012. The highest values reaching 10-12 mg/l are found in the winter season, while summertime lows are typically around 4-6 mg/l. Fig. 2.22 shows the inverse correlation (R^2 = 0.98) between water temperature (°C) and DO (mg/l).

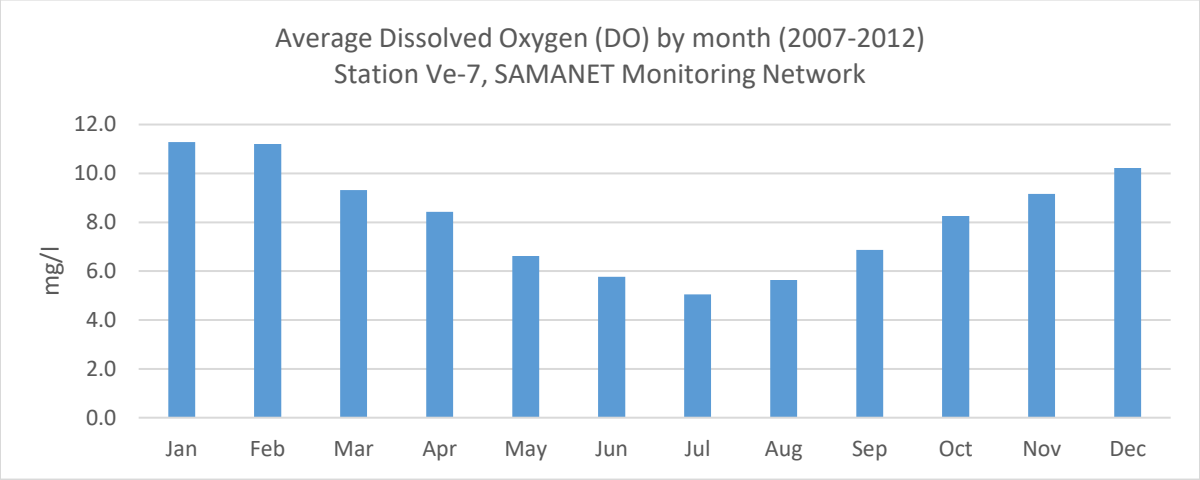

Fig. 2.21 - Average Dissolved Oxygen (DO) by month in PDC. Measures refer to the weather station Ve-7 of the continuous monitoring network SAMANET.

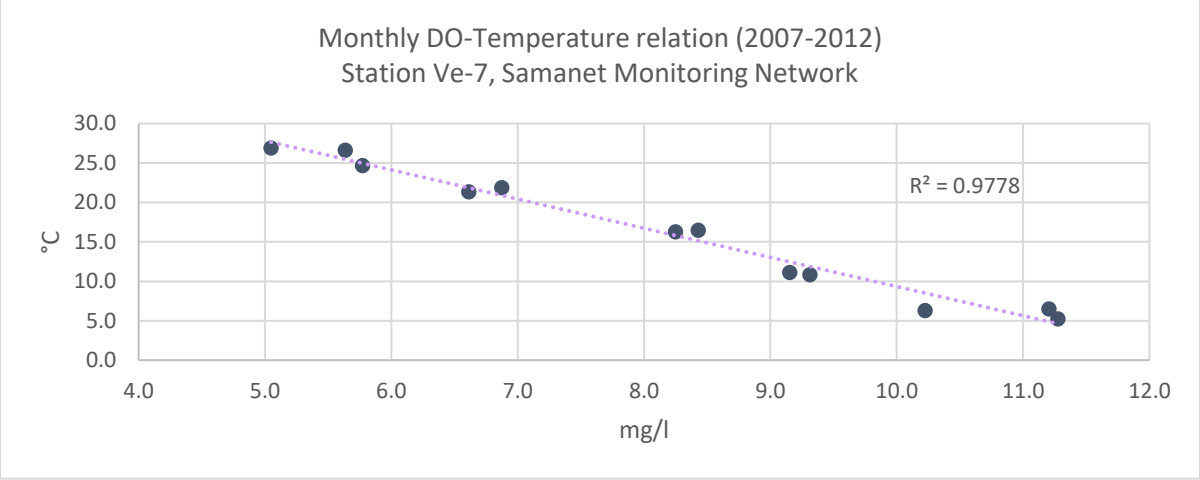

Fig. 2.22 – Inverse correlation between DO and water temperature in PDC. Measures refer to the monitoring station Ve-7 of the continuous monitoring network SAMANET.

2.4.3 Trophic state

The trophic state of a transitional environment such as PDC is the result of multiple variables such as the loadings and concentrations of nutrients, bathymetry, water retention time (water exchanges between sea and lagoon), climate conditions and biological processes (Cloern 2001). This section of the dissertation describes the trophic state of PDC through the concentration of inorganic forms of nutrients, Total Inorganic Nitrogen (TIN) and Total Inorganic Phosphorus (DIP), and the concentrations of chlorophyll-a (Chl-a), the most widely used proxy of phytoplankton biomass in the water column. Considering seasonal variability, PDC's trophic state follows the classic cycle of an aquatic ecosystem in a temperate climate. In the winter period, primary production is low (Fig. 2.23) and the dynamics of nutrients, which are present in higher concentrations (Fig. 2.24 & Fig. 2.25), are mainly influenced by loading and transport phenomena. In the spring time, solar radiation triggers the first phytoplankton blooms, which can be further stimulated or inhibited by the availability of lack of nutrients. Nutrient concentrations show minimum values in the summer period, when phytoplanktonic blooms reach their peak. The dynamics of phytoplankton in PDC, as in the rest of the Venice lagoon, are not only driven by temperature, solar radiation, and nutrient concentrations. Other factors such as turbidity and water retention time influence phytoplankton blooms. In autumn, with the reduction in temperature and light hours, phytoplankton blooms end and nutrient concentrations rise up again.

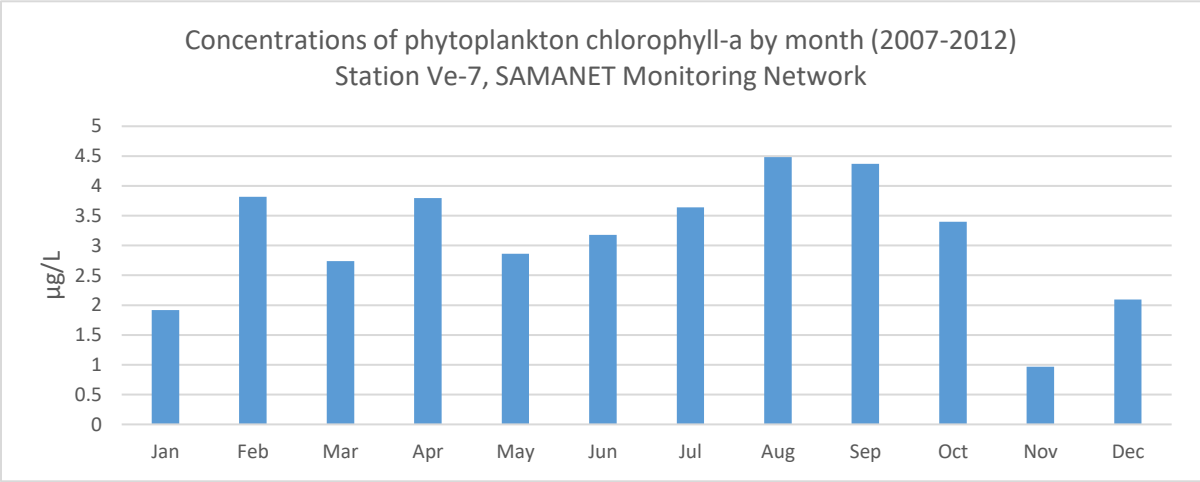

Fig. 2.23 – Concentration of phytoplankton chlorophyll-a by month (2007-2012) in PDC. Measures refer to the monitoring station Ve-7 of the continuous monitoring network SAMANET.

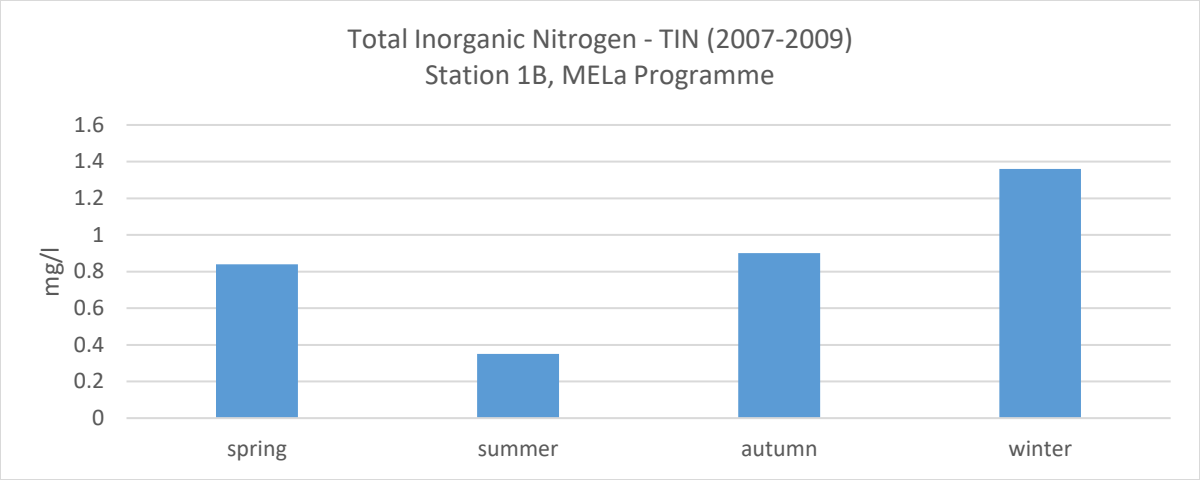

Fig. 2.24 – Seasonal TIN concentrations in the waters of PDC over the period 2007-2009. Data provided by station 1B of the MELa monitoring programme (MAV & CVN 2002).

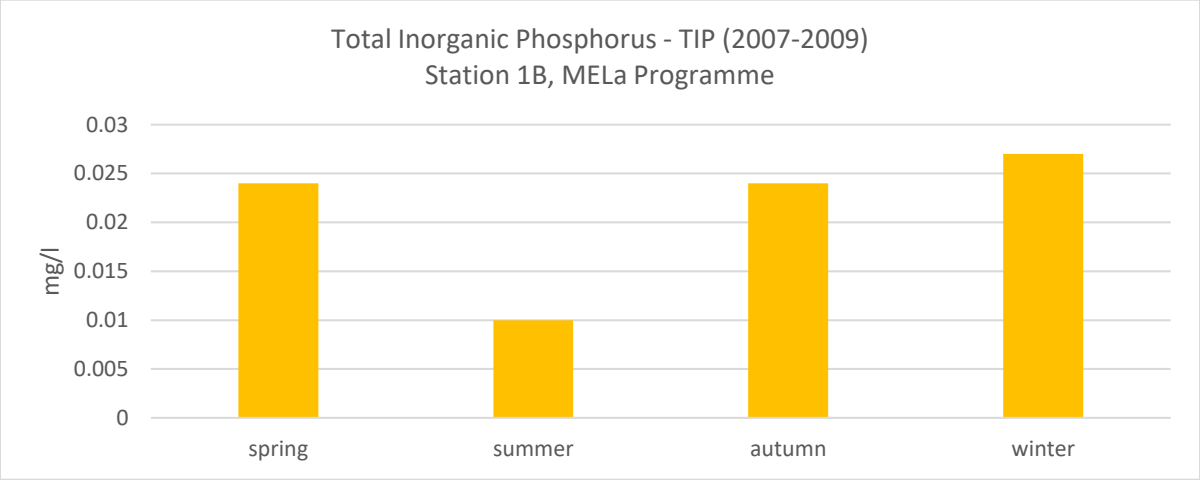

Fig. 2.25 - Seasonal DIP concentrations in the waters of PDC over the period 2007-2009. Data provided by station 1B of the MELa monitoring programme (MAV & CVN 2002).

Fig. 2.26 shows the seasonal variability of the DIN-DIP ratio in PDC over the period 2007-2009. The ratio assumes higher values than the Redfield ratio (16:1), commonly used to describe the composition of marine phytoplankton. This provides evidence of the importance of phosphorus to phytoplankton development in PDC. However, the relationship between N and P is highly variable in estuarine and coastal waters (Zirino et al. 2016b) and other N-P ratios could be representative of these ecosystems. For example, Carstensen and colleagues (2011) indicate that primary production in a body of water with a N-P ratio under 29 could be N-

limited, while a value over 29 would be P-limited. In conclusion, DIN-DIP ratios indicate that, on an annual average, primary production of PDC is limited by P concentrations. However, this condition become less evident in the summer period, where nitrogen may become the limiting factor (Sfriso et al. 1988).

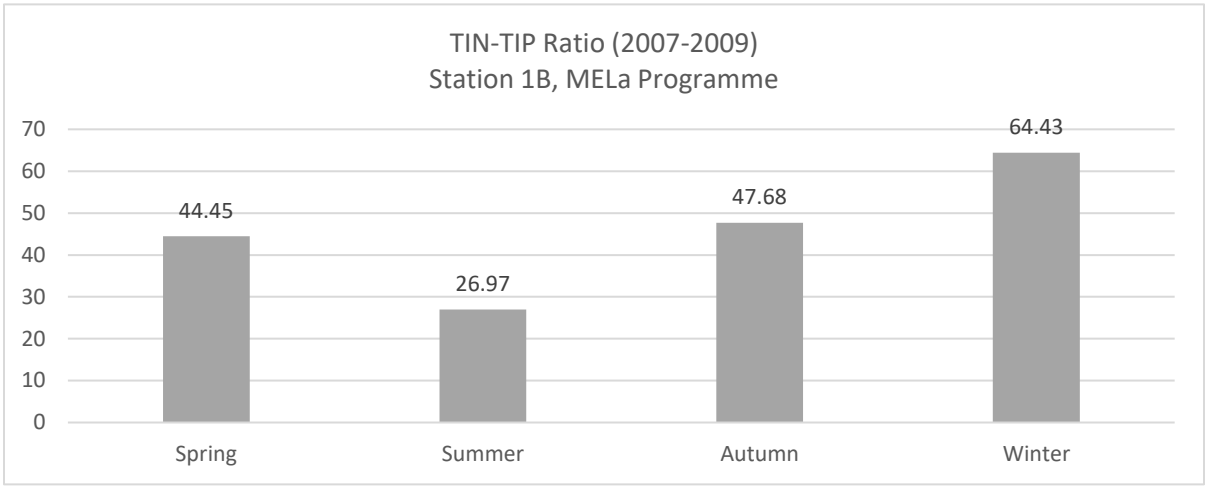

Fig. 2.26 – Seasonal DIN-DIP Ratio in the waters of PDC over the period 2007-2009. Data provided by station 1B of the MELa monitoring programme (MAV & CVN 2002).

Phytoplankton composition in the Lagoon of Venice is dominated by diatoms and flagellates (Facca, Sfriso, and Ghetti 2004). A particular characteristics of water bodies in the lagoon of Venice is the frequent resuspension of sediments from the bed. Many benthic diatoms living attached to the sediment and in its interstitial waters are detached from the bottom and induced to a pelagic life. Therefore, in the Lagoon of Venice, a subtle equilibrium between pelagic phytoplankton and re-suspended microphytobenthos exists. In shallow areas on the landward side of the Lagoon such as PDC, the water temperature in winter often get close to freezing point, and phytoplankton biomass is particularly scarce. In contrast, in summer phytoplankton thermophile species find the most favorable environmental conditions to their metabolism, with temperatures of between 25 and 30 °C, triggering exponential growth (Guerzoni and Tagliapietra 2006).

3 METHODOLOGICAL APPROACH

The integrated modeling approach described in this chapter was applied to the case study described in Chapter 2 of this dissertation to demonstrate its applicability, strengths and limitations. The developed approach (Fig. 3.1) adopted climate scenarios and environmental models to study the effects of climate change on nutrient loadings in coastal watersheds. It is made of 3 components: an ensemble of high resolution climate projections used to describe the future climate conditions, the hydrological model Soil and Water Assessment Tool (SWAT, Arnold et al. 1998) to evaluate the impacts of climate change on the hydrology and nutrient loadings of the watershed (ZRB); and the ecological model AQUATOX (Park et al. 2008) to assess the combined impacts of climate change and nutrient loadings on the aquatic ecosystems of coastal waters (PDC). Figure 3.1 describes the methodology adopted in the research highlighting 3 fundamental steps: climate projections; the hydrological modelling with SWAT; and the ecological modelling with AQUATOX. Paragraphs 3.1, 3.2 and 3.3 3 describe each step of the adopted methodology.

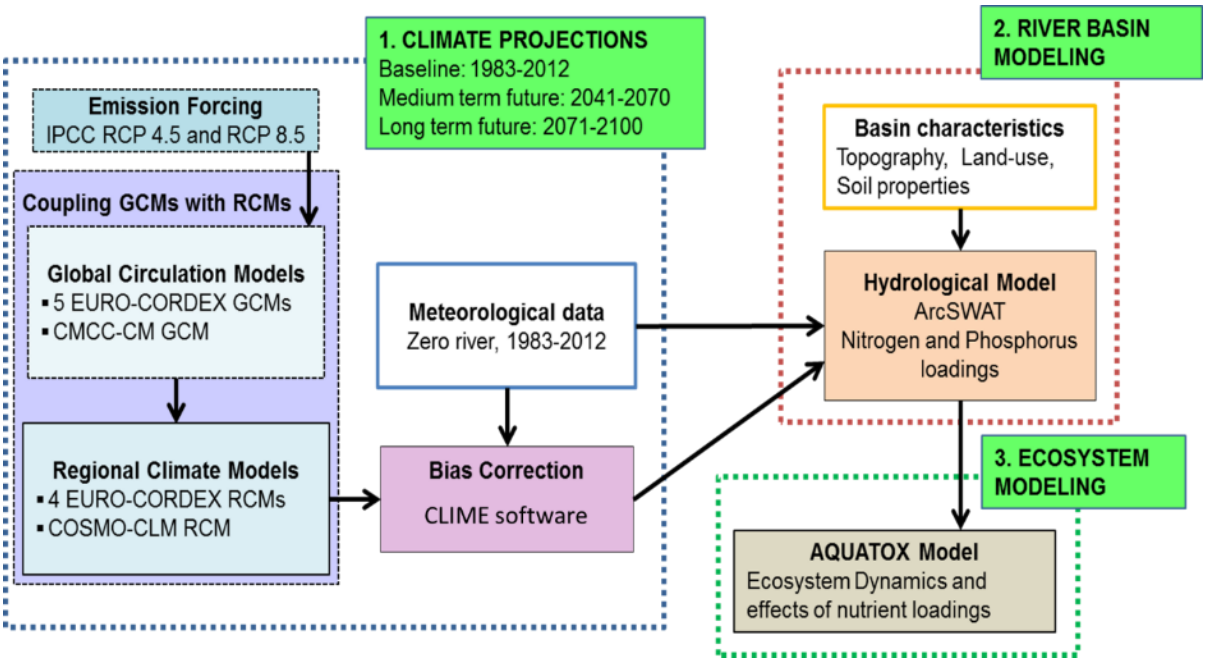

Fig. 3.1 - The developed integrated modelling approach includes 3 fundamental steps: climate projections; the hydrological modeling with SWAT; and the ecological modelling with AQUATOX.

The first component of the methodological approach consists a set of climate projections obtained from the coupling of general circulation models (GCMs) with regional climate models (RCMs), and a bias correction method adopted to reduce the intrinsic biases of climate projections and thus providing reliable climate scenarios of the 21st century (from 2013 to 2100). Future climate projections were estimated for two time periods of 30 years each: a mid-term period (2041-2070) and a long-term period (2071-2100). The second component consists in the modelling of present and future conditions of the hydrology and nutrient loadings of the watershed through the adoption of the hydrological model SWAT. The last component is the ecological model AQUATOX, selected to study the future combined effects of climate change and nutrient loadings on the primary production of coastal aquatic ecosystems. The output of SWAT (freshwater discharge, nitrogen and phosphorous loadings), were implemented in AQUATOX in order to observe the effects on the phytoplankton community. The final output produced information about the potential effects on nutrients and primary producers (phytoplankton) of the coastal aquatic ecosystem. Such information can be used to evaluate how the possible changes in climate can affect hydrological and water quality parameters of watersheds and the ecological aspects of receiving coastal waters. The results can be implemented in environmental risk assessment studies in order to generate potential future scenarios of nutrient pollution and associated environmental impacts.

3.1 Climate projections

3.1.1 Selection of the control period

To correctly assess the differences in climate between present and with future conditions, and to apply the bias-correction method, a control period must be selected. The control period should be sufficiently long in order to obtain representative statistics of the reference climate conditions. Considering this, the reference period from January 1983 to December 2012 was used as a baseline for the study.

3.1.2 Selection of future climate scenarios

The IPCC Data distribution center suggests the use of more than one climate scenario in order to reflect the variability and uncertainties associated to climate models and the resulting climate scenarios (IPCC-TGICA 2007). Uncertainty is intrinsic in the science of climate change. Therefore, it is a fundamental assumption to understand that climate scenarios are not predictions of the future, but rather a plausible description of what might happen to climate in the future. To reduce as much as possible the dependence of the results of the study on the adopted scenarios, an ensemble of 10 climate scenarios was chosen. In order to be selected for the study, climate scenario should be:

- Representative of the study area;
- Representative of the selected time periods: 2041-2070 and 2071-2100 (scenarios that ended in the years 2099 were also selected);
- Open-source and easy to obtain via the internet;
- Forced by RCP4.5 and RCP8.5;
- Characterized by the highest spatial resolution available;

Two RCPs were considered in the study. The "moderate" emission scenario, RCP4.5, that predicts a stabilization of the emissions (approximately 650 ppm) shortly after 2100, with an increase in radiative forcing up to 4.5 W m^{-2} by 2100 (Thomson et al. 2011). The "extreme" emission scenario, RCP8.5, that describes a future without any specific climate mitigation target. In this scenario, the GHGs emissions and concentrations increase considerably over the 21st century, leading to a radiative forcing of 8.5 W m^{-2} by 2100 (Riahi et al. 2011). It was decided to not adopt the RCP2.6 because of the weak effects produced by this pathway.

In agreement with the abovementioned criteria, the CMCC-CM/COSMO-CLM GCM-RCM and an ensemble of 9 GCM-RCM model combinations from the EURO-CORDEX project (Jacob et al. 2014) were selected for this study. The CMCC-CM global model (Scoccimarro et al. 2011) is the coupled atmosphere-ocean general circulation model adopted by the Centro Euro-Mediterraneo sui Cambiamenti Climatici (CMCC). COSMO-CLM (CCLM) (Cattaneo et al. 2012) is a climate regional model that can be used with a spatial resolution between 1 and 50 km.

The coupling of the two models produced climate scenarios at a spatial resolution of 0.0715° (8 km) for the selected region. EURO-CORDEX is the European branch of the CORDEX initiative and aims to provide an ensemble of climate simulations for the European region (Fig. 3.2) based on dynamical statistical downscaling models forced by multiple GCMs. For this study, 9 GCM-RCM model combinations, providing outputs at a spatial scale of 0.11° (12 km), were selected. The model combinations and their characteristics are presented in Table 3.1. Although the selected 9 CORDEX GCM/RCM outputs have been created within the same project, there are specific differences among the adopted calendars. Specifically, the models number 2 and 8 use a 360-day calendar and the model number 3 uses a 365-days calendar (Table 3.1). The remaining scenarios use the standard calendar which contains leap years and can be directly applied to impact models. To prepare the data for additional impact modelling, all climate scenarios were converted to a standard calendar. When a climate model used a 360-days calendar an additional day had to be created in case of January, March, May, July, August, October, and December, and two (one day in the case of a leap year) had to be removed from the month of February. For each added-day a null value (NA) was assigned. The rationale behind removing one/two days from the month of February was that their removal cannot have significant effect on hydrology and ecosystem processes. When a climate model used a 365-days calendar, an additional day with a NA value had to be created every 4 year for the month of February (February 29th). Adding NA values to the time series does not have any effect on statistics and allows the time series to be implemented into SWAT and AQUATOX.

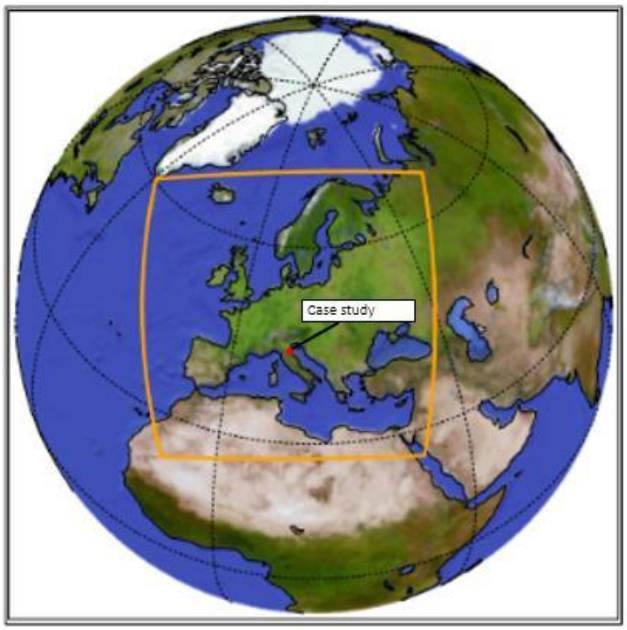

Fig. 3.2 – The EURO-CORDEX region (CORDEX 2015).

Table 3.1 – Future climate scenarios selected and implemented in the models SWAT and AQUATOX.

	N. Scenario	GCM	RCM	Spatial Resolution	Calendar	Time range	Institute
CMCC	1	CMCC-CM	COSMO-CLM	0.0715 deg (8 km)	Standard	1976-2100	CMCC
EURO-CORDEX	2	HadGEM2-ES	RCA4	0.11 deg (12 km)	360-days	1970-2099	SMHI
	3	IPSL-CM5A-MR	RCA4	0.11 deg (12 km)	365-days	1970-2100	SMHI
	4	CNRM-CM5	RCA4	0.11 deg (12 km)	Standard	1970-2100	SMHI
	5	EC-EARTH	RCA4	0.11 deg (12 km)	Standard	1970-2100	SMHI
	6	MPI-ESM-LR	RCA4	0.11 deg (12 km)	Standard	1970-2100	SMHI
	7	CNRM-CM5	CCLM	0.11 deg (12 km)	Standard	1950-2100	CLMcom
	8	HadGEM2-ES	RACMO22E	0.11 deg (12 km)	360-days	1950-2099	KNMI

	9	EC-EARTH	HIRHAM5	0.11 deg (12 km)	Standard	1951-2100	DMI
	10	EC-EARTH	RACMO22E	0.11 deg (12 km)	Standard	1950-2100	KNMI

CTRL: Control period; **SCEN:** future scenario; **CMCC:** Centro Euro-Mediterraneo Cambiamenti Climatici; **KNMI:** Royal Netherlands Meteorological Institute, Ministry of Infrastructure and the Environment; **SMHI:** Rossby Centre, Swedish Meteorological and Hydrological Institute, Norrkoping Sweden; **DMI:** Danish Meteorological Institute, Copenhagen, Denmark.

3.1.3 Bias correction of climate change scenarios with CLIME

GCMs have a spatial resolution too coarse for watershed-scale assessments. Therefore, they are generally coupled with RCMs to provide a better description of the effects of orography, land-sea surface contrast and land surface characteristics. However, also RCMs often show significant biases due to an imperfect conceptualization, discretization and spatial averaging within grid cells (Christensen and Christensen 2007). In order to implement the output of the GCM-RCM into hydrological and ecological models, bias correction is highly recommended (Teutschbein and Seibert 2012). In this study, a simple bias correction post-processing method, the linear scaling (LS) method, was applied to correct the biases in the daily values of temperature (T) and precipitation (P).

The software CLIME was used in this study to apply the LS method to all the selected climate scenarios. CLIME is a GIS software for climate data analysis developed by the REgional Models and geo-Hydrogeological Impacts division (REMHI) of CMCC (Cattaneo et al. 2015). The software CLIME has been here applied to link climate scenarios with environmental impact assessment models, by providing "corrected" and meaningful climate data useful for impact studies. CLIME allows the user to run a bias correction process and to provide the bias corrected results in a readable and usable format (Villani et al. 2015). All the processes run by CLIME are executed by a set of freely consultable functions written in R language and included in the R package named "qmap", available on the R Archive Network[2]. The process consists in comparing the "observation grid", namely the spatial grid containing the weather stations of the study area, with the "model grid", containing the geographical points of the climate

[2] http://www.cran.r-project.org

scenario, for the control period (1983-2012). The bias correction is then applied to a "model box" containing the nearest points of the "model grid" to the selected weather station. This process creates a "correction mask", that is then applied to the "correction period", which corresponds to the future period to be studied (2041-2070 and 2071-2100). The bias corrected values of each of the points in the model box are then averaged and considered as representative of the weather station under exam. In this study, a box of 9 points of the "model grid" was selected for each weather station (Fig. 3.3).

Fig. 3.3 – Representation of the "observation grid" (green dots) and "model grid" (black dots) in CLIME. In this study, the 9 nearest points of the model grid (yellow dots) to the weather station "Castelfranco" were selected as representative. The same process was performed for each of the three weather stations. Elaboration performed by CLIME software.

The method was implemented to all 10 climate scenarios for every weather station of the case study (Fig. 2.3). The longest series of observations available for all the selected weather stations (1993-2012) was used to implement the bias correction method. The time series has a percentage of valid data above 75%, which is considered as acceptable for the application of bias correction in the software CLIME (Cattaneo et al. 2015). The missing values were sporadic and isolated, presenting interruptions not more than 10 days long. Accordingly, it was decided

to leave the values as blank and not substitute them with any interpolation method as they were considered unable to affect long-term statistics (Sachindra et al. 2014).

The LS method aims to perfectly match the monthly mean of corrected values with that of observed ones (Lenderink, Buishand, and van Deursen 2007). The monthly correction is based on the differences between observed and raw RCM data. Precipitation is corrected with a multiplier term while temperature with an additive term on a monthly basis, as shown in Eq. 3.1 and Eq. 3.2:

$$P_{cor,m,d} = P_{RCMraw,m,d} \times \frac{\mu(P_{obs,m})}{\mu(P_{RCMraw,m})} \quad \text{Eq. 3.1}$$

$$T_{cor,m,d} = T_{RCMraw,m,d} + \mu(T_{obs,m}) - \mu(T_{RCMraw,m}) \quad \text{Eq. 3.2}$$

where $P_{cor,m,d}$ and $T_{cor,m,d}$ are corrected precipitation and temperature on the *d*th day of the *m*th month, and $P_{RCMraw,m,d}$ and $T_{RCMraw,m,d}$ are the RCM raw precipitation and temperature on the *d*thday of the *m*th month. Finally, μ represents the mean value. The method was selected for its simplicity and modest data requirements: only the observed daily values for precipitation and temperature are required to calculate the correction factors.

The monthly bias corrections between observed and RCM-simulated variables for the control period for each GCM-RCM model combination were applied at each rainfall and temperature station for both case studies.

The software CLIME was also used to convert the format of climate data into a format readable by the models SWAT and AQUATOX. Climate data are commonly provided to final users in the NetCDF format (Network Common Data Format), an efficient binary data format for large volumes of data. However, this format is generally unreadable by other software and therefore needs to be converted.

3.2 Hydrological modelling: SWAT

3.2.1 Soil and Water Assessment Tool (SWAT)

SWAT was selected for studying the hydrology and water quality parameter of the ZRB. The SWAT model has been developed in order to support the work of managers in assessing the impacts of climate and land management practices in watersheds and large complex river basins. It allows performing studies focusing on hydrology, sediments, non-point source loadings, land management and climate change. The model was selected for the following reasons:

- it has been widely used for modeling nutrient loadings and long-term impacts of climate change on the hydrology of river basins (Cousino, Becker, and Zmijewski 2015; Fan and Shibata 2015; Kim et al. 2016; Sellami et al. 2016);
- the user-friendly interface is based on the software ESRI ArcGIS©, and allows the user to perform a relatively fast implementation of the data into the model and an easy customization of all the parameters involved in the model;
- the input required by SWAT is commonly available from public institutions and government agencies;
- SWAT is a public domain software, freely available on the internet, which receives constant updates and support from the developers; and
- it is well documented and supported by an active user community on the Internet.

SWAT is a semi-distributed and time continuous eco-hydrologic model that operates on a daily time step. SWAT allows to simulate several different physico-chemical and biological processes in a watershed. The model is based on the Hydrologic Response Units (HRUs), areas with identical combinations surface slope, land use and soil type that are able to represent the spatial heterogeneity of a watershed, increasing the accuracy of load computations, and providing an improved description of the water balance (FitzHugh and Mackay 2000). The model components (e.g. soil water content, surface runoff, sediment yield, nutrient cycling) are calculated for every HRU and then are aggregated at a sub-basin level through a weighted average. Finally, water flow, sediment yield and nutrient loadings for each sub-basin are routed through the river network to the watershed outlet (Neitsch et al. 2011). In this section, a brief

description of the main components of the model is provided. A complete description of SWAT equations can be found in Arnold et al. (1998) and Neitsch et al. (2011).

Climate

Climate is the engine of the hydrologic cycle as it provides the energy necessary to regulate the water balance of a watershed. To simulate the climate, SWAT requires daily precipitation (mm), maximum/minimum air temperature (°C), solar radiation (MJ/m^2), wind speed (m/s) and relative humidity (%). SWAT is equipped with a weather generator that can be used to generate missing values on climate time-series based on statistics of the provided data. Specifically, daily precipitation values are generated using a Markov chain model (Nicks 1974) that defines a day as wet or dry by comparing a random number (0.0-1.0) generated by the model with monthly "wet-dry" probabilities obtained from the provided time-series. If the day is "wet", the amount of rainfall is determined from a skewed distribution based on the statistics of the time-series provided to the model. Air temperature and solar radiation are generated from a normal distribution which accounts for temperature and radiation variations caused by dry/rainy days through a continuity equation. Air temperature and solar radiation are reduced when simulating rainy conditions and increased when simulating dry conditions. The goal is to generate long-term statistics in agreement with the averages of the time-series provided to the model. Wind values are generated using a modified exponential equation that reproduces daily mean wind speed based on the mean monthly wind speed of the provided time-series. Daily values of relative humidity are generated using a triangular distribution that makes use of monthly averages of the provided time-series.

Hydrology

Simulation of the hydrology of a watershed can be separated into two phases. The first is the "land phase" (Fig. 3.4), which controls the amount of water, sediment, nutrient and pesticide loadings to the stream channel. The driving force of the model in the land phase is water balance, and the equation the regulates it is formulated as follow (Eq. 3.3):

$$SW_t = SW_0 + \sum(R_{day} + Q_{surf} + E_a + W_{seep} + Q_{gw}) \quad \text{Eq. 3.3}$$

where SW_t is the final soil water content (mm), SW_0 is the initial soil water content (mm), R_{day} is the amount of precipitation for the day (mm), Q_{surf} is the amount of surface runoff for the day (mm), E_a is the amount of evapotranspiration for the day (mm), W_{seep} is the amount of water entering the vadose zone from the soil profile for the day (mm), and Q_{gw} is the amount of return flow to groundwater for the day (mm). Precipitation in SWAT can be intercepted and held by the vegetation or fall to the soil surface. Water on the soil surface will infiltrate into the soil profile or runoff, thus contributing to short-term stream responses. Infiltrated water can be held in the soil and later leave the ground through evapotranspiration, or can reach the underground waters and be removed from the system or making its way back to the surface-water system. The groundwater component of SWAT is a simple conceptual linear reservoir based on information in the form of recharge to and baseflow from the groundwater system. Once SWAT calculates the loadings of water and nutrients, they enter the "routing phase", where they are routed through the stream network of the watershed (Fig. 3.5). In the routing phase water flows downstream. Here, water may be lost due to evaporation and transmission through the bed of the channel, or due to to removal from the network for agricultural purposes. The volume of water may increase as rainfall falls directly on the river network or from point source discharges (e.g. WWTP). Water flow is routed through the channel using a variable storage coefficient method developed by Williams (1969). Hydrologica processes in SWAT are indicated in Fig. 3.6.

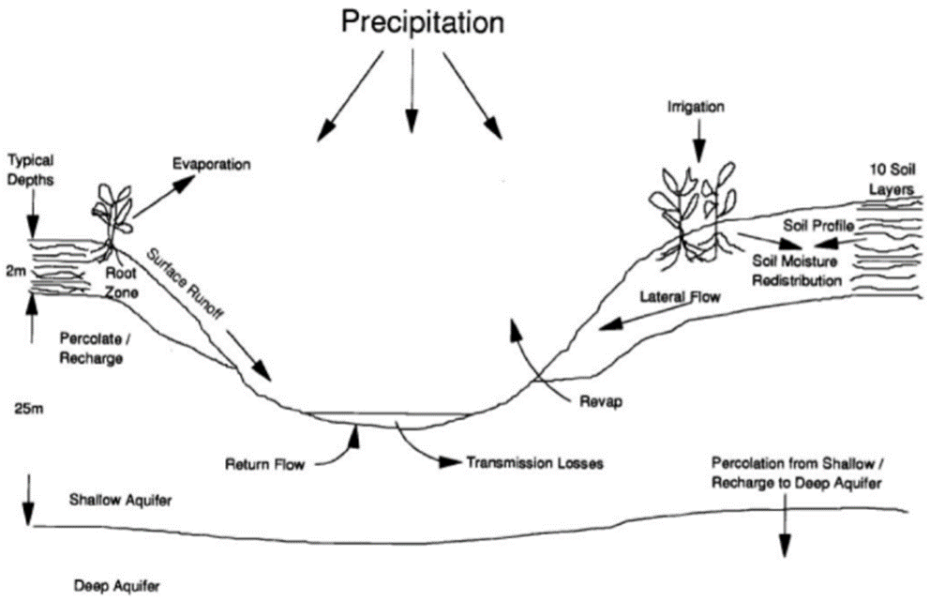

Fig. 3.4 – Land-phase processes modeled by SWAT. Adapted from (Arnold et al. 1998).

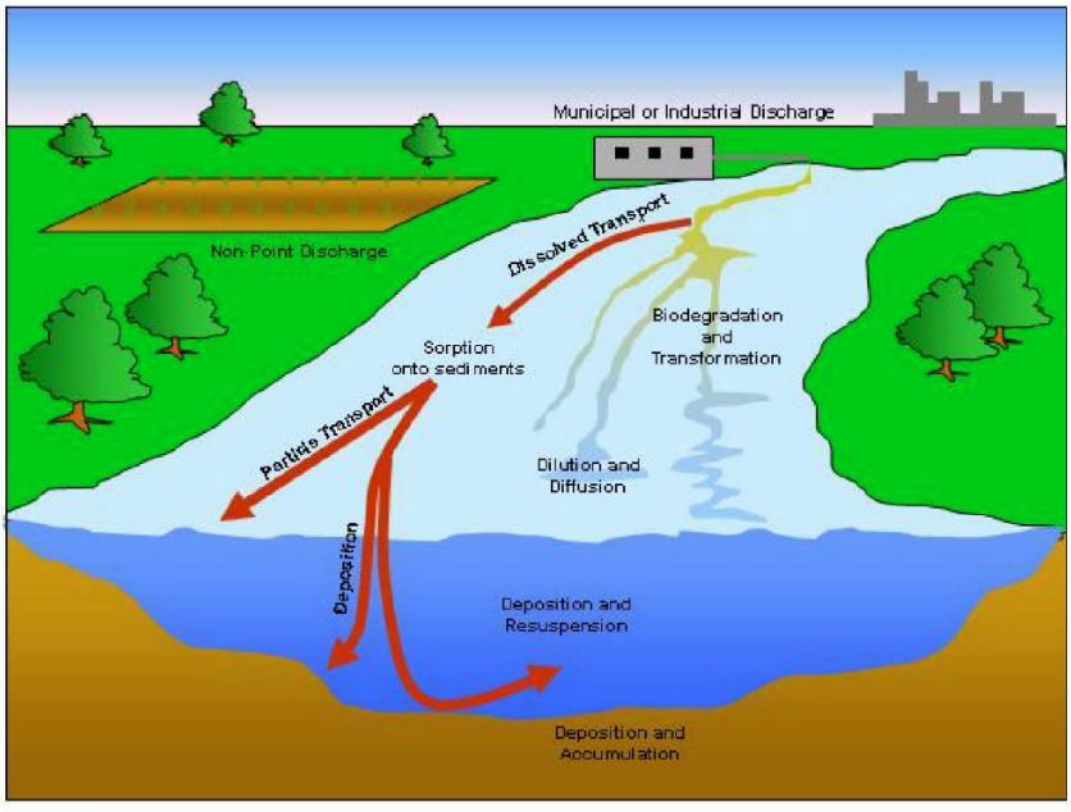

Fig. 3.5 – In-stream processes modeled by SWAT. Adapted from (Arnold et al. 1998).

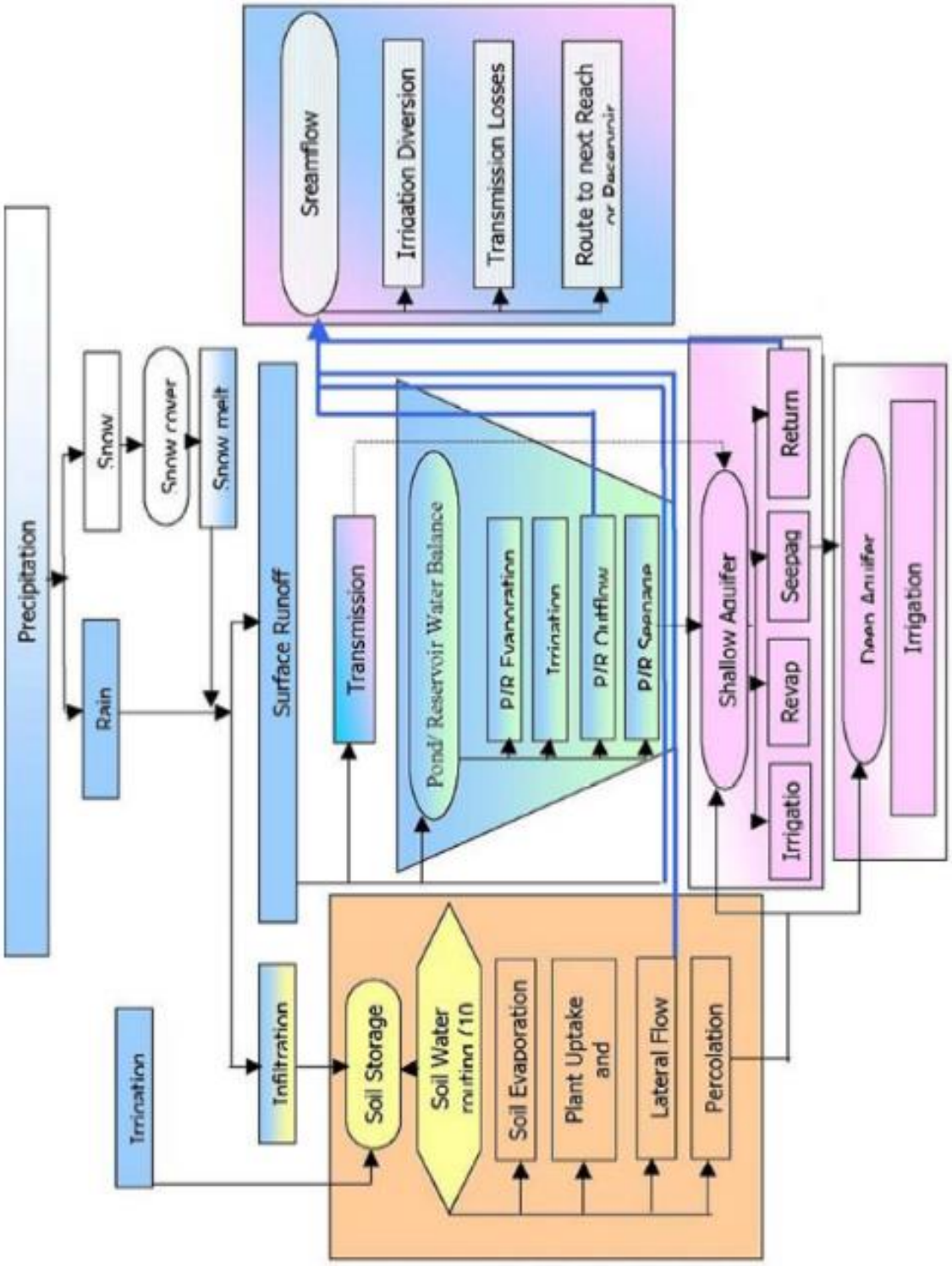

Fig. 3.6 – Schematic representation of hydrology in SWAT.

Nutrient cycles

SWAT can simulate the dynamics of nutrients in the soil profile and in the stream channel. The cycle of nitrogen includes water, atmosphere and soil. While elemental nitrogen is inert, "fixed" nitrogen is an extremely active element and exists in the soil in many valence states. SWAT can simulate all the major forms of nitrogen in the soil, which are subdivided into two main pools, mineral nitrogen and organic Nitrogen (Fig. 3.7). The two forms of inorganic nitrogen in SWAT are ammonium (NH_4^+) and nitrate (NO_3^-). The three forms organic nitrogen are fresh organic nitrogen, representing the crop residue and the microbial mass, stable humic nitrogen, and active humic nitrogen.

The most prevailing form of nitrogen in the soil is organic nitrogen, which is slowly converted to inorganic forms (ammonia and nitrates) through mineralization, which makes nitrogen ready to be assimilated by the plants. Nitrate is very soluble and percolates easily through the soil or is removed by runoff during precipitation events. Ammonium and organic nitrogen are sorbed very readily to soil particles and therefore tend to remain in the soil profile and be removed only during erosion events. The denitrification process facilitates nitrate reduction and produces molecular nitrogen (N_2), causing nitrogen losses toward the atmosphere.

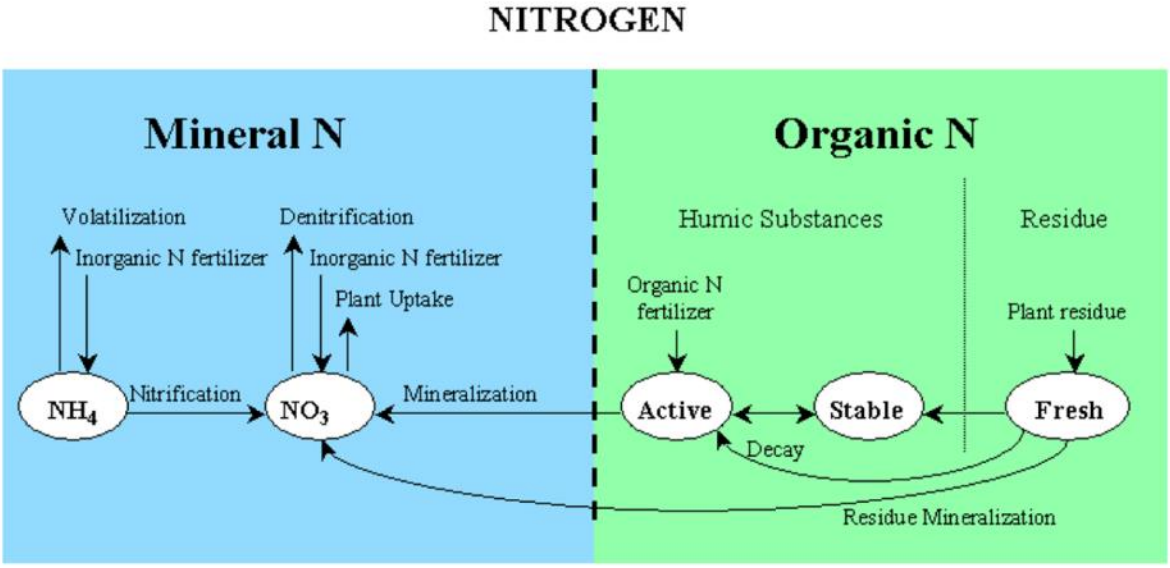

Fig. 3.7 – Soil nitrogen pool and processes simulated in SWAT (Neitsch et al. 2011).

Phosphorus is less mobile than nitrogen, and its cycle differs from the other in that it does not include a gaseous phase. Phosphorous is not very mobile and does not percolate through the soil profile very easily. Phosphorous is sorbed by clays and organic matter and it is removed by erosive processes. For this reason, most of the phosphorous in the soil is not directly available for plants and it remains adsorbed by the soil. Although phosphorous plant demand is considerably less than nitrogen demand, it is necessary for several vital functions such as transfer and storage of energy. Moreover, excess of phosphorus in the water may lead to eutrophication events due to the rapid growth of algae and other organisms rich in chlorophyll. SWAT models six forms of phosphorus, which are subdivided into two main pools, mineral phosphorus and organic phosphorus (Fig. 3.8). Inorganic forms of phosphorus in SWAT are *solution*, *active*, and *stable*. Organic forms of phosphorus are *fresh*, representing the crop residue and the microbial mass, *stable*, and *active*. The major soil processes for nitrogen and phosphorus cycle represented by the SWAT model are: mineralization, decomposition and immobilization.

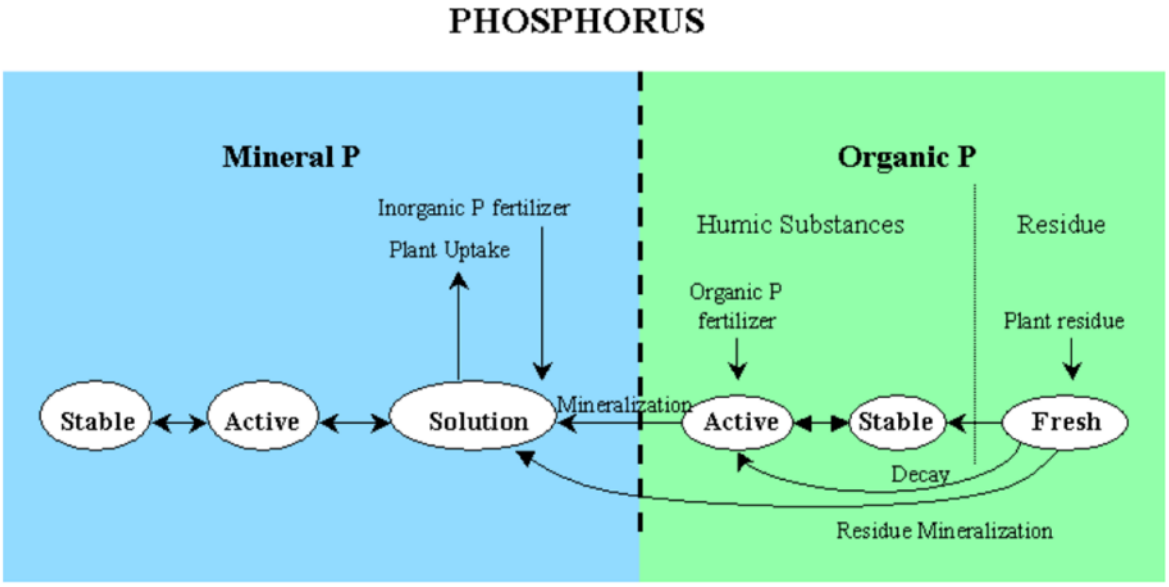

Fig. 3.8 – Soil phosphorus pool and processes simulated in SWAT (Neitsch et al. 2011).

In the "routing phase", SWAT simulates nutrient dynamics by incorporating the kinetic equations of the QUAL2E model (Brown and Barnwell 1987). SWAT model nutrients dissolved

in the stream and nutrients adsorbed to the sediment. Dissolved nutrients are transported with the water while those adsorbed to the sediment can deposit on the bed of the stream.

Agricultural management practices

The impact of agricultural management practices on water quality is very important. SWAT provide an elaborated internal model for the simulation of agricultural practices. Management practices are defined for each crop or vegetative area. For each crop, it is possible to indicate the beginning of the growing season and the harvest period. A harvest efficiency may also be defined as a fraction of harvest plant biomass removed from the HRU. The remaining fraction is converted to residue and remains in the system. Tillage operations in SWAT include the timing of the action and the type of tillage technique. Tillage is very important as it redistributes residue and nutrients in the soil profile, thus defining the fraction of residue and nutrients in each soil layer. SWAT allows for the application of inorganic fertilizers or manure to the soil. The required information includes the timing of operation, the type of fertilizer/manure applied, and the depth to which the fertilizer is applied. Finally, irrigation in SWAT may be scheduled by the user or automatically applied by the model in response to water deficit. Timing, application amount and source of irrigation have to be specified.

3.2.2 Data input for the SWAT model applied to the ZRB

The ability of SWAT to correctly represent the hydrological and water quality processes of a river basin depends on the quality and completeness of input data. In this section, the data collected and implemented for the modeling of the ZRB are described (Fig. 3.9). Table 3.2 shows the list of input data used for the construction of the SWAT model of the ZRB.

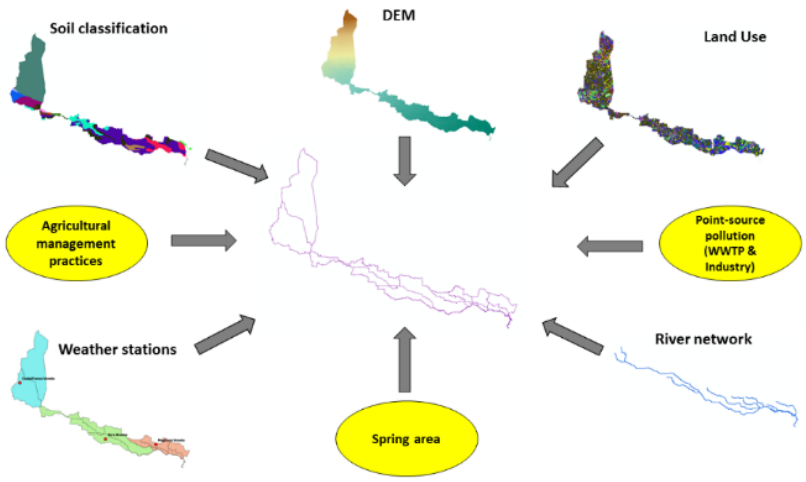

Fig. 3.9 – SWAT input data used for the modeling of the ZRB.

Table 3.2 – List of input data for the SWAT model of the ZRB.

Data type	Description	Resolution/Scale	Source
DEM	Digital Elevation model of the study area	5 meters	Regione del Veneto – Infrastruttura dati territoriali[3]
Sub-basin map	Subdivision of the Zero river basin (adapted for SWAT)	-	Salvetti et al. (2008)
River network map	Network of the main water streams of the study area (adapted for SWAT)	-	Salvetti et al. (2008)
Land Use map	Land use map of the Veneto region for the year 2007	1:10.000	Regione del Veneto – Infrastruttura dati territoriali[1]
Soil map & properties	Soil map of the Venice Lagoon Watershed for the year 2004; soil properties updated to the year 2012	1:50.000	ARPAV (2003)
Weather Data	Daily precipitation, max/min temperature, relative humidity, solar radiation, wind speed (years 2007-2012)	3 stations	ARPAV – Servizio Meteorologico
Hydrologic data	Water flow (Q) and nutrient loadings	2 stations	ARPAV – Servizio Acque Interne MAV – Magistrato Acque Venezia
Point-source pollution	WWTP and Industrial discharges	Constant value	ARPAV & Regione Veneto (2009)
Spring belt contribution	Fluxes from the spring area	Constant value	Expert opinion from ARPAV (Salvetti et al. 2008)
Agricultural management practices	Manure, fertilizer type and application rate, tillage practices, cropping seasons	-	Expert opinion from Veneto Agricoltura (Bonetto and Furlan 2012)

[3] http://idt.regione.veneto.it/app/metacatalog/

Digital Elevation Model

Topographic data are implemented into SWAT through Digital Elevation Models (DEM). For the ZRB, a 5x5 meters DEM of the Veneto Region was available from the Spatial data infrastructure of the Veneto Region website (http://idt.regione.veneto.it/app/metacatalog/). The DEM was developed by the Centro Nazionale Ricerche di Pisa (Italy). The original reference spatial system of the DEM is ROMA40/West. The DEM is presented in Fig. 3.10, and Table 3.3 provides the statistics of the topography of the ZRB.

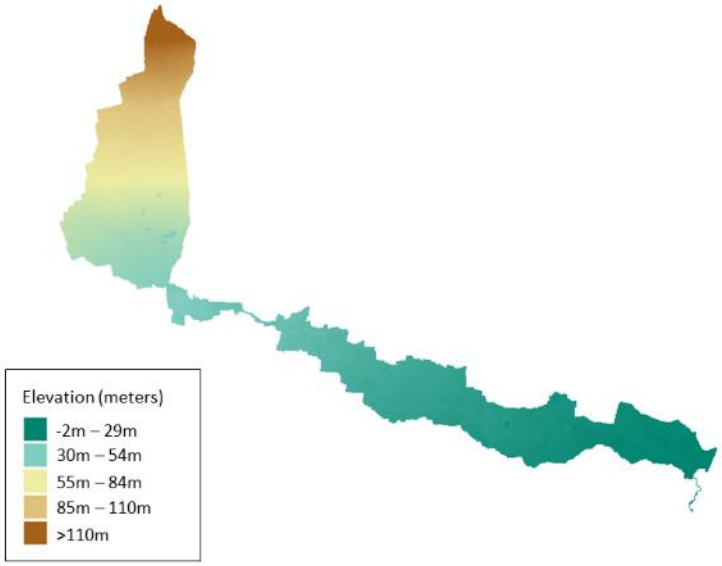

Fig. 3.10 – Digital Elevation Model (DEM) of the ZRB. Source: Regione Veneto.

Table 3.3 –Topographic data of the ZRB.

Min. Elevation	-2 m	
Max. Elevation	127 m	
Mean Elevation	35 m	
Elevation	**% Area Below Elevation**	**Absolute %**
-2m – 0 m	1.59	1.59
0m – 25m	48.49	46.9
25m – 50m	71.98	23.49

Elevation	% Area Below Elevation	Absolute %
50m – 75m	86.76	14.78
75m – 100m	96.38	9.62
100m – 125m	99.97	3.59
> 125m	100	0.03

Sub-basin and river network maps

The sub-basin and river network maps are not mandatory requirements in SWAT. However, in order to correctly represent the river network of the ZRB the maps had to be implemented into the SWAT model. This was necessary because of the flat aspect of the basin, which does not allow the software to automatically delineate the river network through the sole use of the DEM. The ZRB was subdivided into 17 sub-basins. A representation of the sub-basins and the river network is shown in Fig. 3.11.

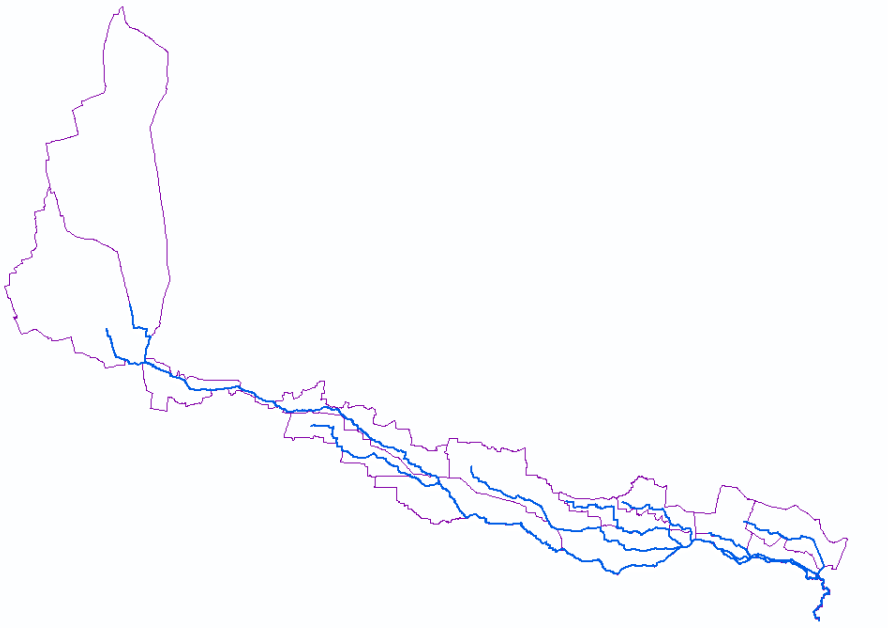

Fig. 3.11 – River network and sub-basin implemented in SWAT for the delineation of the ZRB.

Land-use

The land-use map of the ZRB is based on an adapted version of the CORINE Land Cover classification 2006 (EEA 2006). The CORINE classification is made of 44 classes organized hierarchically in three levels. The version adopted by the Veneto Region (ARPAV 2009) has two additional levels that increase the detail of the classification. The first level contains five main categories: artificial surfaces; agricultural land; forests and semi-natural areas; wetlands; water surfaces). The conversion from CORINE Land Cover to SWAT Land Cover classification was operated at the third level of detail, with the exception of the agricultural land, which was further classified into different crop cultivations. It was decided to assign the CORINE classes 2.1.1 and 2.1.2 to the SWAT class AGRL. The class AGRL was then subdivided into the classes CORN, SOYB and WWHT. The existing surface proportions between the three crops were maintained. The land-use map of the ZRB is presented in Fig. 3.12, and Table 3.4 shows the adopted conversion method between the CORINE and SWAT land-use classification systems.

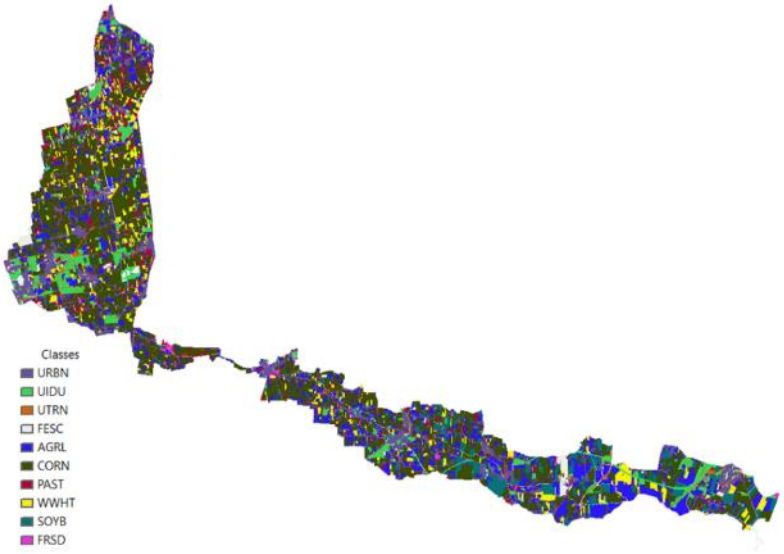

Fig. 3.12 – Land use map of the ZRB based on the SWAT nomenclature.

Table 3.4 – CORINE Land Cover and SWAT classification and correspondence adopted in this study.

CORINE Code	CORINE Nomenclature (Level 3)	SWAT Code	SWAT Nomenclature
1.1.1	Continuous urban fabric	URBN	Residential
1.1.2	Discontinuous urban fabric	URBN	Residential
1.2.1	Industrial or commercial units	UIDU	Industrial
1.2.2	Road, railways, airports	UTRN	Transportation
1.3.1	Mineral extraction sites	UIDU	Industrial
1.3.2	Dump sites	UIDU	Industrial
1.3.3	Construction sites	UIDU	Industrial
1.4.1	Green Urban Areas	FESC	Tall fescue (*Festuca arundinacea*)
1.4.2	Sport and leisure facilities	FESC	Tall fescue (*Festuca arundinacea*)
2.1.1/2.1.2	Non-irrigated/ Irrigated arable land	AGRL	Agricultural Land - Generic
2.1.2.1.1	Arable land: Corn	CORN	Corn (*Zea mays* L.)
2.1.2.1.2	Arable land: Soy	SOYB	Soy (*Glycine max* L., Merr.)
2.1.2.2.1	Arable land: Wheat	WWHT	Winter Wheat (*Triticum aestivum* L.)
2.3.1/2.3.2	Pastures	PAST	Pasture
3.1.1	Broad-level forest	FRSD	Forest Deciduous
3.2.2	Moors and heathland	FRSD	Forest Deciduous
4.1.1	Inland marshes	WETL	Wetlands
4.2.1	Peat bogs	WETL	Wetlands
5.1.1	Water courses	WATR	Water

Soil map and properties

The soil map of the ZRB was developed by ARPAV at a scale of 1:50.000. The field monitoring of ARPAV provided all the parameters required by SWAT. As a result, it was possible to create and implement into SWAT soils specific to the ZRB. The soil map of the ZRB is shown in Fig. 3.13 and the parameters required by SWAT for describing the soil profiles are explicated in Table 3.5. A more detailed description of every soil type is found in ARPAV (2004a) and in Section 2.3.1 of this dissertation .

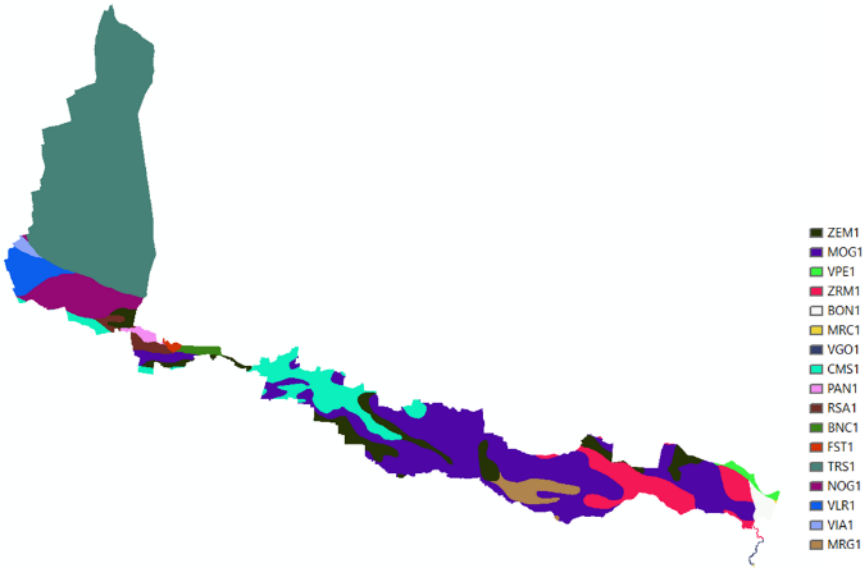

Fig. 3.13 – Soil map classification

Table 3.5 – Soil parameters required by SWAT. Data were input for every layer of every soil of the Zero river basin.

Soil Component Parameter	Description
NLAYERS	Number of layers in soil profile
HYDGRP	Soil hydrologic group
SOL_ZMX	Maximum rooting depth of soil profile (mm)
ANION_EXCL	Fraction of porosity from which anions are excluded
Soil Layer Parameter	**Description**
SOL_Z	Depth to bottom of *n* soil layer (mm)
SOL_BD	Moist bulk density of *n* soil layer (g/cm^3)
SOL_AWC	Available water capacity of *n* soil layer (mm/mm)
SOL_CBN	Organic carbon content of *n* soil layer (%)
SOL_K	Saturated hydraulic conductivity of *n* soil layer (mm/hr)
CLAY	Clay content of *n* soil layer (%)
SILT	Silt content of *n* soil layer (%)
SAND	Sand content of *n* soil layer (%)
SOL_ALB	Moist soil albedo of first soil layer
USLE_K	USLE equation soil erodibility (K) factor

Climate data

SWAT requires daily data of 5 climate parameters, listed in Table 3.6. All the meteorological parameters were provided by the ARPAV meteorological service. The data were obtained for the following weather stations: Castelfranco Veneto; Zero Branco; Mogliano Veneto; Favaro Veneto; Maser; Volpago; Treviso; Roncade; Venezia-Istituto Cavanis; Cavallino; Trebaseleghe.

However, SWAT attributes to every sub-basin only the closest weather station. As a result: only four weather station were selected: Castelfranco Veneto; Zero Branco; Mogliano Veneto; Favaro Veneto. The weather station of Favaro Veneto was not implemented into the model because it became operative in 2009, two years after the beginning of the calibration-validation period (2007-2012, Section **Errore. L'origine riferimento non è stata trovata.**). The selected weather stations are shown in Fig. 3.14.

Table 3.6 – Weather parameters requested by SWAT to describe the climate of the ZRB.

Weather parameter	Unit of measure
Minimum and Maximum Temperature	°C
Precipitation	mm
Relative Humidity	%
Solar Radiation	MJ/m^2
Wind Speed	m/s

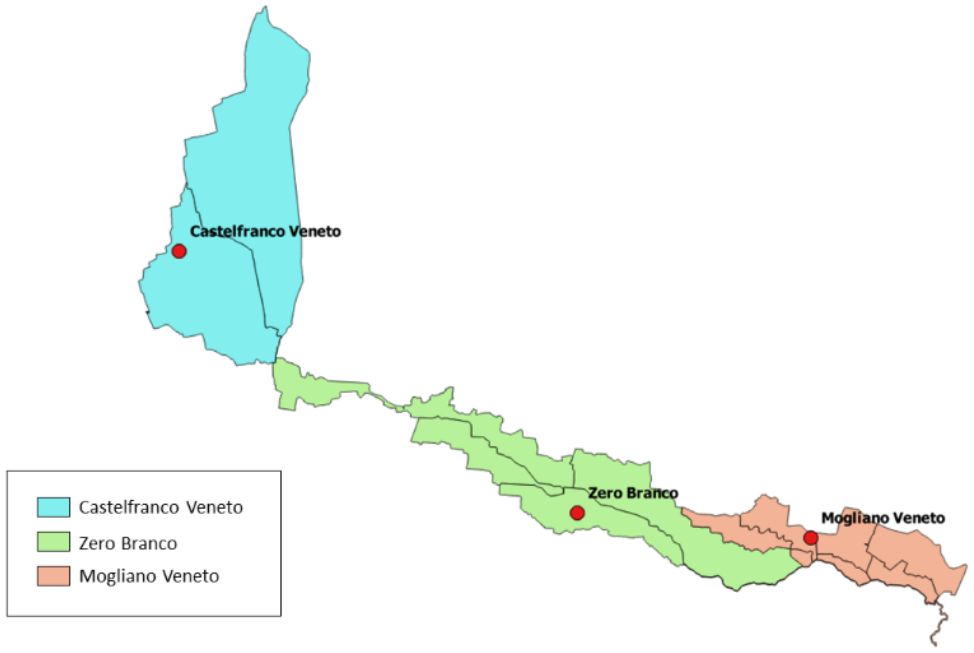

Fig. 3.14 – Weather stations representative of the ZRB and associated sub-basins.

Hydrologic and water quality data

Hydrologic data consisting of water flow (Q) of the Zero river and nutrient concentration were obtained from ARPAV – Servizio Acque Interne and the former MAV (Magistrato alle Acque di

Venezia). Adopted data refers to the hydrologic station “Mogliano”, located at the latitude 45°33’N and longitude 12°15’E. Daily discharge data from the period 2007-2012 were collected. Nutrient concentration data were obtained from 2 monitoring stations: the manual station 122, located at the same site of the hydrologic station “Mogliano”, and the automatic station 2Bi, located at the latitude 45°34’N and longitude 12°17’E. Station 122 provided seasonal data (4 measurements a year) for inorganic species of nitrogen nitrate ($N\text{-}NO_3^-$) and ammonium ($N\text{-}NH_4^+$), and phosphorus as phosphate ($P\text{-}PO_4^{3-}$). Station B2q provided daily concentration data of inorganic species of nitrate ($N\text{-}NO_3^-$) and ammonium ($N\text{-}NH_4^+$). For calibration and validation of the model, nitrogen loadings were obtained using data of the B2q station, while phosphorus loadings were obtained using data from station 122. The position of the monitoring stations is shown in Fig. 3.15.

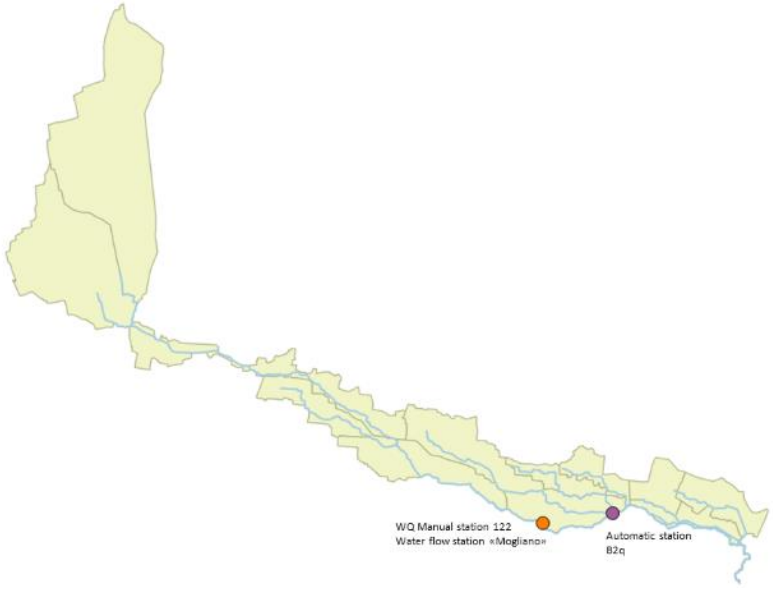

Fig. 3.15 – Position of the monitoring stations used in the study. The orange dot indicates the position of the Water Quality Manual station 122 and Water flow monitoring station “Mogliano”. The purple dot indicates the position of the Water Quality Automatic station B2q.

Contributions of point-source pollution and spring waters

The Zero river basin is not only affected by non-point source pollution from agricultural activities, but also by point-source pollution originating from wastewater treatment plants (WWTP) and industrial discharges. Due to the lack of continuous data, their influence on

nutrient loadings was assumed as constant throughout the year. The adopted values were obtained from ARPAV & Regione Veneto (2007, 2009). The loadings from WWTP and industrial sources implemented into the model are presented in Table 3.7.

Table 3.7 – Non-point source loadings of nutrients from WWTP and Industrial activities implemented into SWAT.

WWTP		Industrial loads	
N (t/year)	P (t/year)	N (t/year)	P (t/year)
23.2	2.8	3.2	0.8

For the same reason, also the influence of external spring waters on the water regime of the ZRB was assumed as constant. Values were obtained from literature review (Salvetti et al. 2008) and discussed with ARPAV experts. The selected values are presented in Table 3.8.

Table 3.8 – Influx of external spring waters implemented into the SWAT model.

Month	Mean flow (m^3/s)
January	0.4
February	0.4
March	0.4
April	0.4
May	0.4
June	0.4
July	0.1
August	0.1
September	0.4
October	0.4
November	0.4
December	0.4

Agricultural Management Practices

Agricultural management practices (e.g. planting and harvest dates, tillage methods, fertilizer applications, etc.) should be implemented into SWAT when the loadings of nutrients and their effects on water quality is the main objective of the study. Land management practices

information for the three crops (Corn, Soy, Winter Wheat) was obtained from literature (Benton Jones Jr. 2003; Giupponi et al. 2012; Tassinari 1976) and interviews with experts of Veneto Agricoltura (Bonetto and Furlan 2012; Regione Veneto 2014). Management operations and their timing are defined in Table 3.9. In this study, agricultural management practices have been considered as constant over the 21st century. See Appendix A for additional details on agricultural management practices in SWAT.

Table 3.9 – Management operations and timing of the crops implemented in SWAT. Irrigation operations were initialized by the model only in the event of water deficit.

	Corn	Soy	Winter Wheat
January			• Tillage operation • Fertilizer application (33-00-00)
February	• Tillage operation	• Tillage operation	
March	• Tillage operation • Fertilizer application (18-46-00)		
April	• Begin growing season		
May	• Fertilizer application (Urea) • Tillage operation	• Fertilizer application (Elemental P) • Begin growing season	
June			• Harvest • Tillage operation
July	• Irrigation (water def.) from external sources	• Irrigation (water def.) from external sources	
August	• Irrigation (water def.) from external sources	• Irrigation (water def.) from external sources	
September			
October	• Harvest • Manure application • Tillage operation	• Harvest • Manure application • Tillage operation	• Manure application • Tillage operation
November	• Manure application	• Manure application	• Fertilizer application (18-46-00) • Tillage operation • Begin growing season
December			

3.2.3 Implementation of SWAT

Parameterization of the model

In order to model the ZRB into SWAT it was necessary to implement the data described in Section 3.2.2. The first step consisted in the definition of the topography and river network of the ZRB. Because of its flat aspect, the GIS software was not able to define a proper delineation of the ZRB river network through the single use of the DEM. For this reason, the maps of the river network and sub-basin had to be created outside SWAT and then implemented into the model. The outlet of the basin was positioned in correspondence of the confluence point of the Zero and Dese river. The Zero river basin was subdivided into 17 sub-basins. A further discretization of the basin was obtained through the implementation of the soil map and land use map. The combinations of slope, defined by the DEM, soil, and land-use, originated the HRUs. To reduce the computational load of the simulation, it was decided to keep only the representative features of each layer (slope, soil, land use). As a result, thresholds were defined and the following classes were included in the model for every sub-basin:

1. each land use class representing over 7% of the sub-basin area;
2. each soil class representing over 15% of that land use area;
3. each slope class representing over 15% of that soil area.

At the end of this characterization procedure, the Zero river basin was subdivided into 17 sub-basins and 125 HRUs in total. This allowed a configuration representative of the physical characteristics of the area and at the same time computationally acceptable.

The third step consisted in assigning for each sub-basin a specific weather station in order to simulate the variability of the local climate along the river basin. SWAT computes this step by automatically looking at the distance between the weather station and the centroid of each sub-basin. The weather station assigned to each sub-basin is shown in Fig. 3.14. During this step observed data on max/min temperature (°C), precipitation (mm), relative humidity (%), solar radiation (MJ/m^2), and wind speed (m/s), relative to the calibration and validation period (2007-2012), were loaded into the simulation.

In the last step, point-source loadings (WWPT and industrial discharges), underground fluxes from external spring areas, and agricultural management practices were implemented into SWAT. Point-source, groundwater fluxes, and agricultural management practices are described in Section 3.2.2.

Once all the data were implemented into the model, they were overwritten into the database of the model. Finally, the simulation was run with a monthly time step for the desired period (2007-2012). It was decided to run a warm-up period of three years (2004-2006) in order to get the model to the steady state. Obtained data relative to the hydrologic and water quality parameters of the ZRB were then implemented into the software SWAT-CUP (Abbaspour 2014), a software designed to apply different sensitivity, calibration and uncertainty analysis for SWAT.

Sensitivity analysis

SWAT contains a wide number of parameters determining flow rate and nutrient processes. A sensitivity analysis was performed to determine which parameters should be selected for calibration. The identification of the most sensitive parameters allows the reduction of the number of parameters subject to calibration. In this study the "global sensitivity analysis" included in the SWAT-CUP software (Abbaspour 2014) was adopted. Through this analysis, parameter sensitivities are estimates of the average changes in the objective function resulting by allowing all the parameters to change. The major disadvantage of the global sensitivity analysis is that a large number of simulations is required (Arnold et al. 2012). A t-test is then used to identify the relative significance of each parameter in the model. The larger the value of *t* the more sensitive the parameter. The most sensitive parameters are presented in Table 3.10 – Most sensitive parameters identified in the simulation of the ZRB. Parameters regulate hydrologic processes (blue), nitrogen processes (orange), and phosphorus processes (green) and were used for the calibration of the model

Calibration and validation of the model

The calibration of the model was performed with the software SWAT-CUP. SWAT-CUP applies the Sequential Uncertainty FItting ver. 2 (SUFI-2) method, a semi-automatic calibration approach that allows the user to adjust watershed parameters between auto-calibration runs (Arnold et al. 2012). This method requires the selection of an objective function to assess the performance of the model. For this study, the Nash-Sutcliffe Efficiency Index *NSE* (Nash and Sutcliffe 1970) was selected. The NSE is defined in the Equation 3.3:

$$NSE = 1 - \left[\frac{\sum_{i=1}^{n}(S_i - O_i)^2}{\sum_{i=1}^{n}(O_i - \bar{O})^2}\right] \quad \text{Eq. 3.3}$$

where O_i and S_i correspond to the observed and simulated values at the time step I, and $\bar{O}$ is the arithmetic mean of all the observations. The optimal value of NSE is 1.0, while values below 0 indicate that mean of the observed values is a better predictor than the simulations. The use of a single objective function to assess the goodness of fit is inappropriate for assessing the predictive capabilities of the model (Legates and McCabe 1999). For this reason, also the square of the correlation coefficient r, the coefficient of determination R^2, was taken into account. A monthly calibration was performed, where flow was calibrated prior to inorganic forms of nutrients. Data for the inorganic form of phosphorus, phosphate (PO_4^{3-}), were not sufficient to perform a meaningful monthly calibration. The 2012 version of the software LOADEST (USGS 2012) was used to obtain monthly values from the daily water flow values and the sporadic values phosphorus values. The calibration of phosphorus is considered as purely indicative. Following calibration, the model was finally validated. Several difficulties in evaluating the real observed values and in comparing the model results with the monitoring observations were found in this phase. The incompleteness of time-series caused by interruptions of the monitoring stations, the location of the monitoring stations, and the different monitoring techniques, may add additional uncertainty to the model created in SWAT. Results of calibration and validation are present in Section 4.2.1 of this dissertation.

Table 3.10 – Most sensitive parameters identified in the simulation of the ZRB. Parameters regulate hydrologic processes (blue), nitrogen processes (orange), and phosphorus processes (green) and were used for the calibration of the model.

Parameter #	Symbol	Method	Value	Parameter #	Symbol	Method	Value
1	GW_DELAY	*Replace*	184.0	11	BC4	*Replace*	0.5
2	OV_N	*Absolute*	9.3	12	RS5	*Replace*	0.1
3	SOL_BD	*Relative*	0.35				
4	REVAPMN	*Replace*	208.68				
5	GW_REVAP	*Replace*	0.23				
6	ALPHA_BF	*Replace*	2				
7	CN2	*Relative*	-0.25				
8	HRU_SLP	*Replace*	0.06				
9	ERORGN	*Absolute*	8.8				
10	HLIFE_NGW	*Replace*	63				

GW_DELAY: Groundwater delay; OV_N: Manning's "n" value for overland flow; SOL_BD: Moist Bulk Density; REVAPMN: Threshold depth of water in the shallow aquifer for "revap" to occur (mm); GW_REVAP: Groundwater "revap" coefficient; ALPHA_BF: Baseflow alpha factor (days); CN2: SCS runoff curve number f; HRU_SLP: Average slope steepness; ERORGN: Organic N enrichment ratio; HLIFE_NGW: Half-life of nitrate in the shallow aquifer (days); BC4: Rate constant for mineralization of organic P to dissolved P in the reach at 20 °C; RS5: Organic phosphorus settling rate in the reach at 20 °C .

Future climate scenarios in SWAT

After performing calibration and validation of the model, daily temperature and precipitation data of future climate scenarios described in Section 3.1.2 were implemented into SWAT to observe the effects of climate change on hydrology and nutrient loadings. At this stage of the study, it was decided to not implement future projections of wind speed, relative humidity and solar radiation due to the high uncertainty in modelling their future variability at both global and local scale (Prosinger, Suhardimand, and Giordano 2015). Daily data for these parameters were automatically generated by the weather generator implemented into SWAT. Daily values were generated based on statistics of the observation period (2007-2012). Each scenario was forced by RCP 4.5 and RCP 8.5, and propagated for two time periods: a mid-term scenario (2041-2070) and a long-term scenario (2071-2100). Missing daily Temperature and Precipitation values for the year 2100 of the climate scenarios 2 and 8 (Table 3.1) were

generated by the SWAT weather generator based on the Temperature and Precipitation statistics of the long-term scenario (2071-2100). As mentioned in Section 3.2.3 “Parameterization of the model”, agricultural management practices and land-use were assumed as constant over the 21st century. Therefore, results are affect only by changes in climate conditions. Results of future scenarios of hydrology and nutrient loadings are presented in Section 4.2.2 of this dissertation.

3.3 Ecological modelling: AQUATOX

3.3.1 AQUATOX

The model AQUATOX was selected to simulate the effects of nutrients released by the ZRB on the primary producers (phytoplankton) of PDC. AQUATOX is a time continuous, process-based, ecological risk assessment model able to simulate different variables of an aquatic ecosystem. The model also represents conventional pollutants, nutrients and sediments, and considers several trophic levels, including attached and planktonic algae, submerged aquatic vegetation, several types of invertebrates, and several types of fish. It can evaluate past, present, and future ecological trends of different aquatic environments such as rivers, lakes, ponds, reservoirs and estuaries. AQUATOX was selected for the following reasons:

- it provides a tool for assessing multiple and concomitant impacts on aquatic ecosystems (i.e. climate change and nutrient pollution);
- it gives the possibility to use SWAT output as input for the model;
- it is a public domain software, freely available on the internet, which receives constant updates and support from the developers; and
- it has been extensively applied in studies on the fate and impacts of nutrients on the ecosystem (Schramm et al. 2009; Taner et al. 2011; Zouiten et al. 2013).

AQUATOX can predict the fate of chemicals in aquatic ecosystems, and their direct and indirect effects on the organisms. It can also predict the effects of non-chemical stressors such as changes in climate (e.g. water temperature), and has the potential to establish causal links between water quality and biological responses of aquatic ecosystems. AQUATOX can be used in several applications related to the management of water resources. For example, in relation to nutrients, it can be applied to develop nutrient targets for river, lakes and reservoirs affected by eutrophication events; identify which factors have a bigger influence on algal blooms; evaluate the effects of land use and climate change on the fate and effects of nutrients (Park et al. 2008). AQUATOX can simulate the transfer of biomass, energy and chemicals such as nutrients and pesticides from one compartment of the ecosystem to another. It is a mechanistic model that computes the most important chemical and biological processes at a

daily time step of the simulation period within a unit volume of water. AQUATOX can simulate both food webs and food chains with multiple trophic levels.

An ecosystem in AQUATOX is described by state variables and driving variables. State variables include nutrient concentrations, dissolved gases, organic detritus, inorganic solids, plant, and animals. Driving variables are those parameters that can force an ecosystem in a particular state. Example of driving variables in AQUATOX are temperature, nutrient input, pH, light, and freshwater inflow.

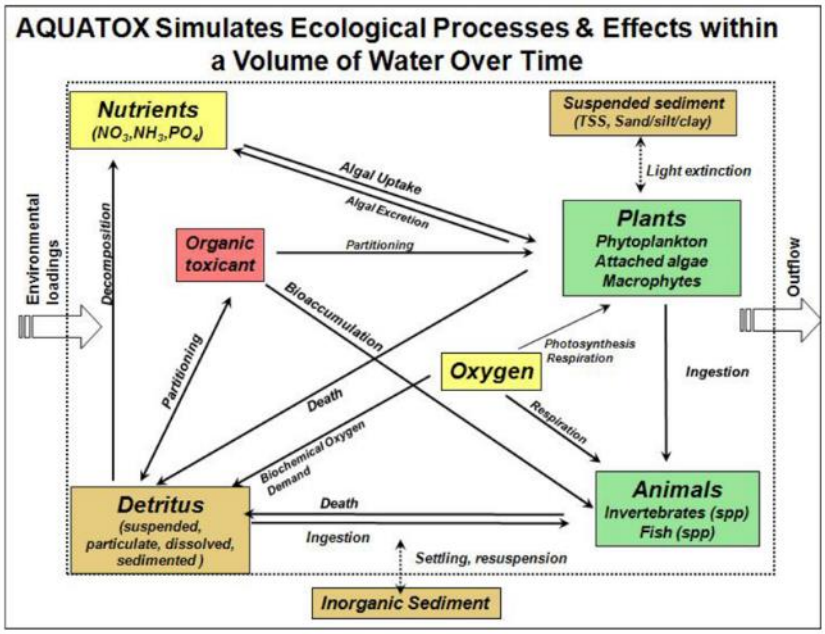

Fig. 3.16 – Biotic and abiotic state variable (boxes) and processes (arrows) simulated in AQUATOX (Park et al. 2008).

State and driving variables represent the average daily conditions of a well-mixed aquatic system. The model is run with a daily maximum time-step (which is not directly related to the temporal scale of the simulation), but numerical instability is avoided by allowing the step size of the integration to vary to achieve a predetermined accuracy in the solution. The length of simulation can be as long as several years or as short as one day. Moreover, results can be integrated to obtain the resulting time period. Results may be plotted in the AQUATOX output screen with the capability to import observed data to examine against model predictions. In this section, a description of the most important parameters for this study is provided.

Functions not implemented in this application (e.g. stream dynamics) are not described. A complete technical description of the AQUATOX model can be found in Park & Clough (2009).

Physical characteristics

Important variables that describe the physical characteristics of PDC in AQUATOX are volume, bathymetry, and retention time. Volume, a state variable, can be computed in several ways depending on the availability of data and the site dynamics. A correct definition of the volume is important for computing the dilution of nutrients and organisms such as phytoplankton and zooplankton. In AQUATOX the change in volume of a water body, except for streams, is computed as indicated in Eq. 3.4:

$$\frac{dVolume}{dt} = Inflow - Discharge - Evap \quad \text{Eq. 3.4}$$

where *dVolume/dt* describes the derivative for volume of water (m^3/d), *Inflow* the inflow of water into the waterbody (m^3/d), *Discharge* the discharge of water from the waterbody (m^3/d), and *Evap* the evaporation (m^3/d). AQUATOX gives several options for computing the volume, including constant volume, dynamic volume (function of inflow, discharge, and evaporation), and time-series of known values. Table 3.11 indicates the necessary input for each of these options.

Table 3.11 – Computation of Volume, Inflow, and Discharge in AQUATOX.

Method	Inflow	Discharge
Constant	InflowLoad	InflowLoad - Evap
Dynamic	InflowLoad	DischargeLoad
Known values	InflowLoad	InflowLoad – Evap + (State – KnownVals) / dt

InflowLoad: user-supplied inflow loading (m^3/d); *DischargeLoad*: user-supplied discharge loading (m^3/d); *State:* computed state variable value for volume (m^3); *KnownVals*: time series of known values of volume (m^3); *dt*: incremental time in simulation (d).

The depth profile of a water body determines the mixing and light penetration of a water body. AQUATOX normally uses an assumption of unchanging mean depth. The shapes of water

bodies in AQUATOX are represented in the model by idealized geometrical approximations, following the topological treatment of Junge (1966), indicated in Eq. 3.5:

$$P = 6.0 \cdot \frac{ZMean}{ZMax} - 3.0 \qquad \text{Eq. 3.5}$$

where *ZMean* is the mean depth (m), *ZMax* the maximum depth (m), and *P* is the shape parameter that characterizes the shape of the site (constrained between -1.0 and 1.0). AQUATOX allows user to model a simpler system, where the bathymetric approximations may be bypassed in favor of a more rudimentary set of assumptions via an option in the software. Retention time is a measure expressing the mean time that water spends in a water body. AQUATOX calculates water retention time as indicated in Eq. 3.6:

$$Retention = \frac{Volume}{TotDischarge} \qquad \text{Eq. 3.6}$$

where *Retention* is the retention time (d), *Volume* the volume of the water body (m^3), and *Discharge* is the discharge of water from the water body (m^3/d).

Climate

In AQUATOX climate is described by water temperature, wind and solar radiation. Water temperature controls several factors in the model such as decomposition, photosynthesis, consumption, respiration, reproduction, and mortality. AQUATOX gives the user different options for computing temperature, including constant temperature, dynamic temperature and time-series of known values. Dynamic water temperature is represented through a sine approximation for seasonal variations (Ward 1963) based on observed means and ranges of variability, as indicated in Eq. 3.7:

$$Temperature = TempMean + \left(-1.0 \cdot \frac{TempRange}{2} \cdot \sin\left(0.0174533 \cdot (0.987 \cdot (Day + PhaseShift) - 30)\right)\right)) \qquad \text{Eq. 3.7}$$

where *Temperature* is the average daily water temperature (°C), *TempMean* is the mean annual temperature (°C), *TempRange* is the annual temperature range (°C), *Day* is the day of the year (d), and *PhaseShift* is the time-lag in heating (=90d).

Wind in AQUATOX determines the stability of blooms of nitrogen-fixing cyanobacteria, affects air-water oxygen exchange, and controls volatilization of organic chemicals. If measured data are not available, AQUATOX gives users the possibility to represent wind speed through a Fourier series of sine and cosine terms (dynamic loading), as indicated in Eq. 3.8:

$$Wind = CosCoeff_0 + \Sigma\left(CosCoeff_n \cdot \mathrm{Cos}\left(\frac{Freq_n \cdot 2\pi \cdot Day}{365} \right) + \mathrm{SinCoeff}_0 \cdot \mathrm{Sin}\left(\frac{Freq_n \cdot 2\pi \cdot Day}{365} \right) \right) \quad \text{Eq. 3.8}$$

where *Wind* is wind speed (m/s), $CosCoeff_0$ is the cosine coefficient for the 0-order harmonic (=3 m/s), $CosCoeff_n$ is the cosine coefficient for the n^{th}-order harmonic, *Day* is the day of the year (d), $SinCoeff_n$ is the sine coefficient for the n^{th}-order harmonic, and $Freq_n$ is the selected frequency for the n^{th}-order harmonic. This default wind dynamic has a 365-day repeat, representative of seasonal variations in wind. The mean and twelve additional harmonics seem to effectively capture the variation of wind. This approach is useful because the user must specify only the mean, while wind variability is imposed by the function.

Solar radiation in AQUATOX controls factors for the photosynthesis of primary producers. The default solar radiation function formulated for AQUATOX is a variation on the temperature equation (Eq. 3.7), but without the lag term, as indicated in Eq. 3.9:

$$Solar = LightMean + \frac{LightRange}{2} \cdot \sin(0.0174533 \cdot Day - 1.76) \cdot Frac_{Light} \quad \text{Eq. 3.9}$$

where *Solar* is average daily incident light intensity (ly/d), *LightMean* is mean annual light intensity (ly/d), *LightRange* is annual range in light intensity (ly/d), *Day* is day of the year (d), $Frac_{Light}$ is fraction of site that is shaded. The derived values are given as average light intensity in Langleys per day (Ly/d = 10 kcal/m2·d). An observed time-series of light also can be supplied by the user.

Detritus

In AQUATOX, detritus (all non-living organic material and associated decomposers, bacteria and fungi) is divided into two categories: labile and refractory. Detritus is modeled as eight compartments: refractory (resistant) dissolved, suspended, sedimented, and buried detritus; and labile (readily decomposed) dissolved, suspended, sedimented, and buried detritus (Fig. 3.17).

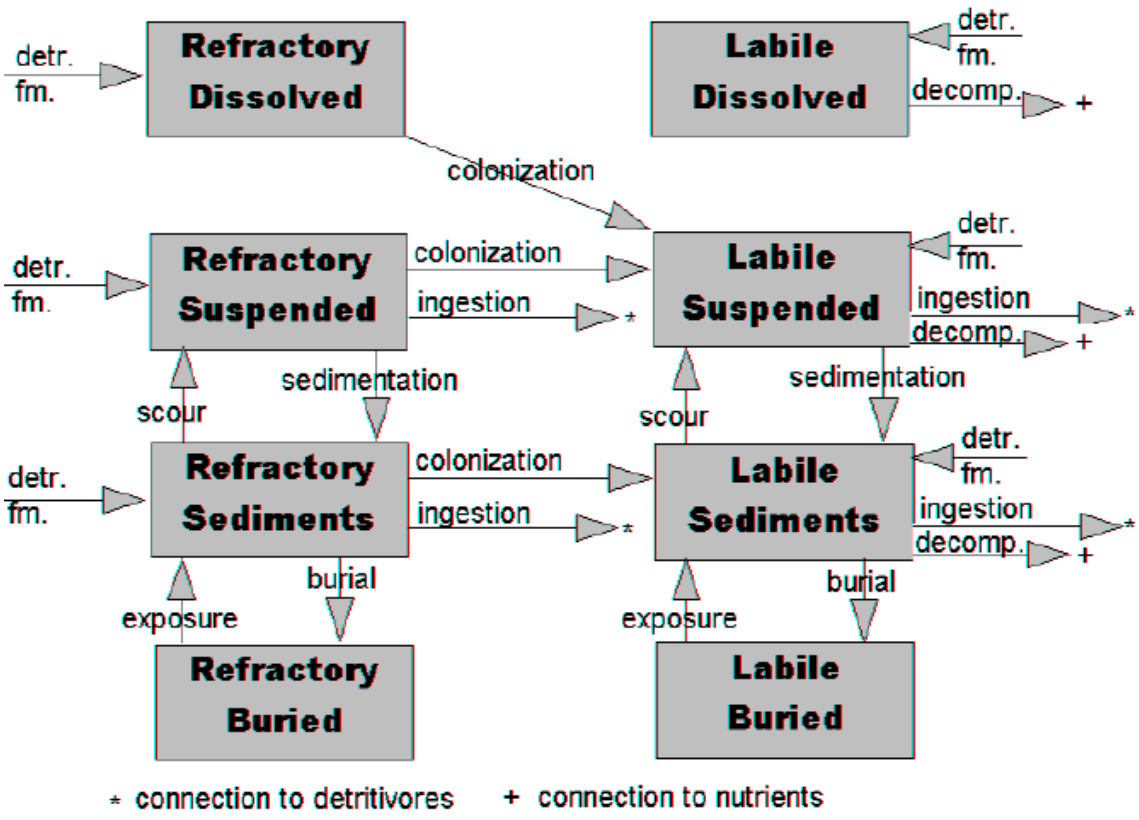

Fig. 3.17 – Detritus compartments in AQUATOX.

Nutrient Cycle

AQUATOX models the cycles of nitrogen and phosphorus in the water column. Two nitrogen compartments, total ammonia (NH_3 + NH_4^+) and nitrate (NO_3^-) are modeled. Nitrite occurs in very low concentrations and is rapidly transformed through nitrification and denitrification, therefore, it is modeled with nitrate. In the basic version of AQUATOX, inorganic nitrogen in the sediment bed is ignored, but organic nitrogen is modeled as component of the sedimented detritus. AQUATOX can model several processes of the nitrogen cycle: remineralization, which includes all the necessary processes to convert organic nitrogen in ammonia; nitrification, which converts ammonia to nitrite and then to nitrate by nitrifying bacteria both at the sediment-water interface and in the water column; denitrification, the anaerobic process that converts nitrate and nitrite to free nitrogen; and ionization of ammonia. In the water column, ammonia is assimilated by algae and macrophytes and is converted to nitrate as a result of nitrification. Nitrate is assimilated by plants and is converted to free nitrogen (and lost) through denitrification. Free nitrogen can be fixed by cyanobacteria. Nitrogen processes are subject to several environmental conditions and are difficult to model with accuracy; therefore, the nitrogen cycle in AQUATOX is represented with considerable uncertainty. The nitrogen cycle in AQUATOX is represent in Fig. 3.18.

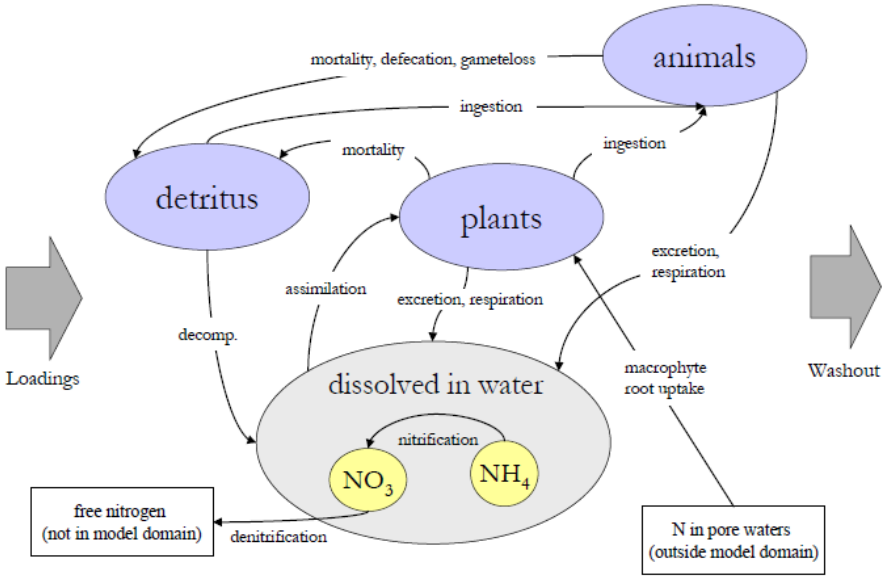

Fig. 3.18 – Nitrogen cycle in AQUATOX.

The phosphorus cycle is simpler than the nitrogen cycle. AQUATOX models only phosphate available for plants. AQUATOX models the remineralization of phosphorus, which includes the processes to convert organic phosphorus in phosphate (PO_4^{3-}). The basic version of AQUATOX does not model fluxes of phosphate from the sediment pore waters to the water column. The nitrogen cycle in AQUATOX is represent in Fig. 3.19.

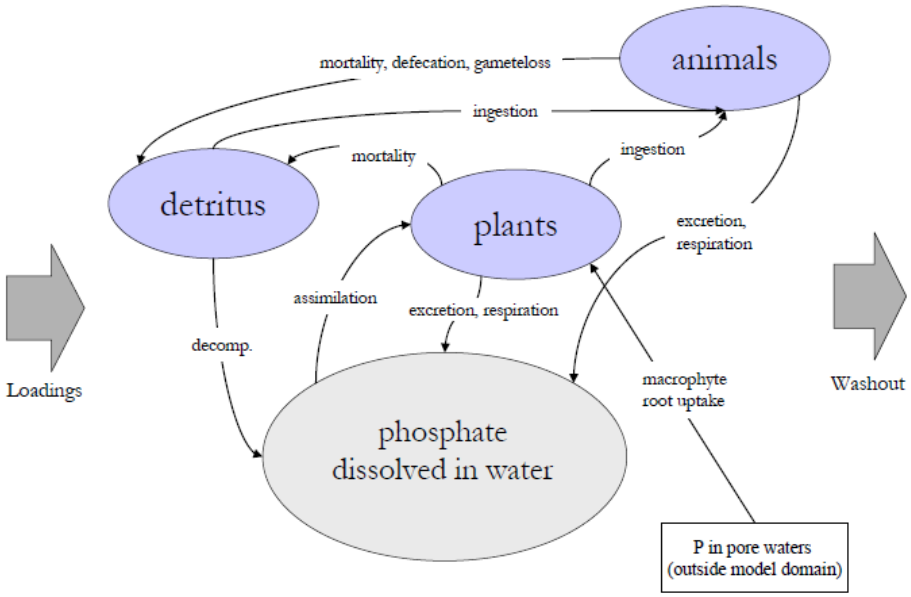

Fig. 3.19 – Phosphorus cycle in AQUATOX.

Phytoplankton

The change in phytoplankton biomass (g/m^3) is function of photosynthesis, respiration, photorespiration, non-predatory mortality, predatory mortality, sinking, sloughing and washout. If the water body is stratified, turbulent diffusion also affects the biomass of phytoplankton. The equation that models the change in phytoplankton is illustrated here below (Eq. 3.10):

$$\frac{dBiomassPhyto}{dt} = Loading + Photosynthesis - Respiration - Photorespiration - Mortality - Predation \pm Sinking \pm Floating - Washout + Washin \pm TurbDiff + \frac{Slough}{3} \qquad \text{Eq. 3.10}$$

where *dBiomass/dt* is the change in biomass of phytoplankton with respect to time (g/m^3·d), *Loading* is the external loading of phytoplankton into the system (g/m^3·d), *Photosynthesis* is the rate of photosynthesis (g/m^3·d), *Respiration* is the respiratory loss (g/m^3·d), *Photorespiration* is the release of photosynthate (dissolved organic material) that occurs in the presence of light (g/m^3·d), *Mortality* is the nonpredatory mortality (g/m^3·d), *Predation* is the predatory mortality (g/m^3·d), *Washout* is the loss due to being carried out of the system (g/m^3·d), *Washin* is the gain from upstream waterbodies (g/m^3·d), *Sinking* is the loss or gain due to sinking between layers of the water body (in case of stratified system) and sedimentation to bottom (g/m^3·d), *Floating* is the loss from the hypolimnion or gain to the epilimnion due to the floatation of "surface-floating" phytoplankton (g/m^3·d), *TurbDiff* is turbulent diffusion (g/m^3·d), *Slough* is the addition to phytoplankton from the scour loss of periphyton (g/m^3·d).

Photosynthesis is modeled as a maximum observed rate multiplied by reduction factors for the effects of toxicants (salinity), habitat, and suboptimal light, temperature, current, and nutrients. The equation that models photosynthesis is illustrated here below (Eq. 3.11 and 3.12):

$$Photosynthesis = PMax \cdot PProdLimit \cdot Biomass \cdot SaltEffect \quad \text{Eq. 3.11}$$

$$PProdLimit = LtLimit \cdot NutrLimit \cdot TCorr \quad \text{Eq. 3.12}$$

where *PMax* is the maximum photosynthetic rate (1/d), *PProdLimit* is the limitation of primary production (Eq. 3.12), *Biomass* is the total biomass of phytoplankton in the system (g/m^3), *SaltEffect* is the effect of salinity of photosynthesis, *LtLimit* is the light limitation (unitless), *NutrLimit* is the nutrient limitation (unitless), and *TCorr* is the limitation due to suboptimal temperature (unitless).

Light is an important limiting variable for phytoplankton. Light limitation in AQUATOX is based on the Steele formulation for light limitation, which is represent by Eq. 3.13:

$$LtLimit = 0.85 \cdot \frac{e \cdot Photoperiod \cdot (LtAtDepth - LtAtTop) \cdot PeriphytExt}{Extinct \cdot (DepthBottom - DepthTop)} \qquad \text{Eq. 3.13}$$

where *LtLimit* is the light limitation (unitless), *e* is the base of natural logarithms (2.71828), *Photoperiod* is the fraction of the day with daylight (unitless), *Extinct* is the total light extinction (1/m), *DepthBottom* is the maximum depth or depth of bottom (m), *DepthTop* si the depth of top of layer (m), *LtAtDepth* is the limitation due to insufficient light (unitless), *LtAtTop* is the limitation of algal growth due to light, and *PeriphytExt* is the extinction due to periphyton (only affects periphyton and macrophytes, unitless).

Nutrient limitation in AQUATOX is modeled, for each individual nutrient, using the Michaelis-Menten equation:

$$PLimit = \frac{Phosphorus}{Phosphorus + KP} \qquad \text{Eq. 3.14}$$

$$NLimit = \frac{Nitrogen}{Nitrogen + KN} \qquad \text{Eq. 3.15}$$

$$CLimit = \frac{Carbon}{Carbon + KCO2} \qquad \text{Eq. 3.16}$$

where *PLimit* is the limitation due to phosphorus (unitless), *Phosphorus* is the available soluble phosphorus (gP/m^3), *KP* is the half-saturation constant for phosphorus (gP/m^3), *NLimit* is the limitation due to nitrogen (unitless), *Nitrogen* is the available soluble nitrogen (gN/m^3), *KN* is the half-saturation constant for nitrogen (gN/m^3), *CLimit* is the limitation due to inorganic carbon (unitless), *Carbon* is the available dissolved inorganic carbon (gC/m^3), *KCO2* is the half-saturation constant for carbon (gC/m^3). The Michaelis-Menten equation is evaluated for each nutrient, and the factor for the nutrient that is most limiting (minimum limiting nutrient) at a particular time is used. The overall nutrient limitation in AQUATOX is calculated as follows (Eq. 3.17):

$$NutrLimit = \min(PLimit, NLimit, CLimit) \qquad \text{Eq. 3.17}$$

where *NutrLimit* is the reduction due to the limiting nutrient (unitless).

Because Chlorphyll-a (Chl-a) is commonly used as an index of water quality, AQUATOX converts phytoplankton biomass into approximate values for Chl-a. The ratio of carbon to Chl-a (C:Chl-a) exhibits a wide range of values depending on the nutrient status of the algae (Harris 1986). AQUATOX adopts values of 45 µgC/µgChl-a.

3.3.2 Data input for the AQUATOX model applied to PDC

AQUATOX requires a series of inputs for describing the abiotic and biotic state of the system. In this section, the data collected and implemented into AQUATOX to simulate PDC are described. Time-series from the SWAT model of the ZRB (i.e. freshwater discharge, nutrient loadings) and monitored observations (e.g. water temperature) were implemented into AQUATOX at a monthly time-step. The list of data implemented in the model is presented in Table 3.12.

Table 3.12 – Summary of principal AQUATOX required input data for the modelling of PDC.

Required Input		Source
Morphology	Length, Average width, Average Depth, Maximum Depth	Guerzoni & Tagliapietra (2006)
Hydrology	Inflows and outflows of water, Water volume, Evaporation	SWAT model; Zuliani et al. (2005)
Climate	Latitude, Wind, Light, Water Temperature	ARPAV – Servizio Meteorologico
Water physico-chemical properties	pH, DIC, Nutrients, Detritus, Inorganic solids	SAMANET; MELa project
Biota	Time-varying biomasses of phytoplankton (chlorophyll a)	SAMANET and scientific literature (Comaschi et al. 1995; Comatti et al. 2006).

Morphology

Implementing correct data of the morphology of the area is necessary for simulating the hydrology of the system. Necessary data, mean depth (*Zmean* in Eq. 3.5) and max depth (*Zmax* in Eq. 3.5) were computed from bathymetry maps of the lagoon of Venice for the year 2002 (Guerzoni and Tagliapietra 2006) using the GIS software ARCGIS. Delimitation of the surface of PDC was defined assuming the lagoon channels and the salt-marshes contouring PDC as the borders of the water body. No data were available for site length, and surface area, so they were calculated using the GIS software ArcGIS.

Hydrology

Freshwater loadings (*Inflow* in Eq. 3.4) were obtained from the SWAT application of the ZRB. No data were available for the volume of PDC. Therefore, volume was calculated as follows (Eq. 3.18):

$$Volume = Surface \cdot MeanDepth \qquad \text{Eq. 3.18}$$

Surface (m^2) and mean depth (m) were computed from geographic and bathymetry maps (Guerzoni and Tagliapietra 2006) using the GIS software ArcGIS.

Climate

Average latitude of PDC was computed using the GIS software ArcGIS by calculating the latitude at its centroid. Time series of both variables were obtained from the weather station "Venezia – Istituto Cavanis" provided by ARPAV for the period 2007-2012**.** Water temperature is at the basis of several processes in AQUATOX. Daily time series of water temperature were obtained from the station Ve-7 of the SAMANET monitoring network.

Water physico-chemical properties

The use of site-specific physico-chemical parameters allows to simulate biotic and abiotic processes correctly. Values of pH and Total Organic Carbon (TOC) were obtained from the station 1-B of the MELa project. Dissolved inorganic carbon (DIC) values were computed using the software CO_2SYS (Robbins et al. 2010), by using values of alkalinity, pH and atmospheric CO_2 provided by the monitoring station VE-1B (MELa project) over the period 2007-2009. Daily values of salinity were obtained from the monitoring station Ve-7 SAMANET monitoring station Ve-7. In AQUATOX, two nitrogen compartments, ammonia and nitrate, are modeled, while phosphorus is present in the system as phosphate (PO_4^{3-}). Dynamic inflow loadings of NH_4^+, NO_3^-, and PO_4^{3-} were obtained from the SWAT model of the ZRB. Seasonal values of nutrients for the period 2007-2009 were used to evaluate the performance of the model and were obtained from the monitoring station Ve-1B of the MELa project. Turbidity caused by suspended solids affects light penetration and photosynthesis processes. As turbidity is an important factor in marsh environments it was decided to implement inorganic sediment

concentrations into the model. Average values of turbidity were obtained from Guerzoni & Tagliapietra (2006).

Biota

Observed data of phytoplankton were retrieved from SAMANET, station Ve-7. The parameter chlorophyll-a (Chl-a) was analysed as a proxy for phytoplankton, as explained in Section 3.3.1. Phytoplankton composition of the Venice lagoon was obtained from scientific literature (Facca et al. 2004). Zooplankton was implemented in the simulation as a predator of phytoplankton in order to regulate its dynamics and avoid exponential growth. Its average concentration values to evaluate model performance were obtained from Comaschi et al. (1995) and Comatti et al. (2006).

3.3.3 Implementation of AQUATOX

Parameterization of the model

This section of the dissertation describes the parameterization of the AQUATOX model of PDC. To parameterize the model, AQUATOX provides a "wizard" that allows to the user to insert initial condition values and time-series for the simulation period for each state and driving variable. This section follows the steps suggested by the wizard of the software.

Simulation type: The environment of PDC was simulated in AQUATOX with the simulation type "Reservoir". AQUATOX integrates an "estuary" sub-model, which was not implemented in the study as it was decided to not consider the effects of the tide in the system. The fundamental reason behind this choice was that the "estuary" sub-model, considered as exploratory by the developers (Park and Clough 2009), was not able to model the complex hydrodynamics of the lagoon of Venice. Therefore, in order to avoid introducing further complexity and uncertainty in the system, the "estuary" sub-model was discarded.

Simulation time period: the system was run for 6 years (2007-2012) with a warm-up period of two years (2005-2006).

Nutrients: initial concentrations of nutrients were input into the model. The values obtained from the measurement performed in the MELa project were used. The averages of the measurements of January for the year 2007-2009 were selected. The following concentrations have been used:

- $N\text{-}NH_4^+$: 0.16 mg/l
- $N\text{-}NO_3^-$: 0.90 mg/l
- $P\text{-}PO_4^{3-}$: 0.03 mg/l
- DIC: 133.25 mg/l
- O_2: 10.45 mg/l

AQUATOX does not simulate silica (Si), and therefore it was not possible to parameterize this aspect. This adds further uncertainty to the results of the study, as Si is required by diatoms, the dominant group in the phytoplankton of PDC.

Detritus in sediment bed and in water column: as no information was available for detritus in sediment bed, both initial conditions were set to 0. The warm-up period was used to bring the system to the steady-state. Initial values of detritus in the water column were obtained from values of total organic carbon (TOC) available from the MELa1 project. The average of the measurements of January for the years 2007-2009 was selected as initial condition for the variable. Initial conditions of TOC were set as 3.0 mg/l. AQUATOX automatically transformed TOC values in organic matter (mg/l).

Phytoplankton: nine phytoplankton compartments were added to represent the possible evolutions of phytoplankton biomass and composition in present and future conditions. It was decided to implement only the species of phytoplankton of the lagoon of Venice that are already present in the AQUATOX database. Phytoplankton implemented in the system belongs to two main-groups: diatoms (D) and cyanobacteria (CB). Initial concentrations were set to 0 mg/l for each species, and the warm-up period was used to bring the species to equilibrium. Moreover, AQUATOX uses “seeds” of phytoplankton, very small concentrations (1E-05 mg/l dry) that are added into the system on a daily basis for preventing the extinction of the species.

Table 3.13 indicates the species of phytoplankton added to the system of PDC in AQUATOX. See Appendix B for details on phytoplankton in AQUATOX.

Table 3.13 – Phytoplankton compartments added to the system.

N.	Species	Optimal T (°C)	N Half-sat K	P Half-sat K
D1	*Navicula ssp.*	15	0.01	0.002
D2	*Cyclotella nana*	20	0.011	0.017
D3	*Cyclotella nana* (High nutrient waters)	20	0.117	0.055
D4	*Fragilaria spp.* (low nutrient waters)	26	0.0154	0.001
D5	*Cyclotella nana* (warm waters)	25	0.011	0.017
D6	Cyclotella nana (extremely warm waters)	30	0.011	0.017
D7	*Cyclotella spp.* (high nutrient and warm waters)	25	0.117	0.055
D8	*Fragilaria spp.* (high nutrient and cold waters)	8	0.117	0.05
CB1	*Microcystis spp*.	30	0.4	0.03

Zooplankton: the species *Acartia clausi* was selected as representative of zooplankton in PDC. Initial concentrations were set to 0 mg/l, and the warm-up period was used to bring the species to equilibrium. Moreover, AQUATOX uses "seeds" of zooplankton, very small concentrations (1E-05 mg/l dry) that are added into the system on a daily basis for preventing the extinction of the species. Table 3.13 indicates the species of phytoplankton added to the system of PDC in AQUATOX.

Table 3.14 - Zooplankton compartments added to the system.

N.	Species	Optimal T (°C)	Maximum Consumption (g/g · d)	Half-saturation feeding (mg/l)
Z1	*Acartia Clausi*	20-25	2.5	2

Site characteristics: Site length and width values were set at 4.5 km and 0.8 km. Surface area was set at 3.6 km^2. Mean depth and Maximum depth were set respectively at 0.8 m and 3 m. Evaporation was assumed as in balance with direct precipitation over the lagoon. As the two

variables tend to cancel each other out (Zirino et al. 2014), evaporation in the model was set constant to the value of 0 inches/year. The latitude was set at 45°3'N.

Water volume data: the water volume of PDC was assumed as constant ($3.8x10^6$ m^3). The effects of seepage of underground water from the watershed was described by increasing the flowrate of freshwater from the ZRB by a multiplicative factor of 1.5. This multiplicative factor was implemented to obtain an acceptable water retention time in PDC. A mean retention time of 15 days was considered as acceptable for the area of PDC (Cucco and Umgiesser 2006).

Water temperature: temperature was computed in AQUATOX as observed time-series. Daily measurements obtained from the SAMANET monitoring network, VE-7 station, were implemented into AQUATOX. Statistics show a mean water temperature of 16°C, and maximum and minimum values of, respectively, 28°C and 3°C.

Wind loading: wind was computed in AQUATOX as dynamic loading (Section 3.3.1, *Climate*) despite the availability of wind speed time-series from the weather station "Venezia – Istituto Cavanis". The rationale behind this choice is that, in this study, wind statistics were not considered as changing over the 21st century in this study. As a result, no wind projections were available. Through the dynamic loading options, AQUATOX computed a 365-day wind speed time-series from the mean value over the period 2007-2012, which was set at 1.5 m/s. The value was obtained from the time series of the weather station "Venezia – Istituto Cavanis". Statistics obtained with the dynamic loading method show a mean value of 1.5 m/s, a maximum of 6.5 m/s and a minimum of 0 m/s.

Light loading: light was computed in AQUATOX as dynamic loading (Section 3.3.1, *Climate*). The rationale supporting this choice is that, in this study, solar radiation statistics were considered as constant throughout the 21st century. As a result, no solar radiation projections were available. Average annual light intensity and annual range light intensity were calculated from solar radiation time series obtained from the weather station "Venezia – Istituto Cavanis" for the period 2007-2012. Their value was set respectively to 332 Ly/day and 559 Ly/day. With these values AQUATOX automatically calculated mean daily value of solar radiation.

pH of water: the pH of PDC is characterised by low variability. For this reason, it was decided to use a constant value into AQUATOX for both present and future time periods. The value was obtained from the monitoring data of the MELa project. A pH value of 7.9 was chosen and it was obtained from the average of available data of the MELa monitoring for the years 2001-2003.

Salinity: salinity is an important factor in PDC, as it is strongly influenced by the influx of freshwater from the watersheds of the Zero and Dese rivers. As a result, daily salinity variations are significant, featuring maximum daily values over 30 ppt and minimum values below 10 ppt. Daily values of salinity were obtained from the SAMANET monitoring station VE-7, and implemented into AQUATOX as monthly averages, as the study focuses on the long-term effects of climate change.

Inorganic sediments: it was decided to implement inorganic sediment concentrations into the model as a constant. AQUATOX can calculate inorganic solids from total suspended sediments (TSS) and organic carbon values. The constant value of TSS was set at 6.5 mg/l.

Non-point source loadings: nutrient loadings obtained with SWAT were implemented into AQUATOX for the period 2007-2012.

Evaluation of model performance

After parameterization, the model performance was evaluated. Developers of AQUATOX do not suggest the adoptions of stringent goodness of fit measures (Park and Clough 2009). As a result, a weight-of-the evidence approach was suggested to measure the appropriateness of the model. First, it was assessed if the model was behaving reasonably. Second, data have been visually inspected by comparing the model plots with the observation points. Third, the overlap between data and model distribution based on relative bias (rB) and variance (F) was performed. Relative bias indicates the correspondence of central tendencies, where rB=0 implies the same mean. The variance ratio or F test (F), describes the similarities in variability between modeled and observed data. Accordingly, F=1 indicates that the variability of the two datasets are the same. Test results with rB close to 0 and F close to 1 indicate models with

good fitness to observed data (Fig. 3.20). The equations to calculate rB and F are illustrated by Eq. 3.19 and Eq. 20:

$$rB = \frac{(\overline{Mod} - \overline{Obs})}{S_{obs}} \qquad \text{Eq. 3.19}$$

$$F = \frac{S^2_{Mod}}{S^2_{Obs}} \qquad \text{Eq. 3.20}$$

where *rB* is relative bias, $\overline{Mod}$ is the mean of predicted (modeled) results, $\overline{Obs}$ is the mean of measured observations, S_{obs} is the standard deviation of observations, *F* is the F test, S^2_{Mod} is the variance of predicted results, and S^2_{Obs} is the variance of monitored observations. Results of the model performance are presented in Section 4.3.1 of this dissertation.

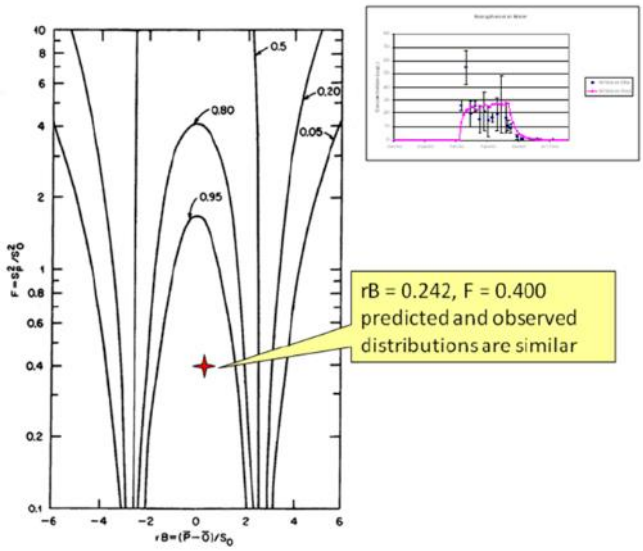

Fig. 3.20 – Relative bias and F test to compare means and variances of observed data and predicted results with AQUATOX. Isopleths indicate the probability that the predicted and observed distributions are the same, assuming normality. (Park and Clough 2009).

Future climate scenarios in AQUATOX

After assessing model performance, nutrient loadings from the SWAT model of the ZRB for each climate scenario were implemented into AQUATOX. Climate scenarios did not provide values for water temperature, salinity, and DIC, which are required by AQUATOX to simulate

PDC. For this reason, they were computed indirectly through regression equations. The air temperature measured by the weather station "Mogliano" (ARPAV – Servizio Meteorologico) and the water temperature measured by the station Ve-7 (SAMANET) for the period 2007-2012 were analysed and a relation among monthly means was drawn. As a result, the linear regression equation y = 1.0462x + 1.5382 (R^2 = 0.99) was computed to predict water temperature in PDC from projected air temperature of Mogliano for each climate scenario (Fig. 3.21).

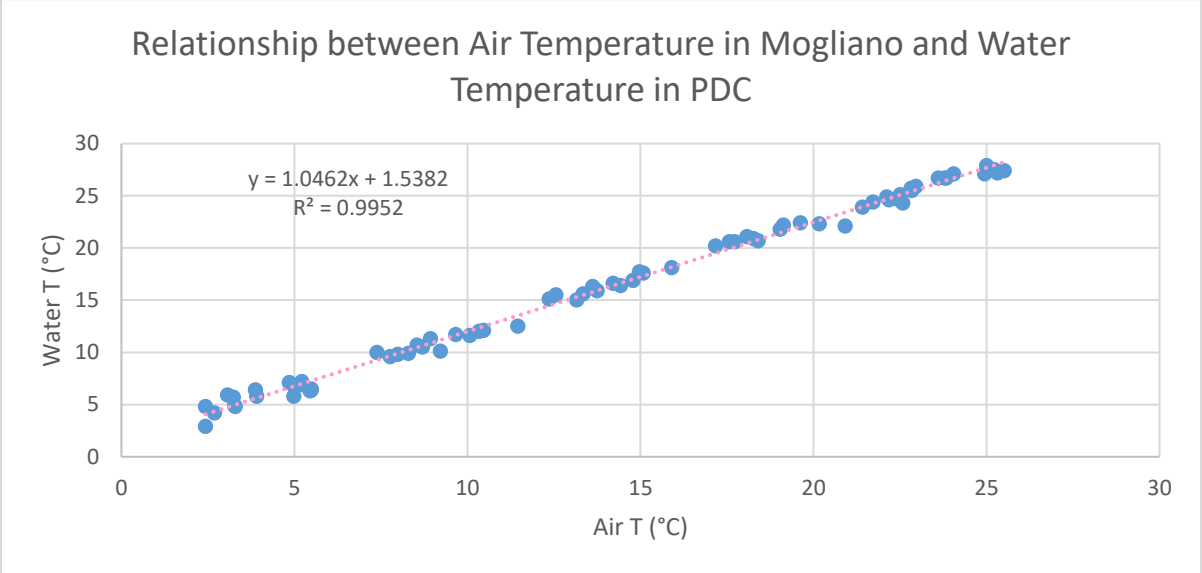

Fig. 3.21 – Relationship between Air Temperature in Mogliano (ARPAV – Servizio Meteorologico) and Water Temperature in PDC (SAMANET).

Water temperature increases notably in the future projections. In the mid-term period, temperatures are on average 2-3°C higher than the control period in both RCP4.5 and RCP8.5 (Fig. 3.22). For the long-term period, differences between the control period and RCP8.5 increase, with differences of 5 to 7 °C over the year (Fig. 3.23).

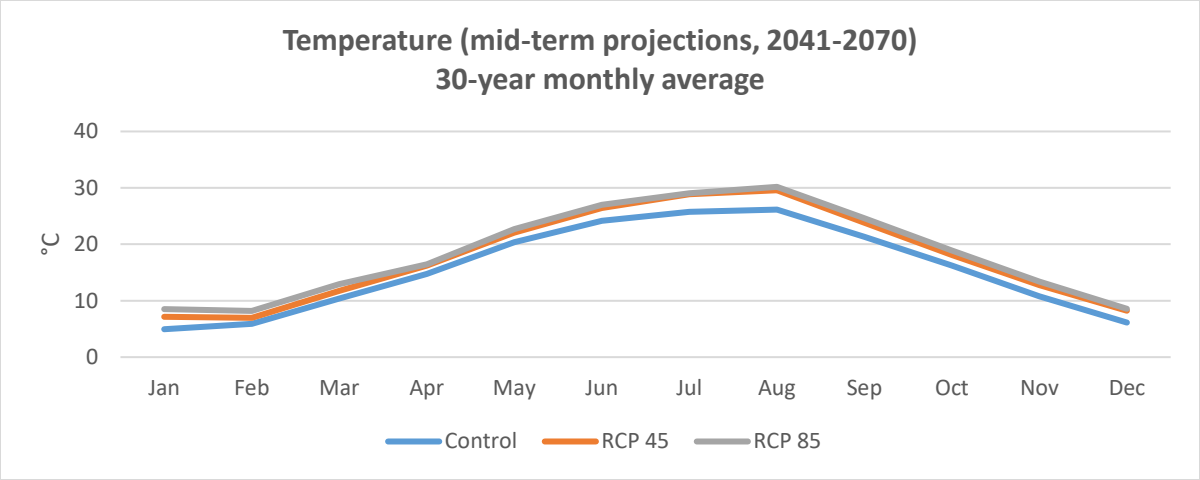

Fig. 3.22 – Differences in the 30-year monthly temperature between the control period (1983-2012) and mid-term projections (2041-2070) of RCP4.5 and RCP 8.5.

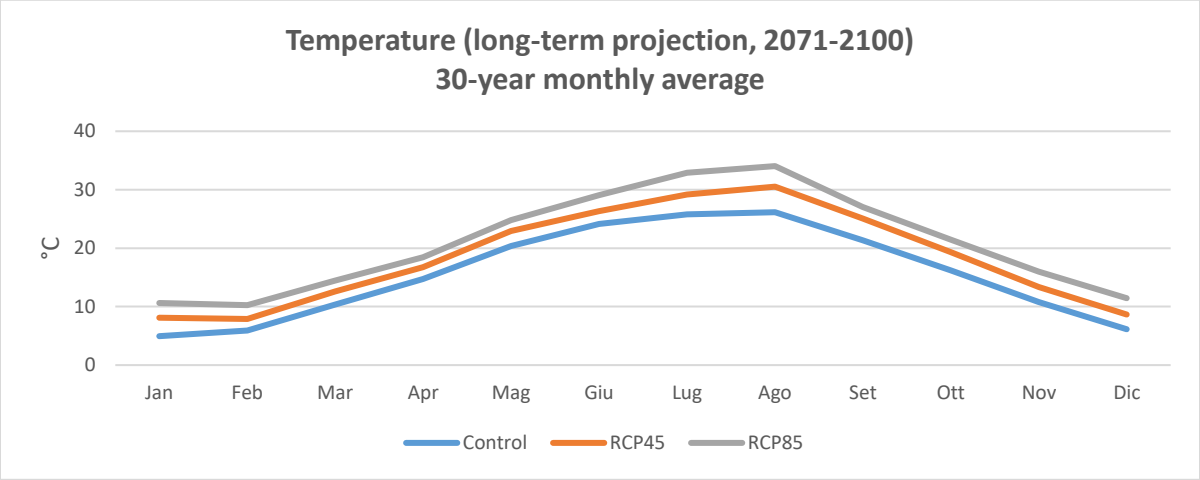

Fig. 3.23 - Differences in the 30-year monthly average temperature between the control period (1983-2012) and long-term projections (2071-2100) of RCP4.5 and RCP 8.5.

Freshwater loadings computed by SWAT for the ZRB and salinity measured by the station Ve-7 (SAMANET) for the period 2007-2012 were analysed and a relation among monthly means was drawn. As a result, the linear regression equation y = -1.8143x + 27.798 (R2 = 0.6) was computed to predict salinity in PDC from projected freshwater discharge from the ZRB for each climate scenario (Fig. 3.24). Salinity was also used to compute alkalinity, a parameter used to determine the future concentrations of DIC in the waters of PDC through the use of the software CO2SYS. The linear regression equation y = -43.216x + 4474.7 (R^2 = 0.4) was computed to predict monthly alkalinity from projected monthly salinity for each climate

scenario associated to the area of PDC (Fig. 3.25). Monthly values of alkalinity, together with monthly values of salinity (ppt), temperature (°C), pressure (dbars), and atmospheric CO_2 (µatm), were implemented into the software to compute projected DIC values for each climate scenario.

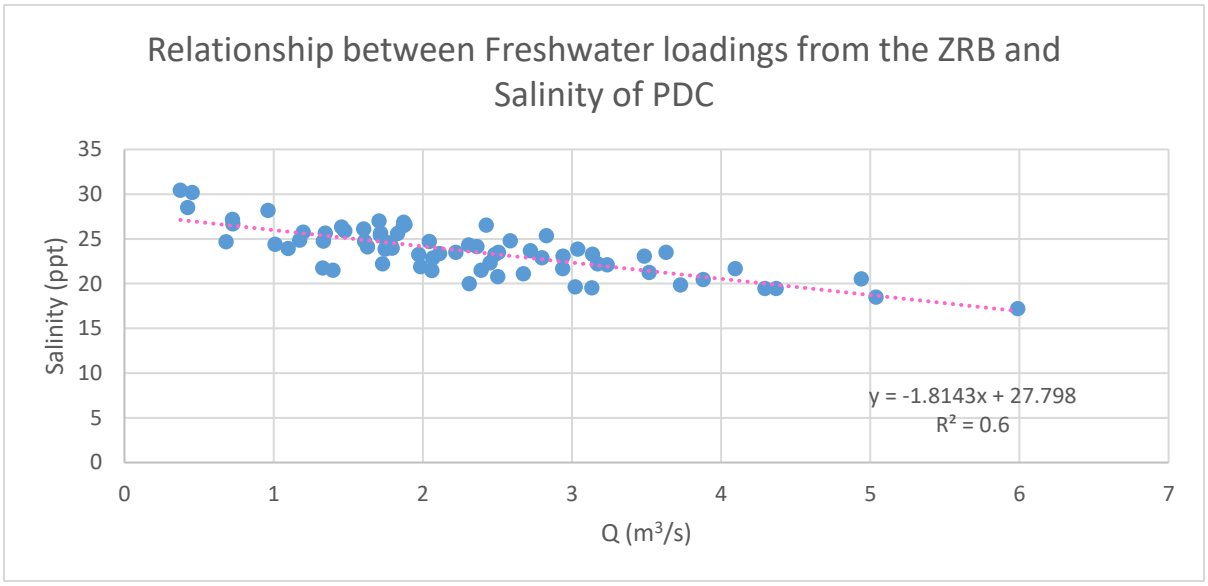

Fig. 3.24 – Relationship between Freshwater loadings from the ZRB and Salinity of PDC.

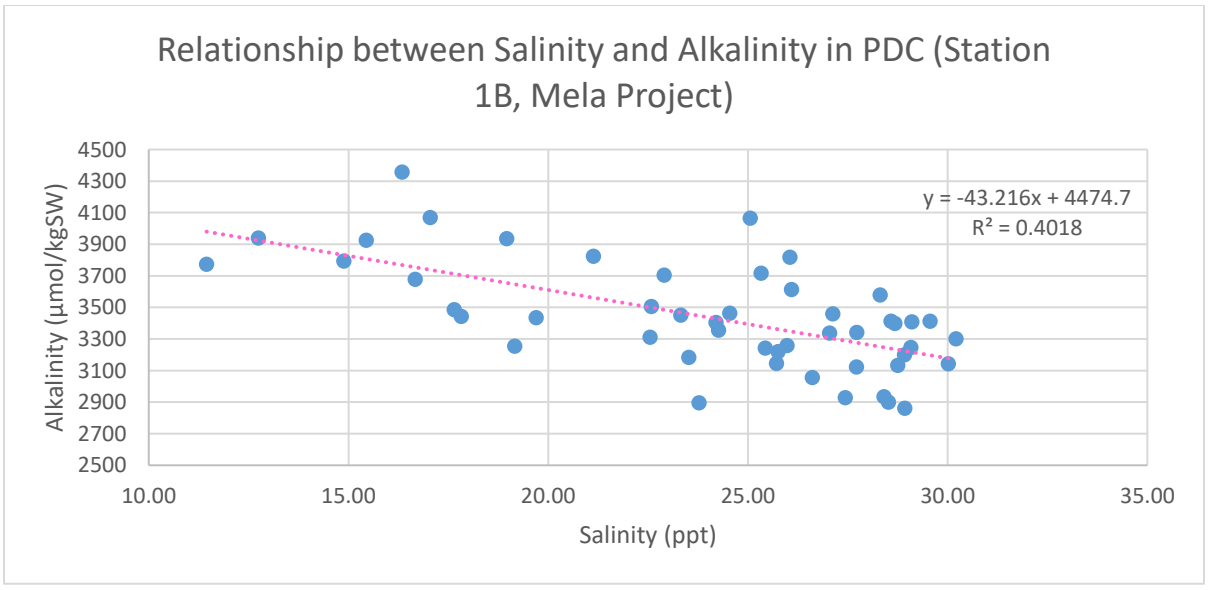

Fig. 3.25 – Relationship between Salinity and Alkalinity in PDC (Station 1B, Mela Project).

As explained above in this section, statistics for wind and light loadings were left unchanged over the 21st century, and daily values were computed automatically by AQUATOX. Finally, it was decided to not consider the effects of sea level rise on PDC and its lagoon of Venice. The rationale behind this choice is the lack of high resolution scenarios and hydrologic models able to simulate the effects of sea-level rise on PDC in an appropriate way. In order to avoid adding additional complexity and uncertainty, sea-level rise was discarded from the study.

Each scenario was forced by two Representative Concentration Pathways (RCPs), RCP 4.5 and RCP 8.5, and propagated for two time periods: a mid-term scenario (2041-2070) and a long-term scenario (2071-2100). Results of future scenarios of nutrient concentrations and phytoplankton biomasses are presented in Section 4.3.2 of this dissertation.

4 RESULTS

4.1 Climate change scenarios for the Zero river basin

4.1.1 Bias correction of future climate change scenarios

As a result of the bias correction, here are presented the future conditions for precipitation and temperature. For simplicity, only the results corresponding to the GCM/RCM 1 (CMCC-CM/COSMO-CLM) for the weather station of Castelfranco Veneto are presented. The method, was able to improve the mean of monthly precipitation (Fig. 4.1a,b) and temperature (Fig. 4.2a,b) while it did not improve the standard deviation (Fig. 4.1c, Fig. 4.2c).

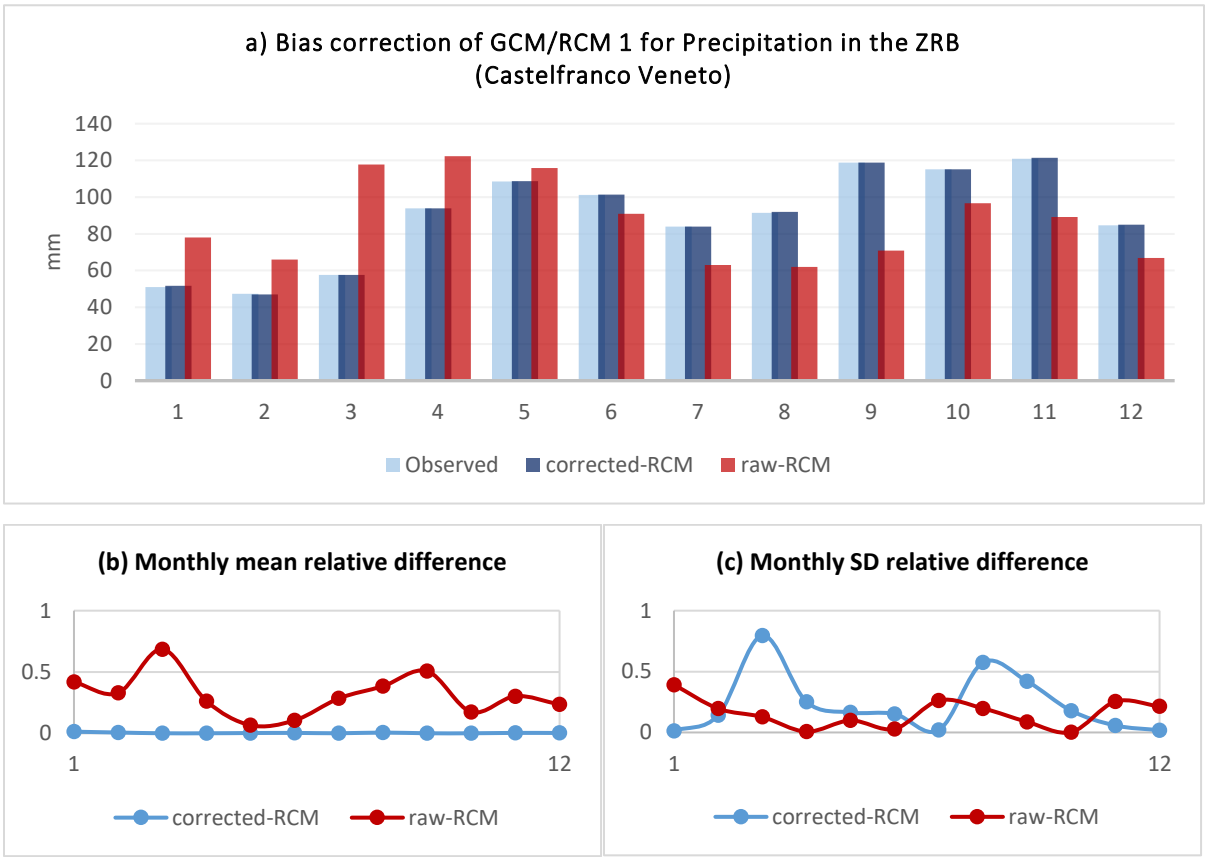

Fig. 4.1 – Bias correction of the GCM/RCM 1 for the variable Precipitation in the ZRB. (a) Differences in the 20-year monthly mean between observed, raw-data and corrected-data precipitation values for the correction period (1993-2012). (b) Relative difference in the 20-year monthly mean between raw-data and corrected-data. (c) Relative difference in the 20-year monthly standard deviation between raw-data and corrected-data.

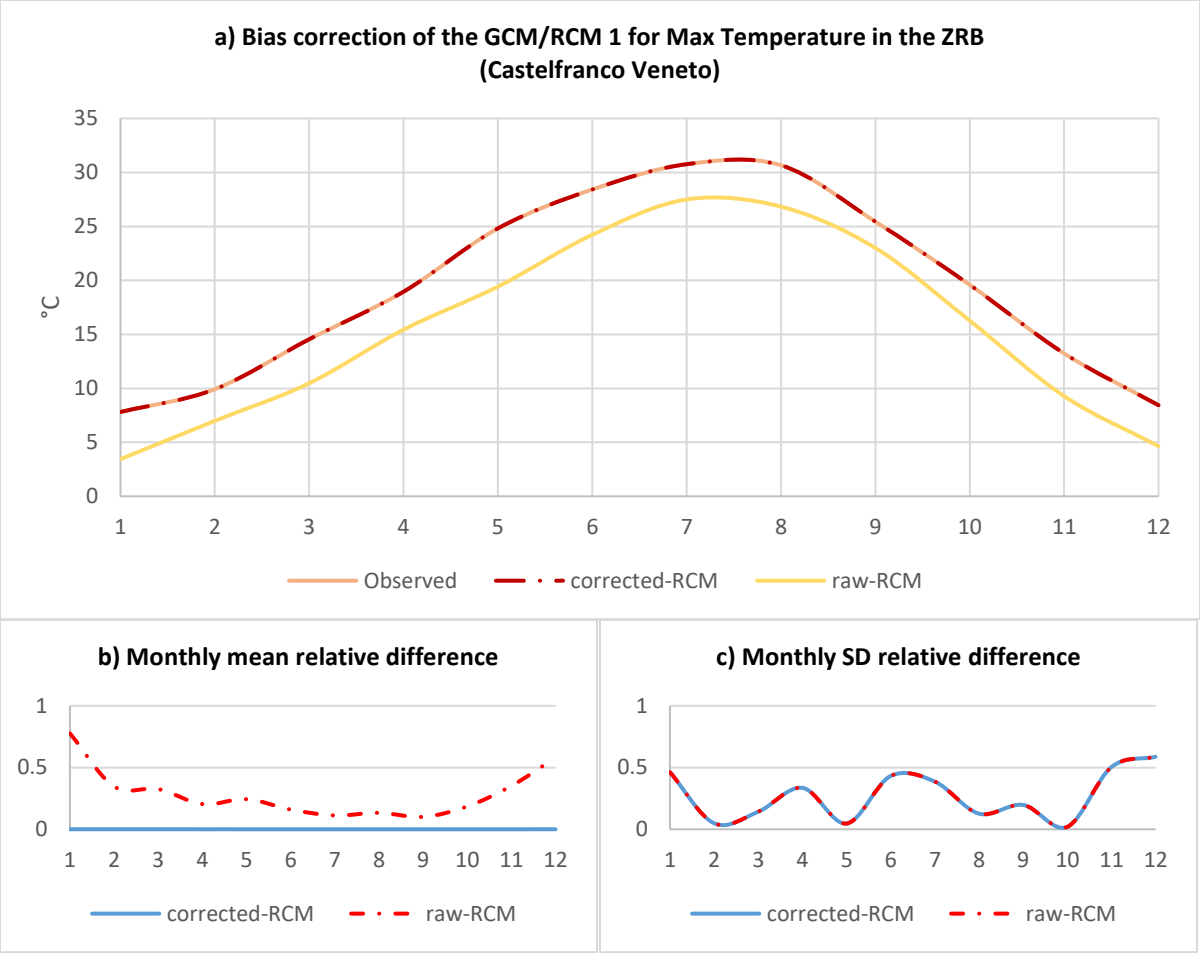

Fig. 4.2 – Bias correction of the GCM/RCM 1 for Max Temperature in the ZRB. (a) Differences in the 20-year monthly mean between observed data, raw-data and corrected-data for the correction period (1993-2012). (b) Relative difference in the 20-year monthly mean between raw-data and corrected-data. (c) Relative difference in the 20-year monthly standard deviation between raw-data and corrected-data.

As a result of the bias correction, suitable climate data temperature and precipitation data for the other models were obtained. Runs with the GCM/RCM 1 show that increases in GHGs are associate with evident changes in precipitation and temperature in the area of the ZRB. Yearly precipitation increases only slightly in both scenarios (Fig. 4.3a). However, precipitation patterns show distinct variations. Winter precipitation will raise up to 30%, and summer precipitation will be reduced up to 40% (Fig. 4.3b and Fig. 4.3c). Differently, it is possible to observe increased temperatures in every month of the year with extremes up to 6°C in the winter period (Fig. 4.4a, b, c).

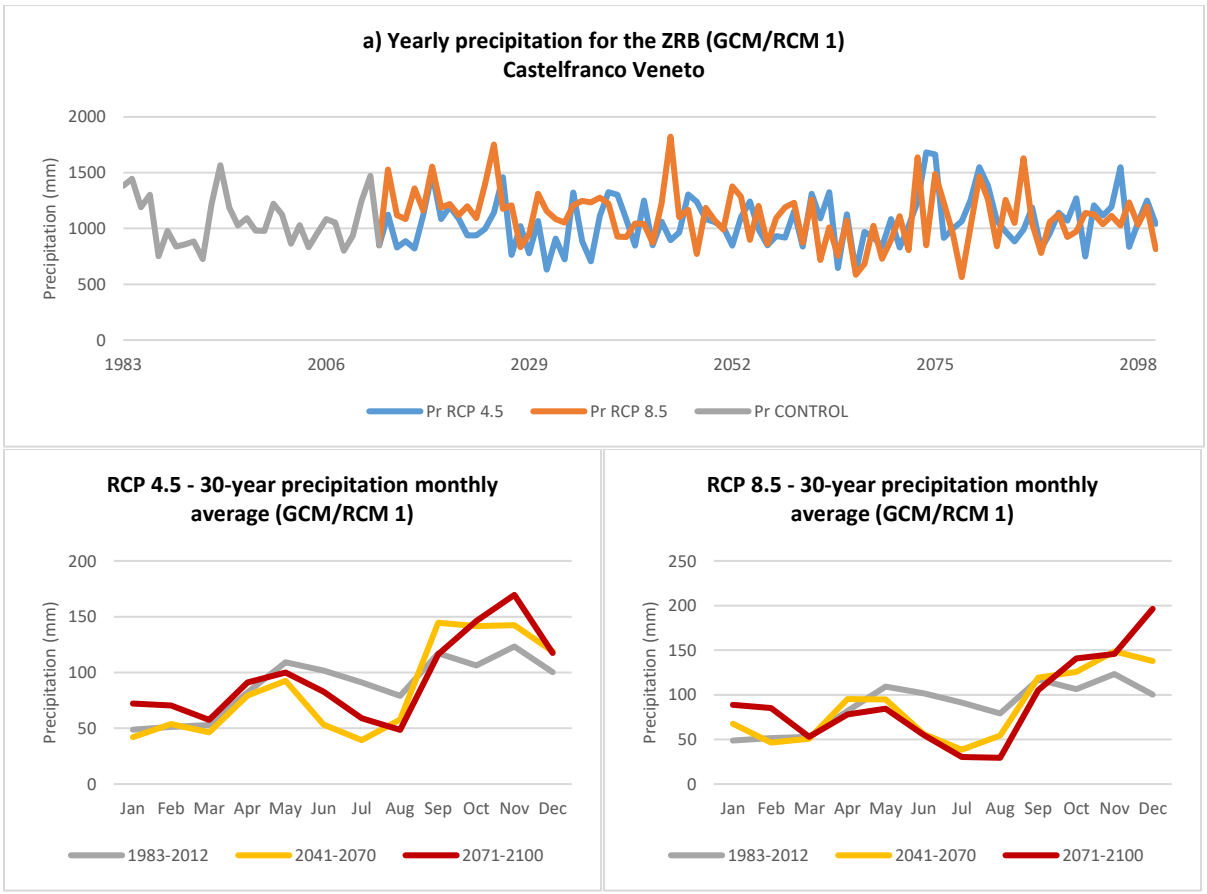

Fig. 4.3 – a) Annual precipitation for the control period (1983-2012) and the mid-term (2041-2070) and long-term (2071-2100) projections for the GCM/RCM 1 in the ZRB. b) differences in the 30-year monthly average between the control period (1983-2012) and the mid-term (2041-2070) and long-term (2071-2100) projections for the RCP4.5 scenario. c) differences in the 30-year monthly average between the control period (1983-2012) and the mid-term (2041-2070) and long-term (2071-2100) projections for the RCP8.5 scenario.

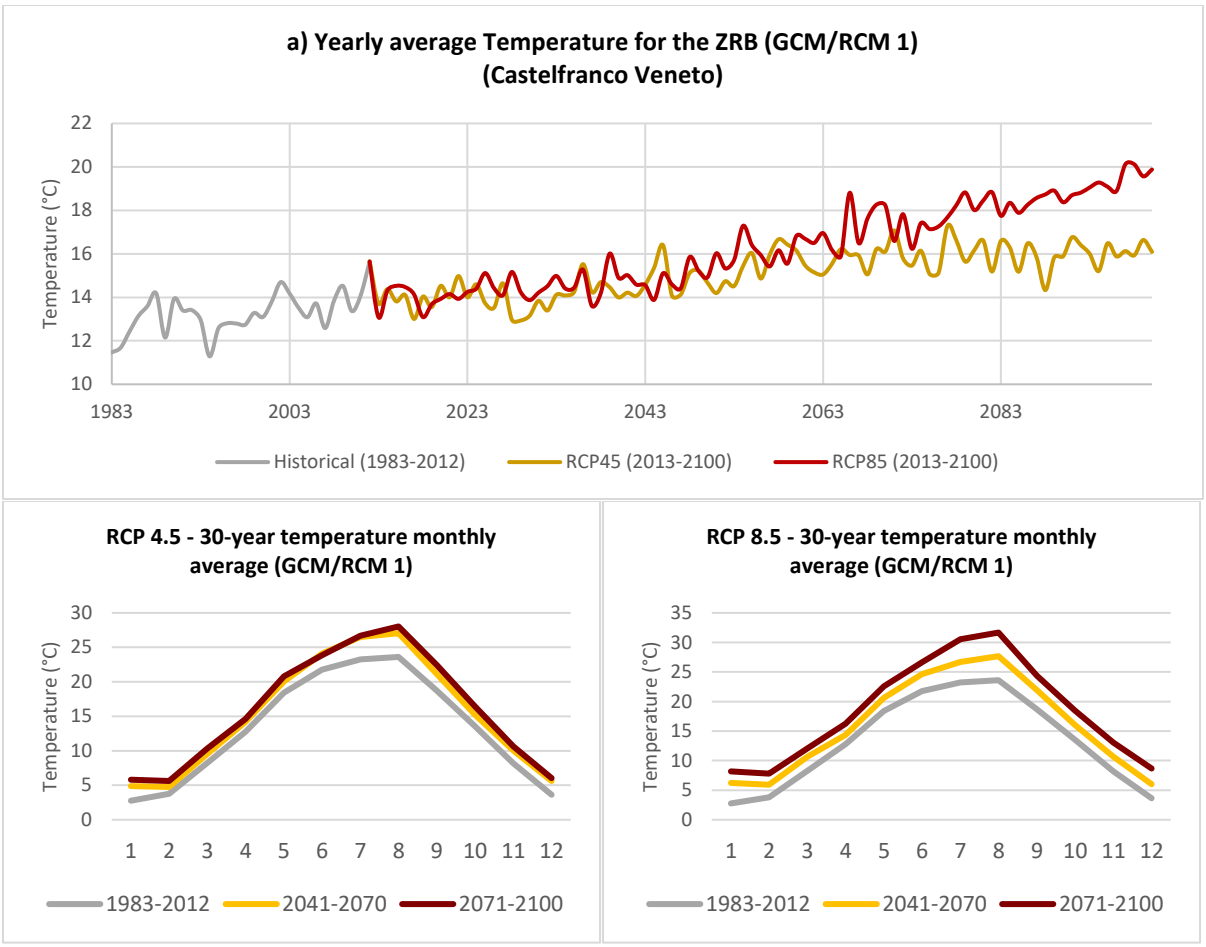

Fig. 4.4 - a) Annual average temperature for the control period (1983-2012) and the mid (2041-2070) and long (2071-2100) term projections in the Zero river basin, Italy. b) Differences in the 30-year monthly average between the control period (1983-2012) and the mid (2041-2070) and long-term (2071-2100) projections for the RCP 4.5 scenario.

4.2 Climate change impacts on hydrology and nutrient loads of the ZRB

4.2.1 Calibration and Validation of the SWAT model for the ZRB

The behavior of the Zero river basin in terms of response to stream flow and nutrient loadings was evaluated by identifying the most sensitive parameters, indicated in Table 3.10. Calibration and validation were performed using observed stream flow and nutrient loadings data (Section 3.2.2). Calibration of the SWAT model for the ZRB was performed at a monthly time step for the 2007-2009 period, following an initial 3-year warm-up (2004-2006). Calibration was possible for the streamflow, nitrate and ammonium loads. The inorganic form of phosphorus was also attempted despite the scarcity of data available.

Calibration for a monthly time step for the 2007-2009 period produced "satisfactory" results (Moriasi et al. 2007) for flow rate (NSE=0.64, R2=0.67), nitrate (NSE=0.59, R2=0.73) and ammonium (NSE=0.51, R2=0.56), as shown in Fig. 4.5, Fig. 4.6, and Fig. 4.7. Validation was performed for the period 2010-2012 and resulted in lower NSE for flow rate (NSE=0.20, R2=0.60) and nitrate (NSE=0.25, R2=0.64). This result can be related to an extreme precipitation event occurred in the area of study at the turn of October and November 2010, and an underestimation of flow rate during the 2011-2012 autumn-winter period, characterised by very low precipitations (Fig. 4.8 and Fig. 4.9). The low performance (NSE=-0.1, R2=0.28) of ammonium during validation period (Fig. 4.10) are attributed to underestimated flow rate during the 2011-2012 autumn-winter period. Moreover, ammonium loadings are also subject to the effect of punctual source of pollution (WWTPs, industrial discharges, direct sewer discharges) which were modeled as constant throughout the calibration and validation periods as no direct observation measures were available. The adoption of methodologies such as the one described in Azzellino et al. (2006) would help to better estimate the loadings of point-source pollution in rain weather conditions.

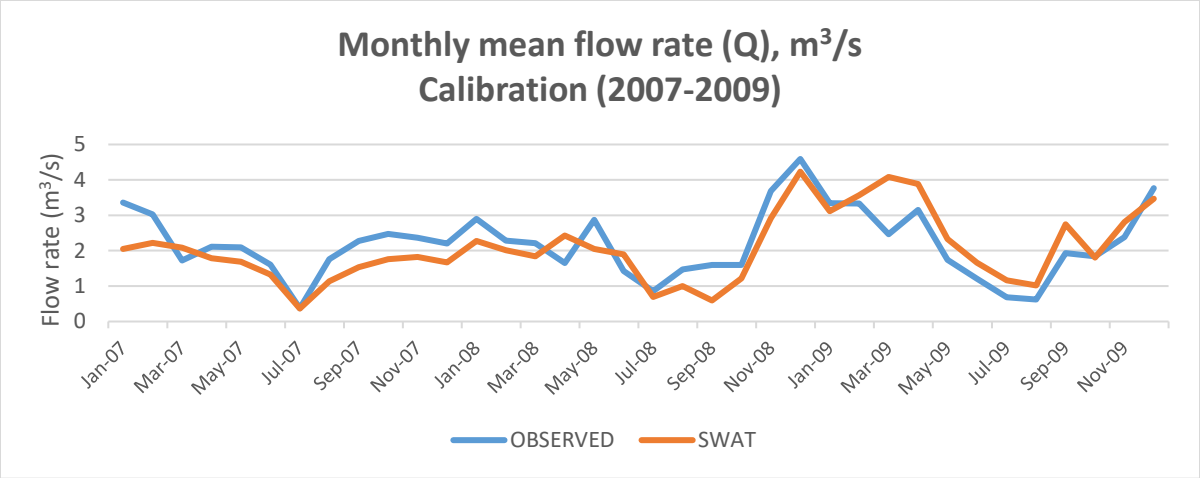

Fig. 4.5 – Mean flow-rate calibration for the period 2007-2009 (NSE=0.64, R2=0.67).

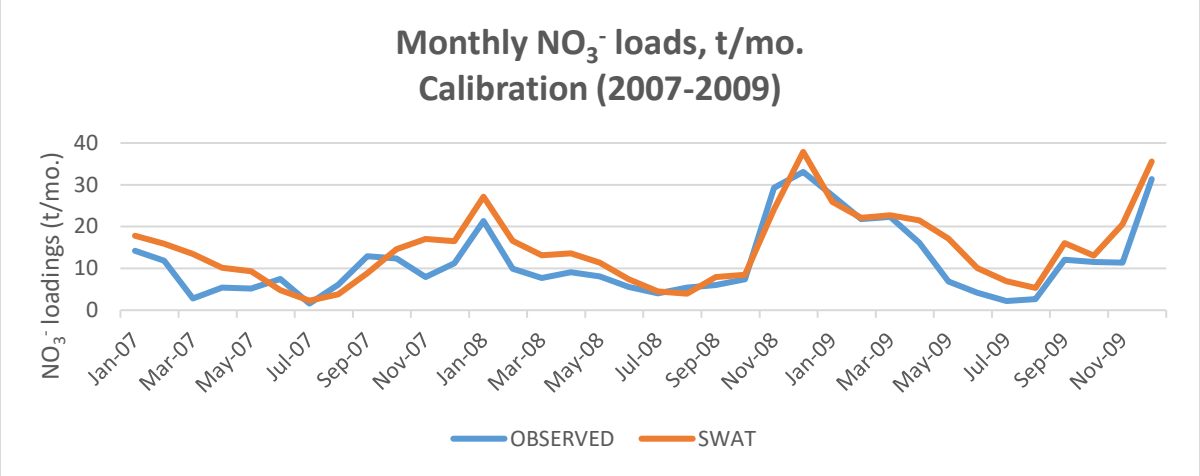

Fig. 4.6 – Nitrate (NO_3^-) loadings calibration for the period 2007-2009 (NSE=0.59, R2=0.73).

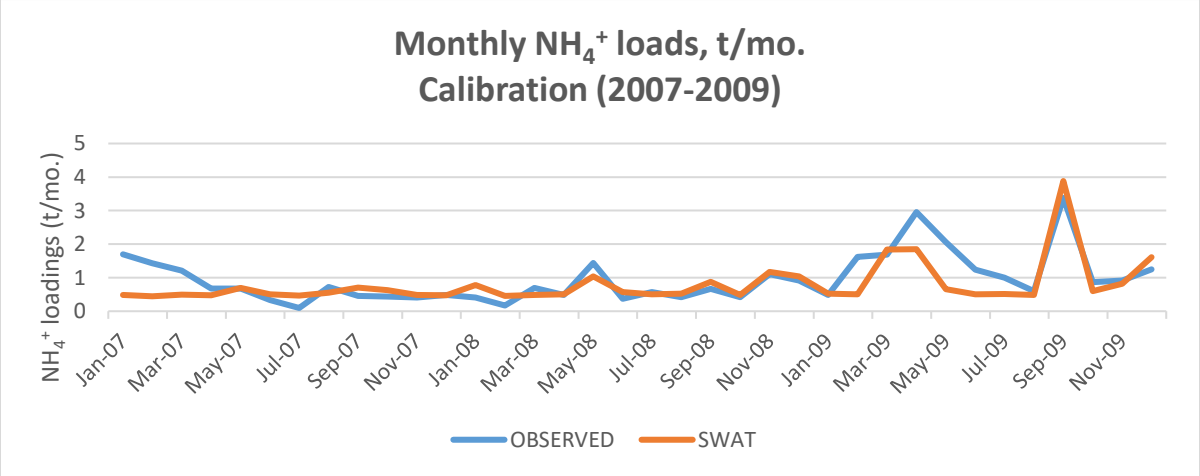

Fig. 4.7 – Ammonium (NH_4^+) loadings calibration for the period 2007-2009 (NSE=0.51, R2=0.56).

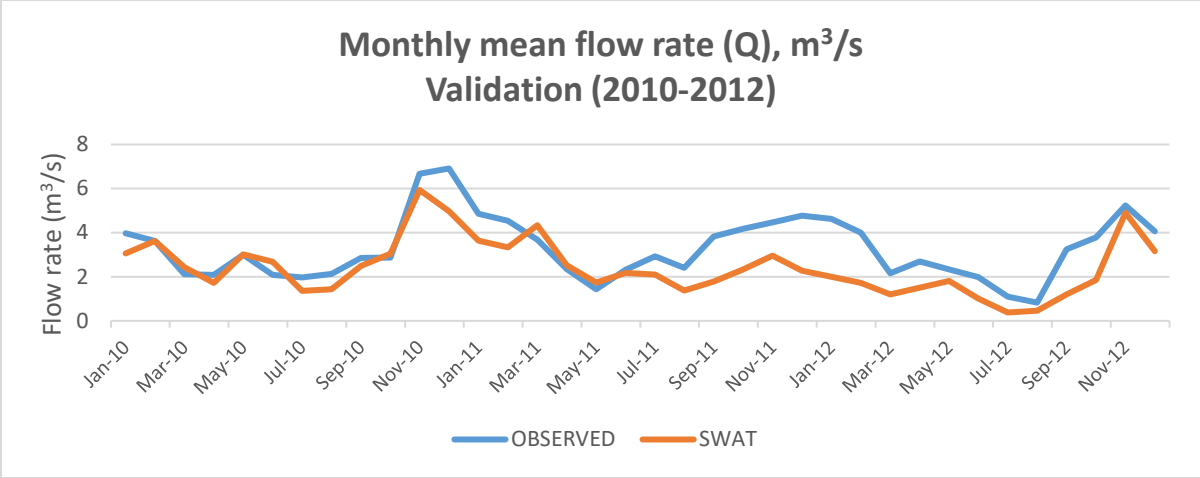

Fig. 4.8 – Mean flow rate validation for the period 2010-2012 (NSE=0.15, R2=0.60).

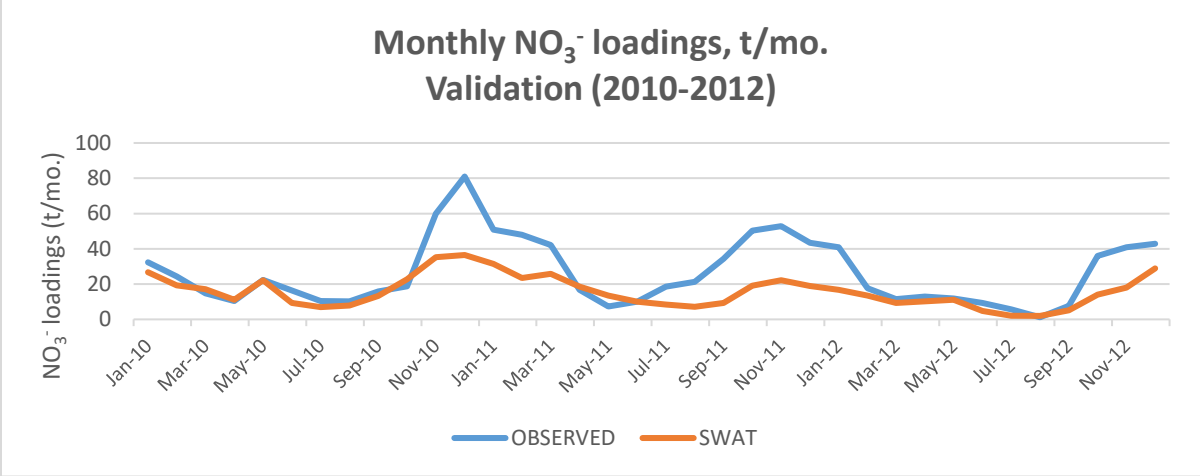

Fig. 4.9 - Nitrate (NO_3^-) loadings validation for the period 2010-2012 (NSE=0.25, R2=0.65).

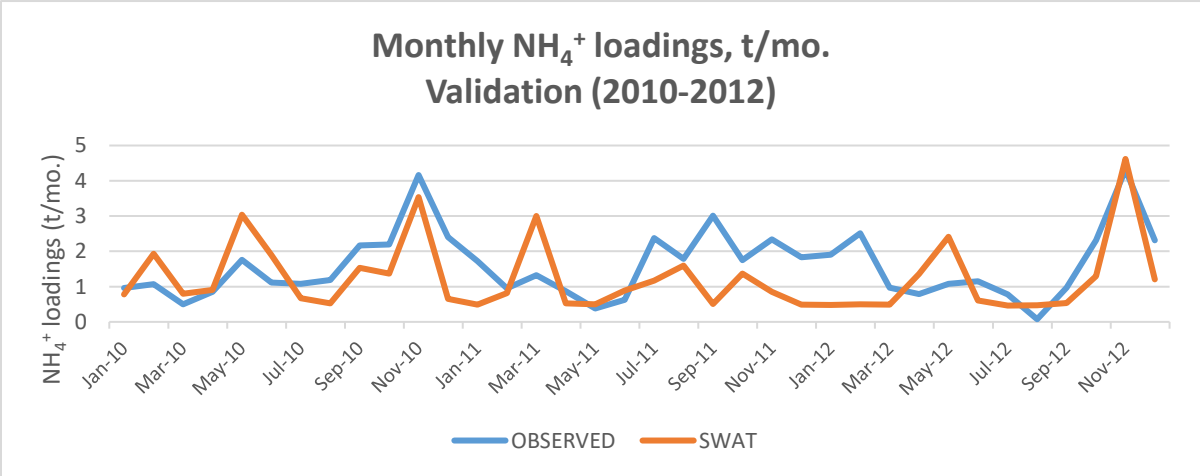

Fig. 4.10 – Validation of ammonium (NH_4^+) for the period 2010-20 (NSE=-0.10, R2=0.25).

Phosphorus calibration (NSE=-0.4, R2=0.1) and validation (NSE=-0.6, R2=0.2) were not satisfying (Fig. 4.11 and Fig. 4.12). The reason behind these results is probably due to the scarce monitoring data available for inorganic phosphorus. The use of the software LOADEST for the computing of potential monthly observed values does not guarantee the validity of the measures.

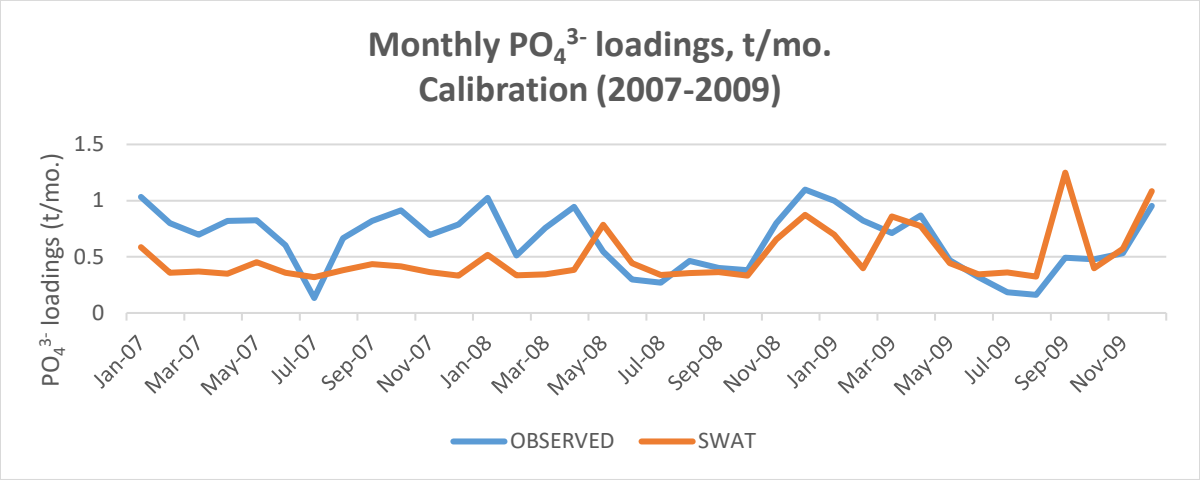

Fig. 4.11 – Calibration of phosphate (PO_4^{3-}) for the period 2007-2009 (NSE=-0.40, R2=0.12). Observed values were computed with the software LOADEST (USGS 2012).

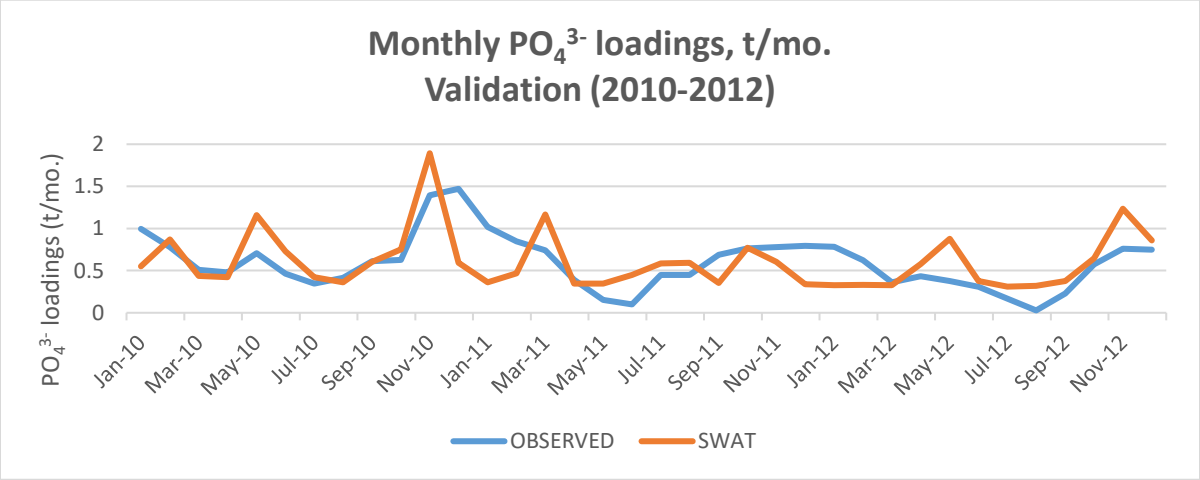

Fig. 4.12 – Validation of phosphate (PO_4^{3-}) for the period 2010-2012 (NSE=0.13, R2=0.29). Observed values were computed with the software LOADEST (USGS 2012).

For completeness, a statistical comparison of means and variances was performed. Relative bias and F-test were computed in order to compare means and variances of the virtual observed loadings of phosphorus computed by LOADEST, and the phosphorus loadings modeled by SWAT. Despite the low R^2 and NSE values, the computed relative bias and F-test

indicated in Table 4.1 shows that observed and modeled distributions are similar, assuming normality (Fig. 4.13). Moreover, the order of magnitude of the average yearly values are in agreement with previous studies on the VLW (Collavini et al. 2005; Giupponi et al. 2012) and support the acceptability of these results for the purposes of this study which focuses on the long-term changes due to the impacts of climate change.

Table 4.1 – Statistical comparison of means and variances between virtual observed phosphorus values computed by LOADEST and phosphorus values modeled by SWAT.

Period	Mean SWAT	Mean LOADEST	St. Dev. LOADEST	Variance SWAT	Variance LOADEST	rb	F
2007-2009	498.49	646.52	264.07	51496.89	69730.59	-0.56	0.74
2010-2012	603.78	593.42	315.62	110629.46	99617.3	0.03	1.11

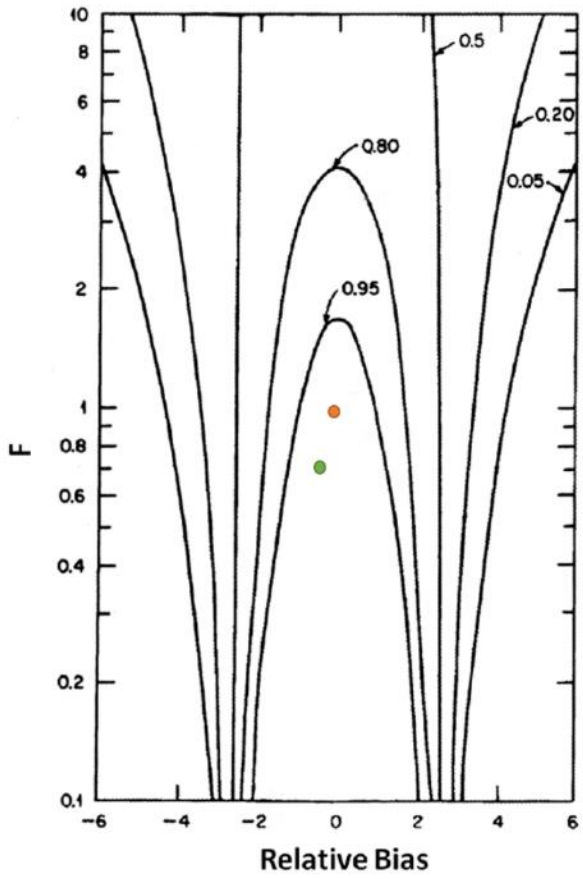

Fig. 4.13 - Relative bias and F-test to compare means and variances of virtual observed values of phosphorus computed with LOADEST and modeled values of phosphorus modeled with SWAT. Isopleths indicate the probability that the predicted and observed distributions are similar, assuming normality.

4.2.2 Impacts of climate change on the ZRB

The calibrated and validated SWAT model was run with the precipitation and temperature data of each GCM/RCM combination. In this section, only the results relative to the GCM/RCM 1 (CMCC-CM/COSMO-CLM) are presented, in order to illustrate synthetically the results of the integrated modelling approach. The effects climate change were evaluated by comparing the 30-year monthly average of the control period (1983-2012), with the mid-term (2041-2070) and long-term (2071-2100) projections. Projections do not show any change in the annual average, with 30-year yearly mean stable at 2 m^3/s. However, an increase in the late autumn-winter flow, and a marked decrease in the months of July and August for both RCP 4.5 and RCP 8.5 scenarios can be observed (Fig. 4.14a,b). These results agree with the future climate projections of the GCM/RCM, which indicate an increase of precipitation in winter and a marked reduction in summer, coupled with an increase in summer evapotranspiration due to the higher temperatures.

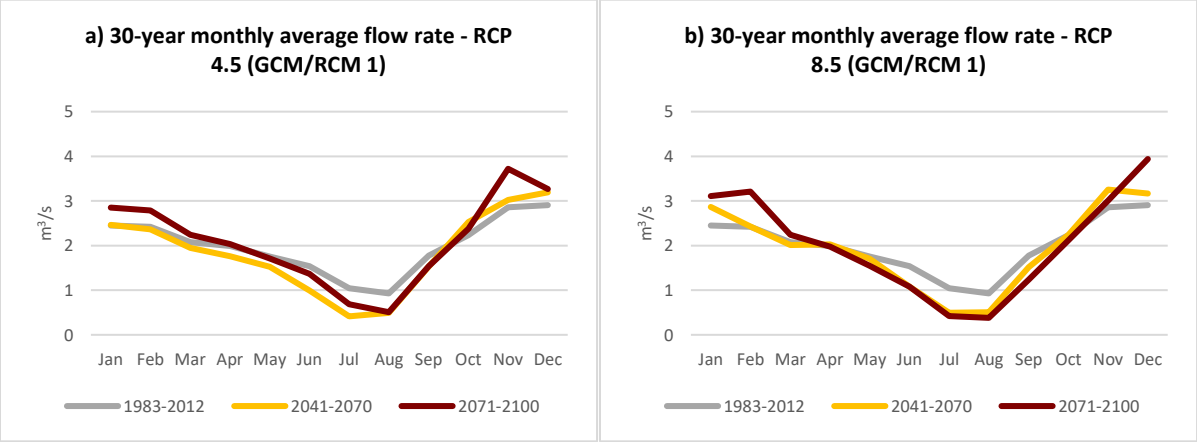

Fig. 4.14 – Flow rate differences in the 30-year monthly average of the control period (1983-2012), mid-term period (2041-2070) and long-term period (2071-2100) for scenarios RCP 4.5 (a) and RCP 8.5 (b) of the GCM/RCM 1.

The capability of the ZRB to export nutrients is controlled by water discharge, which in turn is a function of climate, morphology, soil properties and geology of the basin. Changes in climate and water flow consequently affect the loads of nutrients. Projections of nitrate loadings for both RCP4.5 and RCP 8.5 show an increase in the average yearly loadings over the 21st century, with values that increase of up to 5% by the end of the century. Projections show an increase in winter consequently with projected increased precipitations. The nitrate loads in summer

are influenced mainly by a reduction in precipitation and, therefore, in the water discharge (Fig. 4.15a,b).

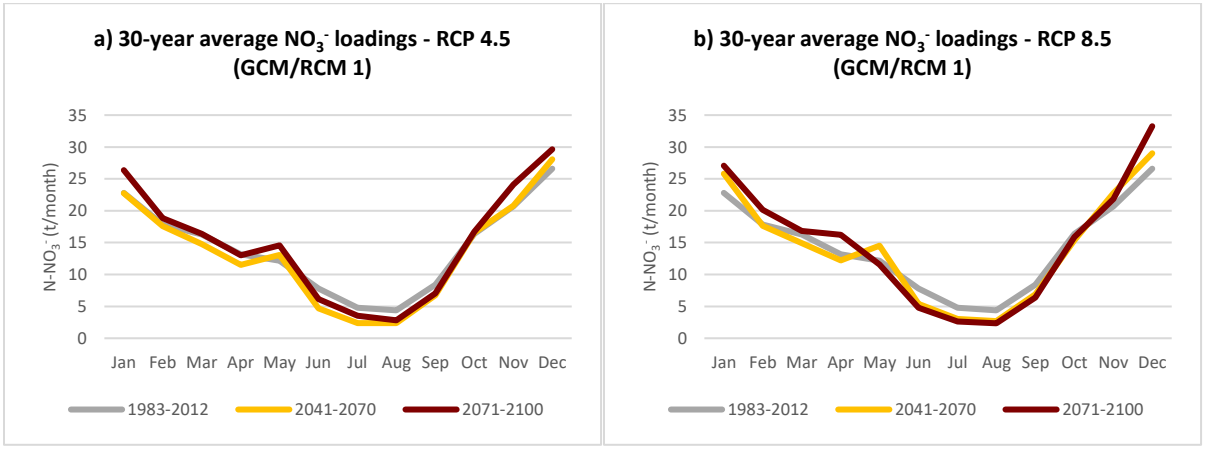

Fig. 4.15 – Nitrate loadings differences in the 30-year monthly average of the control period (1983-2012), mid-term (2041-2070) and long-term (2071-2100) future projections for scenarios RCP 4.5 (a) and RCP 8.5 (b).

The loads of Ammonium show marked differences in the magnitude of changes between RCP4.5 and RCP8.5. RCP4.5 for both mid-term and long-term period show a slight increase in spring and autumn and a reduction of loadings in summer, while RCP8.5 differentiates for the marked increase in the autumn-winter period. Also, it is possible to observe a change in the seasonal pattern between the mid-term and the long-term projection period of RCP8.5. In the mid-term period, loadings are concentrated in the months of April and November, while in the long-term period peaks are concentrated in the winter months, while the peak of April is reduced (Fig. 4.16a,b). Yearly averages show an increase of loadings the mid-term period and a following reduction in the long-term period, that brings loadings closer (RCP4.5) to the average of the control period, or only slightly higher (RCP8.5). The cause is probably related to the higher temperatures reached in the long-term period. Nitrogen transformation processes, such as mineralization, nitrification and volatilization are influenced by temperature and available water, and reach their optimal values within a range of temperature and humidity in the soil.

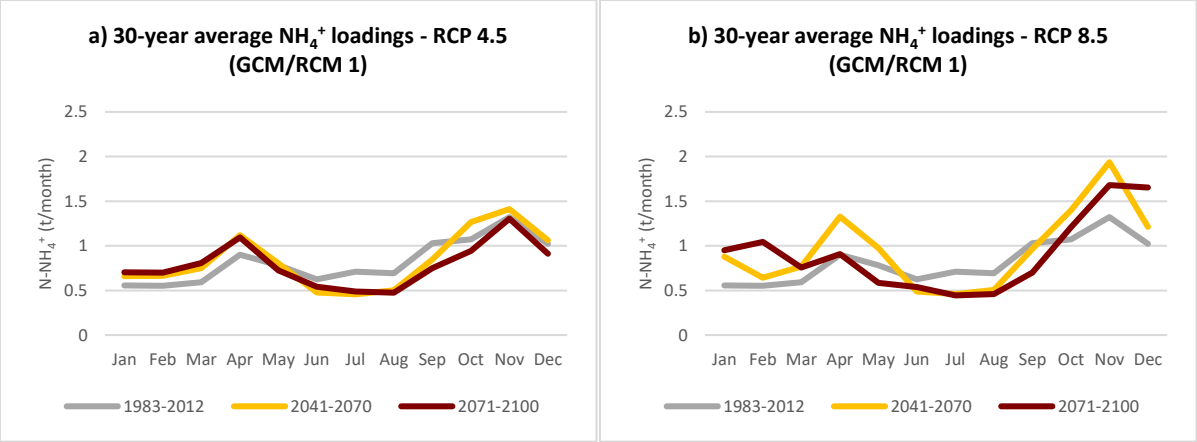

Fig. 4.16 - Ammonium loading differences in the 30-year monthly average of the control period (1983-2012), mid-term (2041-2070) and long-term (2071-2100) future projections for scenarios RCP 4.5 (a) and RCP 8.5 (b).

Changes in phosphorus were also observed. Results indicate marked changes in the magnitude of the winter loads in both RCP4.5 and RCP8.5. Both scenarios show an increase in inorganic phosphorus loadings in winter independently of the trend of the water flow (Fig. 4.17a,b), illustrating a probable enrichment of the topsoil in inorganic phosphorus due to an accelerated remineralization, in conjunction with increased leaching and erosion processes caused by increasing precipitations in the autumn-winter period (Jennings, 2009; Pierson et al., 2010). Moreover, drier conditions in the summer might exacerbate the erosion of soil in the autumn season, and consequently increase the runoff of sediments and adsorbed mineral forms of phosphorus.

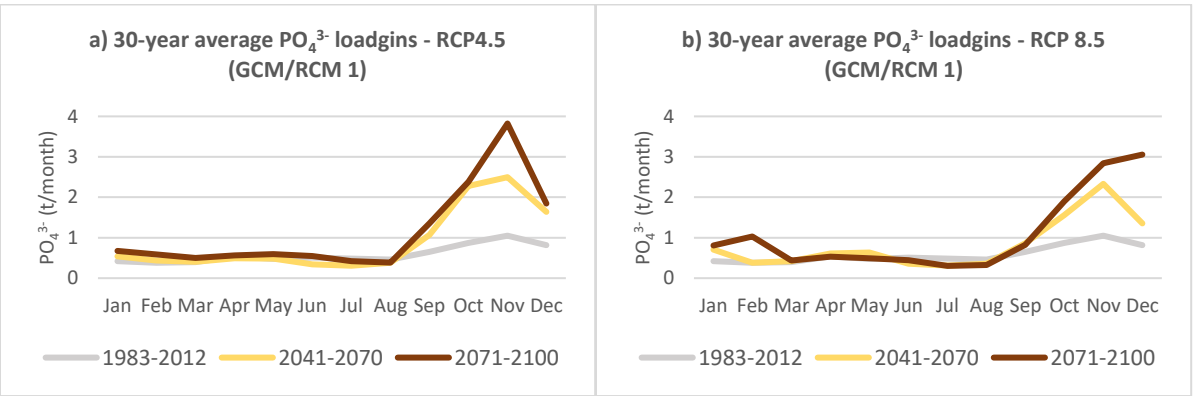

Fig. 4.17 – Inorganic phosphorus loading differences in the 30-year monthly average of the control period (1983-2012), mid-term (2041-2070) and long-term (2071-2100) future projections for scenarios RCP 4.5 (a) and RCP 8.5 (b).

4.3 Climate change impacts on PDC

4.3.1 Performance evaluation of the AQUATOX model for PDC

Model performance was evaluated by comparing simulation results to SAMANET monitoring data from 2007 to 2011 and MELa monitoring data from 2007 to 2009, both visually and statistically. Wind speed, solar radiation, DO, DIN and DIP concentrations, and Chl-a concentrations were used to evaluated the performance of the AQUATOX model of PDC. Table 4.2 and Fig. 4.13 summarise the outcomes of the overlap test through the computed values of relative bias (rb) and F-test (F). This section of the dissertation discusses the performance of the AQUATOX model for PDC in detail.

Table 4.2 – Values of relative bias and F-test for the considered parameters.

Parameter	Mean AQUATOX	Mean Observations	St. Dev. Observations	Variance AQUATOX	Variance Observation	rb	F
Sol. Rad	327.00	334.65	211.06	40325.78	44545.23	-0.03	0.91
Wind	1.38	1.69	0.83	1.67	0.78	-0.38	2.14
DO	8.56	8.16	2.5	2.58	6.25	0.16	0.17
DIN	0.96	0.86	0.69	0.20	0.48	0.14	0.18
DIP	0.03	0.02	0.013	0.00011	0.00017	0.76	0.44
DIN:DIP	30.07	45.35	22.3	303.37	528.9	-0.66	0.34
Chl-a (2007-2011)	3.44	3.5	5.58	35.7	31.09	-0.01	1.32
Chl-a (2007-2012)	4.15	3.1	5.17	61.12	26.74	0.2	5.2

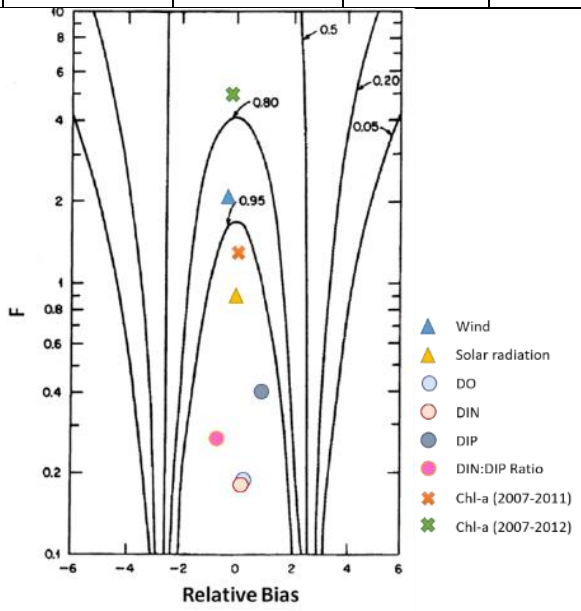

Fig. 4.18 – Overlap between modeled data and observed data, based on relative bias (rB) and variance (F). Isopleths indicate the probability that the predicted and observed distributions are the same, assuming normality.

Daily dissolved oxygen (DO) levels modeled by AQUATOX are in good agreement with the monitoring observation retrieved from the monitoring station VE7 of the SAMANET network Fig. 4.19. Modeled DO concentrations show less variability over the year compared to observations. On average, winter peaks reach 12 mg/l and summer lows 6 mg/l, while the range of observations goes from 15 mg/l to 5 mg/l. This justifies the low value in the F-test (0.17).

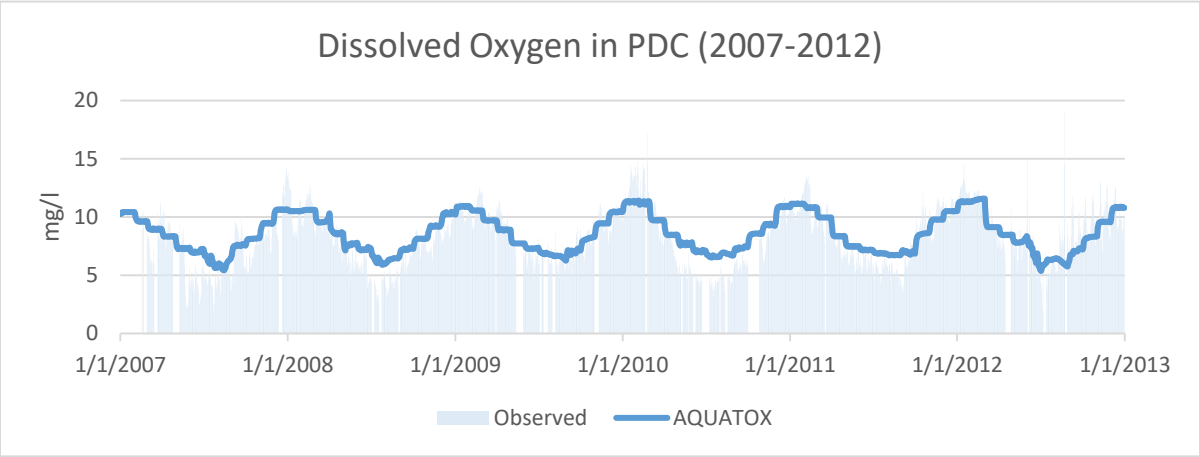

Fig. 4.19 – Relationship between DO modeled by AQUATOX and observations from the station VE-7 of the SAMANET network.

Modeled Dissolved inorganic nitrogen (DIC) shows daily values in good agreement with the observations obtained from the monitoring station 1B of the MELa project (Fig. 4.20). As for DO, fluctuations around the mean are less marked for modeled values than observations. However, the scarcity of available observations might not picture the real variability of data.

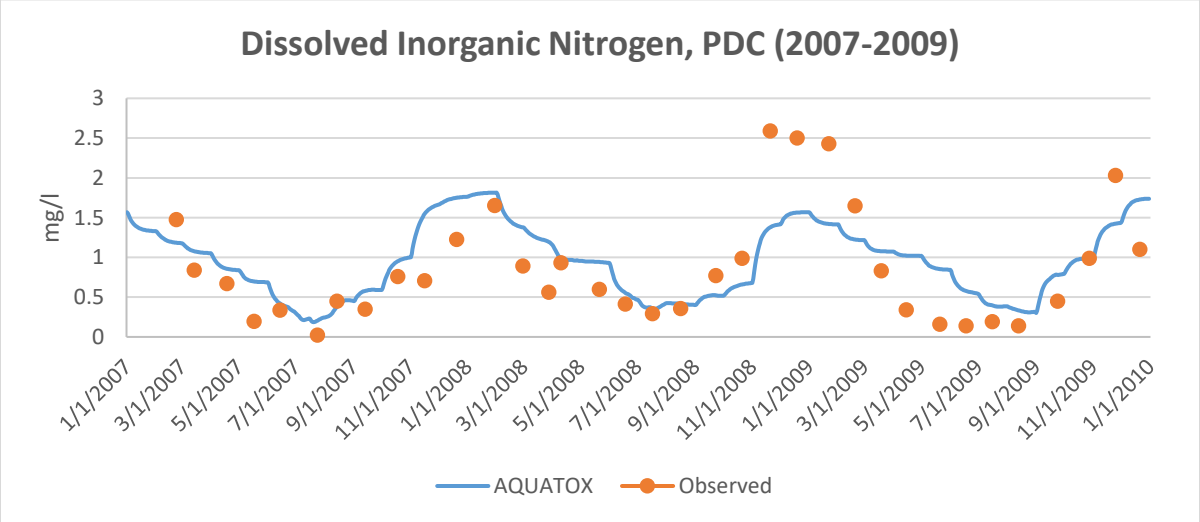

Fig. 4.20 – Relationship between DIN modeled by AQUATOX and observations from the MELa monitoring station 1B.

Daily values of dissolved inorganic phosphorus (DIP) show marked differences between modeled data and observations. The model shows a constant overestimation over the year compared to observed data. This justifies the value of relative bias (0.76) in the overlap test. A plausible explanation may be the difficulty of AQUATOX in modeling the dynamics of nutrient between sediment and water column, specifically the removal of phosphate. Zirino (2016b) describes a mechanism suggested by Di Toro (2001) and Joye et al. (2009) whereby the N:P ratio can increase during the remineralization process that occurs at the bottom of the lagoon: primary production in the water column results in organic particles containing N, P, and other elements necessary for life, most of which settle to the seafloor where they are quickly buried and covered by more production. As a consequence of remineralization of organic detritus settled to the bottom of the lagoon, nitrogen and phosphorus diffuse across the sediment interface into the water where they are re-oxidized: NH_4^+ to NO_3^- and, P to PO_4^{3-}. Nitrate is not adsorbed and is returned to the water column, while a portion of phosphate is adsorbed by hydrated iron oxide. This cause the increasing in the N:P ratio in the water column. Finally it was observed a slight anticipation from the increase of phosphorus concentrations in the autumn period Fig. 2.25. In AQUATOX, phosphorus concentrations begin to rise in August, a month in advance. This is probably due to the remineralization of detritus generated by the phytoplankton bloom of June, which works as internal sink of phosphorus. Given the high water retention time of the summer period, detritus is not removed by the currents.

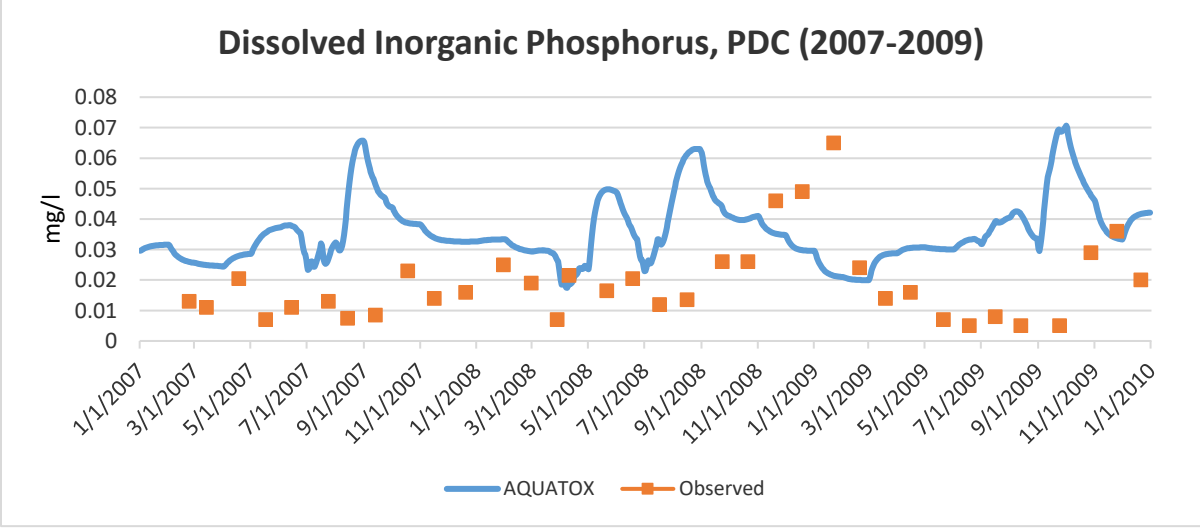

Fig. 4.21 – Relationship between DIP modeled by AQUATOX and observations from the MELa monitoring station 1B.

The DIN:DIP ratio show good agreement between modeled and observed data (Fig. 4.22). It can be observed that AQUATOX underestimates the ratio in the summer months. The reason behind this lies in the overestimation of phosphorus. However, it is possible to observe that AQUATOX portrays the seasonality of the DIN:DIP ratio correctly, with highs in the cold period and lows in the summer.

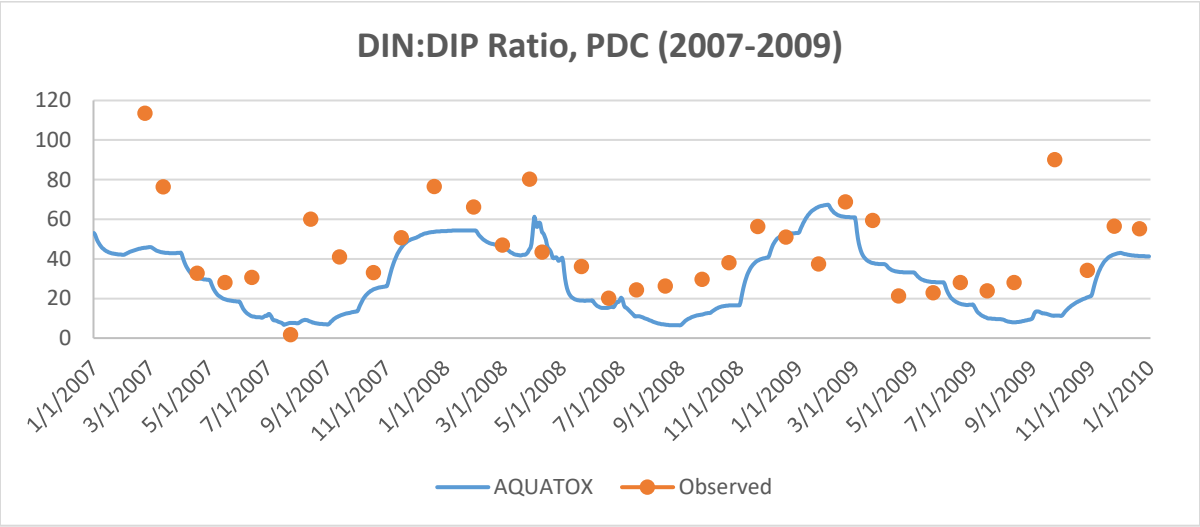

Fig. 4.22 - Relationship between DIN:DIP ratio modeled by AQUATOX and observations from the MELa monitoring station 1B.

The visual comparison of observed against simulated Chl-a was good. Predicted concentrations were slightly higher in summer and lower in winter Fig. 4.23. The years from 2007 to 2011 are in good agreement with observations, while the year 2012 shows substantial differences. While observed data indicate a low production of phytoplankton over the year, AQUATOX features a high peak in the month of June. The peak is caused by high water retention time in the winter months at the turn of 2011 and 2012. This period is characterised by low precipitation and consequent low freshwater discharge from the ZRB. Water retention time is modeled by AQUATOX based on freshwater loadings, and extremely low discharges cause higher water retention times. However, these events are rare and were not cable of affecting long-term (30 years) statistics. The integration of hydrodynamic models able to better simulate water retention times in PDC could solve this problem. However, given the complexity of the study it was not possible to implement another model. The validity of the model is confirmed

by the statistics obtained for the 2007-2011 period, where relative bias (-0.01) and F-test (1.32) indicate strong similarities in the distributions of modeled and observed values.

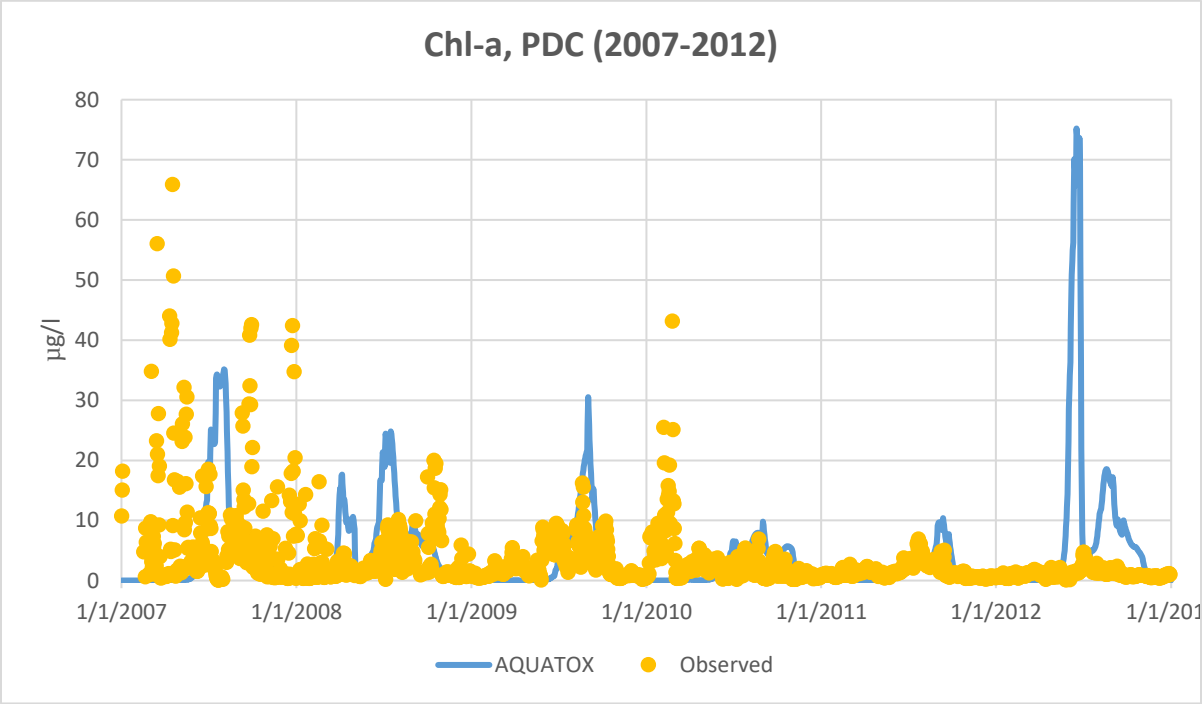

Fig. 4.23 - Relationship between Chl-a modeled by SWAT and observations from the station VE7 of the SAMANET program.

4.3.2 Impacts of climate change and nutrient loadings on PDC

The AQUATOX model for PDC was run with all 10 climate scenarios. Here, only the results relative to the GCM/RCM Number 1 (CMCC-CM/COSMO-CLM) are presented. The effects of future scenarios were evaluated by comparing the 30-year average by month of the control period (1983-2012), and the mid-term (2041-2070) and long-term (2071-2100) periods. In this dissertation, results relative to nutrient concentrations and ratio, chlorophyll-a and abundance of phytoplankton species are presented.

Dissolved Oxygen (DO) concentrations indicate a decrease in both RCP4.5 and RCP8.5 . As expected, the DO decrease in summer, from 7mg/l to 4.5 mg/l, is more marked than in winter. The model does not capture the high excursion that take place in PDC and lagoon of Venice between day and night. As a result, a similar decrease in 30-yr monthly averages might imply an increase in hypoxic conditions.

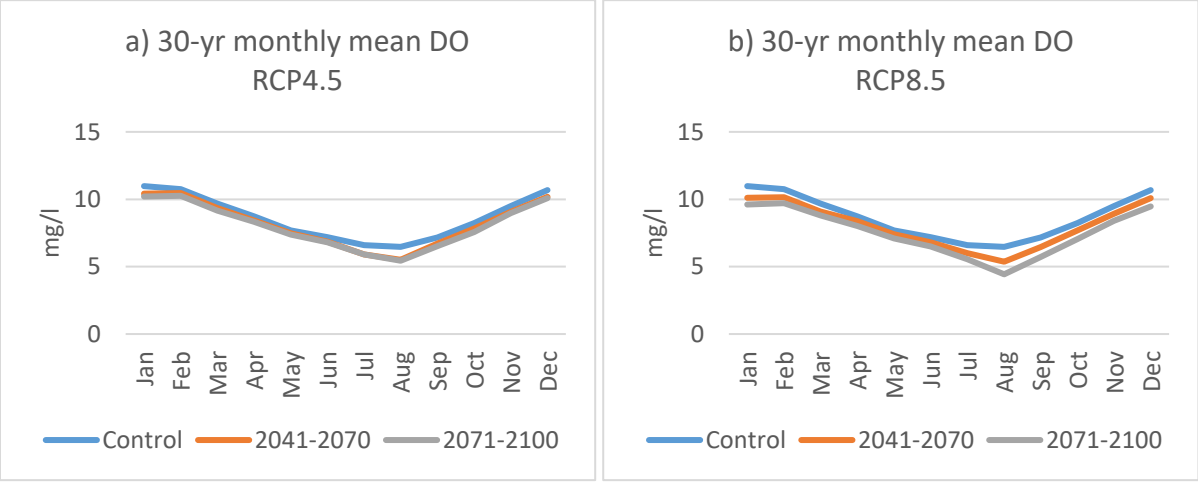

Fig. 4.24 - Differences in the 30-year DO monthly mean between the control period (1983-2012), and the mid-term and long-term projections for RCP4.5 (a) and RCP8.5 (b).

Future projections of DIN concentrations in water don't show substantial changes from the control period (Fig. 4.25a,b). Both RCPs indicate a general decrease of DIN in the summer months and stability over the winter period. This suggests that the surplus of DIN is assimilated by phytoplankton and higher trophic levels of the system (i.e. zooplankton).

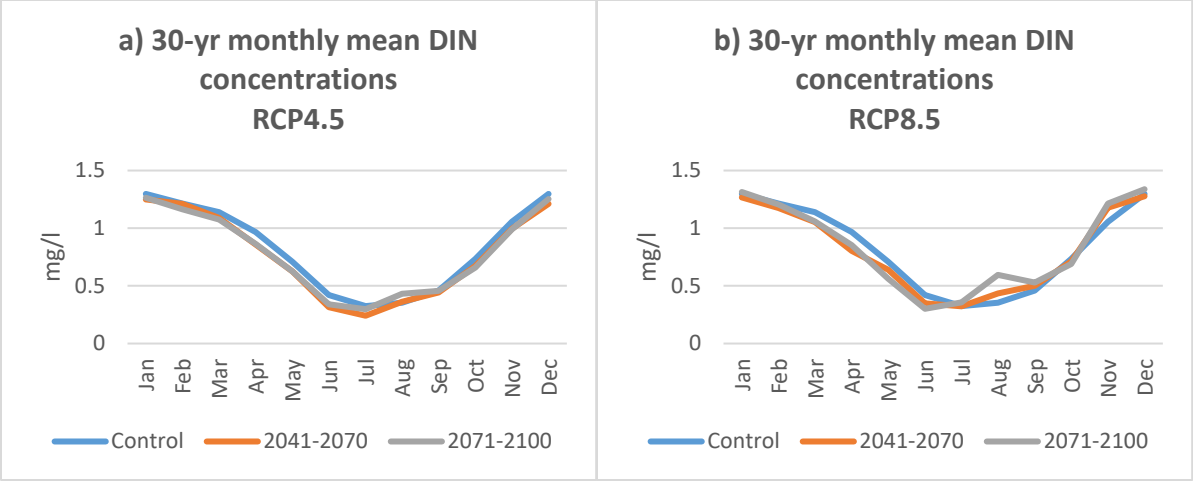

Fig. 4.25 – Differences in the 30-year DIN monthly mean between the control period (1983-2012), and the mid-term and long-term projections for RCP4.5 (a) and RCP8.5 (b).

Differently than DIN, DIP concentrations reflect better the changes in phosphorus loadings from the ZRB. It is possible to observe a substantial increase of phosphorus concentrations in the spring and winter period, while summer concentrations keep the same values of the control period (Fig. 4.26).

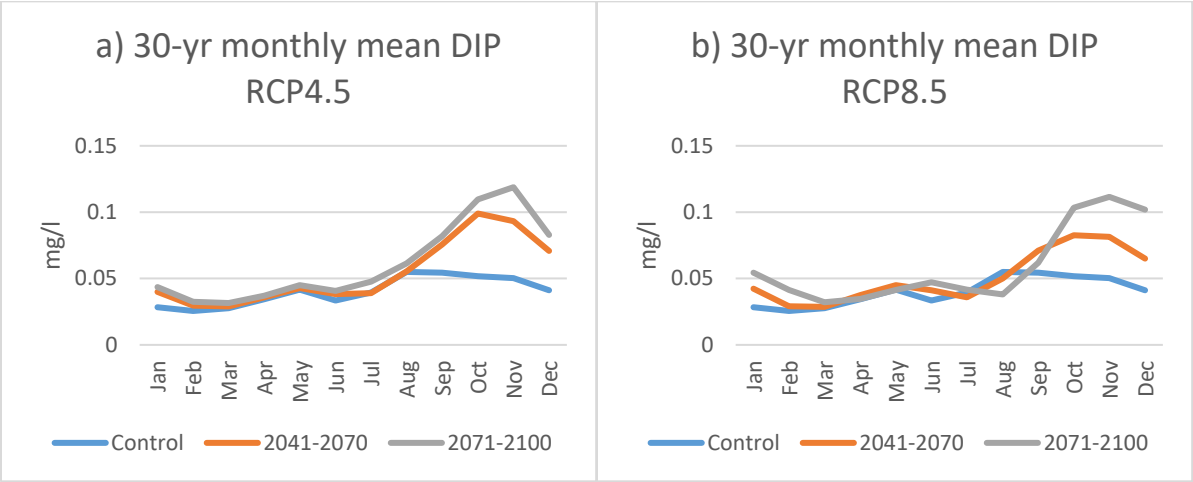

Fig. 4.26 - Differences in the 30-year DIN monthly average concentrations between the control period (1983-2012), and mid-term and long-term projections for RCP4.5 (a) and RCP8.5 (b).

Changes in DIN and DIP concentrations also affect their ratio. Future projection of DIN:DIP ratio indicates marked changes in autumn and winter (Fig. 4.27). Differently, summer months

don't show substantial changes. The higher availability of phosphorus in the winter reduce noticeably the DIN:DIP ratio. However, the same trend of present conditions is still observable also in future projections. As a result, given the overestimation of phosphorus in the model, the complexity of the dynamics of the Venice lagoon, and the limits of the model itself, these results do not allow the forecast of any changes in the limiting conditions of PDC.

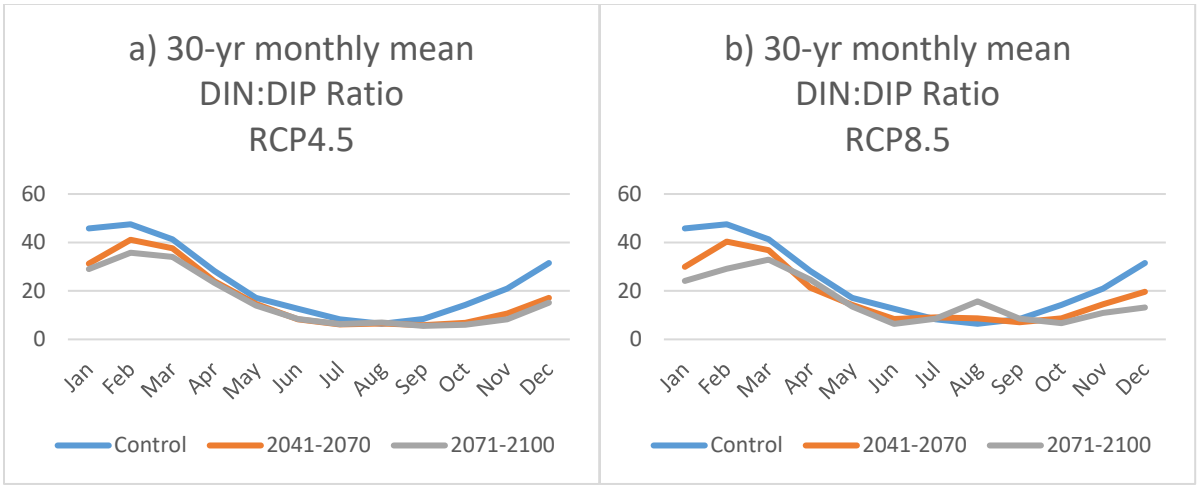

Fig. 4.27 – Differences in the 30-year DIN:DIP monthly mean between the control period (1983-2012), and the mid-term and long-term projections for RCP4.5 (a) and RCP8.5 (b).

30-year averages of Chl-a concentrations were also observed (Fig. 4.28). The RCP4.5 scenario does not indicate marked changes, where only an increase in the summer months is observed. RCP8.5 show more marked differences both in concentration and seasonality. Yearly average concentrations rise from 66.44 µg/l (control period) to 67.7 µg/l (2041-2070) and 89.48 µg/l (2071-2100). It is also observable an evident shift in the peak of Chl-a, from June to August. It is important to consider the fact that Chl-a values are representative of the phytoplankton composition in the system and they cannot model adaptation or addition of new, more tolerant species.

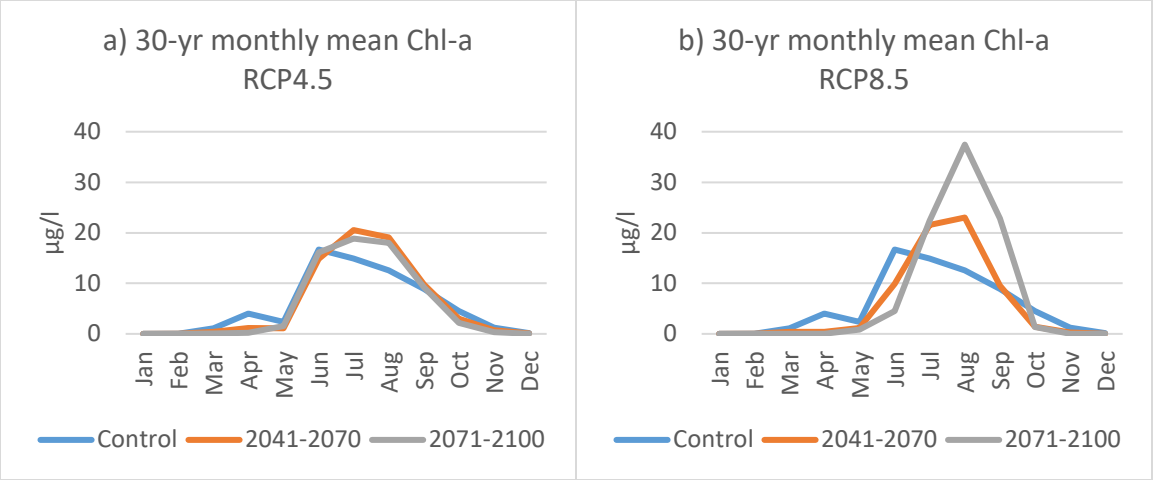

Fig. 4.28 - Differences in the 30-year monthly average Chl-a concentrations between the control period (1983-2012), and mid-term (a) and long-term (b) projections (2071-2100) of RCP4.5 and RCP8.5.

Marked differences are also observable in the composition of phytoplankton (Fig. 4.29 to Fig. 4.33). In the control period, phytoplankton is mainly composed of D1, D2, D5, and D8 (representative of the spring bloom in PDC). The major changes happen in the summer months, where the abundances of Cyanobacteria (CB1) and diatoms adapted to warmer temperatures (D6) increase noticeably. Another observation is that Navicula (D1), a common diatom in PDC and other areas of the lagoon of Venice, tend to disappear in every future scenario. This results show how different climate condition will promote the growth of species which are more resistant to warm temperatures, and inhibit the growth of some of the current species. Change in the composition and seasonality of phytoplankton, due to increased water temperature will also lead to changes in the food-web structure. Warmer temperatures might also trigger a switch from dominance of aquatic macrophytes to phytoplankton (Heino, Virkkala, and Toivonen 2009). Substantial stability in the DIN:DIP ratio does not promote growth of algae with different nutrient ratios, such as D3, D6 and D7. These results indicate that major changes in the phytoplankton community will be caused by higher temperatures, while changes in nutrient loadings will not generate substantial alterations.

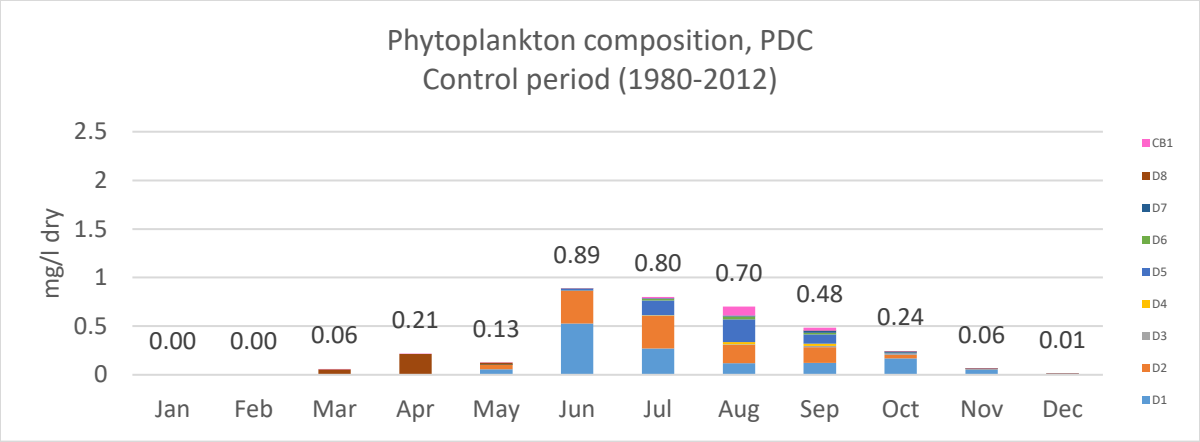

Fig. 4.29 – Abundance of different species of phytoplankton in the control period (1983-2012).

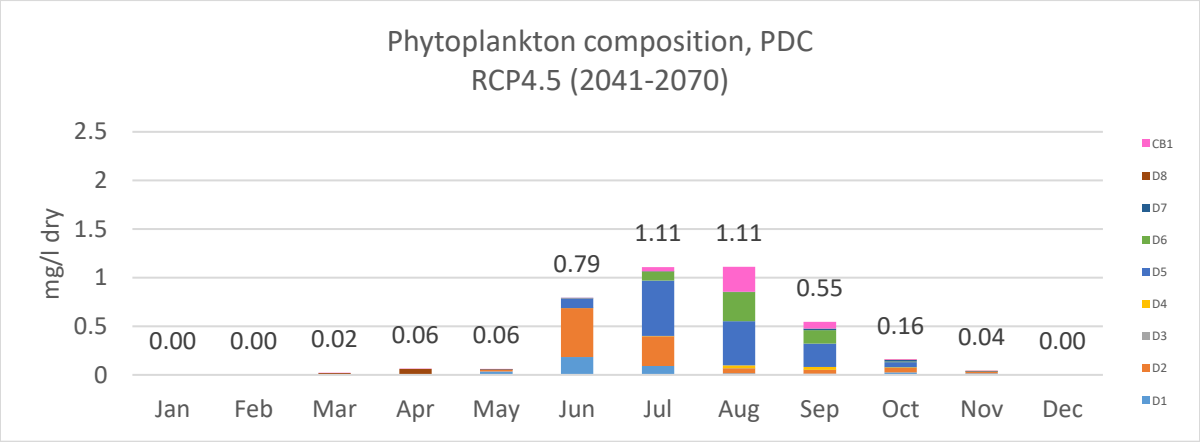

Fig. 4.30 - Abundance of different species of phytoplankton in the mid-term period (1983-2012) for RCP4.5.

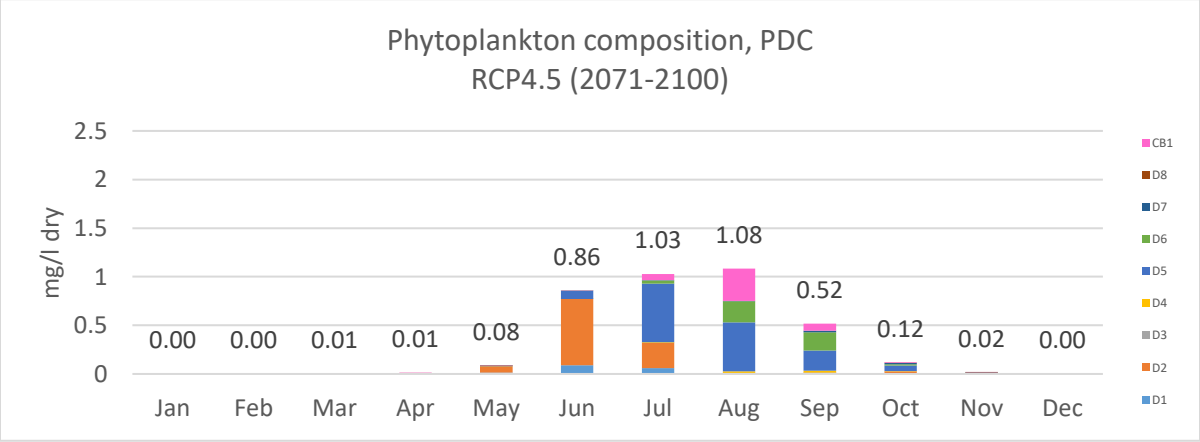

Fig. 4.31 - Abundance of different species of phytoplankton in the mid-term period (1983-2012) for RCP8.5.

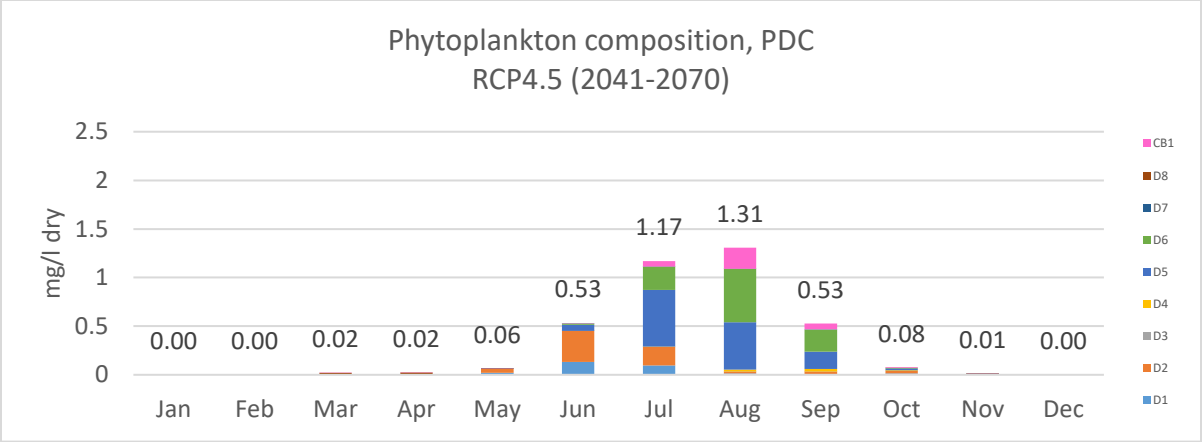

Fig. 4.32 - Abundance of different species of phytoplankton in the long-term period (2071-2100) for RCP4.5.

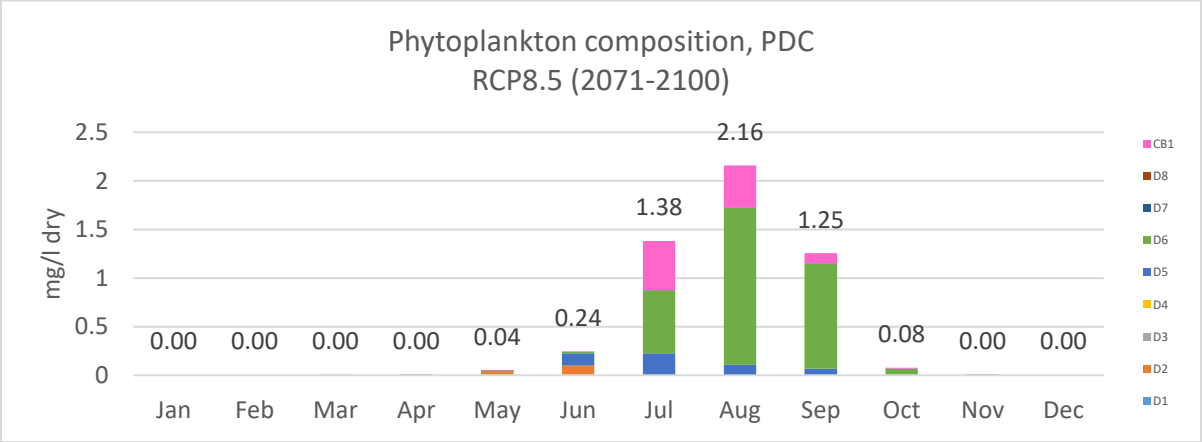

Fig. 4.33 - Abundance of different species of phytoplankton in the long-term period (2071-2100) for RCP8.5.

Finally, it is interesting to observe how the contribution of freshwater will impact on the water retention time of PDC. Fig. 4.34 suggests that contribution of freshwaters will decrease noticeably in summer, as expected from future projections of freshwater loadings described above. This changes increase substantially the water retention time of PDC (>20 days). However, it is important to recall that in this study the effects of the tide, sea level rise, and human infrastructure (i.e. MOSE project) have been neglected.

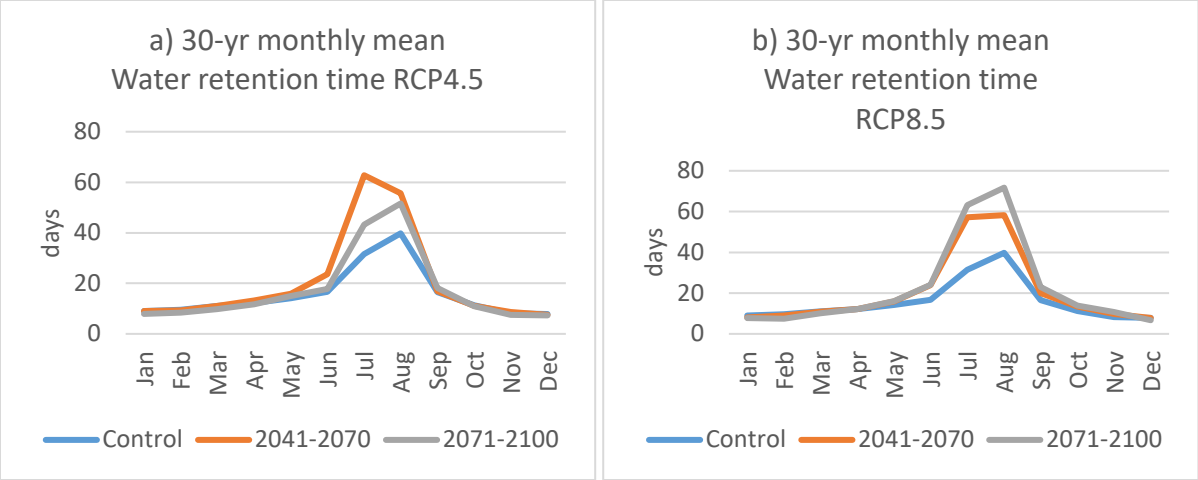

Fig. 4.34 - Differences in the 30-year monthly average water retention time between the control period (1983-2012), and mid-term (a) and long-term (b) projections (2071-2100) of RCP4.5 and RCP8.5.

4.4 Assessment of the variability of results

Different GCMs and RCMs have been developed by a number of research groups. Renowned examples of research groups working with GCM/RCM scenarios are the Danish Meteorological Institute (DMI), the Swedish Meteorological and Hydrological Institute (SMHI), the Met Office Hadley Centre (MOHC), and Euro-Mediterranean Center on Climate Change (CMCC). In this study, an ensemble of ten different climate scenarios and two emission trajectories were adopted, as described in Section 3.1. The motivation behind the use of multiple models in climate change research is to cover different sources of uncertainties. Moreover, reducing the model ensemble one also reduces the information about the uncertainty in the projections and the ensembles (Wilcke and Bärring 2016). The application of an ensemble of climate scenarios provides a spectrum of possible outcomes related to the effects of climate change on the ZRB and PDC, and the basis for further studies on the uncertainty that can be generated from the application of different climate scenarios. To analyse the variability of parameters, the median and the interquartile and interdecile ranges for each month of the 30-year averages have been analysed. Finally, as the bias correction has been calibrated for a period of 20-years, also the control period shows differences between scenarios. This is the result of

the different length of the period (30 years). This indicates that differences among GCM/RCM scenarios are marked even for present periods, and not only for future periods. This section follows the structure of the modelling approach. First, climate variability is described. Second, effects of climate variability on the freshwater discharge and nutrient loadings from the ZRB are discussed. Finally, variability of biological and physico-chemical parameters of PDC are illustrated.

Climate

Fig. 4.33 shows the variability of temperature for different time periods and RCPs. It is possible to observe that temperature variability is not wide and future projections have all the same seasonality. All climate scenarios project the same temperature over the year during the control period (A). The biggest differences are shown in RCP 8.5 where one climate scenarios (GCM/RCM 5) projects lower temperatures in spring and higher temperatures in autumn-winter. The interquartile and interdecile never move away from the median value. Additional details on climate projections can be found in Appendix C.

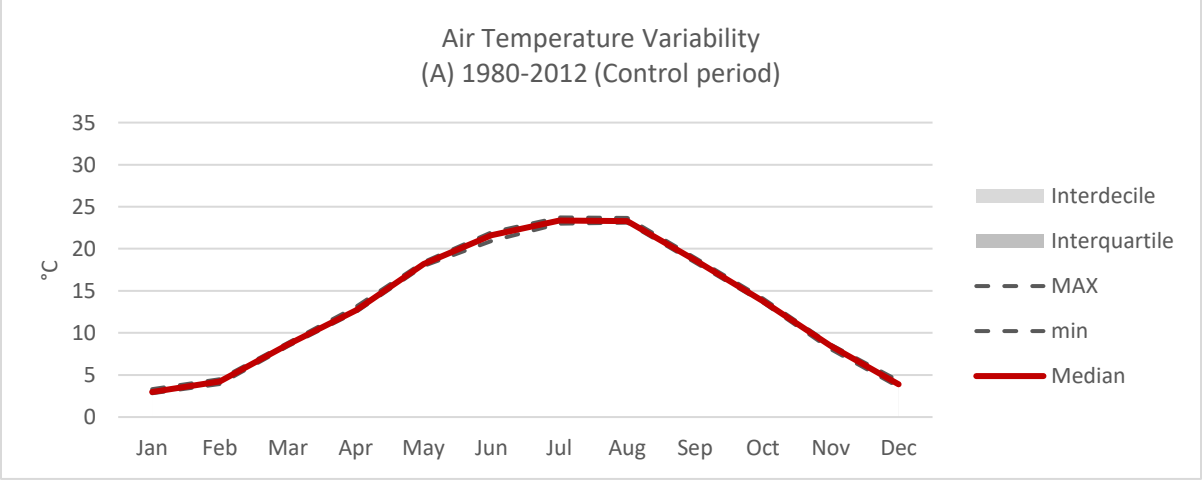

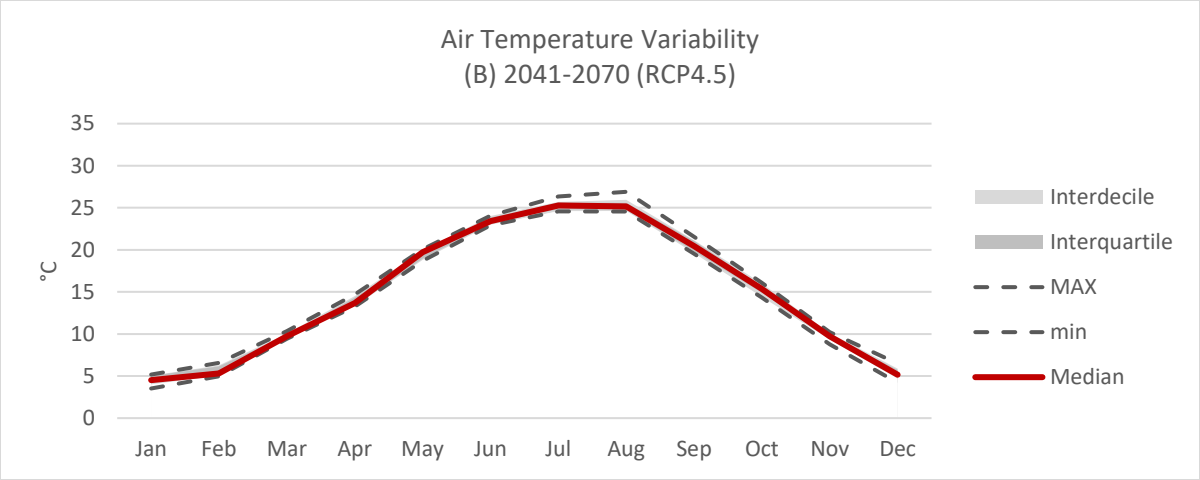
Air Temperature Variability
(B) 2041-2070 (RCP4.5)
35
30
25
20
15
10
5
0
°C
Jan
Feb
Mar
Apr
May
Jun
Jul
Aug
Sep
Oct
Nov
Dec
Interdecile
Interquartile
MAX
min
Median

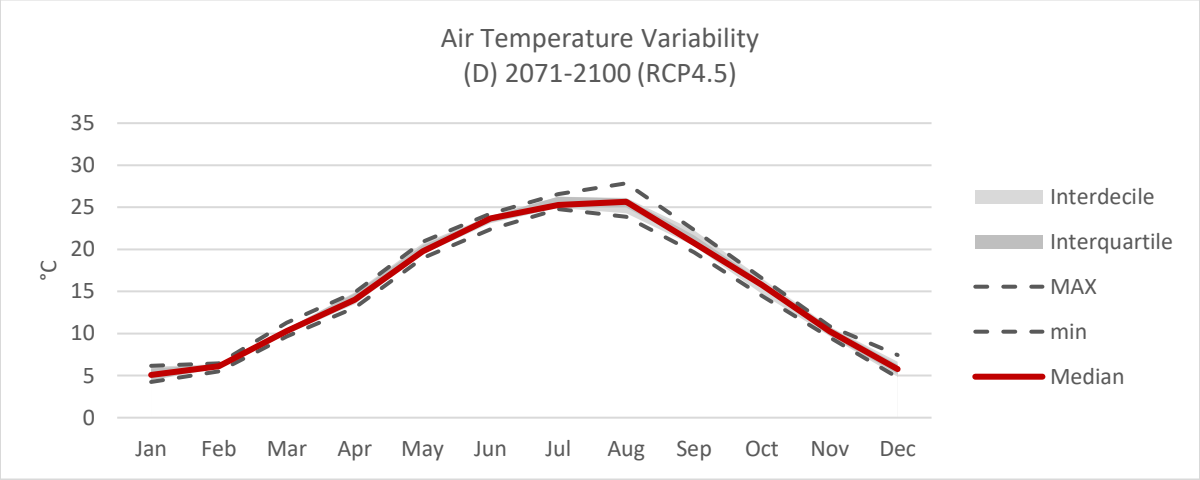
Air Temperature Variability
(D) 2071-2100 (RCP4.5)
35
30
25
20
15
10
5
0
°C
Jan
Feb
Mar
Apr
May
Jun
Jul
Aug
Sep
Oct
Nov
Dec
Interdecile
Interquartile
MAX
min
Median

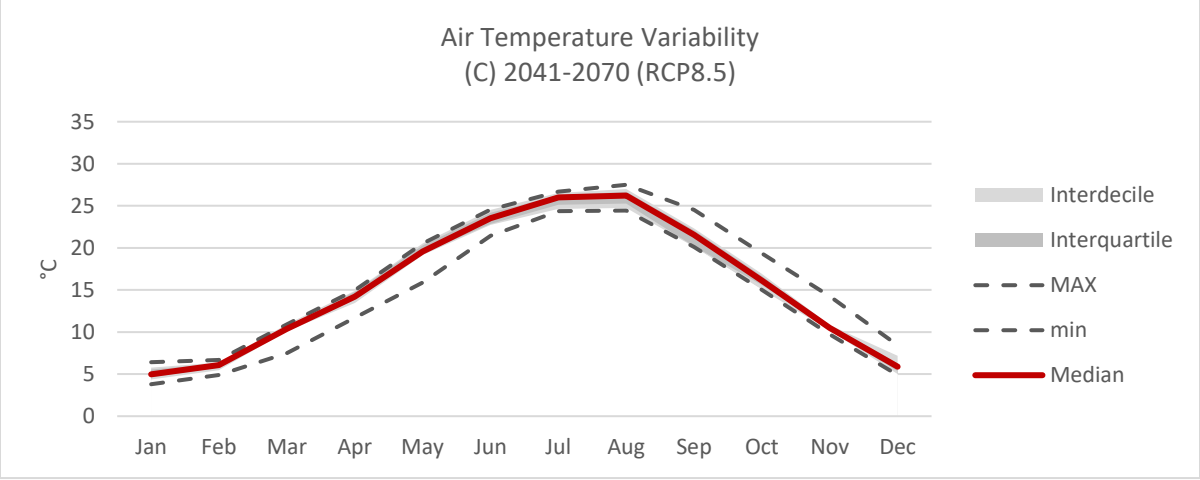
Air Temperature Variability
(C) 2041-2070 (RCP8.5)
35
30
25
20
15
10
5
0
°C
Jan
Feb
Mar
Apr
May
Jun
Jul
Aug
Sep
Oct
Nov
Dec
Interdecile
Interquartile
MAX
min
Median

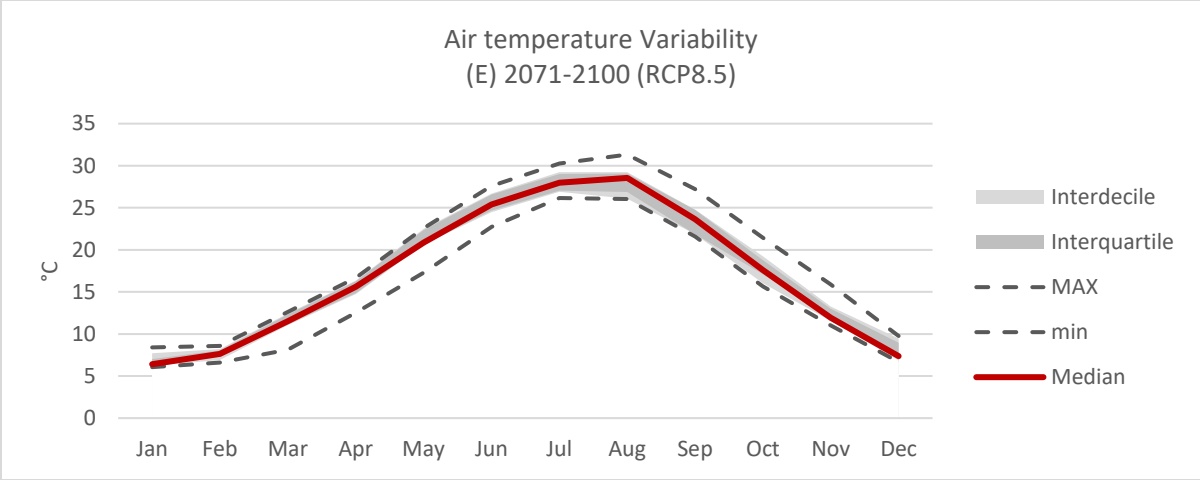

Fig. 4.35 – Variability of air temperature within the GCM/RCM ensemble adopted in the study. (A) Control period (B) RCP4.5 – 2041-2070, (C) RCP4.5 2071-2100, (D) RCP8.5 – 2041-2070 (E) RCP8.5 2071-2100.

Differently, precipitation features a more marked variability in all scenarios shown in Fig. 4.36. It is important to note the increase of variability along the century. All 10 GCMs/RCMs generate very similar statistics for the control period, while they provide different outcomes along the century, especially in the winter period. This validates the widely recognized fact that climate change will increase the variability and the uncertainty related to climate and weather events in the future (Thornton et al. 2014). However, it is possible to observe that the interquartile range (the middle 50% of monthly values) are very close to each other and only the MAX and min monthly values of the ensemble differ noticeably.

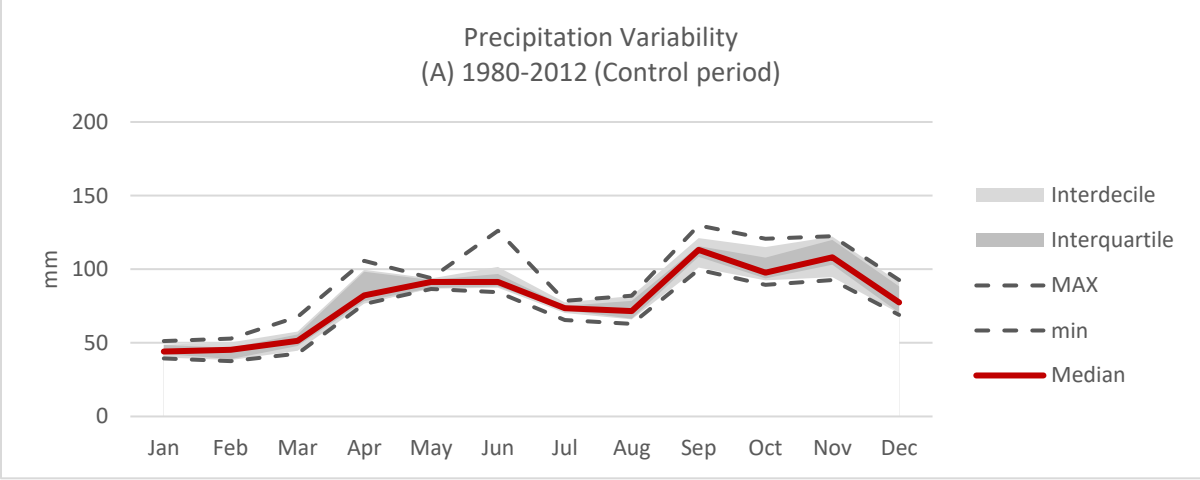

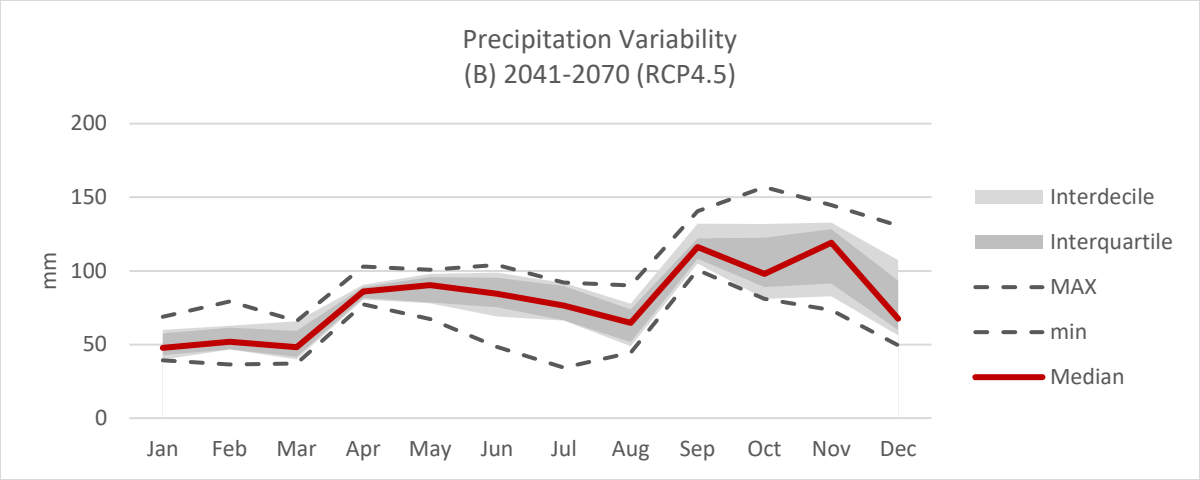
Precipitation Variability
(B) 2041-2070 (RCP4.5)
200
150
100
50
0
mm
Jan
Feb
Mar
Apr
May
Jun
Jul
Aug
Sep
Oct
Nov
Dec
Interdecile
Interquartile
MAX
min
Median

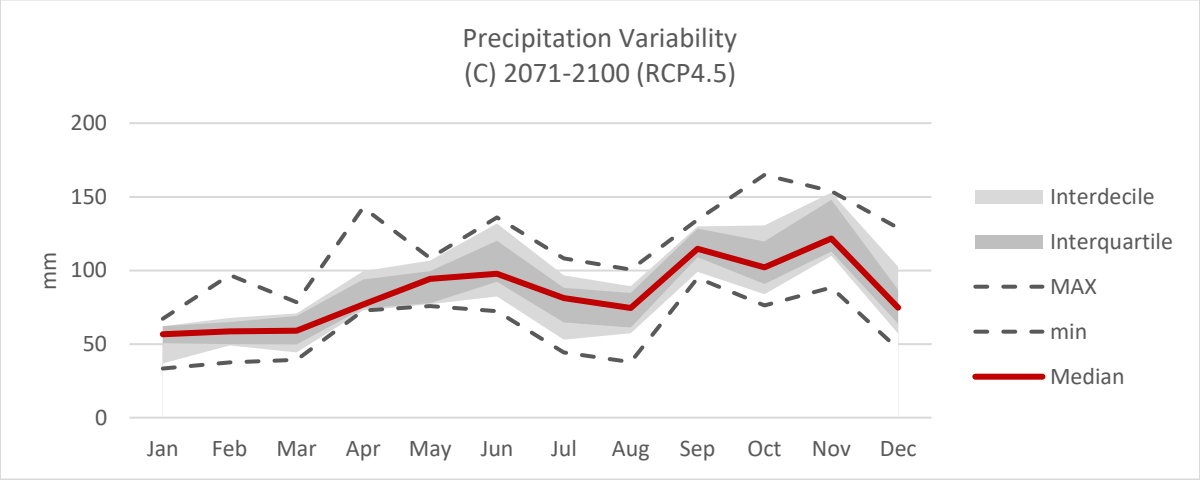
Precipitation Variability
(C) 2071-2100 (RCP4.5)
200
150
100
50
0
mm
Jan
Feb
Mar
Apr
May
Jun
Jul
Aug
Sep
Oct
Nov
Dec
Interdecile
Interquartile
MAX
min
Median

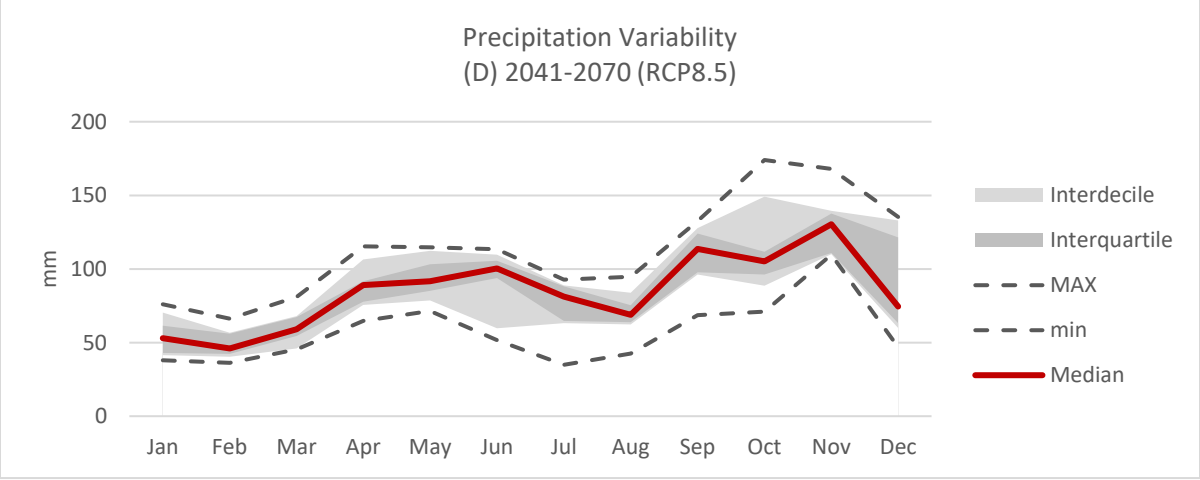
Precipitation Variability
(D) 2041-2070 (RCP8.5)
200
150
100
50
0
mm
Jan
Feb
Mar
Apr
May
Jun
Jul
Aug
Sep
Oct
Nov
Dec
Interdecile
Interquartile
MAX
min
Median

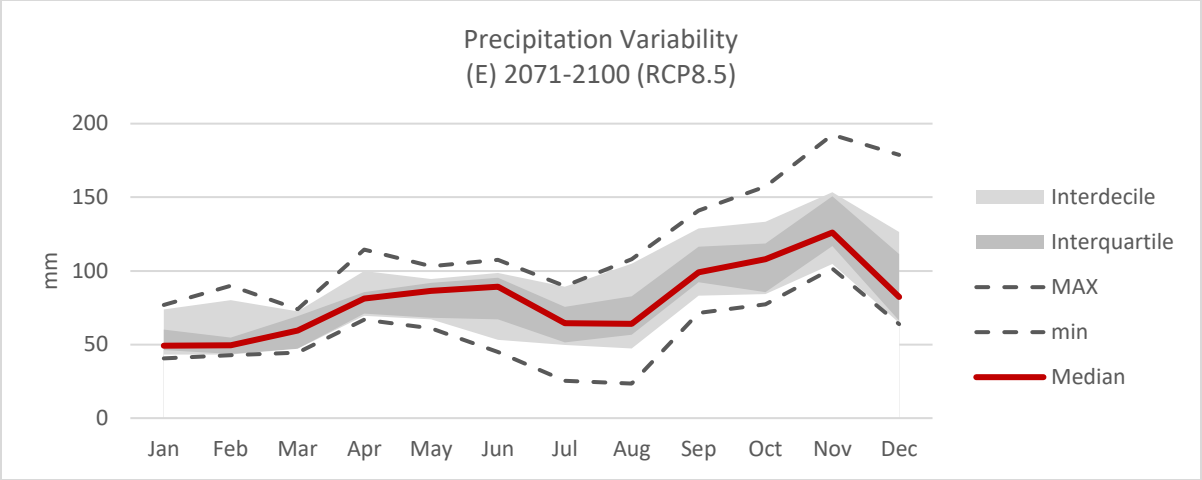

Fig. 4.36 - Variability of precipitation within the GCM/RCM ensemble adopted in the study. (A) Control period, (B) RCP4.5 – 2041-2070, (C) RCP4.5 2071-2100, (D) RCP8.5 – 2041-2070 (E) RCP8.5 2071-2100.

Hydrology and nutrient loadings of the ZRB

Hydrology of ZRB is influenced by changes in climate conditions. As a result, nutrient loadings in the Zero river are also affected. Here, variability of water flow-rate and nutrient loadings are analysed. The water flow-rate in the current period shows a low degree of variability, with GCM/RCMs projection in agreement with each other (Fig. 4.37). RCP4.5 shows the highest degree of variability in water-flow for both medium- and long-term periods. RCP8.5 show a high level of agreement between climate scenarios. The interquartile and interdecile range overlap each other and do not differ significantly from the median.

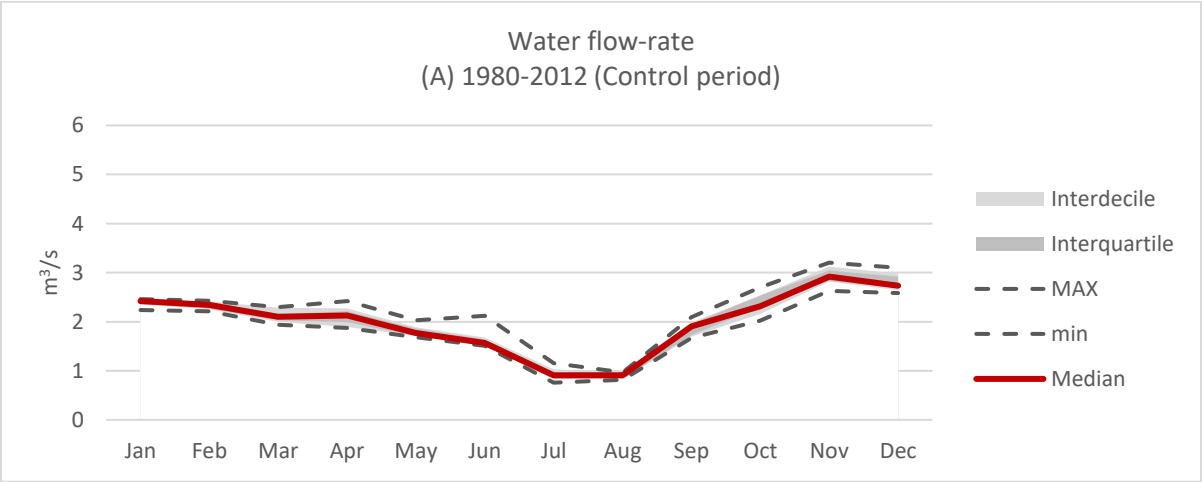

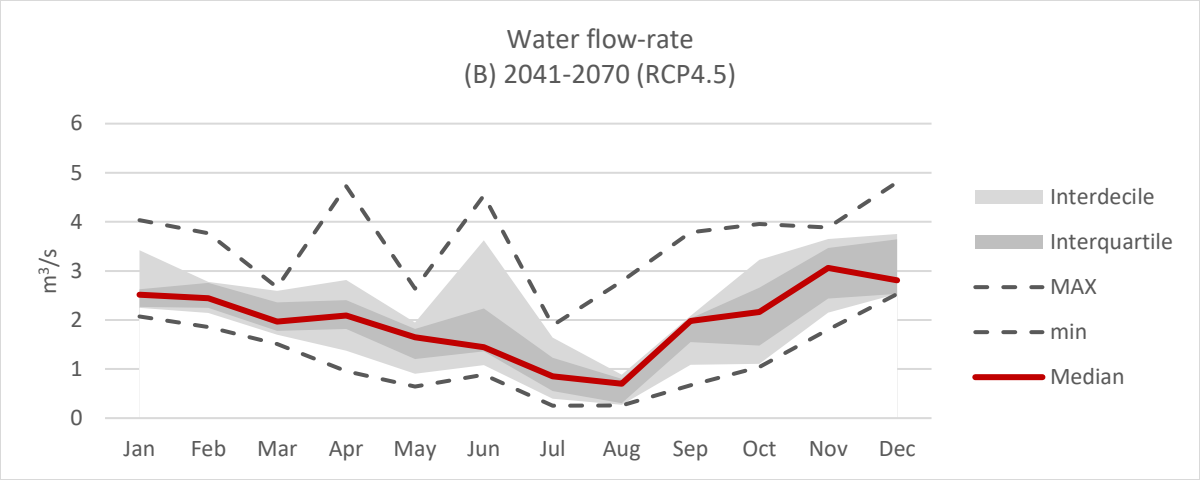
Water flow-rate
(B) 2041-2070 (RCP4.5)
m³/s
0
1
2
3
4
5
6
Jan
Feb
Mar
Apr
May
Jun
Jul
Aug
Sep
Oct
Nov
Dec
Interdecile
Interquartile
MAX
min
Median

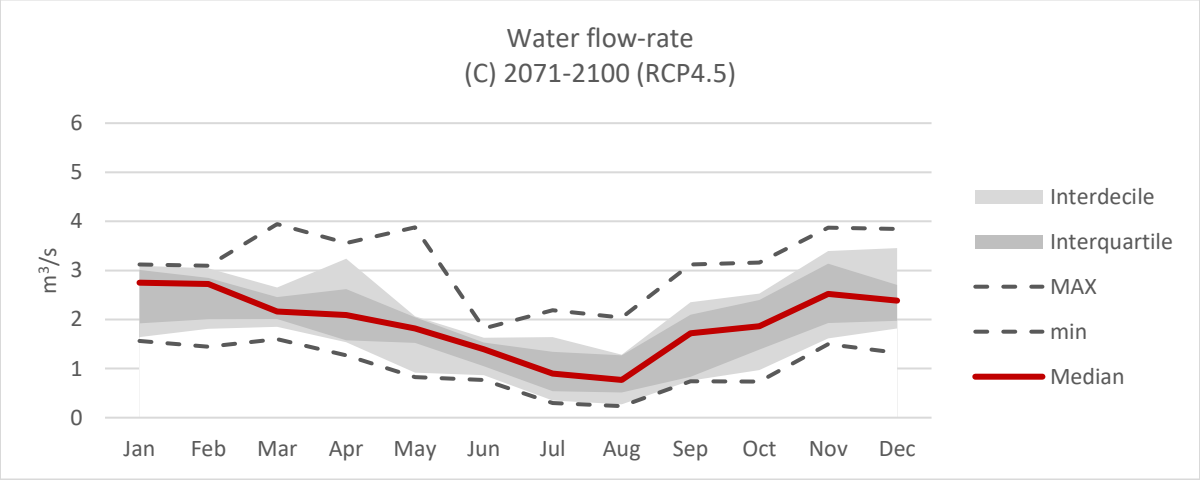
Water flow-rate
(C) 2071-2100 (RCP4.5)
m³/s
0
1
2
3
4
5
6
Jan
Feb
Mar
Apr
May
Jun
Jul
Aug
Sep
Oct
Nov
Dec
Interdecile
Interquartile
MAX
min
Median

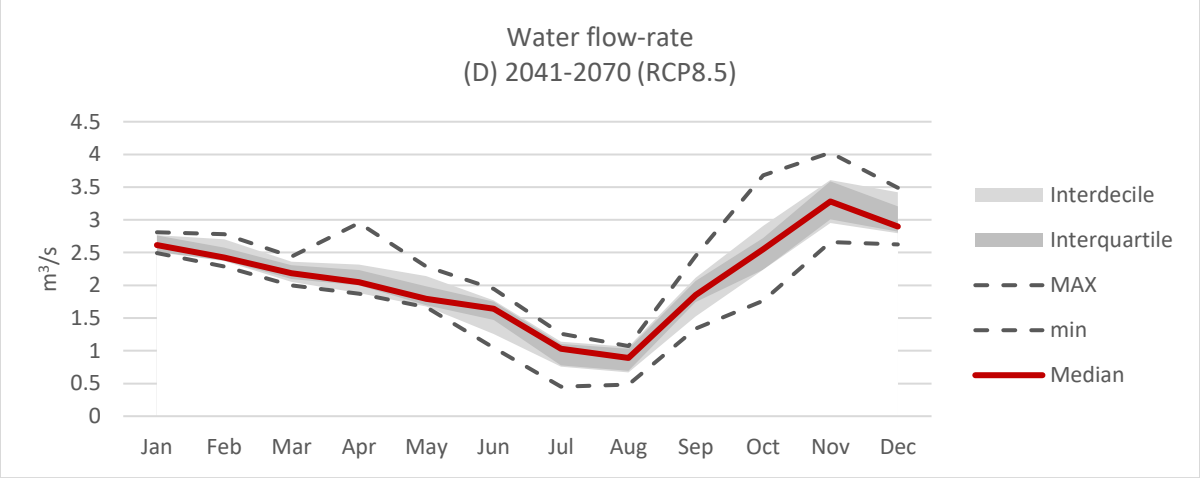
Water flow-rate
(D) 2041-2070 (RCP8.5)
m³/s
0
0.5
1
1.5
2
2.5
3
3.5
4
4.5
Jan
Feb
Mar
Apr
May
Jun
Jul
Aug
Sep
Oct
Nov
Dec
Interdecile
Interquartile
MAX
min
Median

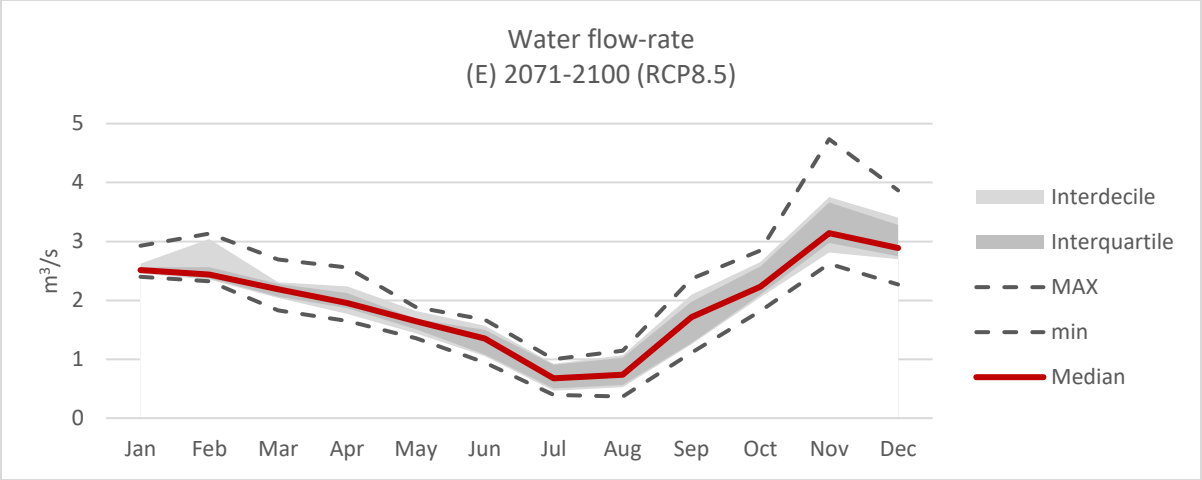

Fig. 4.37 - Variability of water flow-rate within the GCM/RCM ensemble adopted in the study. (A) Control period, (B) RCP4.5 – 2041-2070, (C) RCP4.5 2071-2100, (D) RCP8.5 – 2041-2070 (E) RCP8.5 2071-2100.

Variability of water flow-rate is reflected in nutrient loadings, especially of nitrate (Fig. 4.38). The control period does not show any significant variability both in magnitude and seasonality. Variability increases noticeably in the RCP4.5 scenarios, with the highest differences between models in spring and winter. For example, the MAX value of the month reaches 20 t/month, while the min value is less than 5 t/month. However, the interquartile range does not differ significantly from the median value, with the only exceptions of November in the mid-term period (Fig. 4.38E). RCP8.5 scenarios show a significantly less marked variability, with interquartile and interdecile completely overlapping each other and not differing noticeably from the median monthly values.

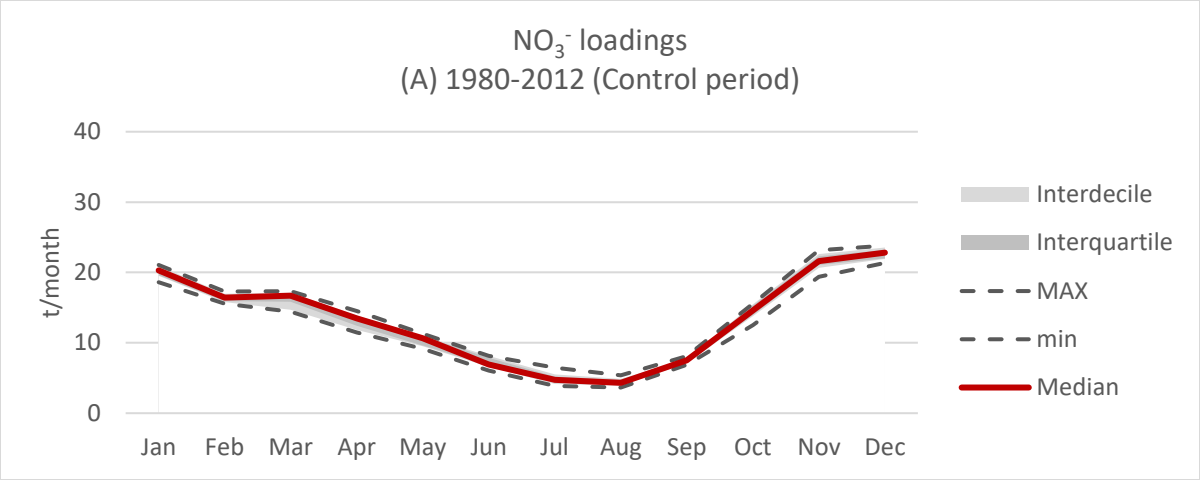
NO_3^- loadings
(A) 1980-2012 (Control period)
t/month
40
30
20
10
0
Jan Feb Mar Apr May Jun Jul Aug Sep Oct Nov Dec
Interdecile
Interquartile
MAX
min
Median

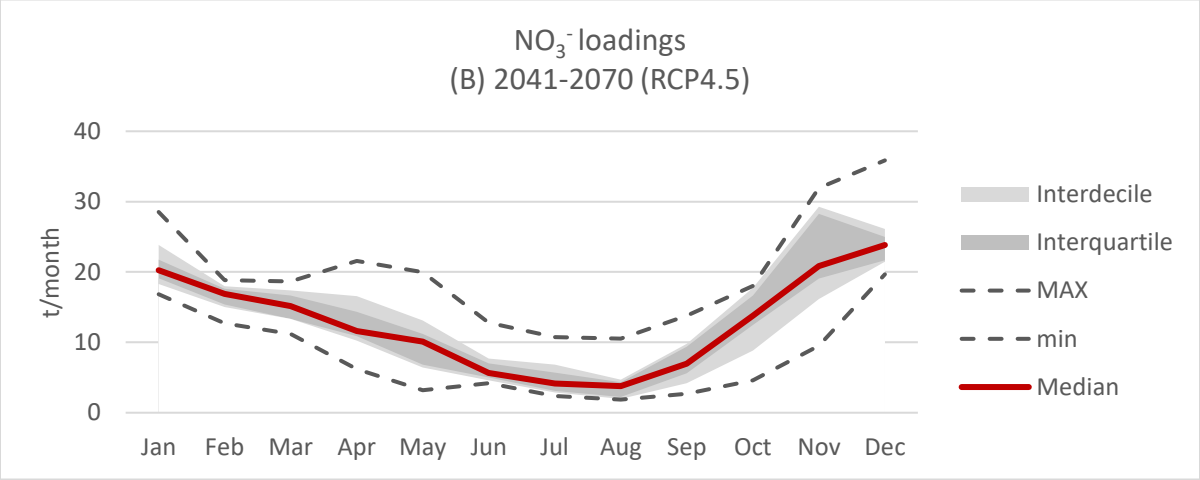
NO_3^- loadings
(B) 2041-2070 (RCP4.5)
t/month
40
30
20
10
0
Jan Feb Mar Apr May Jun Jul Aug Sep Oct Nov Dec
Interdecile
Interquartile
MAX
min
Median

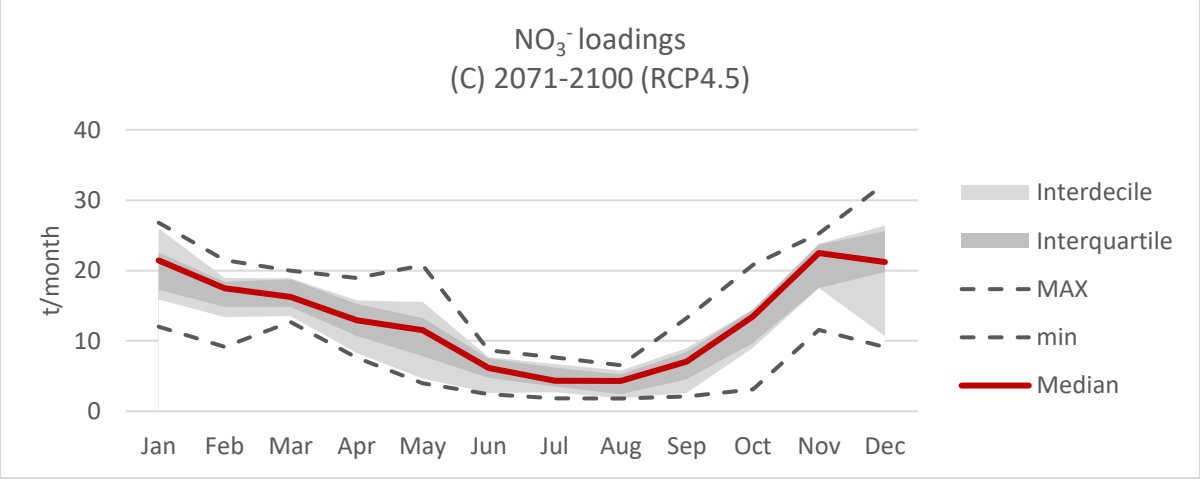
NO_3^- loadings
(C) 2071-2100 (RCP4.5)
t/month
40
30
20
10
0
Jan Feb Mar Apr May Jun Jul Aug Sep Oct Nov Dec
Interdecile
Interquartile
MAX
min
Median

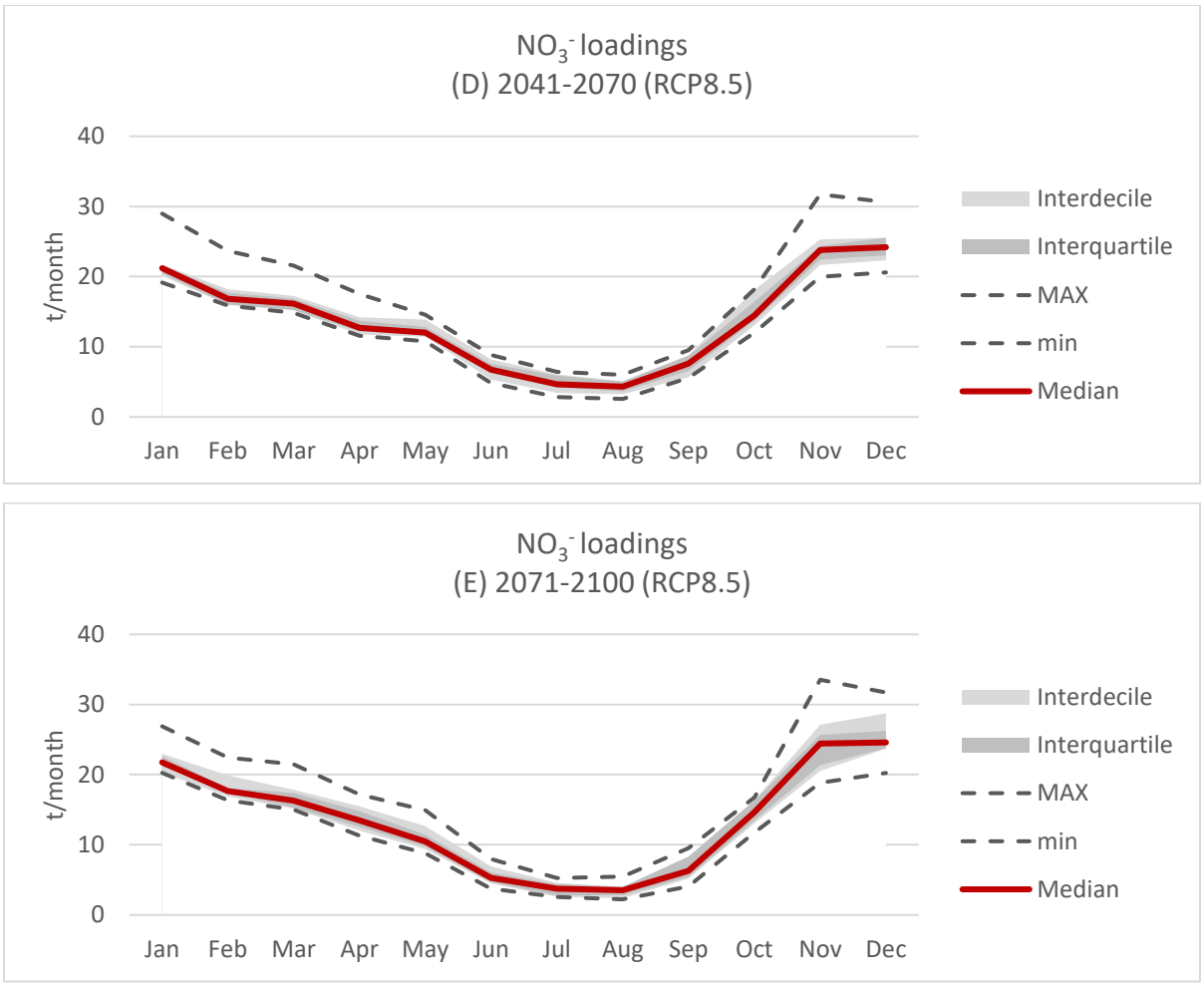

Fig. 4.38 - Variability of nitrate (NO_3^-) loadings within the GCM/RCM ensemble adopted in the study. (A) Control period, (B) RCP4.5 – 2041-2070, (C) RCP4.5 2071-2100, (D) RCP8.5 – 2041-2070 (E) RCP8.5 2071-2100.

Variability of ammonium over the modeled time period is marked for both RCP4.5 and RCP8.5 (Fig. 4.39). The mid-term scenario for the RCP4.5 features the highest degree of variability between models, especially in the months of April and May. 50% of the models (interquartile range) do not differ significantly from the median monthly value in every scenario. Differently, the interdecile range shows more marked differences.

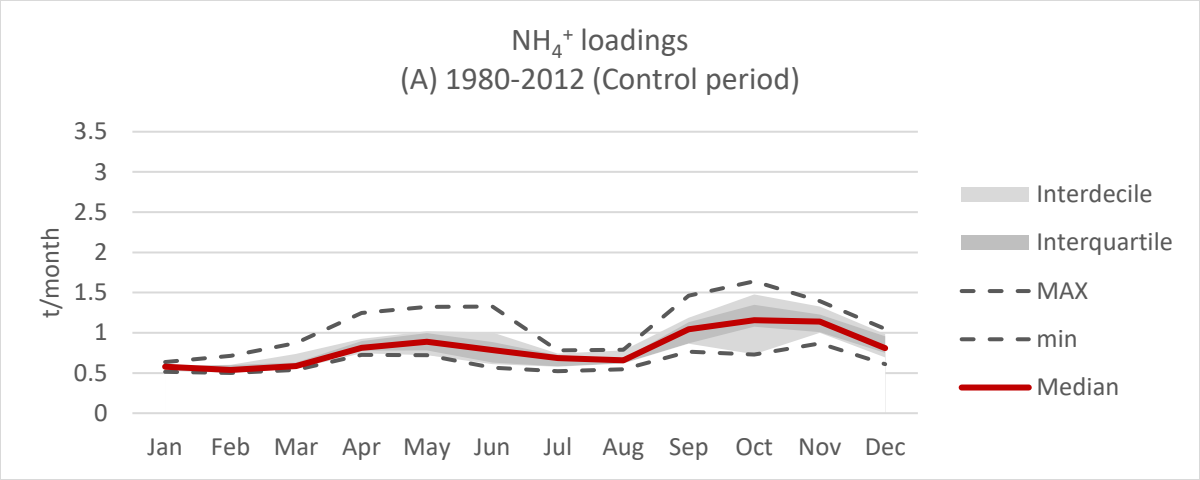
NH4+ loadings
(A) 1980-2012 (Control period)
t/month
3.5
3
2.5
2
1.5
1
0.5
0
Jan Feb Mar Apr May Jun Jul Aug Sep Oct Nov Dec
Interdecile
Interquartile
MAX
min
Median

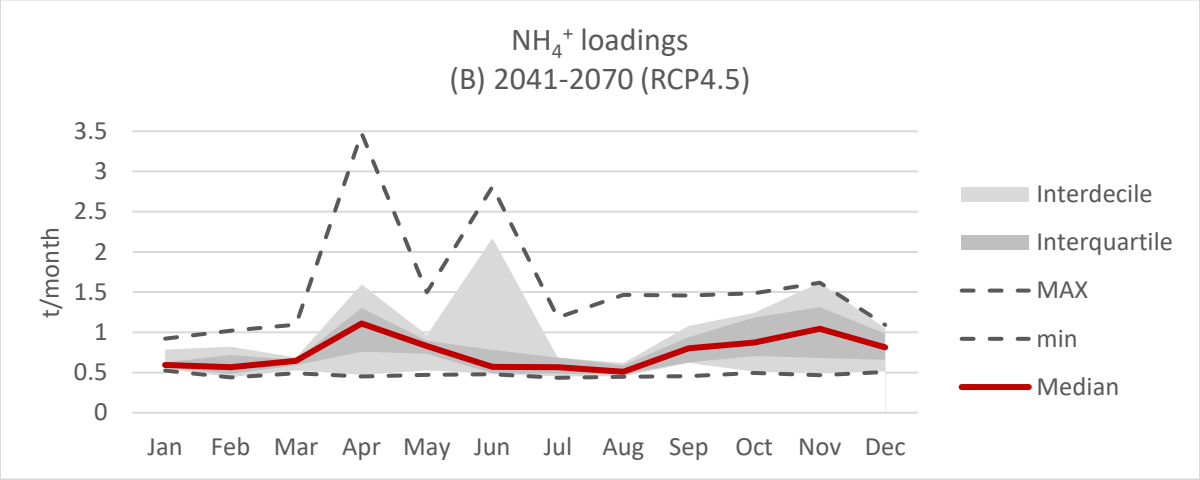
NH4+ loadings
(B) 2041-2070 (RCP4.5)
t/month
3.5
3
2.5
2
1.5
1
0.5
0
Jan Feb Mar Apr May Jun Jul Aug Sep Oct Nov Dec
Interdecile
Interquartile
MAX
min
Median

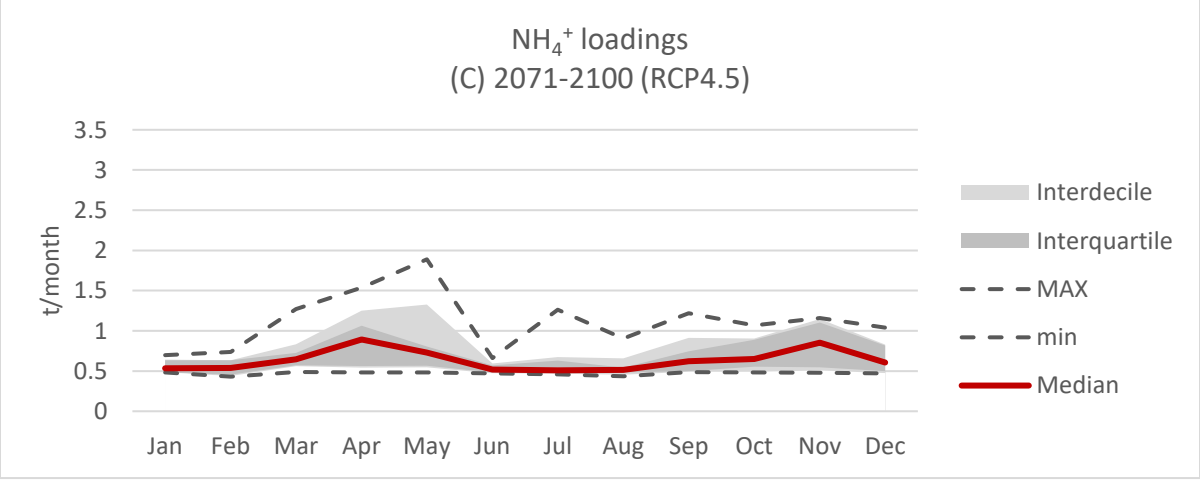
NH4+ loadings
(C) 2071-2100 (RCP4.5)
t/month
3.5
3
2.5
2
1.5
1
0.5
0
Jan Feb Mar Apr May Jun Jul Aug Sep Oct Nov Dec
Interdecile
Interquartile
MAX
min
Median

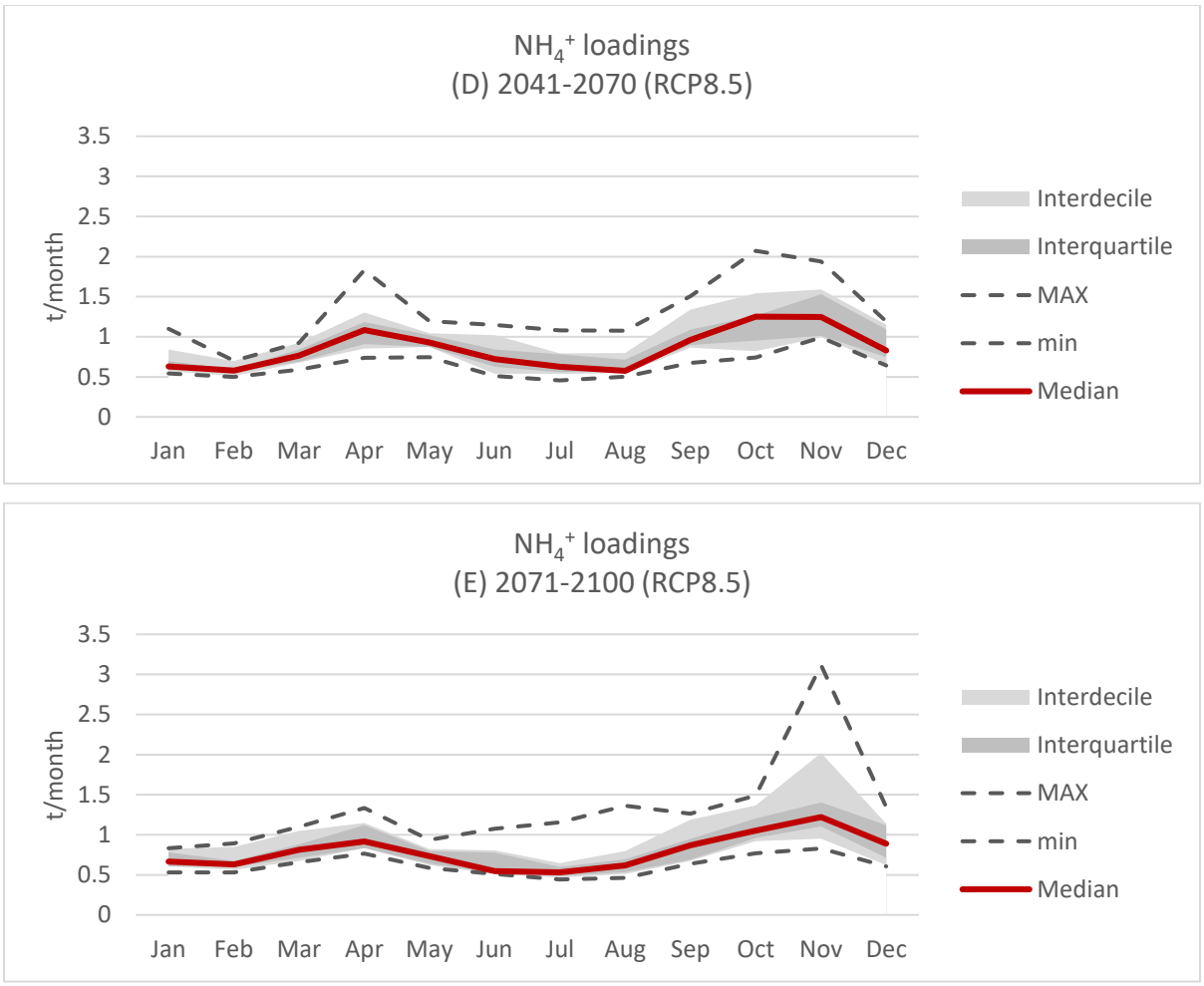

Fig. 4.39 - Variability of ammonium (NH_4^+) loadings within the GCM/RCM ensemble adopted in the study. (A) Control period, (B) RCP4.5 – 2041-2070, (C) RCP4.5 2071-2100, (D) RCP8.5 – 2041-2070 (E) RCP8.5 2071-2100.

Orthophosphate loadings show clear variability, especially in autumn and winter, the time of the year when loadings increase the most Fig. 4.40. Highest variabilities are observed in the RCP4.5 scenarios, where autumn and early-winter projections cover a wide range that goes from 0.5 to 3 t/month in the mid-term period, and from 0.5 to 4 t/month in the long-term period. As with the other nutrients, RCP8.5 scenarios show a less marked variability, even in winter and autumn. However, in this case interquartile and interdecile show noticeable variation from the median monthly value. Additional details can be found in Appendix D.

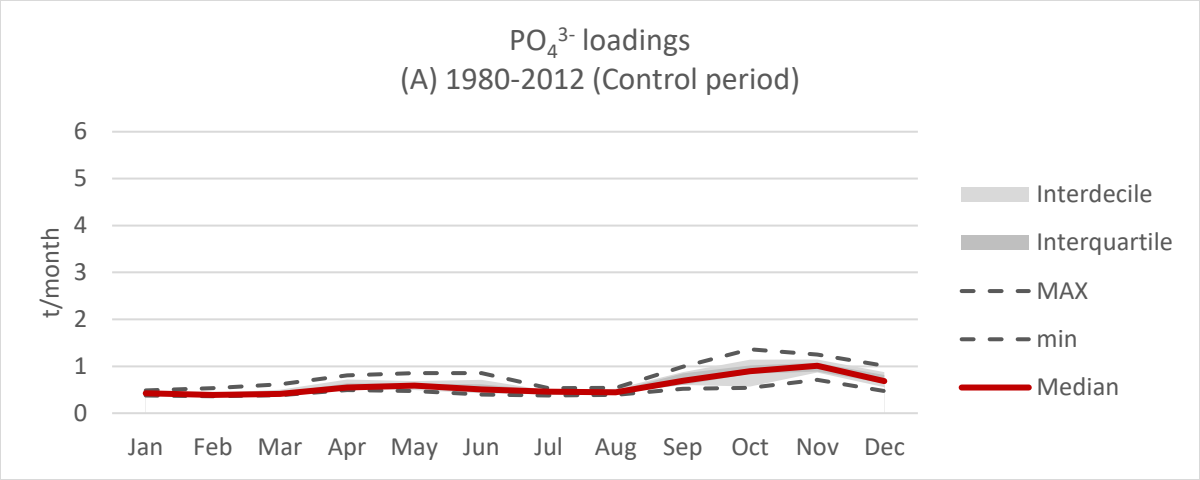
PO_4^{3-} loadings
(A) 1980-2012 (Control period)
t/month
0
1
2
3
4
5
6
Jan
Feb
Mar
Apr
May
Jun
Jul
Aug
Sep
Oct
Nov
Dec
Interdecile
Interquartile
MAX
min
Median

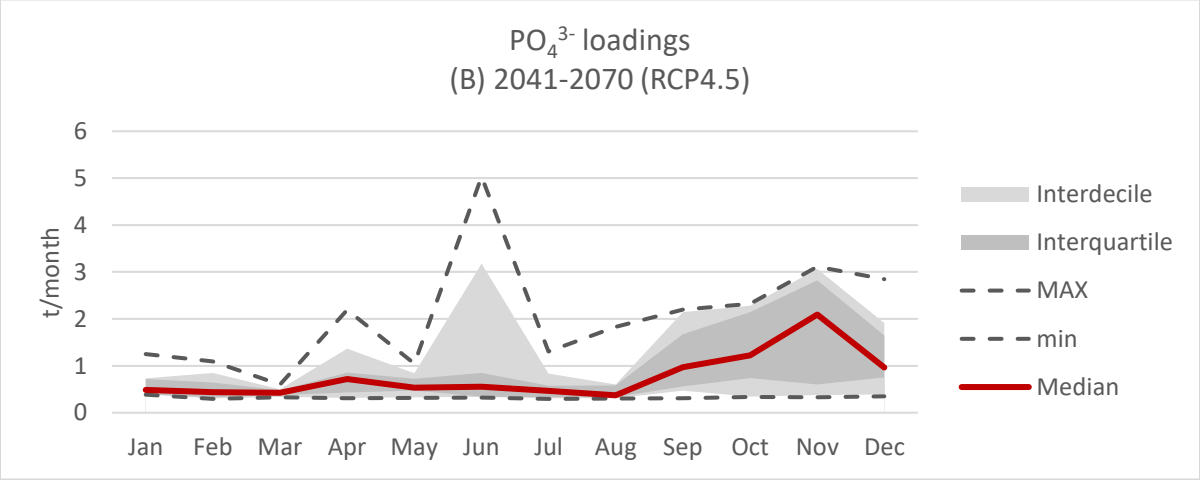
PO_4^{3-} loadings
(B) 2041-2070 (RCP4.5)
t/month
0
1
2
3
4
5
6
Jan
Feb
Mar
Apr
May
Jun
Jul
Aug
Sep
Oct
Nov
Dec
Interdecile
Interquartile
MAX
min
Median

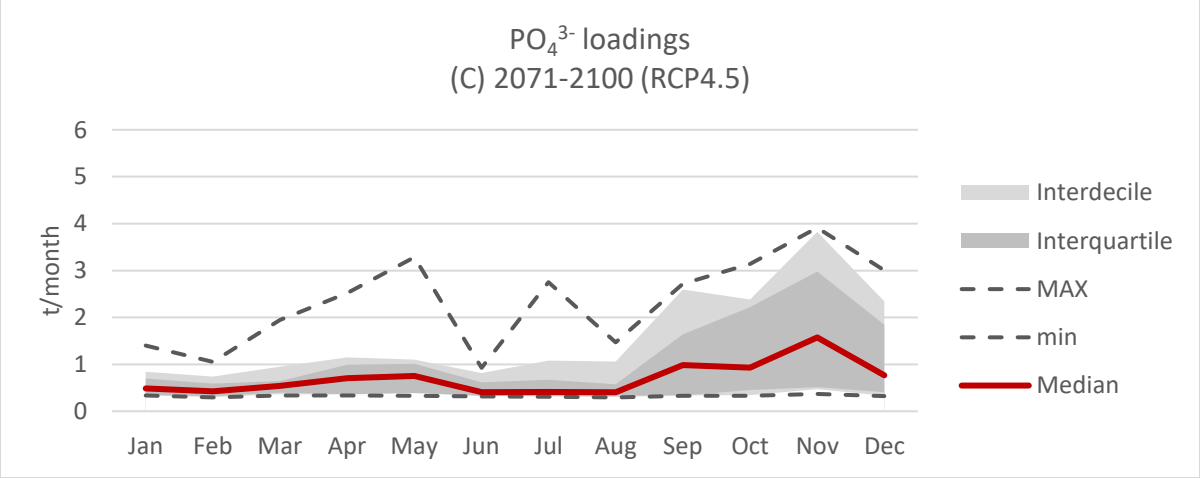
PO_4^{3-} loadings
(C) 2071-2100 (RCP4.5)
t/month
0
1
2
3
4
5
6
Jan
Feb
Mar
Apr
May
Jun
Jul
Aug
Sep
Oct
Nov
Dec
Interdecile
Interquartile
MAX
min
Median

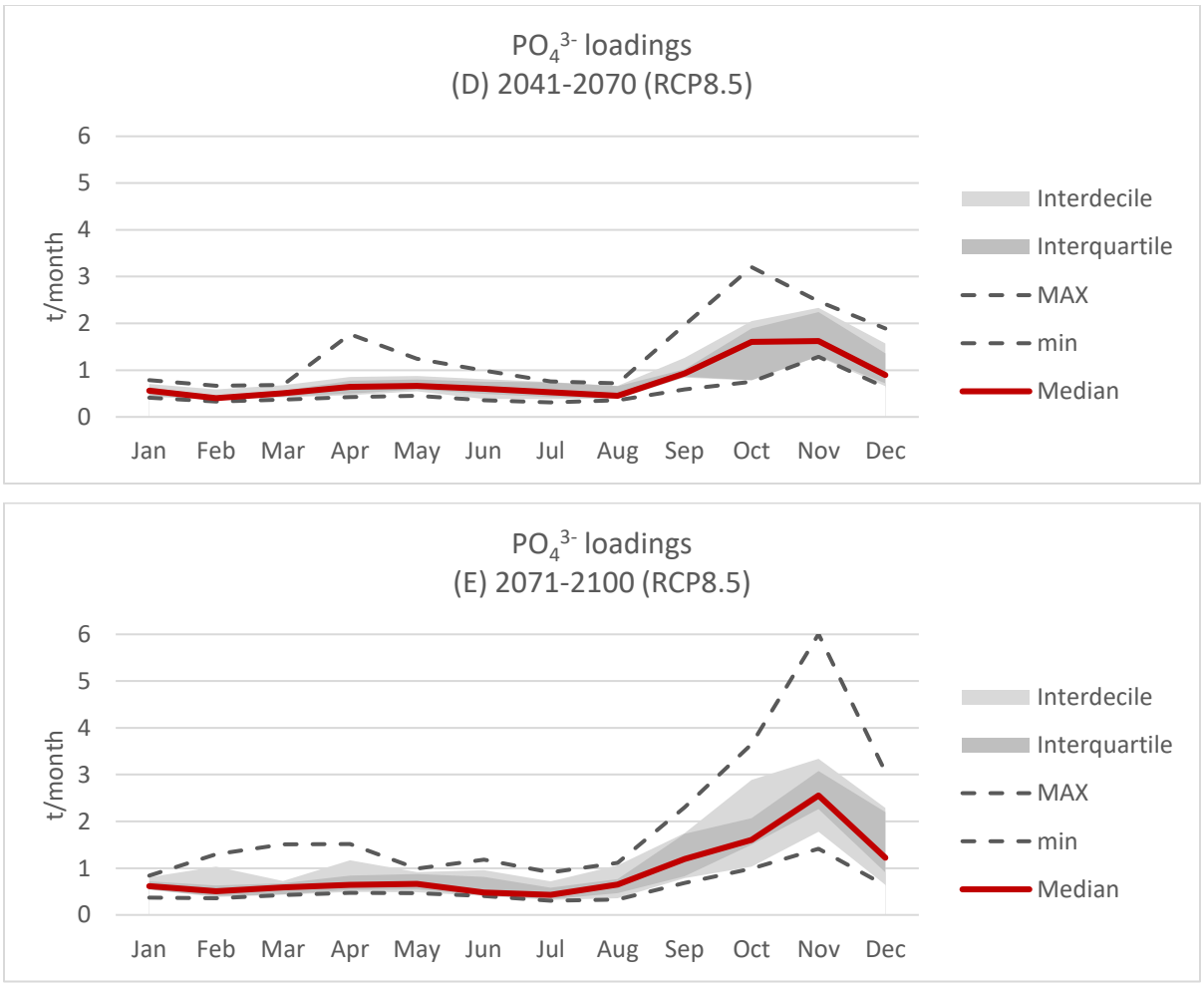

Fig. 4.40 - Variability of orthophosphate (PO_4^{3-}) loadings within the GCM/RCM ensemble adopted in the study. (A) Control period, (B) RCP4.5 – 2041-2070, (C) RCP4.5 2071-2100, (D) RCP8.5 – 2041-2070 (E) RCP8.5 2071-2100.

Physico-chemical and ecological parameters of PDC

Parameters of the AQUATOX model of PDC are subjected to the variability of SWAT outputs and the variability of climate scenarios (i.e. water temperature) (Fig. 4.41). Dissolved oxygen concentrations (DO) do not show any marked variability in simulated scenarios. Both magnitude and seasonality overlap each other, with the only exception of the month of August where minimum differences are shown.

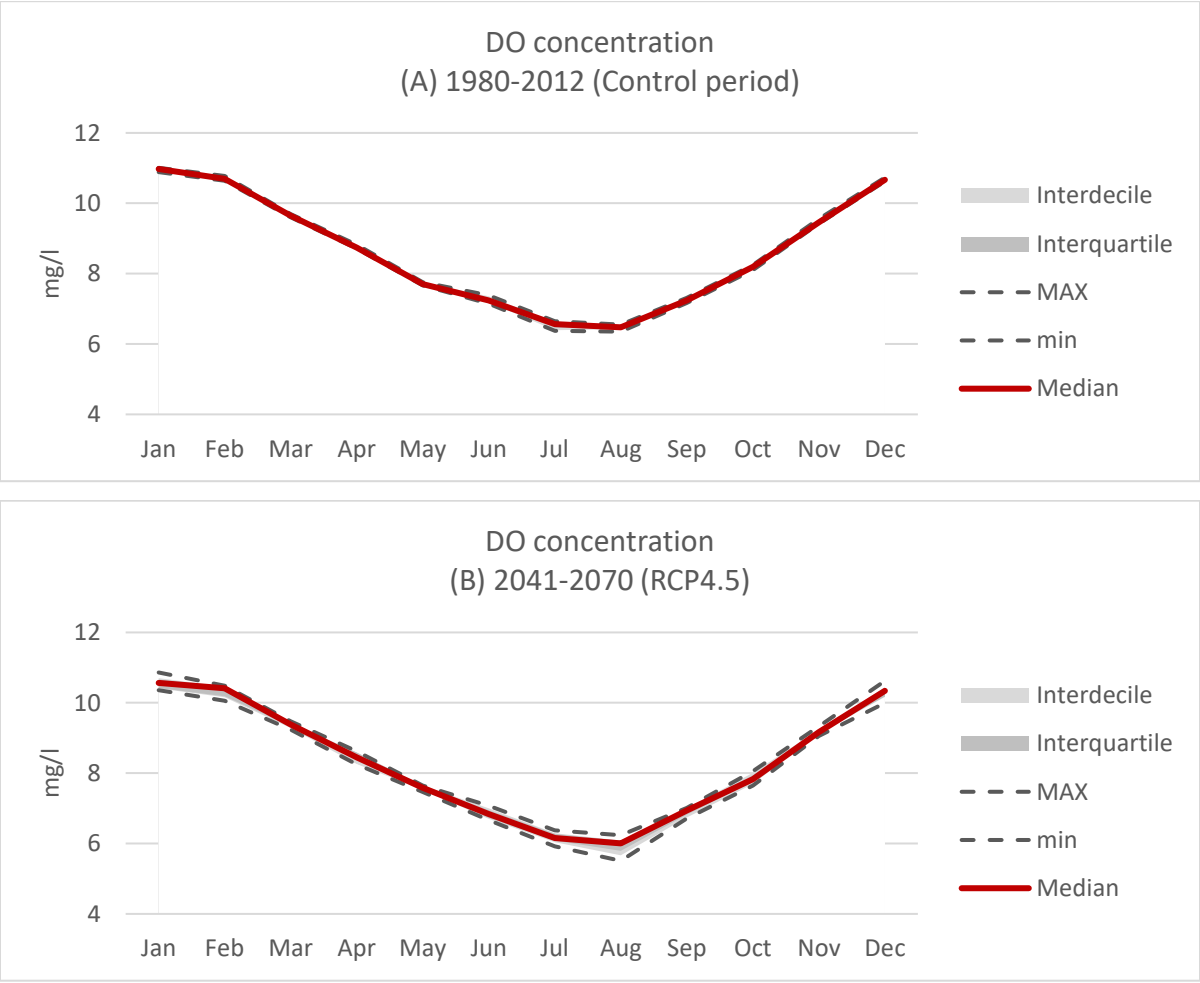

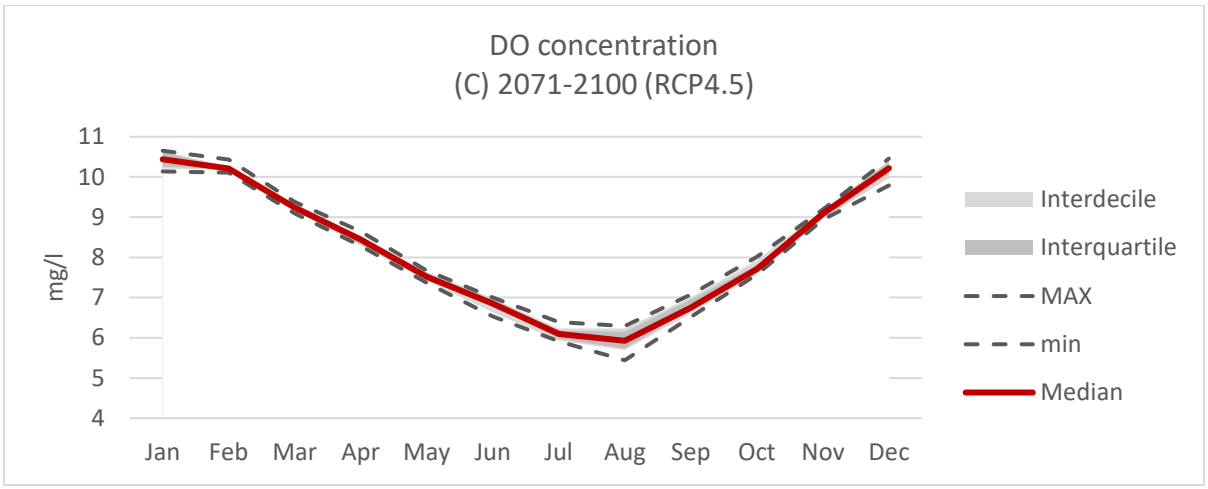

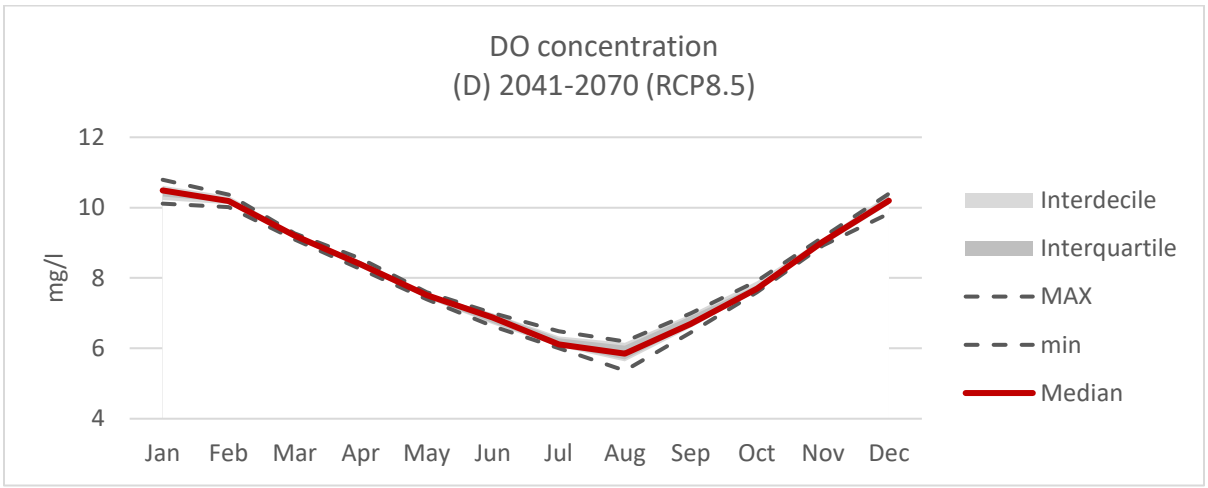

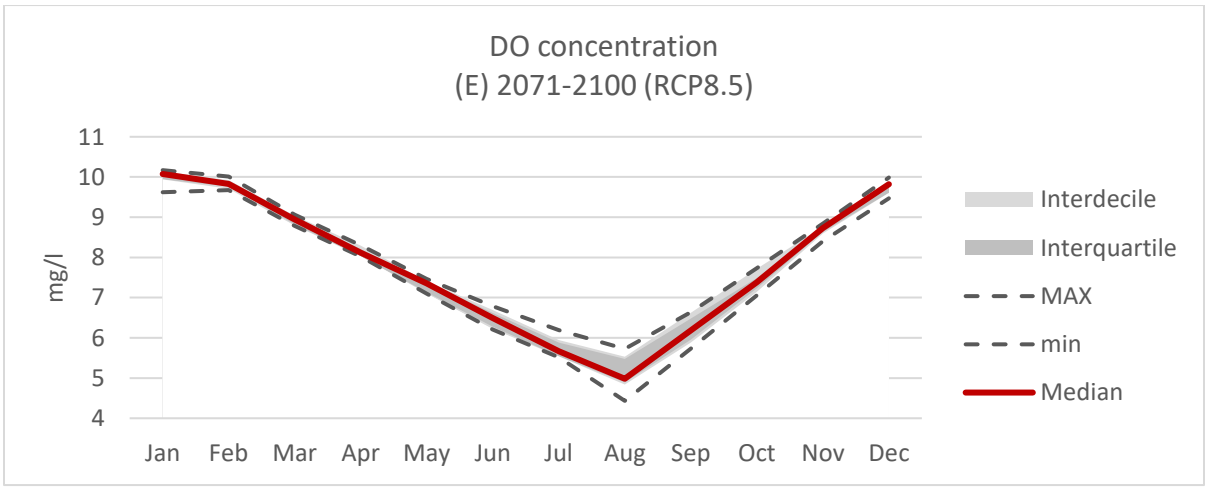

Fig. 4.41 - Variability of DO within the GCM/RCM ensemble adopted in the study. (A) Control period, (B) RCP4.5 – 2041-2070, (C) RCP4.5 2071-2100, (D) RCP8.5 – 2041-2070 (E) RCP8.5 2071-2100.

DIN concentrations reflect the low variability of nitrate loadings from the ZRB. All scenarios indicate low variability and a clear trend. The biggest differences can be observed in the RCP8.5 scenarios where the MAX value for each month differs noticeably from the 9 remaining values. It can be observed that no simulations project sensible changes in DIN concentrations over the 21st century.

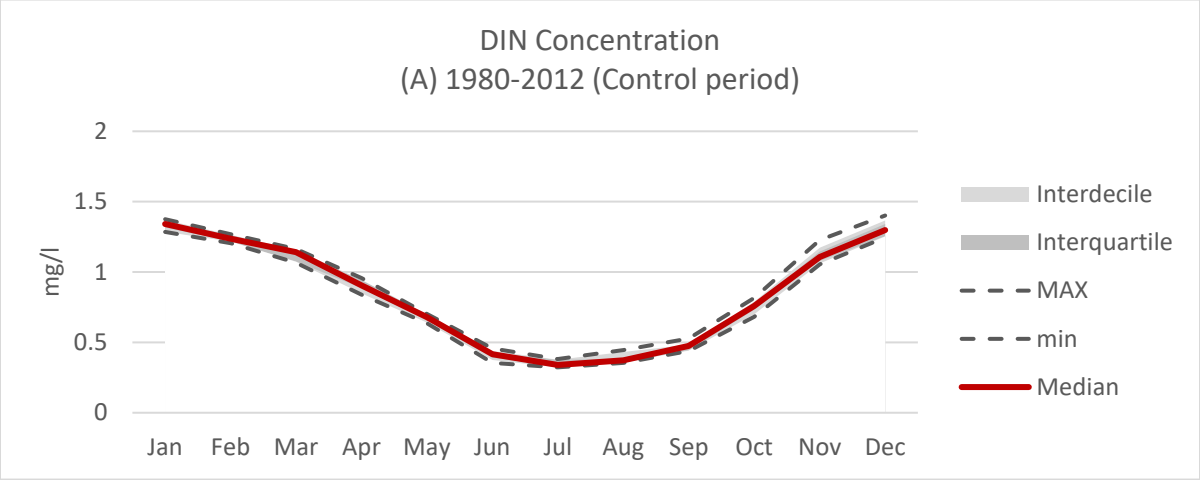

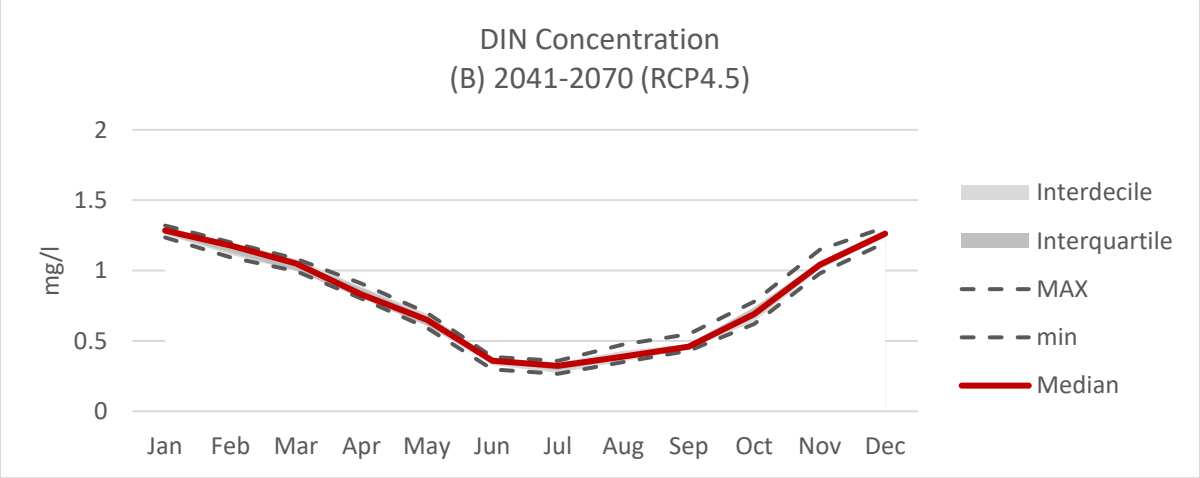

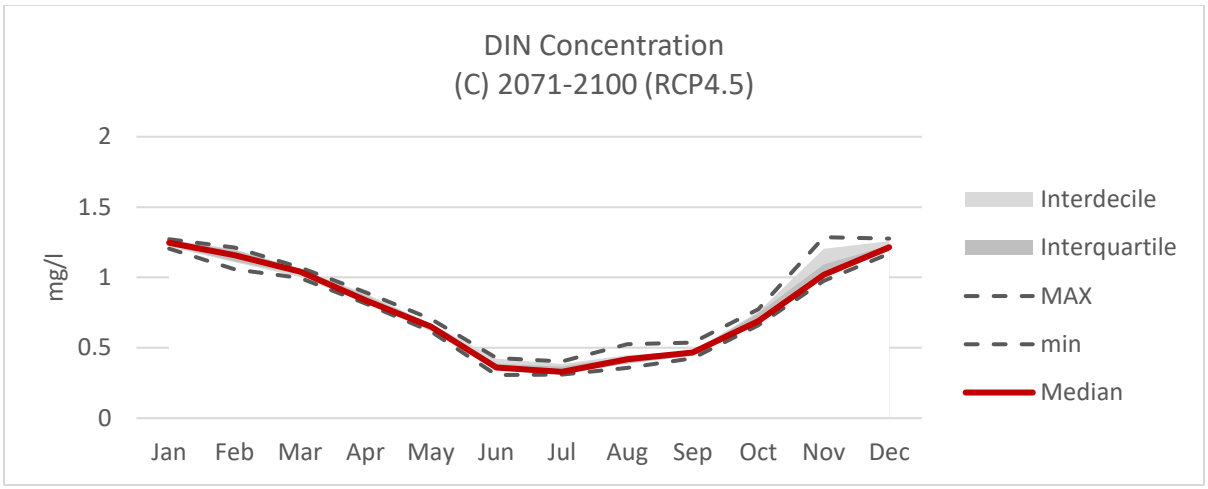

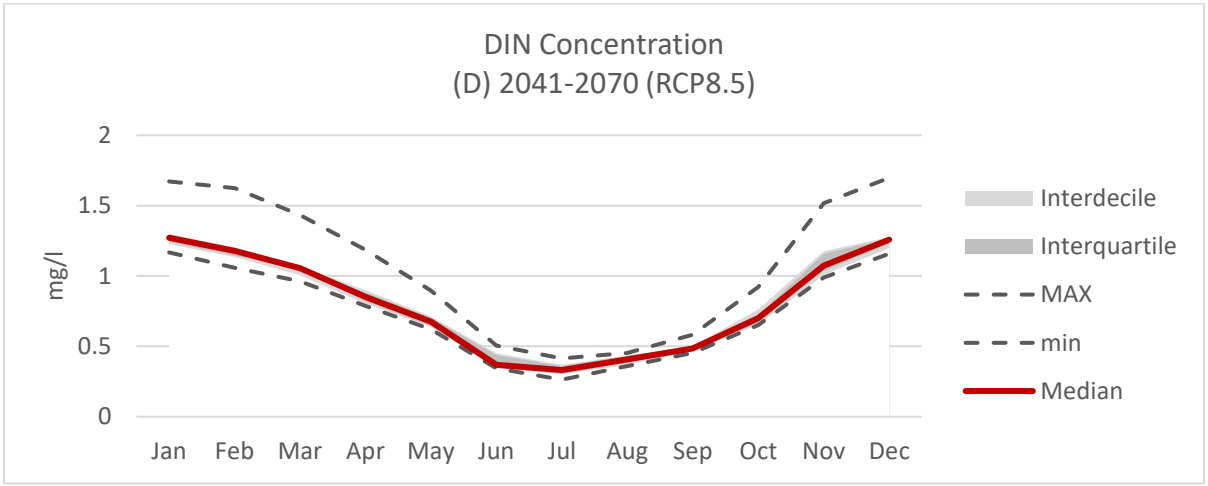

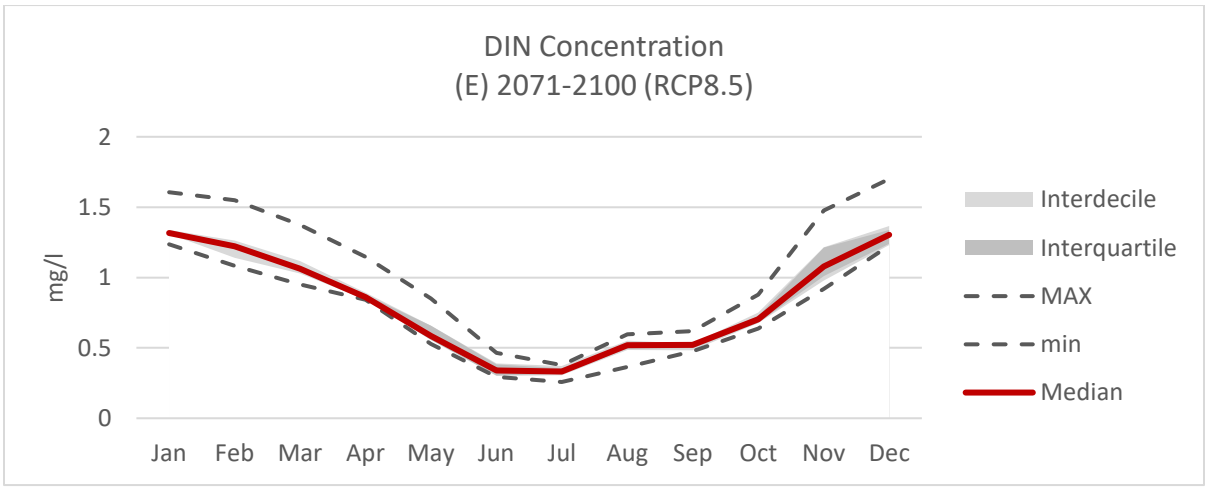

Fig. 4.42 - Variability of DIN within the GCM/RCM ensemble adopted in the study. (A) Control period, (B) RCP4.5 – 2041-2070, (C) RCP4.5 2071-2100, (D) RCP8.5 – 2041-2070 (E) RCP8.5 2071-2100.

DIP concentrations show marked variability, which reflect the variability of phosphate loadings from the ZRB. In the control period, all simulations are in good agreement with each other, with only slight variations in winter, especially in December. The highest variability can be observed in the months of September, October and November. This is due to the different magnitude of loadings simulated by SWAT.

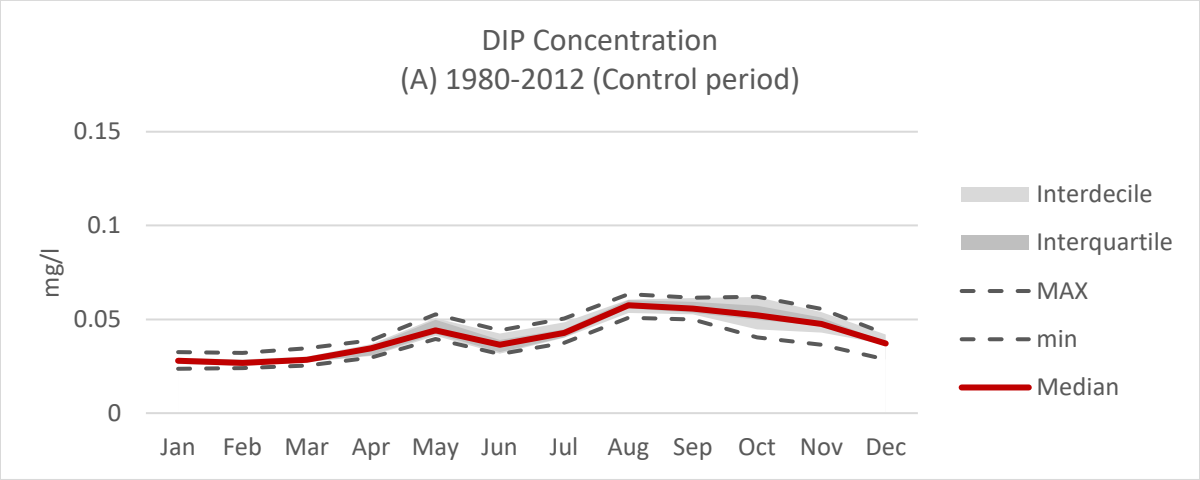

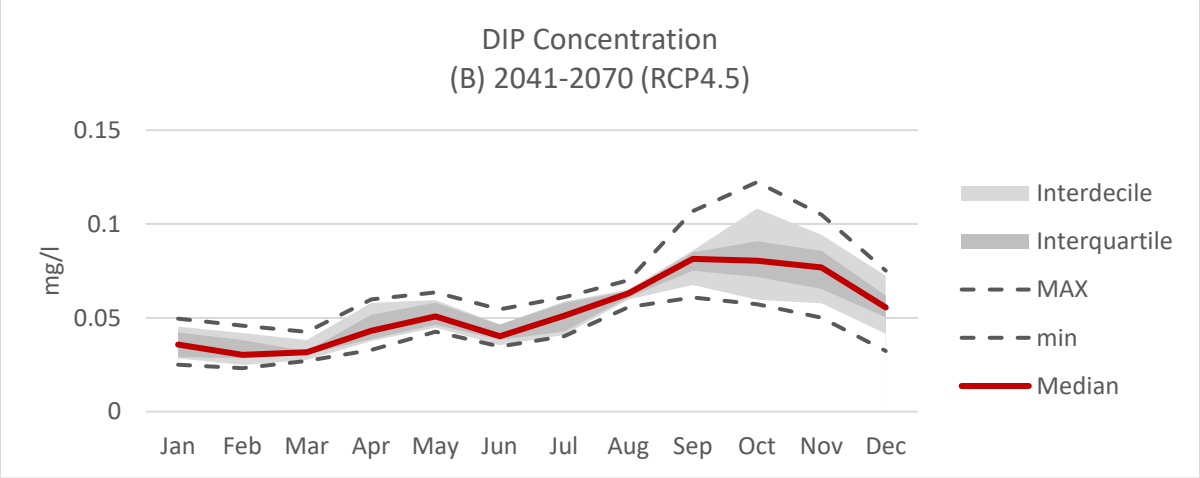

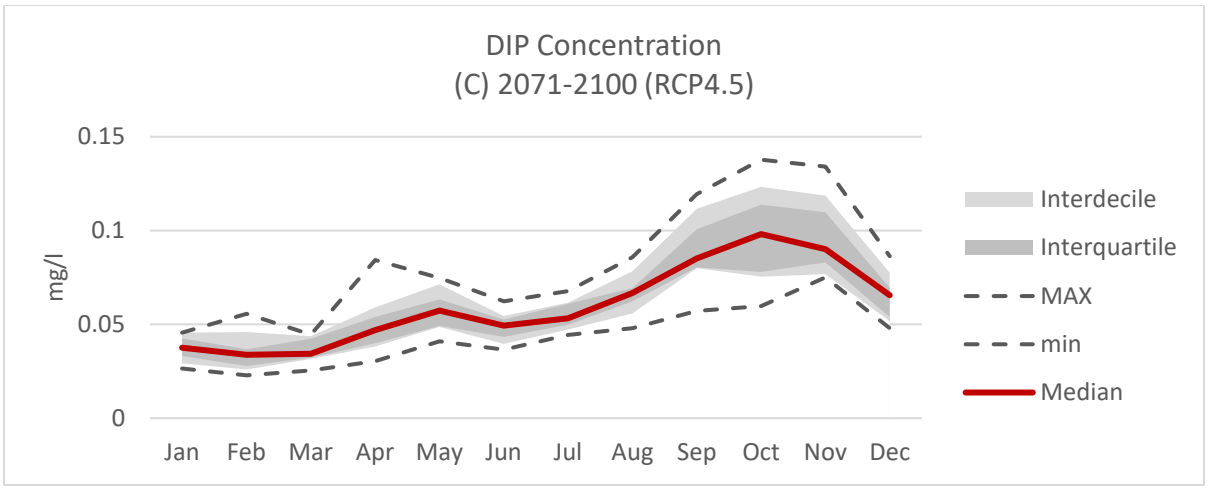

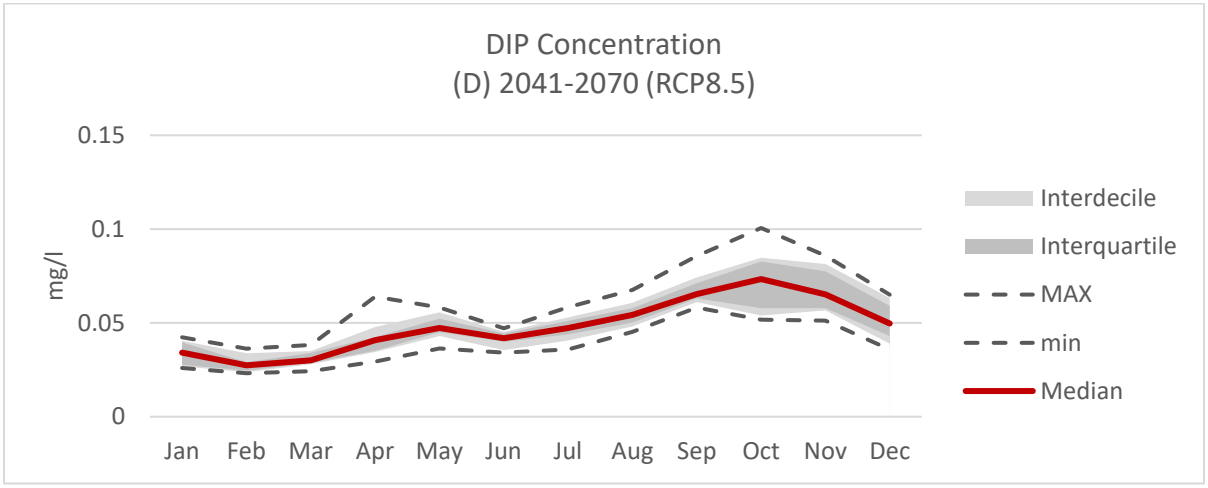

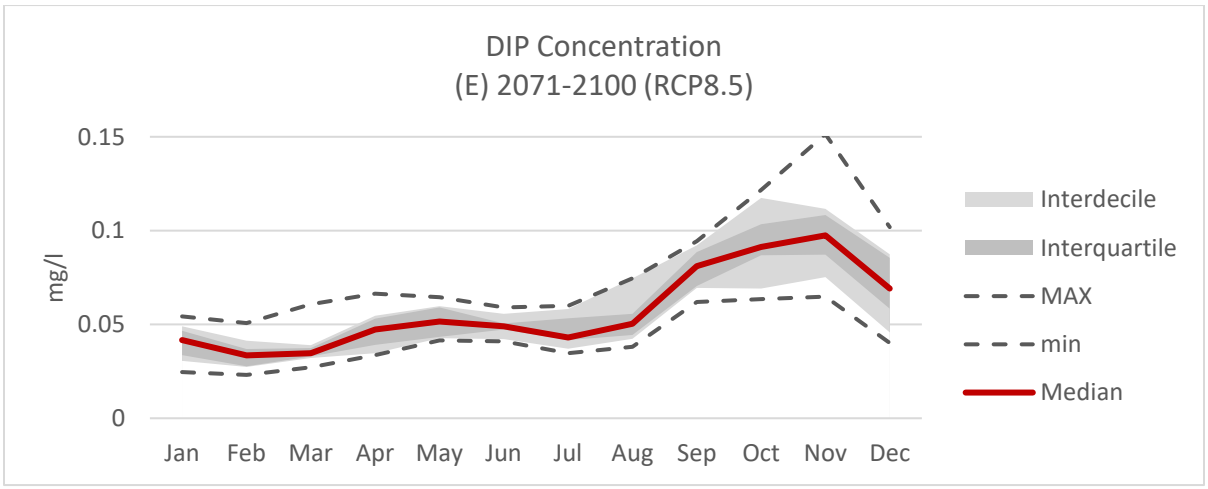

Fig. 4.43 - Variability of DIP within the GCM/RCM ensemble adopted in the study. (A) Control period, (B) RCP4.5 – 2041-2070, (C) RCP4.5 2071-2100, (D) RCP8.5 – 2041-2070 (E) RCP8.5 2071-2100.

Water retention time is directly influenced by water flow-rate from the ZRB. Therefore, its variabilities reflect those of the inflow loads of freshwater. This can be deduced by observing the variability in the summer months, which are extremely critical as the freshwater loadings from the ZRB are low (Fig. 4.44). The control period does not show any marked difference, even in the summer months, where differences are in the order of 7-10 days. The other scenarios show similar variability with the only exception the RCP8.5 long-term scenario. Here, variability in the months of July and August is marked, and the interquartile and interdecile ranges differ noticeably from the median monthly value.

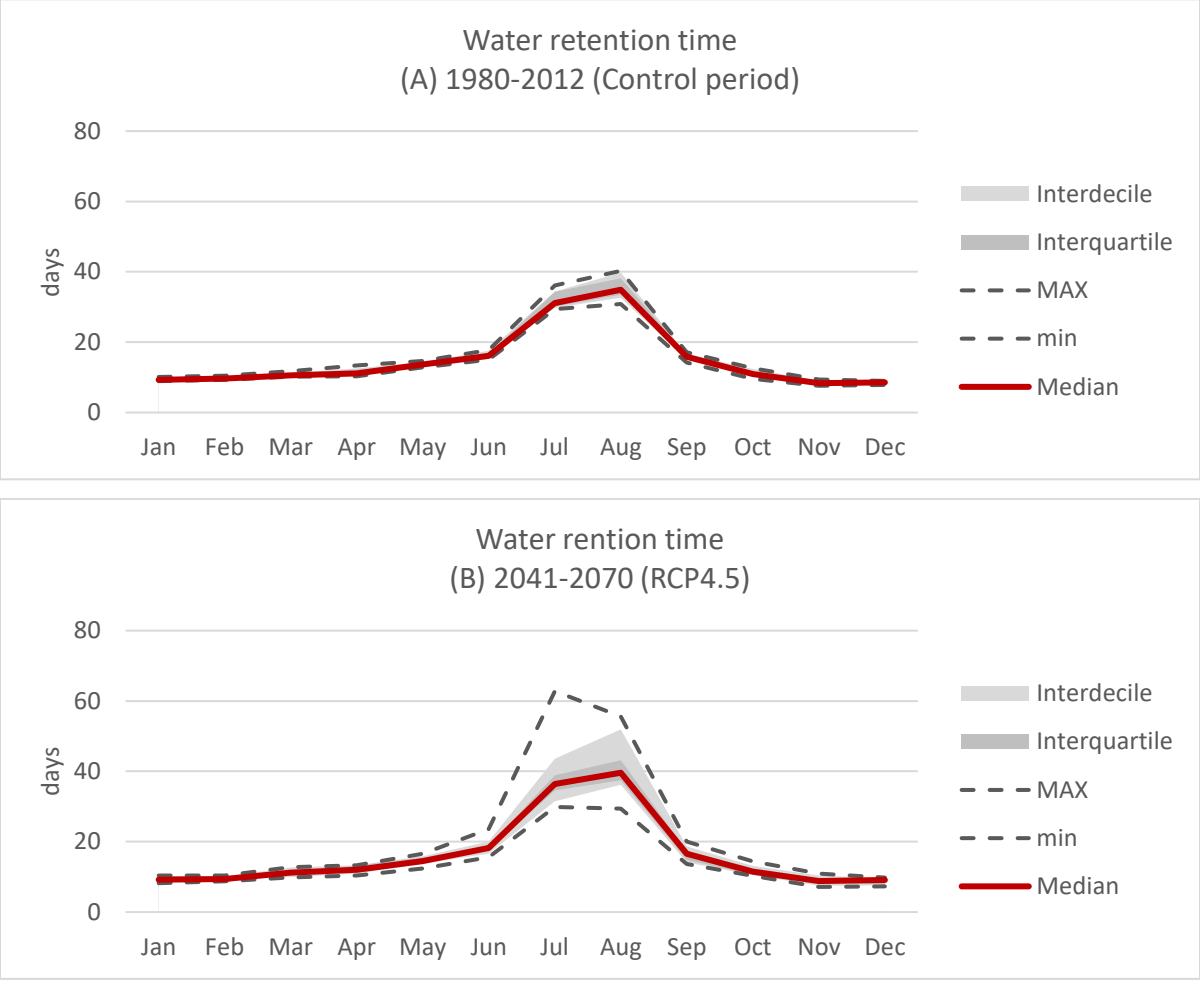

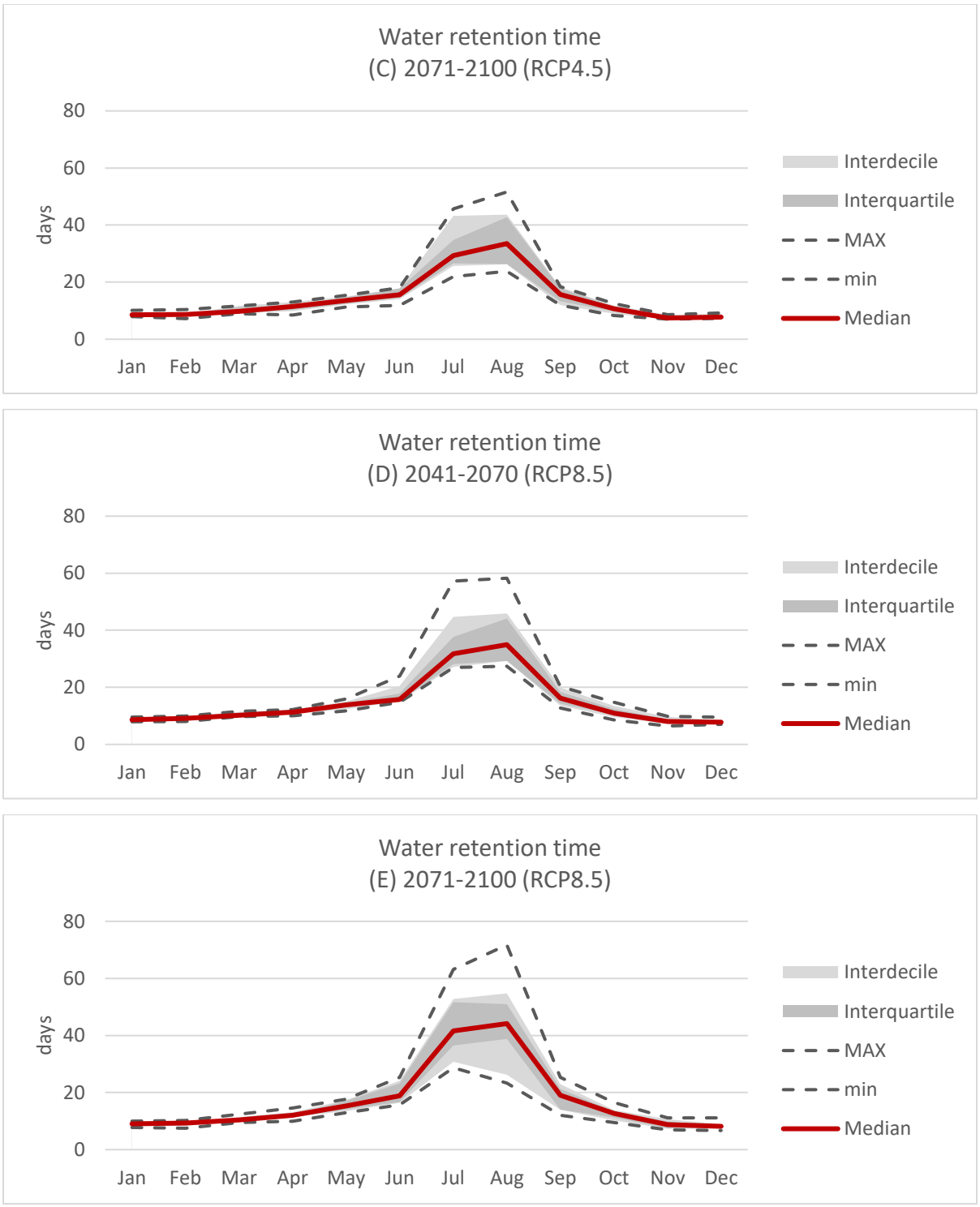

Fig. 4.44 - Variability of Water Retention Time within the GCM/RCM ensemble adopted in the study. (A) Control period, (B) RCP4.5 – 2041-2070, (C) RCP4.5 2071-2100, (D) RCP8.5 – 2041-2070 (E) RCP8.5 2071-2100.

As no significant differences in temperature are identified, the observed variability in Chl-a Fig. 4.45) can be attributed mostly to changes in nutrient concentrations, especially in DIP. Variability in the control period is limited and all simulations are in good agreement with each other, both in magnitude and seasonality. Variability is marked in summer, as winter months feature a low abundance of phytoplankton. The interquartile and interdecile ranges differ noticeably from the median value and their limits are closer to the MAX and min monthly values. The RCP8.5 long-term scenario features the highest variability, both in the spring and summer periods.

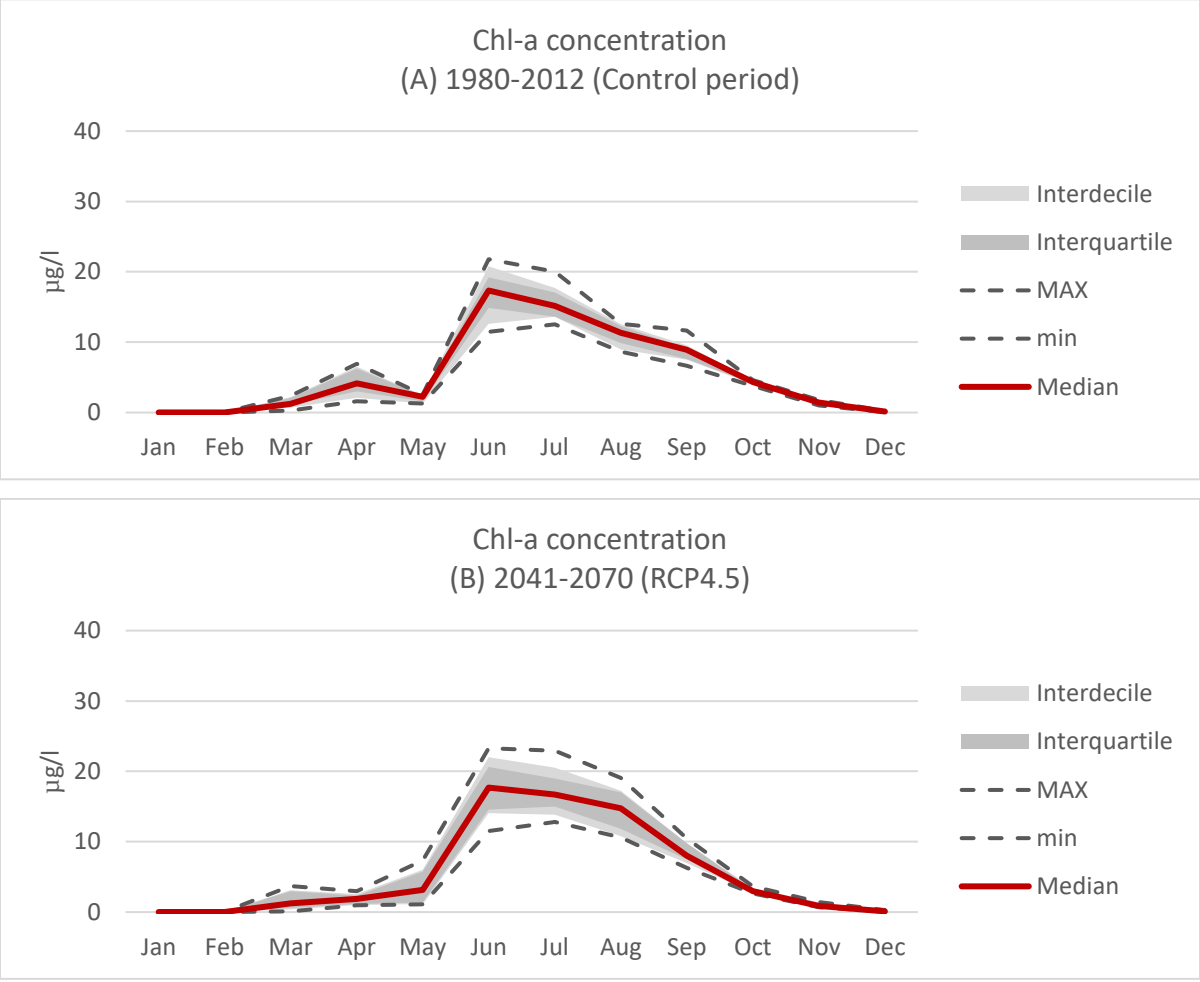

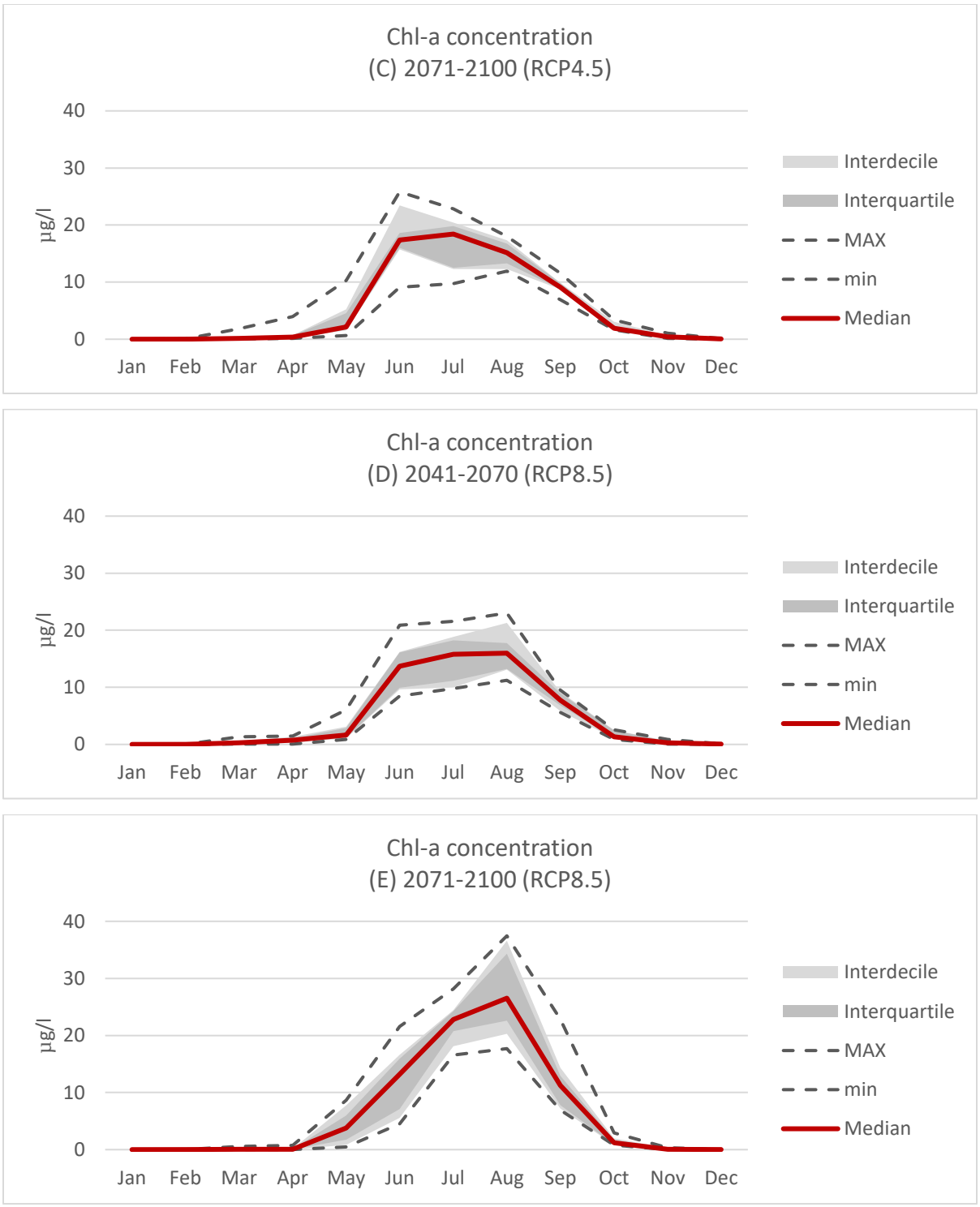

Fig. 4.45 - Variability of Chl-a concentration within the GCM/RCM ensemble adopted in the study. (A) Control period, (B) RCP4.5 – 2041-2070, (C) RCP4.5 2071-2100, (D) RCP8.5 – 2041-2070 (E) RCP8.5 2071-2100.

Here below, the variability of one phytoplankton compartment, the Cyanobacteria Microcystis (CB1), is illustrated . CB1 was chosen because of its ecological importance and the observable changes in concentration between the control period and the long-term period. It is possible to observe that all simulations show the same seasonality for the CB1's bloom. However, differences in concentrations can be observed. Both RCP4.5 and RCP8.5 long-term periods show the highest variability in summer. In the RCP4.5 long-term period, the interquartile and interdecile ranges cover the whole spectrum of monthly values, while in the RCP8.5 the MAX and min values differ slightly. Additional details can be found in Appendix E.

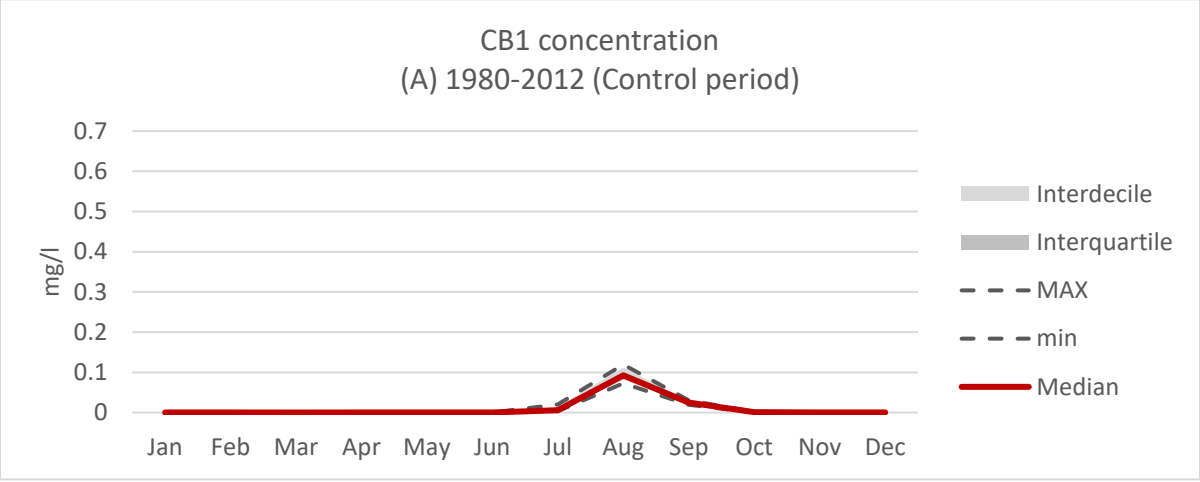

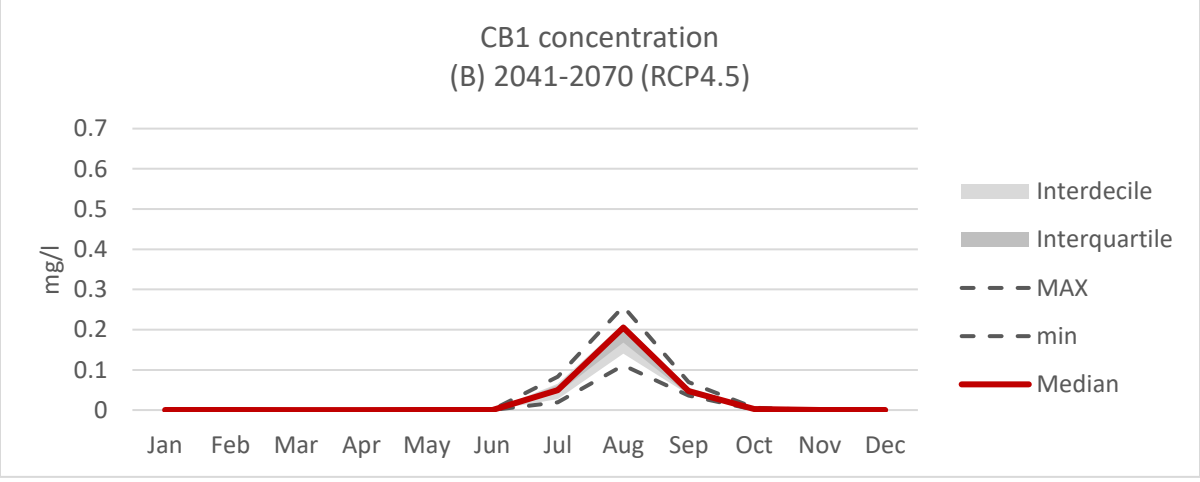

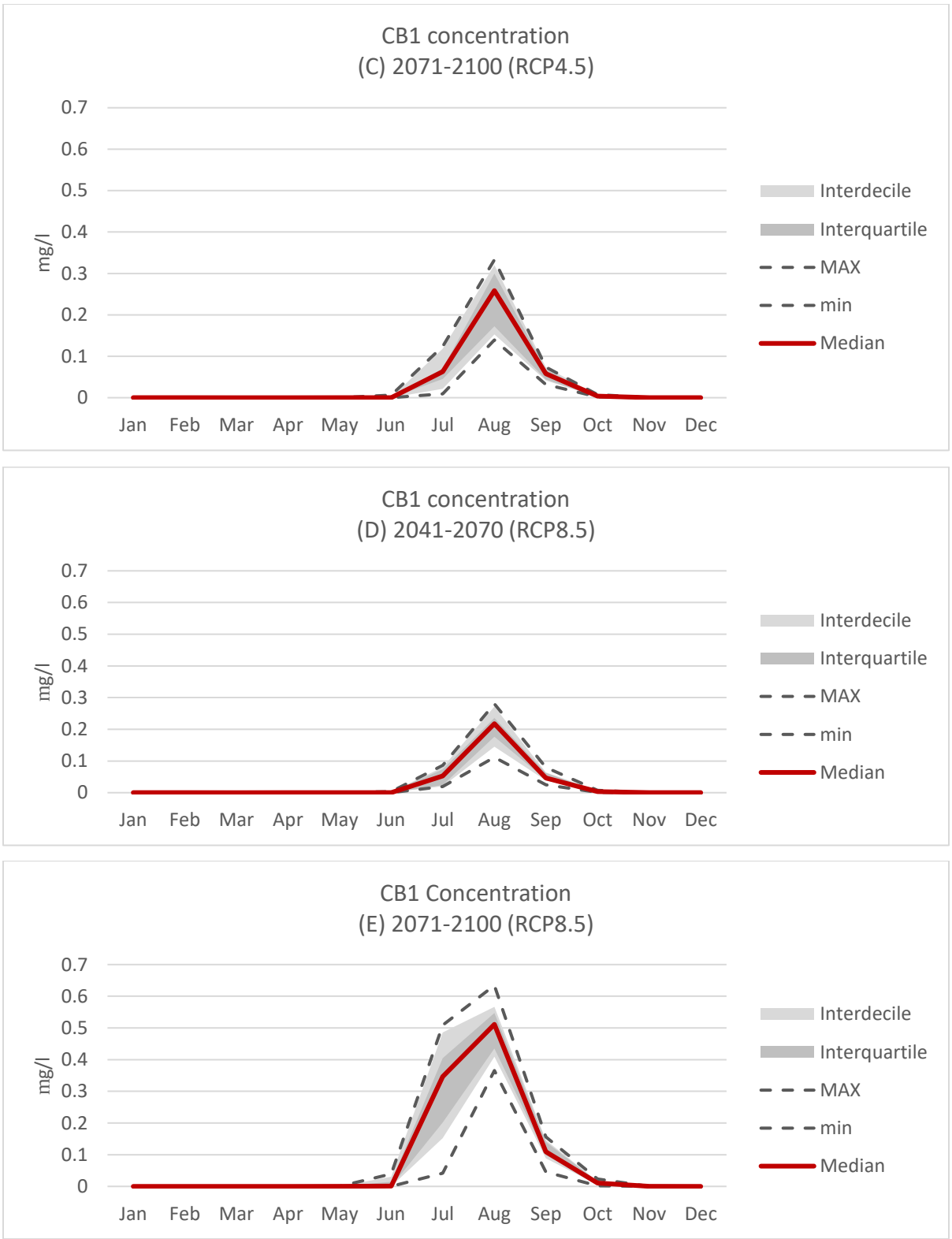

Fig. 4.46 - Variability of CB1 concentration within the GCM/RCM ensemble adopted in the study. (A) Control period, (B) RCP4.5 – 2041-2070, (C) RCP4.5 2071-2100, (D) RCP8.5 – 2041-2070 (E) RCP8.5 2071-2100.

5 SUMMARY AND DISCUSSION

This dissertation describes the development and application of an integrated modeling approach aiming at assessing the impacts of climate change on nutrient loadings and the potential consequent effects on coastal aquatic ecosystems over the 21st century. The overall aim of this study is to develop an approach for assessing potential long-term effects of climate change on the productivity and community structure of coastal phytoplankton at a catchment scale. Phytoplankton is responsible for a large share of photosynthesis and primary production of coastal areas, and plays an important role in several biogeochemical cycles such as carbon, nutrient and oxygen cycles. Furthermore, it is at the base of every aquatic food web, and changes in its processes, dynamics and composition have repercussions on both the environment and higher trophic levels. Finally, phytoplankton can be the cause of several water quality problems in coastal aquatic environments. In particular, eutrophication events can generate elevated biomass, harmful algal blooms (HABs), loss of biodiversity, hypoxic and anoxic conditions, all symptoms that reduce the quality of coastal waters. Therefore, the study of the impacts of climate change on the factors that regulate the dynamics and composition of phytoplankton in coastal areas (i.e. water temperature, nutrient loadings from the hinterland, water retention time, etc.) can help to better represent and understand the underlying processes and interactions between climate, abiotic and biotic factors that will regulate phytoplankton over the 21st century. In this context, the integration of climate, hydrologic, and ecosystem models provides a means to deal with the complex and interrelated nature of recent global environmental change problems, and help to explain, explore, and predict environmental responses to natural and human-induced stressors.

The developed integrated modelling approach is made of 3 components: an ensemble of high-resolution climate projections used to describe the future climate conditions, the hydrological model Soil and Water Assessment Tool (SWAT) to evaluate the impacts of climate change on the hydrology and nutrient loadings of coastal watershed, and the ecological model AQUATOX to assess the combined impacts of climate change and nutrient loadings on the aquatic ecosystems of coastal waters.

In order to demonstrate its applicability, the approach was applied to a local case study: the Zero river basin (ZRB) and the receiving coastal waters of Palude di Cona (PDC), a shallow-water area located in the northern basin of the lagoon of Venice. An ensemble of 10 GCM/RCM combinations, forced by two emission trajectories (RCP4.5 and RCP8.5), was selected for simulating future conditions of climate (temperature and precipitation). While the number of scenarios is consistent and able to represent the whole range of projected changes in climate (Jacob et al. 2014), it is only a partial sample of the climate scenarios available to the scientific community. For this reason, the obtained results are highly dependent on the assumptions of the selected GCM/RCM combinations. Climate scenarios are only a plausible projection of how the climate might unfold over the 21st century, and there is no guarantee that the climate conditions and consequent effects described in this study will manifest in the same form. To reduce the biases intrinsic to GCMs and RCMs, a bias correction methodology, the linear scaling method, was applied. The methodology consistently improved the statistics of precipitation and temperature for the calibration period (1993-2012). The approach was able to perfectly match the monthly mean of corrected values with that of observed ones while it did not reduce the difference in standard deviation (Lenderink et al. 2007). Overall, the number of selected climate scenarios, their spatial resolution (8km and 12km), and the application of one of the most adopted bias correction methods are the current best available approach to limit as much as possible the uncertainty of climate projections.

A SWAT model for the ZRB was constructed. The calibration process provided good results for the objective functions NSE and R2. Validation results show lower performances but were considered acceptable for the purpose of the study. Every objective function used to assess the performance of models should reflect the objectives of the study (Arnold et al. 2012; Diskin and Simon 1977). NSE is very sensitive to peak differences, and less to the long-term trends, which makes it a good indicator for single event modelling studies (i.e. flood events). The coefficient R2, with few exceptions for ammonium and orthophosphate loadings, always indicated good agreement between observed and modelled results. Moreover, numerous dynamics taking place in the ZRB were not modeled by SWAT because of missing data or limits of the model, and assumptions had to be taken. Specifically, the influence of external

groundwaters, irrigation channels, and infrastructure for flooding events were considered as constant throughout the simulation period. Also, agricultural management practices and nutrient dry and wet deposition were considered as constant. Finally, the quality of the available observed data, which in some cases was characterised by several missing values, might have affected the quality of the modelling performance.

The seasonal changes over the 21st century observed in the hydrology and nutrient loadings due to changes in temperature and precipitation are in agreement with previous studies on the Venice Lagoon Watershed (Solidoro et al. 2010). Results indicate an increase of freshwater discharge and nutrient loadings into the lagoon of Venice in the winter, and a decrease in summer. These results indicate that climate change may have important effects on the quality of waters of the Zero river, as the most dramatic changes happen during periods characterised by agricultural activities that influence the quality of waters (e.g. manure application in the fields during the winter period). The AQUATOX model was used to simulate the phytoplankton of PDC. It was possible to assess the performance of the model through several physico-chemical parameters. Results indicate that, despite the complexity of the system of PDC and the limitations of the model (e.g. the effect of tide on the hydrodynamics of the water body was neglected) AQUATOX is able to simulate with good approximation nutrient and phytoplankton concentrations.

Obtained results regarding changes over the 21ste century are in agreement with previous studies (Solidoro et al. 2010). Projected Chl-a concentrations suggest slight changes in yearly concentrations of phytoplankton. However, a marked variation is highlighted in the seasonality of phytoplankton blooms, which are projected to be higher during the summer months. It is also evident the pronounced change in the composition of phytoplankton, with diatoms adapted to warmer waters and cyanobacteria substituting the current species of phytoplankton (e.g. Navicula). From the outcomes of this study it is possible to conclude that changes in nutrient loadings will not have substantial effects on phytoplankton, as nutrient concentration in the warmer months change only slightly. The increase in water temperature seems to be the factor that triggers substantial change in the composition and concentration of phytoplankton in PDC. However, also changes in nutrient concentrations might have

significant effects. For example, the higher availability of phosphorus in the water column might reduce the abundance of phytoplankton to the advantage of other primary producers such as macro-algal species (Conley 2000). Additionally, low N:P ratio conditions may favor the promotion of harmful algal blooms (HAB) and cyanobacteria (Cugier et al. 2005; GEOHAB 2001).

The adoption of a number of climate scenarios and emission trajectories resulted in a spectrum of outcomes for the different parameters analysed in the study. The general conclusion that can be drawn from the assessment of the variability of results is that the selection of climate scenarios is a decision of immense importance as the selection of a more extreme climate scenario will produce more extreme results, and vice versa. The selection of more scenarios can help reducing this risk and indicates that climate change impact assessment studies are always accompanied by a certain degree of uncertainty. The adoption of more scenarios can allow the identification of most sensitive variables of the system under exam.

To generate more informed and useful decisions regarding the management of water environmental issues, the outcomes of this and other similar integrated modeling approaches should be thoroughly analysed and included in a wider decision-making context.

The modeling approach could be further improved to provide more reliable results. First, an underground water modeling tool could be integrated to better model the current and future effects of external and internal groundwaters that affect the hydrology of the ZRB. Second, land-use change and agricultural management practices scenarios responding to changes in climate could be jointly simulated. Furthermore, likely events such as the anticipated shortage of P in coming decades (Glibert et al. 2014) should be take into account in next studies. Third, a hydrodynamic model should be integrated in AQUATOX in order to correctly simulate hydrologic parameters such as water retention time and the effect of tides, which can have profound effects on nutrient and phytoplankton concentrations. Fourth, sea-level rise scenarios could be implemented. Finally, the effects of climate change on silica (Si) could be further explorer and integrated in the approach. Si is required by diatoms, the dominant group in the phytoplankton composition of PDC and lagoon of Venice. Changes in Si loadings might

reduce the abundance of diatoms, with profound effects on energy flows and harmful algal bloom events (Cloern 2001).

Modelling approaches should not be ends in themselves. They should be included in a broader decision-making context in order to provide real and effective benefits. Similar results could be very useful for decision managers that need to develop long-term strategies to protect the quality of water resources. More tools able to provide plausible projections of the future are needed as aquatic ecosystems will have a limited ability to adapt to climate change. Being able to "forecast" possible scenarios and therefore anticipate the possible outcomes might reduce the likelihood of negative events to happen. In relation to future eutrophication events, specific adaptation countermeasures could be adopted at the local and regional level. First, climate policies should be enacted as soon as possible. Addressing climate change is the first and most important measure to reduce the threat to water resources. Second, water management should not only focus on water quantity but also on water quality. Nutrient pollution reduction strategies should be updated and be flexible in order to be consistent with projected future climate change scenarios. A strong consensus claims that eutrophication events in costal ecosystems can be controlled and limited through controls on nitrogen inputs (Boesch 2002; Howarth and Marino 2006). However, as environmental conditions might change, it is important that "N-control" strategies are applied in conjunction with "P-control" strategies, as conveyed in the EU Water Framework Directive (Chave 2015).

Third, adaptation measures should be considered to reduce the unavoidable impacts of climate change. Climate change is expected to increase hydrological extremes such as droughts and floods. These events, could be critical for delicate aquatic environment such as coastal lagoon, which are characterised by shallow waters and high water retention times. The worsening of their environmental conditions could cause serious water eutrophication issues. In similar cases, the application of technological measures able to change the hydrodynamic of the water bodies could dilute the concentration of nutrient loads and restrain the growth of algae and improve the water oxygenation of waters. Finally, local governments should invest in the application of water treatment and water protection technologies, strengthen monitoring networks and implement stricter controls at the source of water pollution (e.g.

agricultural activities). In fact, the correct management of freshwater from upstream watersheds of coastal systems can generate benefits to water quality of coastal ecosystems (Howarth and Marino 2006).

Although water eutrophication modeling studies considering the effects of climate change have increased and have gained more attention from international researchers in the last decades, more scientific work is needed. This study highlights the fact that there could be significant changes in water environmental quality due to climate change in the waters of the lagoon of Venice. The proposed formulation of combined models might serve as a "blueprint" for other coastal environments and can assist environmental managers in their decisions. However, a great deal of uncertainty concerning the impact of climate change still exists and further studies are needed. Future studies should focus on improving and expand the integration of modeling tools as well as improving monitoring practices, in order to develop methods that allows the integration of knowledge from different disciplines and provide a synthetic outcome that could lead to a better management of the Earth’s natural resources.

APPENDIX A – AGRICULTURAL MANAGEMENT PRACTICES FROM SWAT, TABLES

CORN		
Date (mm/dd)	Operation	kg
01/01	Auto Irrigation initialization	
02/15	Tillage operation	
03/19	Tillage operation	
03/20	Fertilizer application (18-46-00)	200
03/20	Plant/begin. Growing season	
05/01	Tillage operation	
05/01	Fertilizer application (Urea)	300
05/17	Fertilizer application (Urea)	300
05/17	Tillage operation	
10/10	Harvest	
10/15	Manure application (Cow)	N: 60 P: 20
11/15	Manure application (Cow)	N: 60 P: 20
12/15	Manure application (Cow)	N: 60 P: 20

SOY		
Date (mm/dd)	Operation	kg
01/01	Auto Irrigation initialization	
02/15	Tillage operation	
05/01	Fertilizer application (Elemental P)	96
05/01	Fertilizer application (Elemental N)	32
05/02	Plant/begin. Growing season	
10/10	Harvest	
10/15	Manure (cow) application	N: 60 P: 20
11/15	Manure (cow) application	N: 60 P: 20
12/15	Manure (cow) application	N: 60 P: 20

WINTER WHEAT		
Date (mm/dd)	Operation	kg
01/01	Auto Irrigation initialization	
01/15	Tillage operation	
01/15	Fertilizer application (33-00-00)	200
06/10	Harvest	
06/15	Tillage operation	
09/15	Manure (cow) application	N: 60 P: 20
10/30	Fertilizer application (18-46-00)	200
10/31	Tillage operation	
11/01	Plant/begin. Growing season	
11/15	Manure (cow) application	N: 60 P: 20
12/15	Manure (cow) application	N: 60 P: 20

APPENDIX B – PHYTOPLANKTON IN AQUATOX, TABLES

Diatom, Navicula	
Saturating light (Ly/d)	58
P Half-saturation (mg/L)	0.01
N Half-saturation (mg/L)	0.002
C Half-saturation (mg/L)	0.054
Optimum T (°C)	15
Maximum T (°C)	39
Minimum T (°C)	10
Max. Photosynthetic rate (1/d)	1.6
Photorespiration coefficient (1/d)	0.05

Diatom, Cyclotella nana	
Saturating light (Ly/d)	22.5
P Half-saturation (mg/L)	0.017
N Half-saturation (mg/L)	0.011
C Half-saturation (mg/L)	0.054
Optimum T (°C)	20
Maximum T (°C)	35
Minimum T (°C)	2
Max. Photosynthetic rate (1/d)	3.4
Photorespiration coefficient (1/d)	0.026

Diatom, Cyclotella (High-nutrient)	
Saturating light (Ly/d)	22.5
P Half-saturation (mg/L)	0.055
N Half-saturation (mg/L)	0.117
C Half-saturation (mg/L)	0.054
Optimum T (°C)	20
Maximum T (°C)	35
Minimum T (°C)	2
Max. Photosynthetic rate (1/d)	1.87
Photorespiration coefficient (1/d)	0.026

Diatom, Fragilaria (Low-nutrient, warm waters)	
Saturating light (Ly/d)	56
P Half-saturation (mg/L)	0.001
N Half-saturation (mg/L)	0.0154
C Half-saturation (mg/L)	0.054
Optimum T (°C)	26
Maximum T (°C)	39
Minimum T (°C)	2
Max. Photosynthetic rate (1/d)	1.4
Photorespiration coefficient (1/d)	0.02

Diatom, Cyclotella nana (Warm waters)	
Saturating light (Ly/d)	22.5
P Half-saturation (mg/L)	0.017
N Half-saturation (mg/L)	0.011
C Half-saturation (mg/L)	0.054
Optimum T (°C)	25
Maximum T (°C)	39
Minimum T (°C)	2
Max. Photosynthetic rate (1/d)	3.4
Photorespiration coefficient (1/d)	0.026

Diatom, Cyclotella nana (Very warm waters)	
Saturating light (Ly/d)	22.5
P Half-saturation (mg/L)	0.017
N Half-saturation (mg/L)	0.011
C Half-saturation (mg/L)	0.054
Optimum T (°C)	30
Maximum T (°C)	39
Minimum T (°C)	2
Max. Photosynthetic rate (1/d)	3.4
Photorespiration coefficient (1/d)	0.026

Diatom, Cyclotella (High-nutrient, warm waters)	
Saturating light (Ly/d)	22.5
P Half-saturation (mg/L)	0.055
N Half-saturation (mg/L)	0.117
C Half-saturation (mg/L)	0.054
Optimum T (°C)	25
Maximum T (°C)	35
Minimum T (°C)	2
Max. Photosynthetic rate (1/d)	1.87
Photorespiration coefficient (1/d)	0.026

Diatom, Fragilaria (High-nutrient, cold waters)	
Saturating light (Ly/d)	20
P Half-saturation (mg/L)	0.055
N Half-saturation (mg/L)	0.117
C Half-saturation (mg/L)	0.054
Optimum T (°C)	8
Maximum T (°C)	20
Minimum T (°C)	2
Max. Photosynthetic rate (1/d)	3
Photorespiration coefficient (1/d)	0.02

Cyanobacteria, Microcystis	
Saturating light (Ly/d)	150
P Half-saturation (mg/L)	0.03
N Half-saturation (mg/L)	0.4
C Half-saturation (mg/L)	0.024
Optimum T (°C)	30
Maximum T (°C)	50
Minimum T (°C)	5
Max. Photosynthetic rate (1/d)	3.9
Photorespiration coefficient (1/d)	0.01

APPENDIX C – CLIMATE SCENARIOS

Monthly Mean Temperature (°C) ZRB– Control period (1983-2012)

	S1	S2	S3	S4	S5	S6	S7	S8	S9	S10	MAX	Median	MIN	Interquartile	Interdecile
Jan	2.97	2.99	3.32	3.20	2.88	2.89	3.09	2.85	2.83	3.28	3.32	2.98	2.83	3.20	3.28
Feb	3.97	4.01	4.39	4.33	4.22	4.28	4.21	3.93	4.21	4.50	4.50	4.22	3.93	4.33	4.39
Mar	8.43	8.46	8.42	8.69	8.50	8.67	8.65	8.58	8.61	8.78	8.78	8.59	8.42	8.67	8.69
Apr	12.73	12.62	12.72	12.69	12.49	12.64	12.69	12.73	12.65	13.10	13.10	12.69	12.49	12.73	12.73
May	18.29	18.18	18.07	18.20	18.12	17.96	18.42	17.96	18.28	18.28	18.42	18.19	17.96	18.28	18.29
Jun	21.78	21.66	20.92	21.44	21.97	21.43	21.78	21.56	21.51	21.90	21.97	21.61	20.92	21.78	21.90
Jul	23.21	23.25	22.99	23.49	23.64	23.45	23.26	23.20	23.73	23.49	23.73	23.36	22.99	23.49	23.64
Aug	23.54	23.29	23.27	23.11	23.66	23.35	23.17	23.30	23.27	23.42	23.66	23.29	23.11	23.42	23.54
Sep	18.66	18.65	18.58	18.84	18.66	18.75	18.92	18.63	18.39	18.90	18.92	18.66	18.39	18.84	18.90
Oct	13.64	13.76	13.65	13.65	13.96	13.98	13.65	13.79	13.91	14.10	14.10	13.78	13.64	13.96	13.98
Nov	8.32	8.61	8.09	8.62	8.52	8.43	8.61	8.21	8.46	8.31	8.62	8.44	8.09	8.61	8.61
Dec	3.90	3.85	3.68	3.97	3.70	4.01	3.99	3.60	3.81	4.32	4.32	3.88	3.60	3.99	4.01

Monthly Mean Temperature (°C) ZRB– RCP4.5 mid-term (2041-2070)

	S1	S2	S3	S4	S5	S6	S7	S8	S9	S10	MAX	Median	MIN	Interquartile	Interdecile
Jan	5.06	5.03	4.49	4.67	4.27	4.02	4.42	5.18	4.55	3.52	5.18	4.52	3.52	5.03	5.06
Feb	4.95	6.26	6.15	5.11	5.67	5.13	5.05	6.59	5.35	5.24	6.59	5.29	4.95	6.15	6.26
Mar	9.76	9.65	10.02	9.83	9.43	9.51	9.70	10.35	9.59	9.83	10.35	9.73	9.43	9.83	10.02
Apr	14.18	14.52	13.84	13.27	13.47	13.32	13.33	14.69	13.51	14.32	14.69	13.67	13.27	14.32	14.52
May	19.91	19.73	20.09	18.72	19.73	18.82	18.95	19.11	19.71	19.71	20.09	19.71	18.72	19.73	19.91
Jun	24.02	23.58	23.35	22.93	24.06	23.30	23.50	23.15	22.98	23.83	24.06	23.43	22.93	23.83	24.02
Jul	26.35	25.69	25.15	24.58	25.47	25.41	24.83	25.60	24.92	24.57	26.35	25.28	24.57	25.60	25.69
Aug	26.90	25.12	25.59	24.56	25.94	25.29	24.74	25.20	25.08	24.62	26.90	25.16	24.56	25.59	25.94
Sep	21.04	21.54	20.54	19.63	20.51	19.53	19.86	21.14	20.16	20.37	21.54	20.44	19.53	21.04	21.14
Oct	15.34	16.01	15.33	14.34	15.68	14.88	14.42	16.07	15.28	15.46	16.07	15.33	14.34	15.68	16.01
Nov	10.21	9.66	8.78	10.10	9.71	9.79	9.85	9.70	9.34	9.52	10.21	9.71	8.78	9.85	10.10
Dec	5.90	5.75	4.22	5.31	4.71	5.01	4.87	6.50	5.56	4.96	6.50	5.16	4.22	5.75	5.90

Monthly Mean Temperature (°C) ZRB– RCP4.5 long-term (2071-2100)

	S1	S2	S3	S4	S5	S6	S7	S8	S9	S10	MAX	Median	MIN	Interquartile	Interdecile
Jan	6.02	5.44	5.85	5.18	4.47	4.46	4.97	6.16	4.25	4.54	6.16	5.08	4.25	5.85	6.02
Feb	5.83	6.06	6.14	6.04	6.30	5.96	6.19	6.45	5.51	6.38	6.45	6.10	5.51	6.30	6.38
Mar	10.57	10.01	10.30	10.27	10.11	9.65	10.30	10.57	9.93	11.28	11.28	10.28	9.65	10.57	10.57
Apr	14.64	14.88	14.20	13.78	13.88	13.49	13.86	14.90	13.06	14.77	14.90	14.04	13.06	14.77	14.88
May	20.73	20.92	19.81	19.75	19.41	18.98	19.51	20.50	19.58	20.16	20.92	19.78	18.98	20.50	20.73
Jun	23.85	24.24	23.77	23.12	24.00	23.21	23.52	23.63	22.40	23.93	24.24	23.70	22.40	23.93	24.00
Jul	26.58	26.25	26.01	24.96	25.37	26.27	24.79	25.07	25.17	24.92	26.58	25.27	24.79	26.25	26.27
Aug	27.85	25.87	26.05	23.87	26.10	26.03	24.30	25.44	25.17	24.96	27.85	25.66	23.87	26.05	26.10
Sep	22.27	21.68	22.32	20.40	20.76	20.67	20.78	21.57	19.66	20.70	22.32	20.77	19.66	21.68	22.27
Oct	16.53	16.15	15.98	14.70	16.20	15.54	14.46	16.56	15.57	15.52	16.56	15.78	14.46	16.20	16.53
Nov	10.78	10.87	9.68	10.42	9.75	10.07	10.30	10.77	9.52	10.19	10.87	10.25	9.52	10.77	10.78
Dec	6.31	6.64	5.20	5.77	4.79	4.85	5.80	7.44	5.20	6.03	7.44	5.79	4.79	6.31	6.64

Monthly Mean Temperature (°C) ZRB– RCP8.5 mid-term (2041-2070)

	S1	S2	S3	S4	S5	S6	S7	S8	S9	S10	MAX	Median	MIN	Interquartile	Interdecile
Jan	6.42	5.19	5.55	5.02	4.93	4.35	4.80	5.75	4.64	3.80	6.42	4.97	3.80	5.55	5.75
Feb	6.12	6.16	6.39	6.01	4.89	6.28	6.05	6.67	5.48	5.77	6.67	6.09	4.89	6.28	6.39
Mar	10.89	10.22	10.40	10.49	7.50	10.11	10.54	10.91	10.20	10.34	10.91	10.37	7.50	10.54	10.89
Apr	14.32	14.92	14.58	13.82	11.71	14.12	13.46	14.77	14.01	14.98	14.98	14.22	11.71	14.77	14.92
May	20.52	20.52	20.30	19.38	15.90	19.40	19.38	20.20	19.74	19.14	20.52	19.57	15.90	20.30	20.52
Jun	24.56	24.17	24.10	22.94	21.45	23.66	22.86	24.52	22.75	23.42	24.56	23.54	21.45	24.17	24.52
Jul	26.53	26.17	26.68	24.36	26.08	26.24	24.65	25.95	25.13	25.22	26.68	26.02	24.36	26.24	26.53
Aug	27.50	26.24	26.67	24.44	27.00	26.20	24.75	26.38	25.27	25.59	27.50	26.22	24.44	26.67	27.00
Sep	21.82	22.07	22.30	20.10	24.54	21.27	20.17	21.98	20.10	20.98	24.54	21.55	20.10	22.07	22.30
Oct	16.14	16.66	16.11	15.01	19.36	16.11	15.05	16.91	15.94	15.59	19.36	16.11	15.01	16.66	16.91
Nov	10.84	10.78	10.25	10.48	14.24	10.40	10.49	10.80	9.72	10.19	14.24	10.48	9.72	10.80	10.84
Dec	6.26	6.03	5.36	5.86	8.42	4.91	5.86	7.18	5.91	5.03	8.42	5.89	4.91	6.26	7.18

Monthly Mean Temperature (°C) ZRB– RCP8.5 long-term (2071-2100)

	S1	S2	S3	S4	S5	S6	S7	S8	S9	S10	MAX	Median	MIN	Interquartile	Interdecile
Jan	8.41	7.04	6.73	6.41	6.34	6.41	6.30	7.70	6.06	6.21	8.41	6.41	6.06	7.04	7.70
Feb	8.04	7.58	8.20	7.45	6.60	7.72	7.48	8.60	6.93	7.93	8.60	7.65	6.60	8.04	8.20
Mar	12.30	11.65	12.06	11.38	8.12	11.40	11.05	12.63	11.16	12.44	12.63	11.53	8.12	12.30	12.44
Apr	16.25	16.21	15.84	15.27	12.56	15.43	14.74	16.67	14.86	16.34	16.67	15.63	12.56	16.25	16.34
May	22.50	22.57	22.35	20.68	17.31	20.86	20.72	22.09	20.76	20.85	22.57	20.86	17.31	22.35	22.50
Jun	26.57	27.59	26.70	24.66	22.75	25.37	24.47	26.49	24.78	25.39	27.59	25.38	22.75	26.57	26.70
Jul	30.26	29.01	29.23	26.90	27.56	28.95	26.16	28.41	27.04	27.40	30.26	27.99	26.16	29.01	29.23
Aug	31.32	28.40	29.07	26.08	29.23	28.70	26.02	28.96	26.87	27.42	31.32	28.55	26.02	29.07	29.23
Sep	24.17	24.75	24.74	21.84	27.23	23.03	21.59	24.80	21.87	23.13	27.23	23.65	21.59	24.75	24.80
Oct	18.59	18.79	17.67	16.05	21.43	17.12	15.65	19.22	17.31	17.51	21.43	17.59	15.65	18.79	19.22
Nov	13.26	12.52	11.54	11.85	15.87	11.95	11.84	13.01	11.00	11.93	15.87	11.94	11.00	13.01	13.26
Dec	8.96	8.25	6.66	7.28	9.77	7.09	7.42	9.46	7.14	6.88	9.77	7.35	6.66	8.96	9.46

Monthly Mean Precipitation (mm) ZRB– Control period (1983-2012)

	S1	S2	S3	S4	S5	S6	S7	S8	S9	S10	MAX	Median	MIN	Interquartile	Interdecile
Jan	44.10	43.38	51.20	48.48	42.45	39.33	48.66	44.16	44.08	40.05	51.20	44.09	39.33	48.48	48.66
Feb	50.32	37.58	46.19	44.29	46.63	38.94	46.20	38.34	52.90	42.57	52.90	45.24	37.58	46.63	50.32
Mar	47.93	42.56	67.55	55.15	48.03	57.59	53.54	44.59	55.63	49.25	67.55	51.39	42.56	55.63	57.59
Apr	76.36	78.38	105.79	89.73	79.91	81.83	98.25	76.64	82.52	99.52	105.79	82.18	76.36	98.25	99.52
May	92.64	86.48	91.81	88.65	92.21	94.06	87.30	90.68	86.70	93.70	94.06	91.24	86.48	92.64	93.70
Jun	91.82	88.31	126.02	96.88	84.43	90.74	90.65	96.13	101.47	87.42	126.02	91.28	84.43	96.88	101.47
Jul	75.04	70.37	78.57	77.42	73.72	72.24	74.81	72.46	65.59	73.43	78.57	73.57	65.59	75.04	77.42
Aug	66.32	65.95	67.83	81.79	69.27	74.02	76.86	62.86	78.46	82.05	82.05	71.65	62.86	78.46	81.79
Sep	108.42	121.11	113.03	99.66	108.60	115.68	101.10	113.25	129.74	113.49	129.74	113.14	99.66	115.68	121.11
Oct	92.33	93.77	94.32	89.37	120.62	115.01	96.45	98.65	103.61	107.82	120.62	97.55	89.37	107.82	115.01
Nov	108.00	122.16	92.74	107.11	122.38	103.15	107.96	113.70	94.62	119.90	122.38	107.98	92.74	119.90	122.16
Dec	92.55	68.94	85.31	71.12	91.03	78.55	70.41	69.94	88.31	76.20	92.55	77.38	68.94	88.31	91.03

Monthly Mean Precipitation (mm) ZRB– RCP4.5 mid-term (2041-2070)

	S1	S2	S3	S4	S5	S6	S7	S8	S9	S10	MAX	Median	MIN	Interquartile	Interdecile
Jan	39.37	45.26	50.19	60.00	68.77	42.70	51.65	43.45	57.50	39.67	68.77	47.72	39.37	57.50	60.00
Feb	53.76	62.64	61.54	46.72	58.78	36.46	50.12	48.71	79.19	46.73	79.19	51.94	36.46	61.54	62.64
Mar	41.68	37.14	51.35	59.24	44.80	65.83	45.00	39.91	65.92	52.49	65.92	48.17	37.14	59.24	65.83
Apr	77.35	90.54	102.90	80.46	82.75	86.75	85.19	88.92	88.94	81.72	102.90	85.97	77.35	88.94	90.54
May	77.94	100.87	67.38	97.91	95.81	78.68	93.13	92.66	87.98	86.94	100.87	90.32	67.38	95.81	97.91
Jun	48.39	75.52	91.55	104.07	69.04	84.33	75.39	95.28	98.79	84.72	104.07	84.53	48.39	95.28	98.79
Jul	34.28	89.69	79.81	92.16	66.36	78.89	71.44	73.80	66.12	91.91	92.16	76.34	34.28	89.69	91.91
Aug	44.45	57.07	65.81	90.04	48.82	63.79	77.80	66.39	51.65	73.83	90.04	64.80	44.45	73.83	77.80
Sep	132.08	108.23	118.25	108.63	100.62	114.12	122.09	104.98	118.77	140.56	140.56	116.19	100.62	122.09	132.08
Oct	122.58	98.58	81.05	80.98	156.92	131.87	101.24	91.34	89.11	97.42	156.92	98.00	80.98	122.58	131.87
Nov	123.42	127.56	91.48	132.79	128.36	144.76	106.40	114.85	73.35	82.79	144.76	119.14	73.35	128.36	132.79
Dec	107.26	59.83	130.85	70.47	64.33	85.38	49.43	64.63	93.37	56.27	130.85	67.55	49.43	93.37	107.26

Monthly Mean Precipitation (mm) ZRB– RCP4.5 long-term (2071-2100)

	S1	S2	S3	S4	S5	S6	S7	S8	S9	S10	MAX	Median	MIN	Interquartile	Interdecile
Jan	62.18	55.86	67.16	55.17	57.43	36.85	50.51	58.15	62.09	33.36	67.16	56.65	33.36	62.09	62.18
Feb	63.84	67.80	56.48	49.89	60.80	37.46	49.08	64.87	96.77	54.11	96.77	58.64	37.46	64.87	67.80
Mar	49.71	44.27	78.37	68.97	63.32	53.64	59.21	39.33	58.81	70.71	78.37	59.01	39.33	68.97	70.71
Apr	77.13	93.77	142.79	76.42	74.48	72.79	74.18	72.69	99.48	90.14	142.79	76.77	72.69	93.77	99.48
May	76.99	77.78	75.87	86.94	106.75	99.33	108.29	99.47	96.45	91.94	108.29	94.20	75.87	99.47	106.75
Jun	72.38	108.02	82.25	120.23	97.56	97.83	92.29	131.81	136.09	95.86	136.09	97.69	72.38	120.23	131.81
Jul	44.23	87.32	72.24	88.09	74.95	53.02	96.56	108.13	64.73	87.95	108.13	81.14	44.23	88.09	96.56
Aug	37.76	61.21	64.68	100.63	57.32	76.68	82.12	72.35	89.21	84.66	100.63	74.52	37.76	84.66	89.21
Sep	94.83	134.49	99.02	118.32	117.48	112.08	109.92	109.05	128.42	129.86	134.49	114.78	94.83	128.42	129.86
Oct	116.77	94.21	76.31	90.87	164.87	119.78	93.68	83.91	110.17	130.61	164.87	102.19	76.31	119.78	130.61
Nov	147.96	153.73	117.30	140.79	123.28	112.83	152.82	120.08	88.31	109.91	153.73	121.68	88.31	147.96	152.82
Dec	102.61	46.71	128.82	74.42	63.92	83.89	71.69	57.19	86.76	74.96	128.82	74.69	46.71	86.76	102.61

Monthly Mean Precipitation (mm) ZRB– RCP8.5 mid-term (2041-2070)

	S1	S2	S3	S4	S5	S6	S7	S8	S9	S10	MAX	Median	MIN	Interquartile	Interdecile
Jan	61.49	58.04	55.37	75.90	37.92	43.02	70.41	50.74	44.67	41.56	75.90	53.05	37.92	61.49	70.41
Feb	45.08	56.64	43.24	42.42	56.00	36.25	54.37	46.92	66.23	40.47	66.23	46.00	36.25	56.00	56.64
Mar	45.46	57.49	80.92	54.50	60.56	60.79	45.92	56.14	68.01	67.31	80.92	59.02	45.46	67.31	68.01
Apr	91.69	91.10	115.34	84.51	64.65	75.58	77.74	106.40	87.49	90.55	115.34	89.02	64.65	91.69	106.40
May	78.65	103.12	71.50	85.07	102.07	92.31	89.51	90.84	114.70	112.26	114.70	91.58	71.50	103.12	112.26
Jun	51.70	105.55	100.91	113.49	59.78	104.69	99.08	109.67	99.59	93.92	113.49	100.25	51.70	105.55	109.67
Jul	34.89	88.83	68.30	88.15	64.76	63.15	86.87	92.82	85.44	76.93	92.82	81.19	34.89	88.15	88.83
Aug	42.50	63.90	65.70	94.78	70.08	62.32	75.43	70.06	83.75	67.62	94.78	68.84	42.50	75.43	83.75
Sep	112.93	97.83	68.59	96.15	119.25	114.11	132.62	98.00	124.11	127.71	132.62	113.52	68.59	124.11	127.71
Oct	111.64	107.62	71.05	88.67	173.99	149.10	96.13	104.42	96.68	105.73	173.99	105.07	71.05	111.64	149.10
Nov	134.54	139.49	119.89	110.86	167.87	126.18	137.60	110.05	109.67	136.52	167.87	130.36	109.67	137.60	139.49
Dec	132.96	46.84	135.42	75.79	84.95	72.98	69.53	63.20	121.38	59.84	135.42	74.39	46.84	121.38	132.96

Monthly Mean Precipitation (mm) ZRB– RCP8.5 long-term (2071-2100)

	S1	S2	S3	S4	S5	S6	S7	S8	S9	S10	MAX	Median	MIN	Interquartile	Interdecile
Jan	76.77	48.40	48.52	49.86	73.75	60.18	43.29	40.57	46.18	57.84	76.77	49.19	40.57	60.18	73.75
Feb	80.03	48.00	43.24	42.66	51.16	51.38	43.53	54.64	89.81	45.16	89.81	49.58	42.66	54.64	80.03
Mar	44.52	47.14	72.60	63.98	47.36	67.68	54.84	47.09	73.97	69.16	73.97	59.41	44.52	69.16	72.60
Apr	69.57	84.08	114.45	74.49	70.95	66.80	79.41	99.95	82.84	85.62	114.45	81.13	66.80	85.62	99.95
May	67.09	73.68	60.94	91.34	91.94	68.08	94.43	84.28	88.68	103.20	103.20	86.48	60.94	91.94	94.43
Jun	44.87	72.16	67.08	107.46	53.25	95.24	93.96	93.77	98.49	84.58	107.46	89.18	44.87	95.24	98.49
Jul	25.43	70.62	63.18	89.23	49.64	51.45	89.62	75.52	65.96	57.65	89.62	64.57	25.43	75.52	89.23
Aug	23.48	74.78	57.98	104.80	56.74	64.26	108.00	47.36	82.78	63.93	108.00	64.09	23.48	82.78	104.80
Sep	92.30	94.23	83.14	95.83	71.48	116.47	128.70	113.73	102.03	140.96	140.96	98.93	71.48	116.47	128.70
Oct	115.57	133.42	85.56	77.31	157.28	117.88	100.36	84.31	86.28	118.64	157.28	107.97	77.31	118.64	133.42
Nov	116.86	192.43	150.66	128.84	101.57	123.29	121.88	153.43	104.68	143.14	192.43	126.06	101.57	150.66	153.43
Dec	178.78	74.37	126.35	84.82	64.64	79.73	66.22	88.30	111.45	63.73	178.78	82.28	63.73	111.45	126.35

APPENDIX D – SWAT OUTPUT

Monthly mean water discharge, Q (m^3/s) – Control period (1983-2012)

	S1	S2	S3	S4	S5	S6	S7	S8	S9	S10	MAX	Median	MIN	Interquartile	Interdecile
Jan	2.42	2.24	2.46	2.41	2.42	2.42	2.46	2.37	2.35	2.44	2.46	2.42	2.24	2.44	2.46
Feb	2.42	2.21	2.32	2.27	2.43	2.26	2.37	2.32	2.42	2.37	2.43	2.34	2.21	2.42	2.42
Mar	2.07	1.94	2.29	2.10	2.10	2.12	2.16	1.99	2.30	2.08	2.30	2.10	1.94	2.16	2.29
Apr	1.99	1.99	2.42	2.12	2.14	2.03	2.27	1.87	2.18	2.21	2.42	2.13	1.87	2.21	2.27
May	1.76	1.71	2.03	1.71	1.84	1.86	1.72	1.68	1.81	1.89	2.03	1.78	1.68	1.86	1.89
Jun	1.54	1.57	2.12	1.57	1.52	1.64	1.56	1.51	1.68	1.57	2.12	1.57	1.51	1.64	1.68
Jul	1.04	0.76	1.15	0.96	0.88	0.93	0.88	0.90	0.83	0.92	1.15	0.91	0.76	0.96	1.04
Aug	0.93	0.82	0.91	0.97	0.81	0.89	0.93	0.84	0.91	0.94	0.97	0.91	0.81	0.93	0.94
Sep	1.77	1.93	1.98	1.70	1.96	1.73	1.67	1.80	2.09	1.94	2.09	1.86	1.67	1.96	1.98
Oct	2.23	2.30	2.31	2.03	2.70	2.54	2.16	2.33	2.53	2.52	2.70	2.32	2.03	2.53	2.54
Nov	2.86	3.04	2.82	2.83	3.20	2.88	2.85	2.96	2.63	3.12	3.20	2.87	2.63	3.04	3.12
Dec	2.91	2.59	2.74	2.69	3.10	2.73	2.64	2.72	2.84	2.98	3.10	2.73	2.59	2.91	2.98

Monthly mean water discharge, Q (m^3/s) – RCP4.5 mid-term (2041-2070)

	S1	S2	S3	S4	S5	S6	S7	S8	S9	S10	MAX	Median	MIN	Interquartile	Interdecile
Jan	2.46	2.24	2.59	4.03	2.31	2.49	3.42	2.27	2.07	2.55	4.03	2.47	2.07	2.59	3.42
Feb	2.36	2.53	2.44	2.75	1.85	2.35	2.45	2.25	3.77	2.78	3.77	2.44	1.85	2.75	2.78
Mar	1.94	1.83	2.10	2.66	1.51	1.78	2.09	1.81	2.36	2.59	2.66	2.02	1.51	2.36	2.59
Apr	1.76	1.96	2.40	2.81	0.96	2.26	1.82	1.88	1.37	4.73	4.73	1.92	0.96	2.40	2.81
May	1.52	1.80	1.58	1.95	0.65	1.82	1.21	1.71	0.90	2.64	2.64	1.65	0.65	1.82	1.95
Jun	1.00	1.39	1.36	1.43	3.62	1.52	0.89	1.46	4.54	2.23	4.54	1.44	0.89	2.23	3.62
Jul	0.41	1.03	0.77	0.39	0.55	1.64	0.56	0.93	1.23	1.89	1.89	0.85	0.39	1.23	1.64
Aug	0.49	0.80	0.73	0.55	0.30	0.69	0.27	0.88	0.71	2.79	2.79	0.70	0.27	0.80	0.88
Sep	1.53	2.08	2.00	2.03	0.67	1.93	1.55	1.97	1.99	3.79	3.79	1.98	0.67	2.03	2.08
Oct	2.53	2.31	2.05	1.48	1.04	2.15	2.66	2.17	3.23	3.96	3.96	2.24	1.04	2.66	3.23
Nov	3.03	3.23	2.44	3.65	3.88	3.47	3.04	3.08	1.80	2.56	3.88	3.06	1.80	3.47	3.65
Dec	3.19	2.53	3.64	2.79	2.83	3.46	2.53	2.53	3.75	2.66	3.75	2.81	2.53	3.46	3.64

Monthly mean water discharge, Q (m^3/s) – RCP4.5 long-term (2071-2100)

	S1	S2	S3	S4	S5	S6	S7	S8	S9	S10	MAX	Median	MIN	Interquartile	Interdecile
Jan	2.85	2.57	2.93	1.64	3.09	1.56	1.92	2.53	2.94	3.01	3.09	2.71	1.56	2.94	3.01
Feb	2.78	2.85	2.70	1.45	2.66	1.81	2.01	2.75	3.10	3.05	3.10	2.72	1.45	2.85	3.05
Mar	2.24	2.15	2.65	1.60	2.46	1.85	2.07	2.01	3.94	2.18	3.94	2.17	1.60	2.46	2.65
Apr	2.03	2.21	3.24	1.27	2.46	1.54	1.58	1.97	3.56	1.85	3.56	2.00	1.27	2.46	3.24
May	1.71	1.78	2.02	0.92	2.07	1.53	0.83	1.85	3.88	1.60	3.88	1.74	0.83	2.02	2.07
Jun	0.14	1.63	1.53	0.86	1.10	1.05	0.76	1.82	1.38	1.42	1.82	1.24	0.14	1.53	1.63
Jul	0.69	0.94	0.88	2.19	0.62	0.30	0.54	1.34	0.92	1.64	2.19	0.90	0.30	1.34	1.64
Aug	0.51	0.84	0.86	2.04	0.23	0.27	0.54	1.28	1.27	0.70	2.04	0.77	0.23	1.27	1.28
Sep	1.54	2.35	1.79	1.65	1.17	0.75	0.83	2.10	1.79	3.12	3.12	1.72	0.75	2.10	2.35
Oct	2.38	2.53	2.07	1.57	1.66	1.39	0.73	2.31	3.16	2.40	3.16	2.19	0.73	2.40	2.53
Nov	3.72	3.87	2.66	2.99	3.14	1.50	2.39	3.40	1.93	2.33	3.87	2.82	1.50	3.40	3.72
Dec	3.26	2.70	3.46	1.82	1.97	2.37	1.32	2.66	2.13	3.84	3.84	2.52	1.32	3.26	3.46

Monthly mean water discharge, Q (m^3/s) – RCP8.5 mid-term (2041-2070)

	S1	S2	S3	S4	S5	S6	S7	S8	S9	S10	MAX	Median	MIN	Interquartile	Interdecile
Jan	2.86	2.52	2.69	2.81	2.62	2.51	2.76	2.51	2.61	2.49	2.86	2.62	2.49	2.76	2.81
Feb	2.43	2.58	2.41	2.44	2.56	2.29	2.78	2.38	2.70	2.37	2.78	2.44	2.29	2.58	2.70
Mar	2.01	2.18	2.44	2.19	2.31	2.10	2.17	2.05	2.36	2.23	2.44	2.19	2.01	2.31	2.36
Apr	2.03	2.03	2.95	2.07	1.88	1.87	2.00	2.31	2.23	2.23	2.95	2.05	1.87	2.23	2.31
May	1.71	1.98	1.75	1.68	1.84	1.70	1.69	1.90	2.29	2.14	2.29	1.79	1.68	1.98	2.14
Jun	1.08	1.94	1.47	1.69	1.25	1.77	1.48	1.75	1.67	1.62	1.94	1.64	1.08	1.75	1.77
Jul	0.49	1.14	0.78	1.11	0.76	0.79	1.06	1.26	1.03	1.03	1.26	1.03	0.49	1.11	1.14
Aug	0.50	0.91	0.76	1.07	0.67	0.70	0.86	1.06	1.03	0.93	1.07	0.89	0.50	1.03	1.06
Sep	1.52	1.80	1.34	1.77	1.95	1.75	2.11	1.91	2.45	2.07	2.45	1.85	1.34	2.07	2.11
Oct	2.24	2.64	1.76	2.24	3.68	2.91	2.38	2.72	2.59	2.51	3.68	2.55	1.76	2.72	2.91
Nov	3.25	3.59	2.66	3.01	4.03	3.46	3.31	3.16	2.95	3.61	4.03	3.28	2.66	3.59	3.61
Dec	3.17	2.62	3.49	2.84	3.21	2.80	2.96	2.84	3.42	2.82	3.49	2.90	2.62	3.21	3.42

Monthly mean water discharge, Q (m^3/s) – RCP8.5 long-term (2071-2100)

	S1	S2	S3	S4	S5	S6	S7	S8	S9	S10	MAX	Median	MIN	Interquartile	Interdecile
Jan	3.11	2.56	2.52	2.62	2.47	2.50	2.50	2.46	2.40	2.56	3.11	2.51	2.40	2.56	2.62
Feb	3.21	2.56	2.46	2.32	2.35	2.41	2.37	2.46	3.04	2.41	3.21	2.44	2.32	2.56	3.04
Mar	2.24	2.11	2.31	2.27	1.83	2.17	2.06	2.04	2.69	2.28	2.69	2.20	1.83	2.28	2.31
Apr	1.97	1.95	2.56	1.95	1.65	1.77	1.87	2.23	1.96	2.12	2.56	1.96	1.65	2.12	2.23
May	1.55	1.44	1.62	1.68	1.66	1.36	1.64	1.65	1.82	1.89	1.89	1.64	1.36	1.68	1.82
Jun	1.08	1.18	1.08	1.57	0.94	1.49	1.34	1.36	1.67	1.50	1.67	1.35	0.94	1.50	1.57
Jul	0.42	0.67	0.56	1.00	0.46	0.51	0.85	0.92	0.90	0.68	1.00	0.68	0.42	0.90	0.92
Aug	0.38	0.84	0.56	1.14	0.52	0.72	1.02	0.76	1.07	0.71	1.14	0.74	0.38	1.02	1.07
Sep	1.24	1.63	1.27	1.70	1.11	1.77	2.10	1.73	1.97	2.37	2.37	1.72	1.11	1.97	2.10
Oct	2.12	2.84	1.82	2.09	2.57	2.20	2.46	2.05	2.26	2.65	2.84	2.23	1.82	2.57	2.65
Nov	3.01	4.74	2.99	3.44	2.81	2.98	3.29	3.66	2.62	3.75	4.74	3.15	2.62	3.66	3.75
Dec	3.94	2.95	3.40	2.83	2.27	2.70	2.80	3.09	3.28	2.75	3.94	2.89	2.27	3.28	3.40

Monthly mean $N\text{-}NO_3^-$ loads (t/mt.) – Control period (1983-2012)

	S1	S2	S3	S4	S5	S6	S7	S8	S9	S10	MAX	Median	MIN	Interquartile	Interdecile
Jan	22.83	18.63	20.61	21.06	19.61	20.33	20.94	20.23	20.42	20.25	22.83	20.37	18.63	20.94	21.06
Feb	17.82	15.54	17.28	16.25	16.63	16.27	16.97	15.78	15.91	16.81	17.82	16.45	15.54	16.97	17.28
Mar	16.28	14.41	17.36	16.79	16.89	17.10	16.88	14.69	15.82	16.57	17.36	16.68	14.41	16.89	17.10
Apr	13.17	11.48	13.64	13.90	13.71	13.48	14.52	11.85	12.43	13.48	14.52	13.48	11.48	13.71	13.90
May	12.18	9.14	10.93	10.57	10.94	10.56	10.98	9.59	9.52	11.27	12.18	10.75	9.14	10.98	11.27
Jun	7.82	6.07	8.16	7.05	6.78	6.86	8.15	6.79	6.59	7.88	8.16	6.95	6.07	7.88	8.15
Jul	4.80	3.87	6.48	4.64	4.31	4.57	5.21	4.88	4.16	5.52	6.48	4.72	3.87	5.21	5.52
Aug	4.38	3.65	5.38	4.27	3.92	4.33	4.75	4.48	3.92	4.88	5.38	4.35	3.65	4.75	4.88
Sep	8.41	6.87	7.52	7.51	7.10	7.64	7.55	7.67	7.22	8.10	8.41	7.54	6.87	7.67	8.10
Oct	16.36	12.50	14.93	13.95	15.49	15.58	15.04	14.28	13.78	15.28	16.36	14.98	12.50	15.49	15.58
Nov	20.71	21.09	21.60	21.58	22.30	21.37	22.63	21.74	19.39	23.14	23.14	21.59	19.39	22.30	22.63
Dec	26.60	21.92	23.55	22.60	23.20	21.35	23.04	22.01	22.30	23.13	26.60	22.82	21.35	23.20	23.55

Monthly mean $N\text{-}NO_3^-$ loads (t/mt.) – RCP4.5 mid-term (2041-2070)

	S1	S2	S3	S4	S5	S6	S7	S8	S9	S10	MAX	Median	MIN	Interquartile	Interdecile
Jan	22.73	19.13	20.72	28.53	19.74	21.76	23.83	18.30	16.83	21.58	28.53	21.15	16.83	22.73	23.83
Feb	17.57	15.37	16.96	17.40	12.71	16.77	17.59	15.04	18.82	17.99	18.82	17.18	12.71	17.59	17.99
Mar	14.78	13.34	15.44	18.66	11.20	14.58	16.06	13.33	16.67	17.39	18.66	15.11	11.20	16.67	17.39
Apr	11.53	10.94	12.09	16.58	6.18	14.35	12.35	10.89	10.24	21.58	21.58	11.81	6.18	14.35	16.58
May	13.06	11.22	9.89	13.11	3.18	10.34	6.84	11.12	6.44	19.99	19.99	10.73	3.18	13.06	13.11
Jun	4.68	5.71	5.58	7.69	4.62	5.15	4.99	6.51	7.02	12.80	12.80	5.65	4.62	7.02	7.69
Jul	2.38	3.96	4.37	3.16	3.12	5.70	2.89	4.84	6.82	10.76	10.76	4.17	2.38	5.70	6.82
Aug	2.37	3.69	3.87	2.93	1.98	4.23	1.87	4.35	4.68	10.53	10.53	3.78	1.87	4.35	4.68
Sep	6.76	6.18	6.82	9.38	2.68	9.80	4.22	7.11	8.71	13.81	13.81	6.97	2.68	9.38	9.80
Oct	16.59	12.45	13.09	8.82	4.61	16.65	17.73	13.49	15.02	18.02	18.02	14.25	4.61	16.65	17.73
Nov	20.79	20.46	19.05	29.27	31.95	28.26	24.90	21.17	9.53	16.14	31.95	20.98	9.53	28.26	29.27
Dec	28.07	21.67	24.99	24.35	19.67	26.11	21.90	21.46	35.86	23.32	35.86	23.84	19.67	26.11	28.07

Monthly mean $N\text{-}NO_3^-$ loads (t/mt.) – RCP4.5 long-term (2071-2100)

	S1	S2	S3	S4	S5	S6	S7	S8	S9	S10	MAX	Median	MIN	Interquartile	Interdecile
Jan	26.36	21.46	22.35	15.90	25.97	12.00	17.26	21.39	21.17	26.81	26.81	21.43	12.00	25.97	26.36
Feb	18.84	17.16	18.92	9.18	18.40	13.39	14.83	16.73	17.76	21.49	21.49	17.46	9.18	18.84	18.92
Mar	16.37	15.48	18.30	12.69	18.87	13.53	15.13	14.84	19.99	18.77	19.99	15.93	12.69	18.77	18.87
Apr	13.00	12.87	15.77	7.61	15.24	8.29	10.68	11.77	18.95	14.06	18.95	12.94	7.61	15.24	15.77
May	14.57	11.58	13.27	3.98	15.54	7.85	4.64	11.86	20.76	11.47	20.76	11.72	3.98	14.57	15.54
Jun	6.15	6.17	7.50	2.41	6.14	4.75	2.62	7.42	8.66	7.69	8.66	6.16	2.41	7.50	7.69
Jul	3.55	4.42	5.48	4.23	4.27	1.85	2.72	6.19	6.69	7.67	7.67	4.34	1.85	6.19	6.69
Aug	2.82	4.08	4.78	5.23	1.81	1.81	2.45	5.78	6.54	4.54	6.54	4.31	1.81	5.23	5.78
Sep	7.03	7.53	6.56	8.44	4.56	2.09	2.62	8.17	8.99	13.23	13.23	7.28	2.09	8.44	8.99
Oct	16.72	14.45	13.31	9.01	10.80	9.70	3.10	13.68	20.81	14.12	20.81	13.50	3.10	14.45	16.72
Nov	24.13	23.81	23.66	22.26	20.18	17.49	25.25	22.71	11.55	17.51	25.25	22.48	11.55	23.81	24.13
Dec	29.64	21.26	24.31	10.70	19.82	26.37	9.10	21.14	19.76	32.36	32.36	21.20	9.10	26.37	29.64

Monthly mean $N\text{-}NO_3^-$ loads (t/mt.) – RCP8.5 mid-term (2041-2070)

	S1	S2	S3	S4	S5	S6	S7	S8	S9	S10	MAX	Median	MIN	Interquartile	Interdecile
Jan	25.80	21.00	21.43	28.98	21.46	20.89	21.57	20.12	19.16	20.50	28.98	21.21	19.16	21.57	25.80
Feb	17.65	16.85	16.62	23.67	17.70	16.03	18.21	15.96	15.87	16.79	23.67	16.82	15.87	17.70	18.21
Mar	14.90	15.94	17.24	21.57	16.82	15.18	16.34	14.82	15.29	16.41	21.57	16.14	14.82	16.82	17.24
Apr	12.22	12.56	14.20	17.53	12.19	11.55	13.06	13.69	11.73	12.84	17.53	12.70	11.55	13.69	14.20
May	14.51	11.93	12.00	14.55	11.73	11.41	12.01	12.84	12.15	13.86	14.55	12.08	11.41	13.86	14.51
Jun	5.40	6.78	6.35	8.83	5.35	6.22	7.53	7.54	6.71	8.18	8.83	6.75	5.35	7.54	8.18
Jul	3.04	4.70	4.64	6.45	3.42	4.18	5.21	6.05	4.62	5.89	6.45	4.67	3.04	5.89	6.05
Aug	2.69	4.31	3.98	6.00	3.26	3.67	4.59	5.11	4.33	5.02	6.00	4.32	2.69	5.02	5.11
Sep	6.90	7.48	5.66	9.51	6.55	6.87	8.80	8.08	7.72	8.68	9.51	7.60	5.66	8.68	8.80
Oct	15.38	14.40	12.04	18.10	18.19	15.27	14.56	14.26	13.75	16.41	18.19	14.92	12.04	16.41	18.10
Nov	22.73	24.12	22.44	31.73	24.35	23.50	24.14	23.36	19.98	25.30	31.73	23.81	19.98	24.35	25.30
Dec	29.01	20.60	25.55	30.64	25.53	23.03	23.94	22.32	24.45	23.05	30.64	24.19	20.60	25.55	29.01

Monthly mean $N\text{-}NO_3^-$ loads (t/mt.) – RCP8.5 long-term (2071-2100)

	S1	S2	S3	S4	S5	S6	S7	S8	S9	S10	MAX	Median	MIN	Interquartile	Interdecile
Jan	27.08	22.25	21.35	26.90	21.22	21.63	20.23	21.88	20.28	22.61	27.08	21.76	20.23	22.61	26.90
Feb	20.13	18.08	17.79	22.45	17.54	17.46	16.33	17.52	16.90	18.08	22.45	17.66	16.33	18.08	20.13
Mar	16.83	16.18	17.38	21.50	15.01	16.40	15.15	15.31	16.19	16.71	21.50	16.30	15.01	16.83	17.38
Apr	16.22	12.80	15.48	17.17	11.28	12.55	12.02	14.10	12.70	14.78	17.17	13.45	11.28	15.48	16.22
May	11.56	8.78	10.68	14.91	9.89	9.39	11.43	10.25	11.14	12.66	14.91	10.91	8.78	11.56	12.66
Jun	4.78	4.70	4.92	7.96	3.76	4.65	6.08	5.98	5.62	6.92	7.96	5.27	3.76	6.08	6.92
Jul	2.64	3.18	3.51	5.26	2.55	2.79	4.18	4.57	3.93	4.37	5.26	3.72	2.55	4.37	4.57
Aug	2.35	3.38	3.27	5.47	2.40	2.82	4.01	3.96	3.66	3.81	5.47	3.52	2.35	3.96	4.01
Sep	6.37	6.28	5.44	9.50	4.07	5.93	8.35	7.12	6.27	8.31	9.50	6.33	4.07	8.31	8.35
Oct	15.90	15.30	11.74	16.74	15.38	13.99	16.36	13.48	13.05	16.31	16.74	15.34	11.74	16.31	16.36
Nov	21.87	25.32	25.67	33.52	18.84	23.70	23.90	24.98	21.34	27.13	33.52	24.44	18.84	25.67	27.13
Dec	33.25	24.56	26.24	31.71	20.23	24.30	23.79	24.61	25.85	23.71	33.25	24.58	20.23	26.24	31.71

Monthly mean $N\text{-}NH_4^+$ loads (t/mt.) – Control period (1983-2012)

	S1	S2	S3	S4	S5	S6	S7	S8	S9	S10	MAX	Median	MIN	Interquartile	Interdecile
Jan	0.56	0.53	0.58	0.59	0.58	0.58	0.51	0.58	0.64	0.53	0.64	0.58	0.51	0.58	0.59
Feb	0.55	0.54	0.50	0.54	0.60	0.51	0.50	0.60	0.71	0.53	0.71	0.54	0.50	0.60	0.60
Mar	0.59	0.59	0.74	0.56	0.56	0.63	0.54	0.63	0.87	0.55	0.87	0.59	0.54	0.63	0.74
Apr	0.90	0.88	1.25	0.78	0.81	0.73	0.80	0.74	0.92	0.90	1.25	0.84	0.73	0.90	0.92
May	0.78	1.00	1.32	0.78	0.97	0.89	0.72	0.80	1.02	0.88	1.32	0.89	0.72	1.00	1.02
Jun	0.63	0.84	1.32	0.76	0.81	0.88	0.57	0.63	1.01	0.61	1.32	0.79	0.57	0.88	1.01
Jul	0.71	0.58	0.72	0.78	0.71	0.71	0.52	0.59	0.67	0.58	0.78	0.69	0.52	0.71	0.72
Aug	0.69	0.66	0.55	0.78	0.66	0.66	0.62	0.62	0.79	0.65	0.79	0.66	0.55	0.69	0.78
Sep	1.03	1.19	1.11	0.87	1.13	0.87	0.77	1.00	1.46	1.09	1.46	1.06	0.77	1.13	1.19
Oct	1.07	1.26	1.08	0.73	1.64	1.35	0.73	1.10	1.48	1.21	1.64	1.16	0.73	1.35	1.48
Nov	1.32	1.33	1.12	1.01	1.39	1.07	0.87	1.16	1.00	1.18	1.39	1.14	0.87	1.32	1.33
Dec	1.02	0.69	0.79	0.80	1.05	0.82	0.61	0.75	0.96	0.87	1.05	0.81	0.61	0.96	1.02

Monthly mean $N\text{-}NH_4^+$ loads (t/mt.) – RCP4.5 mid-term (2041-2070)

	S1	S2	S3	S4	S5	S6	S7	S8	S9	S10	MAX	Median	MIN	Interquartile	Interdecile
Jan	0.66	0.59	0.62	0.92	0.57	0.60	0.78	0.58	0.52	0.55	0.92	0.60	0.52	0.66	0.78
Feb	0.66	0.72	0.56	0.48	0.44	0.53	0.44	0.57	1.02	0.82	1.02	0.57	0.44	0.72	0.82
Mar	0.75	0.65	0.69	0.66	0.53	0.49	0.59	0.63	0.65	1.10	1.10	0.65	0.49	0.69	0.75
Apr	1.12	1.13	1.30	1.30	0.45	1.60	0.76	1.09	0.47	3.48	3.48	1.12	0.45	1.30	1.60
May	0.80	0.88	0.83	0.96	0.53	1.50	0.90	0.82	0.47	0.79	1.50	0.83	0.47	0.90	0.96
Jun	0.48	0.59	0.57	0.49	2.17	0.78	0.48	0.57	2.81	0.50	2.81	0.57	0.48	0.78	2.17
Jul	0.46	0.69	0.53	0.43	0.49	1.18	0.50	0.60	0.69	0.62	1.18	0.56	0.43	0.69	0.69
Aug	0.50	0.59	0.52	0.48	0.46	0.52	0.45	0.62	0.49	1.47	1.47	0.51	0.45	0.59	0.62
Sep	0.85	1.08	0.88	0.63	0.46	0.83	0.78	0.94	0.62	1.46	1.46	0.84	0.46	0.94	1.08
Oct	1.27	1.02	0.78	0.51	0.50	0.71	0.88	0.86	1.24	1.49	1.49	0.87	0.50	1.24	1.27
Nov	1.41	1.08	0.73	1.62	1.62	1.31	0.68	1.01	0.47	0.49	1.62	1.04	0.47	1.41	1.62
Dec	1.06	0.69	1.09	0.91	0.80	0.83	0.51	0.66	1.05	0.50	1.09	0.81	0.50	1.05	1.06

Monthly mean $N\text{-}NH_4^+$ loads (t/mt.) – RCP4.5 long-term (2071-2100)

	S1	S2	S3	S4	S5	S6	S7	S8	S9	S10	MAX	Median	MIN	Interquartile	Interdecile
Jan	0.70	0.61	0.64	0.48	0.51	0.48	0.48	0.56	0.70	0.51	0.70	0.54	0.48	0.64	0.70
Feb	0.70	0.74	0.57	0.43	0.45	0.51	0.44	0.63	0.63	0.50	0.74	0.54	0.43	0.63	0.70
Mar	0.81	0.69	0.83	0.56	0.60	0.73	0.57	0.59	1.27	0.49	1.27	0.64	0.49	0.81	0.83
Apr	1.10	1.02	1.54	0.54	0.89	1.06	0.48	0.90	1.25	0.56	1.54	0.96	0.48	1.10	1.25
May	0.73	0.76	0.80	0.55	0.69	1.33	0.48	0.77	1.89	0.56	1.89	0.75	0.48	0.80	1.33
Jun	0.54	0.59	0.54	0.50	0.47	0.57	0.48	0.66	0.47	0.49	0.66	0.52	0.47	0.57	0.59
Jul	0.49	0.55	0.51	1.26	0.47	0.46	0.51	0.68	0.48	0.63	1.26	0.51	0.46	0.63	0.68
Aug	0.47	0.54	0.51	0.91	0.44	0.45	0.51	0.66	0.53	0.49	0.91	0.51	0.44	0.54	0.66
Sep	0.75	0.91	0.71	0.52	0.50	0.49	0.49	0.75	0.57	1.22	1.22	0.64	0.49	0.75	0.91
Oct	0.94	0.91	0.70	0.49	0.55	0.61	0.48	0.75	1.07	0.58	1.07	0.65	0.48	0.91	0.94
Nov	1.30	1.16	0.71	0.81	1.10	0.55	0.89	0.93	0.51	0.48	1.30	0.85	0.48	1.10	1.16
Dec	0.91	0.64	0.83	0.47	0.54	0.70	0.47	0.58	0.50	1.04	1.04	0.61	0.47	0.83	0.91

Monthly mean N-NH_4^+ loads (t/mt.) – RCP8.5 mid-term (2041-2070)

	S1	S2	S3	S4	S5	S6	S7	S8	S9	S10	MAX	Median	MIN	Interquartile	Interdecile
Jan	0.88	0.66	0.70	1.10	0.58	0.57	0.60	0.62	0.64	0.54	1.10	0.63	0.54	0.70	0.88
Feb	0.64	0.70	0.56	0.58	0.59	0.50	0.56	0.57	0.70	0.51	0.70	0.58	0.50	0.64	0.70
Mar	0.77	0.79	0.92	0.92	0.81	0.73	0.59	0.69	0.84	0.73	0.92	0.78	0.59	0.84	0.92
Apr	1.33	1.08	1.83	1.18	0.85	0.91	0.74	1.30	1.17	1.09	1.83	1.13	0.74	1.30	1.33
May	0.98	1.05	0.87	1.02	0.94	0.87	0.75	0.92	1.20	0.99	1.20	0.96	0.75	1.02	1.05
Jun	0.49	1.02	0.69	1.15	0.67	0.84	0.54	0.75	0.79	0.63	1.15	0.72	0.49	0.84	1.02
Jul	0.46	0.79	0.54	1.08	0.62	0.56	0.64	0.78	0.77	0.59	1.08	0.63	0.46	0.78	0.79
Aug	0.51	0.65	0.55	1.08	0.57	0.56	0.57	0.72	0.80	0.58	1.08	0.57	0.51	0.72	0.80
Sep	0.97	0.86	0.67	1.34	1.09	0.90	0.99	0.93	1.50	1.00	1.50	0.98	0.67	1.09	1.34
Oct	1.40	1.26	0.74	1.26	2.07	1.54	0.82	1.23	1.25	0.95	2.07	1.25	0.74	1.40	1.54
Nov	1.94	1.39	0.99	1.94	1.59	1.33	0.99	1.17	1.01	1.16	1.94	1.25	0.99	1.59	1.94
Dec	1.21	0.76	1.19	1.15	0.83	0.75	0.66	0.83	1.09	0.64	1.21	0.83	0.64	1.15	1.19

Monthly mean N-NH_4^+ loads (t/mt.) – RCP8.5 long-term (2071-2100)

	S1	S2	S3	S4	S5	S6	S7	S8	S9	S10	MAX	Median	MIN	Interquartile	Interdecile
Jan	0.95	0.69	0.66	0.82	0.78	0.67	0.53	0.61	0.60	0.61	0.95	0.67	0.53	0.78	0.82
Feb	1.04	0.66	0.62	0.62	0.64	0.60	0.53	0.67	0.89	0.56	1.04	0.63	0.53	0.67	0.89
Mar	0.76	0.76	0.87	1.05	0.71	0.88	0.67	0.75	1.10	0.87	1.10	0.81	0.67	0.88	1.05
Apr	0.91	0.93	1.34	1.15	0.83	0.83	0.87	1.12	0.90	1.00	1.34	0.92	0.83	1.12	1.15
May	0.59	0.64	0.75	0.94	0.80	0.62	0.75	0.68	0.82	0.71	0.94	0.73	0.59	0.80	0.82
Jun	0.54	0.54	0.51	1.08	0.51	0.78	0.53	0.56	0.81	0.58	1.08	0.55	0.51	0.78	0.81
Jul	0.44	0.54	0.49	1.15	0.47	0.49	0.55	0.60	0.64	0.52	1.15	0.53	0.44	0.60	0.64
Aug	0.46	0.63	0.51	1.36	0.53	0.63	0.69	0.60	0.80	0.56	1.36	0.62	0.46	0.69	0.80
Sep	0.70	0.85	0.69	1.26	0.64	0.95	0.88	0.80	0.91	1.19	1.26	0.87	0.64	0.95	1.19
Oct	1.21	1.49	0.92	1.20	1.36	1.03	0.77	0.96	0.97	1.07	1.49	1.05	0.77	1.21	1.36
Nov	0.17	2.02	1.20	3.12	1.19	1.10	0.95	1.40	0.83	1.24	3.12	1.20	0.17	1.40	2.02
Dec	1.65	0.88	1.14	1.12	0.71	0.79	0.60	0.90	0.97	0.62	1.65	0.89	0.60	1.12	1.14

Monthly mean $P\text{-}PO_4^{3-}$ loads (t/mt.) – Control period (1983-2012)

	S1	S2	S3	S4	S5	S6	S7	S8	S9	S10	MAX	Median	MIN	Interquartile	Interdecile
Jan	0.42	0.39	0.43	0.45	0.44	0.42	0.37	0.42	0.49	0.40	0.49	0.42	0.37	0.44	0.45
Feb	0.38	0.40	0.36	0.39	0.43	0.37	0.36	0.43	0.54	0.38	0.54	0.39	0.36	0.43	0.43
Mar	0.40	0.42	0.50	0.40	0.40	0.44	0.38	0.44	0.61	0.40	0.61	0.41	0.38	0.44	0.50
Apr	0.54	0.63	0.81	0.53	0.55	0.49	0.53	0.52	0.72	0.59	0.81	0.55	0.49	0.63	0.72
May	0.48	0.63	0.86	0.54	0.62	0.61	0.49	0.53	0.68	0.57	0.86	0.59	0.48	0.63	0.68
Jun	0.51	0.60	0.85	0.50	0.51	0.62	0.40	0.44	0.71	0.43	0.85	0.51	0.40	0.62	0.71
Jul	0.48	0.41	0.47	0.53	0.45	0.47	0.38	0.41	0.48	0.40	0.53	0.46	0.38	0.48	0.48
Aug	0.46	0.48	0.39	0.54	0.43	0.45	0.44	0.42	0.52	0.43	0.54	0.44	0.39	0.48	0.52
Sep	0.65	0.85	0.88	0.60	0.81	0.60	0.52	0.66	0.99	0.72	0.99	0.69	0.52	0.85	0.88
Oct	0.87	0.98	0.88	0.57	1.36	1.02	0.54	0.84	1.14	0.91	1.36	0.89	0.54	1.02	1.14
Nov	1.05	1.14	1.07	0.87	1.25	0.89	0.71	0.97	0.89	1.07	1.25	1.01	0.71	1.07	1.14
Dec	0.81	0.56	0.66	0.67	1.01	0.70	0.47	0.64	0.87	0.76	1.01	0.68	0.47	0.81	0.87

Monthly mean $P\text{-}PO_4^{3-}$ loads (t/mt.) – RCP4.5 mid-term (2041-2070)

	S1	S2	S3	S4	S5	S6	S7	S8	S9	S10	MAX	Median	MIN	Interquartile	Interdecile
Jan	0.54	0.48	0.72	1.25	0.41	0.39	0.73	0.49	0.40	0.38	1.25	0.49	0.38	0.72	0.73
Feb	0.44	0.85	0.44	0.34	0.29	0.33	0.30	0.45	1.09	0.64	1.09	0.44	0.29	0.64	0.85
Mar	0.40	0.48	0.50	0.43	0.34	0.33	0.38	0.41	0.48	0.60	0.60	0.42	0.33	0.48	0.50
Apr	0.50	0.86	1.36	0.78	0.31	0.66	0.43	0.77	0.31	2.19	2.19	0.72	0.31	0.86	1.36
May	0.48	0.84	0.73	0.55	0.33	1.05	0.47	0.64	0.32	0.52	1.05	0.53	0.32	0.73	0.84
Jun	0.43	0.60	0.60	0.34	3.18	0.85	0.32	0.51	5.03	0.35	5.03	0.56	0.32	0.85	3.18
Jul	0.31	0.83	0.41	0.29	0.33	1.31	0.34	0.56	0.58	0.52	1.31	0.47	0.29	0.58	0.83
Aug	0.38	0.58	0.40	0.34	0.31	0.36	0.30	0.60	0.34	1.83	1.83	0.37	0.30	0.58	0.60
Sep	1.07	2.20	1.55	0.47	0.31	0.88	0.74	1.67	0.56	2.14	2.20	0.97	0.31	1.67	2.14
Oct	2.28	1.91	1.18	0.35	0.34	0.74	0.92	1.27	2.32	2.15	2.32	1.22	0.34	2.15	2.28
Nov	2.50	2.31	1.17	3.11	2.82	3.07	0.60	1.87	0.33	0.38	3.11	2.09	0.33	2.82	3.07
Dec	1.64	0.89	2.85	0.95	0.97	1.14	0.35	0.75	1.91	0.39	2.85	0.96	0.35	1.64	1.91

Monthly mean $P\text{-}PO_4^{3-}$ loads (t/mt.) – RCP4.5 long-term (2071-2100)

	S1	S2	S3	S4	S5	S6	S7	S8	S9	S10	MAX	Median	MIN	Interquartile	Interdecile
Jan	0.68	0.70	0.84	0.34	0.45	0.33	0.35	0.52	1.40	0.37	1.40	0.49	0.33	0.70	0.84
Feb	0.59	1.05	0.56	0.30	0.30	0.33	0.33	0.74	0.50	0.35	1.05	0.42	0.30	0.59	0.74
Mar	0.50	0.63	0.95	0.40	0.37	0.65	0.58	0.41	1.95	0.34	1.95	0.54	0.34	0.65	0.95
Apr	0.56	1.15	2.52	0.36	0.72	0.69	0.36	0.84	0.99	0.34	2.52	0.71	0.34	0.99	1.15
May	0.59	0.94	1.10	0.39	0.43	1.01	0.33	0.91	3.28	0.38	3.28	0.75	0.33	1.01	1.10
Jun	0.55	0.82	0.61	0.34	0.32	0.46	0.33	0.93	0.32	0.35	0.93	0.41	0.32	0.61	0.82
Jul	0.42	0.60	0.40	2.75	0.32	0.31	0.35	1.08	0.32	0.67	2.75	0.41	0.31	0.67	1.08
Aug	0.39	0.58	0.50	1.47	0.30	0.30	0.35	1.06	0.43	0.34	1.47	0.41	0.30	0.58	1.06
Sep	1.36	2.72	1.63	0.41	0.34	0.33	0.34	1.64	0.62	2.60	2.72	0.99	0.33	1.64	2.60
Oct	2.39	2.22	1.24	0.34	0.45	0.61	0.33	1.45	3.14	0.60	3.14	0.93	0.33	2.22	2.39
Nov	3.82	3.91	1.48	1.47	2.98	0.47	1.67	2.73	0.51	0.37	3.91	1.57	0.37	2.98	3.82
Dec	1.84	1.14	2.34	0.32	0.54	0.70	0.33	0.84	0.41	3.00	3.00	0.77	0.32	1.84	2.34

Monthly mean $P\text{-}PO_4^{3-}$ loads (t/mt.) – RCP8.5 mid-term (2041-2070)

	S1	S2	S3	S4	S5	S6	S7	S8	S9	S10	MAX	Median	MIN	Interquartile	Interdecile
Jan	0.71	0.59	0.62	0.78	0.46	0.43	0.48	0.53	0.63	0.41	0.78	0.56	0.41	0.63	0.71
Feb	0.38	0.59	0.40	0.37	0.43	0.33	0.40	0.43	0.67	0.37	0.67	0.40	0.33	0.43	0.59
Mar	0.42	0.56	0.68	0.55	0.53	0.46	0.37	0.44	0.68	0.49	0.68	0.51	0.37	0.56	0.68
Apr	0.61	0.63	1.77	0.66	0.46	0.50	0.42	0.77	0.85	0.73	1.77	0.64	0.42	0.77	0.85
May	0.63	0.87	0.66	0.59	0.68	0.55	0.45	0.68	1.24	0.80	1.24	0.67	0.45	0.80	0.87
Jun	0.35	0.99	0.58	0.75	0.52	0.80	0.38	0.62	0.75	0.49	0.99	0.60	0.35	0.75	0.80
Jul	0.31	0.76	0.38	0.68	0.55	0.42	0.50	0.74	0.75	0.44	0.76	0.53	0.31	0.74	0.75
Aug	0.36	0.57	0.39	0.66	0.45	0.41	0.40	0.65	0.72	0.45	0.72	0.45	0.36	0.65	0.66
Sep	0.86	0.92	0.59	0.84	1.27	0.91	1.02	0.94	1.96	0.94	1.96	0.93	0.59	1.02	1.27
Oct	1.56	1.65	0.75	0.78	3.20	2.05	0.78	1.89	1.77	0.98	3.20	1.60	0.75	1.89	2.05
Nov	2.33	2.24	1.29	1.30	2.47	1.93	1.29	1.61	1.34	1.64	2.47	1.62	1.29	2.24	2.33
Dec	1.36	0.83	1.89	0.79	0.97	0.72	0.66	0.96	1.57	0.63	1.89	0.89	0.63	1.36	1.57

Monthly mean $P\text{-}PO_4^{3-}$ loads (t/mt.) – RCP8.5 long-term (2071-2100)

	S1	S2	S3	S4	S5	S6	S7	S8	S9	S10	MAX	Median	MIN	Interquartile	Interdecile
Jan	0.81	0.66	0.72	0.62	0.84	0.62	0.37	0.54	0.59	0.54	0.84	0.62	0.37	0.72	0.81
Feb	1.03	0.63	0.50	0.38	0.52	0.40	0.35	0.59	1.30	0.41	1.30	0.51	0.35	0.63	1.03
Mar	0.44	0.60	0.73	0.61	0.43	0.55	0.42	0.58	1.51	0.68	1.51	0.59	0.42	0.68	0.73
Apr	0.53	0.82	1.52	0.63	0.63	0.49	0.47	1.17	0.66	0.84	1.52	0.65	0.47	0.84	1.17
May	0.49	0.60	0.88	0.63	0.92	0.47	0.55	0.70	0.99	0.74	0.99	0.66	0.47	0.88	0.92
Jun	0.45	0.46	0.42	0.82	0.41	0.96	0.41	0.50	1.18	0.52	1.18	0.48	0.41	0.82	0.96
Jul	0.30	0.47	0.34	0.91	0.33	0.38	0.45	0.58	0.72	0.41	0.91	0.43	0.30	0.58	0.72
Aug	0.33	0.68	0.36	1.06	0.46	0.76	0.75	0.62	1.11	0.47	1.11	0.65	0.33	0.76	1.06
Sep	0.82	1.28	0.78	1.00	0.68	1.73	1.21	1.18	1.75	2.30	2.30	1.20	0.68	1.73	1.75
Oct	1.90	3.65	1.53	0.99	2.89	1.53	1.03	1.50	1.67	2.07	3.65	1.60	0.99	2.07	2.89
Nov	2.84	6.01	2.50	3.08	2.49	2.26	1.78	3.34	1.42	2.61	6.01	2.55	1.42	3.08	3.34
Dec	3.06	1.37	2.28	0.92	0.91	1.07	0.64	1.56	2.20	0.63	3.06	1.22	0.63	2.20	2.28

APPENDIX D – AQUATOX OUTPUT TABLES

Monthly mean Dissolved Inorganic Nitrogen, DIN (mg/l) – Control period (1983-2012)

	S1	S2	S3	S4	S5	S6	S7	S8	S9	S10	MAX	Median	MIN	Interquartile	Interdecile
Jan	1.30	1.32	1.34	1.38	1.29	1.32	1.35	1.34	1.37	1.29	1.38	1.33	1.29	1.35	1.37
Feb	1.21	1.22	1.26	1.26	1.21	1.25	1.25	1.22	1.22	1.22	1.26	1.22	1.21	1.25	1.26
Mar	1.14	1.07	1.14	1.16	1.15	1.16	1.14	1.07	1.07	1.14	1.16	1.14	1.07	1.15	1.16
Apr	0.97	0.84	0.90	0.96	0.94	0.94	0.94	0.89	0.85	0.91	0.97	0.92	0.84	0.94	0.96
May	0.71	0.64	0.68	0.70	0.70	0.70	0.70	0.66	0.64	0.68	0.71	0.69	0.64	0.70	0.70
Jun	0.42	0.36	0.43	0.42	0.41	0.40	0.46	0.39	0.38	0.44	0.46	0.42	0.36	0.43	0.44
Jul	0.32	0.32	0.38	0.33	0.32	0.33	0.35	0.35	0.33	0.38	0.38	0.33	0.32	0.35	0.38
Aug	0.35	0.35	0.43	0.37	0.36	0.38	0.37	0.38	0.35	0.38	0.43	0.37	0.35	0.38	0.38
Sep	0.46	0.44	0.48	0.48	0.45	0.47	0.48	0.47	0.44	0.48	0.48	0.47	0.44	0.48	0.48
Oct	0.73	0.68	0.77	0.77	0.74	0.77	0.79	0.73	0.70	0.75	0.79	0.75	0.68	0.77	0.77
Nov	1.06	1.05	1.17	1.11	1.08	1.11	1.15	1.10	1.06	1.12	1.17	1.10	1.05	1.12	1.15
Dec	1.30	1.31	1.37	1.32	1.25	1.25	1.34	1.29	1.26	1.26	1.37	1.29	1.25	1.32	1.34

Monthly mean Dissolved Inorganic Nitrogen, DIN (mg/l) – RCP4.5 mid-term (2041-2070)

	S1	S2	S3	S4	S5	S6	S7	S8	S9	S10	MAX	Median	MIN	Interquartile	Interdecile
Jan	1.25	1.32	1.29	1.27	1.29	1.28	1.29	1.26	1.24	1.26	1.32	1.28	1.24	1.29	1.29
Feb	1.21	1.11	1.19	1.18	1.16	1.20	1.17	1.13	1.09	1.19	1.21	1.18	1.09	1.19	1.20
Mar	1.09	0.99	1.05	1.05	1.06	1.08	1.05	1.00	0.99	1.09	1.09	1.05	0.99	1.08	1.09
Apr	0.86	0.80	0.81	0.88	0.88	0.91	0.87	0.81	0.80	0.85	0.91	0.85	0.80	0.88	0.88
May	0.62	0.63	0.59	0.70	0.67	0.67	0.69	0.65	0.61	0.65	0.70	0.65	0.59	0.67	0.69
Jun	0.32	0.35	0.33	0.38	0.37	0.35	0.39	0.37	0.35	0.37	0.39	0.36	0.32	0.37	0.38
Jul	0.24	0.30	0.36	0.33	0.27	0.27	0.29	0.35	0.34	0.32	0.36	0.31	0.24	0.34	0.35
Aug	0.36	0.37	0.43	0.39	0.39	0.38	0.35	0.40	0.41	0.35	0.43	0.38	0.35	0.40	0.41
Sep	0.44	0.43	0.45	0.48	0.46	0.48	0.46	0.46	0.45	0.44	0.48	0.46	0.43	0.46	0.48
Oct	0.67	0.62	0.68	0.73	0.64	0.70	0.74	0.68	0.66	0.72	0.74	0.68	0.62	0.72	0.73
Nov	1.00	0.98	1.06	1.03	1.01	1.05	1.06	1.03	1.05	1.02	1.06	1.03	0.98	1.05	1.06
Dec	1.21	1.29	1.26	1.20	1.25	1.24	1.26	1.27	1.26	1.26	1.29	1.26	1.20	1.26	1.27

Monthly mean Dissolved Inorganic Nitrogen, DIN (mg/l) – RCP4.5 long-term (2071-2100)

	S1	S2	S3	S4	S5	S6	S7	S8	S9	S10	MAX	Median	MIN	Interquartile	Interdecile
Jan	1.26	1.26	1.22	1.23	1.27	1.27	1.24	1.26	1.20	1.25	1.27	1.25	1.20	1.26	1.27
Feb	1.16	1.11	1.20	1.15	1.16	1.19	1.18	1.11	1.06	1.15	1.20	1.16	1.06	1.18	1.19
Mar	1.07	1.02	1.06	1.04	1.04	1.06	1.05	1.00	1.00	1.03	1.07	1.04	1.00	1.06	1.06
Apr	0.87	0.83	0.82	0.89	0.87	0.84	0.89	0.81	0.84	0.83	0.89	0.84	0.81	0.87	0.89
May	0.63	0.62	0.63	0.66	0.67	0.65	0.70	0.62	0.65	0.67	0.70	0.65	0.62	0.67	0.67
Jun	0.34	0.35	0.43	0.37	0.35	0.31	0.42	0.35	0.34	0.39	0.43	0.35	0.31	0.39	0.42
Jul	0.30	0.31	0.39	0.33	0.31	0.31	0.33	0.31	0.37	0.36	0.39	0.32	0.30	0.36	0.37
Aug	0.43	0.43	0.45	0.39	0.41	0.44	0.36	0.43	0.40	0.39	0.45	0.42	0.36	0.43	0.44
Sep	0.46	0.45	0.47	0.44	0.48	0.47	0.47	0.47	0.43	0.45	0.48	0.46	0.43	0.47	0.47
Oct	0.66	0.67	0.70	0.71	0.68	0.68	0.75	0.66	0.66	0.75	0.75	0.68	0.66	0.71	0.75
Nov	0.99	1.01	1.20	1.05	0.98	1.01	1.09	1.01	1.01	1.03	1.20	1.01	0.98	1.05	1.09
Dec	1.25	1.19	1.23	1.19	1.21	1.26	1.21	1.17	1.22	1.22	1.26	1.22	1.17	1.23	1.25

Monthly mean Dissolved Inorganic Nitrogen, DIN (mg/l) – RCP8.5 mid-term (2041-2070)

	S1	S2	S3	S4	S5	S6	S7	S8	S9	S10	MAX	Median	MIN	Interquartile	Interdecile
Jan	1.27	1.30	1.26	1.67	1.28	1.30	1.24	1.23	1.17	1.29	1.67	1.27	1.17	1.30	1.30
Feb	1.17	1.18	1.17	1.62	1.19	1.19	1.14	1.14	1.06	1.20	1.62	1.18	1.06	1.19	1.20
Mar	1.05	1.06	1.06	1.43	1.07	1.05	1.06	1.00	0.96	1.07	1.43	1.06	0.96	1.07	1.07
Apr	0.80	0.85	0.82	1.19	0.88	0.85	0.90	0.85	0.79	0.83	1.19	0.85	0.79	0.88	0.90
May	0.64	0.64	0.64	0.90	0.67	0.68	0.71	0.69	0.62	0.70	0.90	0.68	0.62	0.70	0.71
Jun	0.35	0.35	0.38	0.51	0.35	0.36	0.45	0.40	0.34	0.44	0.51	0.37	0.34	0.44	0.45
Jul	0.32	0.30	0.36	0.41	0.26	0.30	0.33	0.35	0.34	0.37	0.41	0.33	0.26	0.36	0.37
Aug	0.43	0.41	0.43	0.45	0.37	0.40	0.36	0.41	0.38	0.39	0.45	0.41	0.36	0.43	0.43
Sep	0.50	0.49	0.48	0.58	0.47	0.47	0.48	0.49	0.45	0.50	0.58	0.48	0.45	0.50	0.50
Oct	0.71	0.67	0.69	0.92	0.72	0.69	0.72	0.65	0.65	0.76	0.92	0.70	0.65	0.72	0.76
Nov	1.18	1.03	1.16	1.52	1.01	1.05	1.07	1.08	0.99	1.10	1.52	1.07	0.99	1.16	1.18
Dec	1.28	1.20	1.27	1.70	1.25	1.27	1.24	1.23	1.16	1.27	1.70	1.26	1.16	1.27	1.28

Monthly mean Dissolved Inorganic Nitrogen, DIN (mg/l) – RCP8.5 long-term (2071-2100)

	S1	S2	S3	S4	S5	S6	S7	S8	S9	S10	MAX	Median	MIN	Interquartile	Interdecile
Jan	1.31	1.32	1.31	1.61	1.32	1.34	1.24	1.32	1.31	1.33	1.61	1.32	1.24	1.33	1.34
Feb	1.21	1.22	1.20	1.55	1.26	1.22	1.14	1.22	1.08	1.24	1.55	1.22	1.08	1.24	1.26
Mar	1.06	1.07	1.07	1.37	1.12	1.08	1.03	1.05	0.95	1.05	1.37	1.06	0.95	1.08	1.12
Apr	0.85	0.85	0.87	1.15	0.87	0.89	0.85	0.85	0.84	0.88	1.15	0.86	0.84	0.88	0.89
May	0.56	0.53	0.57	0.85	0.56	0.61	0.66	0.56	0.60	0.66	0.85	0.58	0.53	0.66	0.66
Jun	0.30	0.32	0.36	0.46	0.31	0.29	0.38	0.36	0.30	0.39	0.46	0.34	0.29	0.38	0.39
Jul	0.36	0.31	0.37	0.38	0.32	0.33	0.26	0.35	0.32	0.33	0.38	0.33	0.26	0.36	0.37
Aug	0.60	0.49	0.55	0.52	0.51	0.53	0.36	0.53	0.50	0.50	0.60	0.52	0.36	0.53	0.55
Sep	0.53	0.53	0.52	0.62	0.53	0.51	0.48	0.52	0.48	0.50	0.62	0.52	0.48	0.53	0.53
Oct	0.69	0.69	0.68	0.88	0.73	0.72	0.75	0.68	0.64	0.72	0.88	0.70	0.64	0.73	0.75
Nov	1.21	0.92	1.21	1.48	0.98	1.14	1.07	1.01	1.06	1.09	1.48	1.08	0.92	1.21	1.21
Dec	1.34	1.23	1.33	1.70	1.24	1.37	1.26	1.23	1.32	1.28	1.70	1.30	1.23	1.34	1.37

Monthly mean Dissolved Inorganic Phosphorus, DIP (mg/l) – Control period (1983-2012)

	S1	S2	S3	S4	S5	S6	S7	S8	S9	S10	MAX	Median	MIN	Interquartile	Interdecile
Jan	0.028	0.028	0.028	0.029	0.029	0.027	0.024	0.028	0.033	0.027	0.033	0.028	0.024	0.029	0.029
Feb	0.026	0.028	0.026	0.027	0.027	0.026	0.024	0.029	0.032	0.025	0.032	0.027	0.024	0.028	0.029
Mar	0.028	0.030	0.029	0.027	0.027	0.028	0.025	0.030	0.035	0.027	0.035	0.028	0.025	0.030	0.030
Apr	0.034	0.035	0.039	0.032	0.030	0.030	0.031	0.035	0.036	0.035	0.039	0.034	0.030	0.035	0.036
May	0.042	0.050	0.053	0.042	0.044	0.044	0.039	0.043	0.051	0.041	0.053	0.044	0.039	0.050	0.051
Jun	0.033	0.038	0.044	0.033	0.039	0.039	0.033	0.032	0.042	0.032	0.044	0.036	0.032	0.039	0.042
Jul	0.040	0.048	0.041	0.043	0.043	0.045	0.037	0.040	0.050	0.040	0.050	0.042	0.037	0.045	0.048
Aug	0.055	0.063	0.056	0.060	0.056	0.060	0.051	0.056	0.061	0.053	0.063	0.056	0.051	0.060	0.061
Sep	0.054	0.061	0.055	0.056	0.057	0.054	0.050	0.055	0.062	0.053	0.062	0.055	0.050	0.057	0.061
Oct	0.052	0.057	0.051	0.045	0.062	0.054	0.040	0.050	0.062	0.050	0.062	0.052	0.040	0.057	0.062
Nov	0.050	0.054	0.047	0.043	0.056	0.047	0.036	0.047	0.051	0.048	0.056	0.048	0.036	0.051	0.054
Dec	0.041	0.037	0.037	0.037	0.042	0.037	0.029	0.037	0.042	0.038	0.042	0.037	0.029	0.041	0.042

Monthly mean Dissolved Inorganic Phosphorus, DIP (mg/l) – RCP4.5 mid-term (2041-2070)

	S1	S2	S3	S4	S5	S6	S7	S8	S9	S10	MAX	Median	MIN	Interquartile	Interdecile
Jan	0.040	0.037	0.045	0.034	0.042	0.028	0.025	0.034	0.050	0.029	0.050	0.036	0.025	0.042	0.045
Feb	0.029	0.042	0.031	0.028	0.038	0.023	0.025	0.032	0.046	0.029	0.046	0.030	0.023	0.038	0.042
Mar	0.029	0.038	0.032	0.031	0.032	0.028	0.027	0.032	0.043	0.031	0.043	0.032	0.027	0.032	0.038
Apr	0.036	0.052	0.060	0.042	0.043	0.038	0.033	0.047	0.058	0.043	0.060	0.043	0.033	0.052	0.058
May	0.043	0.058	0.060	0.050	0.054	0.045	0.043	0.052	0.064	0.050	0.064	0.051	0.043	0.058	0.060
Jun	0.038	0.042	0.039	0.046	0.046	0.045	0.038	0.035	0.055	0.036	0.055	0.040	0.035	0.046	0.046
Jul	0.039	0.059	0.052	0.058	0.049	0.050	0.041	0.053	0.061	0.043	0.061	0.051	0.039	0.058	0.059
Aug	0.055	0.065	0.061	0.064	0.062	0.064	0.056	0.064	0.070	0.060	0.070	0.063	0.055	0.064	0.065
Sep	0.076	0.086	0.078	0.068	0.084	0.079	0.061	0.083	0.085	0.075	0.086	0.079	0.061	0.084	0.085
Oct	0.099	0.091	0.076	0.060	0.108	0.085	0.057	0.079	0.082	0.072	0.108	0.080	0.057	0.091	0.099
Nov	0.093	0.085	0.068	0.076	0.094	0.086	0.050	0.077	0.066	0.058	0.094	0.077	0.050	0.086	0.093
Dec	0.071	0.057	0.075	0.056	0.056	0.054	0.032	0.050	0.062	0.042	0.075	0.056	0.032	0.062	0.071

Monthly mean Dissolved Inorganic Phosphorus, DIP (mg/l) – RCP4.5 long-term (2071-2100)

	S1	S2	S3	S4	S5	S6	S7	S8	S9	S10	MAX	Median	MIN	Interquartile	Interdecile
Jan	0.044	0.041	0.046	0.033	0.041	0.035	0.026	0.033	0.046	0.029	0.046	0.038	0.026	0.044	0.046
Feb	0.033	0.046	0.033	0.028	0.034	0.028	0.023	0.037	0.056	0.026	0.056	0.033	0.023	0.037	0.046
Mar	0.032	0.042	0.044	0.032	0.035	0.035	0.025	0.033	0.045	0.034	0.045	0.034	0.025	0.042	0.044
Apr	0.037	0.059	0.084	0.038	0.042	0.046	0.030	0.048	0.054	0.048	0.084	0.047	0.030	0.054	0.059
May	0.045	0.063	0.071	0.049	0.058	0.058	0.041	0.057	0.075	0.052	0.075	0.057	0.041	0.063	0.071
Jun	0.041	0.053	0.048	0.048	0.051	0.054	0.036	0.050	0.062	0.040	0.062	0.049	0.036	0.053	0.054
Jul	0.048	0.054	0.052	0.050	0.058	0.062	0.044	0.061	0.068	0.047	0.068	0.053	0.044	0.061	0.062
Aug	0.062	0.065	0.056	0.069	0.066	0.069	0.048	0.078	0.086	0.062	0.086	0.065	0.048	0.069	0.078
Sep	0.082	0.101	0.082	0.080	0.080	0.096	0.057	0.087	0.119	0.084	0.119	0.083	0.057	0.096	0.101
Oct	0.110	0.108	0.078	0.075	0.123	0.109	0.060	0.082	0.114	0.089	0.123	0.098	0.060	0.110	0.114
Nov	0.119	0.119	0.077	0.087	0.107	0.110	0.075	0.090	0.091	0.083	0.119	0.090	0.075	0.110	0.119
Dec	0.083	0.070	0.077	0.060	0.065	0.068	0.048	0.054	0.066	0.052	0.083	0.066	0.048	0.070	0.077

Monthly mean Dissolved Inorganic Phosphorus, DIP (mg/l) – RCP8.5 mid-term (2041-2070)

	S1	S2	S3	S4	S5	S6	S7	S8	S9	S10	MAX	Median	MIN	Interquartile	Interdecile
Jan	0.042	0.035	0.040	0.037	0.030	0.028	0.026	0.033	0.041	0.027	0.042	0.034	0.026	0.040	0.041
Feb	0.029	0.034	0.028	0.027	0.027	0.024	0.023	0.028	0.036	0.025	0.036	0.027	0.023	0.029	0.034
Mar	0.029	0.035	0.034	0.031	0.030	0.028	0.024	0.030	0.038	0.029	0.038	0.030	0.024	0.034	0.035
Apr	0.038	0.043	0.064	0.041	0.034	0.035	0.029	0.042	0.048	0.041	0.064	0.041	0.029	0.043	0.048
May	0.045	0.052	0.056	0.047	0.045	0.043	0.036	0.048	0.058	0.047	0.058	0.047	0.036	0.052	0.056
Jun	0.041	0.047	0.040	0.044	0.045	0.044	0.034	0.040	0.042	0.035	0.047	0.042	0.034	0.044	0.045
Jul	0.036	0.053	0.051	0.051	0.045	0.046	0.041	0.048	0.058	0.044	0.058	0.047	0.036	0.051	0.053
Aug	0.050	0.058	0.055	0.061	0.053	0.052	0.048	0.057	0.068	0.045	0.068	0.054	0.045	0.058	0.061
Sep	0.071	0.068	0.063	0.065	0.074	0.066	0.058	0.064	0.086	0.061	0.086	0.065	0.058	0.071	0.074
Oct	0.083	0.075	0.061	0.054	0.101	0.083	0.052	0.072	0.085	0.058	0.101	0.073	0.052	0.083	0.085
Nov	0.081	0.077	0.062	0.057	0.086	0.076	0.051	0.064	0.066	0.058	0.086	0.065	0.051	0.077	0.081
Dec	0.065	0.052	0.063	0.043	0.051	0.045	0.036	0.049	0.059	0.039	0.065	0.050	0.036	0.059	0.063

Monthly mean Dissolved Inorganic Phosphorus, DIP (mg/l) – RCP8.5 long-term (2071-2100)

	S1	S2	S3	S4	S5	S6	S7	S8	S9	S10	MAX	Median	MIN	Interquartile	Interdecile
Jan	0.054	0.043	0.049	0.034	0.047	0.039	0.025	0.040	0.043	0.030	0.054	0.042	0.025	0.047	0.049
Feb	0.041	0.035	0.033	0.027	0.037	0.029	0.023	0.034	0.051	0.028	0.051	0.034	0.023	0.037	0.041
Mar	0.032	0.037	0.039	0.034	0.034	0.033	0.027	0.037	0.061	0.035	0.061	0.035	0.027	0.037	0.039
Apr	0.035	0.050	0.066	0.043	0.047	0.039	0.034	0.055	0.053	0.048	0.066	0.047	0.034	0.053	0.055
May	0.042	0.052	0.065	0.049	0.060	0.043	0.043	0.055	0.059	0.051	0.065	0.052	0.042	0.059	0.060
Jun	0.047	0.050	0.049	0.049	0.050	0.056	0.041	0.049	0.059	0.042	0.059	0.049	0.041	0.050	0.056
Jul	0.042	0.037	0.044	0.058	0.042	0.053	0.035	0.042	0.060	0.045	0.060	0.043	0.035	0.053	0.058
Aug	0.038	0.042	0.044	0.075	0.052	0.055	0.056	0.045	0.075	0.049	0.075	0.050	0.038	0.056	0.075
Sep	0.062	0.082	0.069	0.086	0.080	0.092	0.072	0.070	0.094	0.089	0.094	0.081	0.062	0.089	0.092
Oct	0.103	0.122	0.087	0.069	0.117	0.095	0.064	0.089	0.088	0.094	0.122	0.091	0.064	0.103	0.117
Nov	0.112	0.151	0.099	0.096	0.108	0.093	0.065	0.108	0.075	0.087	0.151	0.097	0.065	0.108	0.112
Dec	0.102	0.087	0.086	0.058	0.069	0.065	0.040	0.074	0.069	0.046	0.102	0.069	0.040	0.086	0.087

REFERENCES

Abbaspour, K. C. 2014. “SWAT-CUP 2012: SWAT Calibration and Uncertainty Programs - A User Manual.” *Science And Technology* 106.

Abberton, Michael et al. 2016. “Global Agricultural Intensification during Climate Change: A Role for Genomics.” *Plant Biotechnology Journal* 14(4):1095–98. Retrieved (http://doi.wiley.com/10.1111/pbi.12467).

Alam, Md Jahangir and Dushmanta Dutta. 2013. “Predicting Climate Change Impact on Nutrient Pollution in Waterways: A Case Study in the Upper Catchment of the Latrobe River, Australia.” *Ecohydrology* 6(1):73–82. Retrieved (http://doi.wiley.com/10.1002/eco.282).

Amin, M. Z. M. et al. 2017. “Future Climate Change Impact Assessment of Watershed Scale Hydrologic Processes in Peninsular Malaysia by a Regional Climate Model Coupled with a Physically-Based Hydrology Modelo.” *Science of The Total Environment* 575:12–22. Retrieved (http://linkinghub.elsevier.com/retrieve/pii/S004896971632174X).

Arnell, N. W. et al. 2004. “Climate and Socio-Economic Scenarios for Global-Scale Climate Change Impacts Assessments: Characterising the SRES Storylines.” *Global Environmental Change* 14(1):3–20.

Arnell, Nigel W. 1999. “The Effect of Climate Change on Hydrological Regimes in Europe: A Continental Perspective.” *Global Environmental Change* 9(1):5–23.

Arnell, Nigel W. 2003. “Relative Effects of Multi-Decadal Climatic Variability and Changes in the Mean and Variability of Climate due to Global Warming: Future Streamflows in Britain.” *Journal of Hydrology* 270(3–4):195–213.

Arnold, J. G. et al. 2012. “Swat: Model Use, Calibration, and Validation.” *Asabe* 55(4):1491–1508.

Arnold, J. G., R. Srinivasan, R. S. Muttiah, and J. R. Williams. 1998. “Large Area Hydrologic Modeling and Assessment Part I: Model Development.” *Journal of the American Water Resources Association* 34(1):73–89. Retrieved (http://doi.wiley.com/10.1111/j.1752-1688.1998.tb05961.x).

ARPAV. 2001. “La Carta Dei Suoli Del Bacino Scolante in Laguna Di Venezia.” *Bollettino della Società Italiana della Scienza del Suolo* 50:273–80.

ARPAV. 2004a. *Carta Dei Suoli Del Bacino Scolante in Laguna Di Venezia*.

ARPAV. 2004b. *Carta Dei Suoli Della Regione Veneto Alla Scala 1:250.000*.

ARPAV. 2009. “Banca Dati Della Copertura Del Suolo Della Regione Veneto.” Retrieved January 1, 2016 (http://idt.regione.veneto.it).

ARPAV. 2010. “Rete Idrografica Del Veneto.”

ARPAV and Regione Veneto. 2007. *Bacino Scolante Nella Laguna Di Venezia. Rapporto Sullo Stato Ambientale Dei Corpi Idrici, Anni 2003-2004*.

ARPAV and Regione Veneto. 2009. *Bacino Scolante Nella Laguna Di Venezia: Rapporto Sullo Stato Ambientale Dei Corpi Idrici. Anni 2005-2007*.

Aydinalp, Cumhur and Malcolm S. Cresser. 2008. “The Effects of Global Climate Change on Agriculture.” *American-Eurasian J. Agric. & Environ. Sci.* 3(5):672–76. Retrieved (http://idosi.org/aejaes/jaes3(5)/1.pdf).

Azzellino, A., R. Salvetti, R. Vismara, and L. Bonomo. 2006. “Combined Use of the EPA-QUAL2E Simulation Model and Factor Analysis to Assess the Source Apportionment of Point and Non Point Loads of Nutrients to Surface Waters.” *Science of The Total Environment* 371(1–3):214–22. Retrieved (http://linkinghub.elsevier.com/retrieve/pii/S004896970600252X).

Benton Jones Jr., J. 2003. *Agronomic Handbook - Management of Crops, Soil. and Their Fertility*.

Bintanja, R., G. J. van Oldenborgh, S. S. Drijfhout, B. Wouters, and C. A. Katsman. 2013. “Important Role for Ocean Warming and Increased Ice-Shelf Melt in Antarctic Sea-Ice Expansion.” *Nature Geoscience* 6(5):376–79. Retrieved (http://www.nature.com/doifinder/10.1038/ngeo1767).

Blanchard, J. L. et al. 2012. “Potential Consequences of Climate Change for Primary Production and Fish Production in Large Marine Ecosystems.” *Philosophical Transactions of the Royal Society B: Biological Sciences* 367(1605):2979–89. Retrieved (http://rstb.royalsocietypublishing.org/cgi/doi/10.1098/rstb.2012.0231).

Blanco, Maria. 2011. *Supply of and Access to Key Nutrients NPK for Fertilizers for Feeding the World in 2050*.

Blankespoor, Brian, Susmita Dasgupta, and Benoit Laplante. 2012. “Sea-Level Rise and Coastal Wetlands Impacts and Costs.” *World Bank Policy …* (November):1–27. Retrieved (http://papers.ssrn.com/sol3/papers.cfm?abstract_id=2181286).

Bloom, Nicolas S., Ligia M. Moretto, Paolo Scopece, and Paolo Ugo. 2004. “Seasonal Cycling of Mercury and Monomethyl Mercury in the Venice Lagoon (Italy).” *Marine Chemistry* 91(1–4):85–99. Retrieved (http://linkinghub.elsevier.com/retrieve/pii/S0304420304001756).

Boesch, Donald F. 2002. “Challenges and Opportunities for Science in Reducing Nutrient over-Enrichment of Coastal Ecosystems.” *Estuaries* 25(4):886–900. Retrieved (http://link.springer.com/10.1007/BF02804914).

Bonetto, Christian and Lorenzo Furlan. 2012. *Gestione Fertilizzanti E Contributi Tecnici Sulla Problematica Dei Nitrati*.

Bouraoui, F., L. Galbiati, and G. Bidoglio. 2002. “Climate Change Impacts on Nutrient Loads in the Yorkshire Ouse Catchment (UK).” *Hydrology and Earth System Sciences* 6(2):197–209. Retrieved (https://hal.archives-ouvertes.fr/hal-00304659/document).

Boxall, Alistair B. A. et al. 2009. “Impacts of Climate Change on Indirect Human Exposure to Pathogens and Chemicals from Agriculture.” *Environmental Health Perspectives* 117(4):508–14.

Brevik, Eric. 2013. “The Potential Impact of Climate Change on Soil Properties and Processes and Corresponding Influence on Food Security.” *Agriculture* 3(3):398–417. Retrieved (http://www.mdpi.com/2077-0472/3/3/398/).

Brito, Ana C., Alice Newton, Paul Tett, and Teresa F. Fernandes. 2012. “How Will Shallow Coastal Lagoons Respond to Climate Change? A Modelling Investigation.” *Estuarine, Coastal and Shelf Science* 112:98–104. Retrieved (http://linkinghub.elsevier.com/retrieve/pii/S0272771411003829).

Brown, L. C. and T. O.Jr. Barnwell. 1987. “The Enhanced Water Quality Models QUAL2E and Evaluate the Impacts of Water Quality Management Plans Implemented in a Watershed in Texas.” *Environ. Model. Soft.* 21(8):1141–57.

Bussi, Gianbattista, Paul G. Whitehead, et al. 2016. “Impacts of Climate Change, Land-Use Change and Phosphorus Reduction on Phytoplankton in the River Thames (UK).” *Science*

of The Total Environment. Retrieved (http://linkinghub.elsevier.com/retrieve/pii/S0048969716303199).

Bussi, Gianbattista, Simon J. Dadson, Christel Prudhomme, and Paul G. Whitehead. 2016. "Modelling the Future Impacts of Climate and Land-Use Change on Suspended Sediment Transport in the River Thames (UK)." *Journal of Hydrology* 542:357–72. Retrieved (http://linkinghub.elsevier.com/retrieve/pii/S0022169416305625).

Cadée, Gerhard C. and Jan Hegeman. 2002. "Phytoplankton in the Marsdiep at the End of the 20th Century; 30 Years Monitoring Biomass, Primary Production, and Phaeocystis Blooms." *Journal of Sea Research* 48(2):97–110. Retrieved (http://linkinghub.elsevier.com/retrieve/pii/S1385110102001612).

Camatti, E. et al. 2006. "Analisi Dei Popolamenti Zooplanctonici Nella Laguna Di Venezia Dal 1975 Al 2004." *Biol. Mar. Medit.* 1:46–53.

Carstensen, Jacob, María Sánchez-Camacho, Carlos M. Duarte, Dorte Krause-Jensen, and Núria Marbà. 2011. "Connecting the Dots: Responses of Coastal Ecosystems to Changing Nutrient Concentrations." *Environmental Science & Technology* 45(21):9122–32. Retrieved (http://pubs.acs.org/doi/abs/10.1021/es202351y).

Cattaneo, L. et al. 2012. "Assessment of COSMO-CLM Performances over Mediterranean Area." *SSRN Electronic Journal*. Retrieved (http://papers.ssrn.com/abstract=2195524).

Cattaneo, L., V. Rillo, M. P. Manzi, V. Villani, and P. Mercogliano. 2015. "Clime: Climate Data Processing in GIS Environment." *CMCC Research Papers* (RP0257).

Chan, F. et al. 2008. "Emergence of Anoxia in the California Current Large Marine Ecosystem." *Science (New York, N.Y.)* 319(5865):920.

Charlson, R. J. 2001. "ATMOSPHERIC SCIENCE: Reshaping the Theory of Cloud Formation." *Science* 292(5524):2025–26. Retrieved (http://www.sciencemag.org/cgi/doi/10.1126/science.1060096).

Chave, P. 2015. "The EU Water Framework Directive - An Introduction." *Water Intelligence Online* 6(0):9781780402239–9781780402239. Retrieved (http://wio.iwaponline.com/cgi/doi/10.2166/9781780402239).

Chen, Jie, François P. Brissette, and Philippe Lucas-Picher. 2015. "Assessing the Limits of Bias-

Correcting Climate Model Outputs for Climate Change Impact Studies." *Journal of Geophysical Research: Atmospheres* 120(3):1123–36. Retrieved September 7, 2016 (http://onlinelibrary.wiley.com/doi/10.1002/2014JD022635/full).

Christensen, Jens Hesselbjerg and Ole B??ssing Christensen. 2007. "A Summary of the PRUDENCE Model Projections of Changes in European Climate by the End of This Century." *Climatic Change* 81(SUPPL. 1):7–30.

Church, John A. and Neil J. White. 2006. "A 20th Century Acceleration in Global Sea-Level Rise." *Geophysical Research Letters* 33(1).

Cloern, J. E. 2001. "Our Evolving Conceptual Model of the Coastal Eutrophication Problem." *Marine Ecology Progress Series* 210:223–53.

Cole, Thomas M. and Edward M. Buchak. 1995. "CE-QUAL-W2: A Two-Dimensional, Laterally Averaged, Hydrodynamic and Water Quality Model, Version 2.0." *Instruction Report EL-95* EL-95-(March):379. Retrieved (%5C%5CIBSERVER%5CID_enl%5CReports%5CInstruction Report EL-95%5CCole_Model EPA.PDF).

Collavini, Flaviano, Cinzia Bettiol, Luca Zaggia, and Roberto Zonta. 2005. "Pollutant Loads from the Drainage Basin to the Venice Lagoon (Italy)." *Environment International* 31(7):939–47. Retrieved (http://linkinghub.elsevier.com/retrieve/pii/S016041200500070X).

Comaschi, Alessandra, Franco Bianchi, and Giorgio Socal. 1995. *Osservazioni Sulla Distribuzione E Sul Ciclo Stagionale Delle Specie Appartenenti Al Genere Acartia Presenti Nella Palude Di Cona (Bacino Settentrionale Della Laguna Di Venezia)*.

Conley, Daniel J. 2000. "Biogeochemical Nutrient Cycles and Nutrient Management Strategies." *Hydrobiologia* 410:87–96.

Cook, John et al. 2016. "Consensus on Consensus : A Synthesis of Consensus Estimates on Human - Caused Global Warming." *Environmental Research Letters* 11(2016):1–24. Retrieved (http://dx.doi.org/10.1088/1748-9326/11/4/048002).

Cooney, Catherine M. 2012. "Downscaling Climate Models: Sharpening the Focus on Local-Level Changes." *Environmental Health Perspectives* 120(1):a22–28. Retrieved (http://ehp.niehs.nih.gov/120-a22).

CORDEX. 2015. *CORDEX Domains for Model Integrations. Technical Report CORDEX.*

Cousino, Luke K., Richard H. Becker, and Kirk A. Zmijewski. 2015. "Modeling the Effects of Climate Change on Water, Sediment, and Nutrient Yields from the Maumee River Watershed." *Journal of Hydrology: Regional Studies* 4:762–75.

Cucco, Andrea and Georg Umgiesser. 2006. "Modeling the Venice Lagoon Residence Time." *Ecological Modelling* 193(1–2):34–51. Retrieved (http://linkinghub.elsevier.com/retrieve/pii/S0304380005004552).

Cugier, P., G. Billen, J. F. Guillaud, J. Garnier, and A. Ménesguen. 2005. "Modelling the Eutrophication of the Seine Bight (France) under Historical, Present and Future Riverine Nutrient Loading." *Journal of Hydrology* 304(1–4):381–96. Retrieved (http://linkinghub.elsevier.com/retrieve/pii/S0022169404005074).

Culbertson, Andreas M., Jay F. Martin, Noel Aloysius, and Stuart A. Ludsin. 2016. "Anticipated Impacts of Climate Change on 21st Century Maumee River Discharge and Nutrient Loads." *Journal of Great Lakes Research*. Retrieved (http://linkinghub.elsevier.com/retrieve/pii/S0380133016301502).

CVN. 2006. *Regime Degli Apporti Di Acqua Dolce in Laguna Di Venezia*.

Davidson, K., K. J. Flynn, and A. Cunningham. 1992. "Non-Steady State Ammonium-Limited Growth of the Marine Phytoflagellate, Isochrysis Galbana Parke." *New Phytologist* 122(3):433–38.

Davidson, Keith et al. 2014. "Anthropogenic Nutrients and Harmful Algae in Coastal Waters." *Journal of Environmental Management* 146:206–16. Retrieved (http://linkinghub.elsevier.com/retrieve/pii/S030147971400334X).

Diskin, M. H. and E. Simon. 1977. "A Procedure for the Selection of Objective Functions for Hydrologic Simulation Models." *Journal of Hydrology* 34(1–2):129–49. Retrieved (http://linkinghub.elsevier.com/retrieve/pii/002216947790066X).

EEA. 2006. "CORINE Land Cover 2006." *Final report on interpreta*. Retrieved (http://www.statistiques.developpement-durable.gouv.fr/donnees-ligne/li/1825.html).

Eghball, Bahman, Brian J. Wienhold, John E. Gilley, and Roger A. Eigenberg. 2002. "Mineralization of Manure Nutrients." *Journal of Soil and Water Conservation* 57(6):470–

73. Retrieved (http://digitalcommons.unl.edu/cgi/viewcontent.cgi?article=1138&context=biosysengfacpub%5Cnhttp://www.jswconline.org/content/57/6/470.abstract%5Cnhttp://www.jswconline.org/content/57/6/470.short).

El-Khoury, A. et al. 2015. "Combined Impacts of Future Climate and Land Use Changes on Discharge, Nitrogen and Phosphorus Loads for a Canadian River Basin." *Journal of Environmental Management* 151:76–86.

Elmgren, R. and U. Larsson. 2001. "Nitrogen and the Baltic Sea: Managing Nitrogen in Relation to Phosphorus." *The Scientific World* 1(S2):371–77.

EPA. 2008. *Integrated Modeling for Integrated Environmental Decision Making*. Retrieved (https://www.epa.gov/sites/production/files/2015-02/documents/im4iedm_white_paper_final_epa100r08010_0.pdf).

EPA. 2009. *Guidance on the Development, Evaluation, and Application of Environmental Models*. Retrieved (https://www.epa.gov/sites/production/files/2015-04/documents/cred_guidance_0309.pdf).

EPA. 2015. "BASINS 4.1 (Better Assessment Science Integrating Point & Non-Point Source) Modeling Framework. National Exposure Research Laboratory, RTP, North Carolina." Retrieved January 1, 2016 (https://www.epa.gov/exposure-assessment-models/basins).

Essenfelder, A. H., S. Giove, and C. Giupponi. 2016. "Identifying the Factors Influencing the Total External Hydraulic Loads to the Dese-Zero Watershed." P. 8 in *8th International Environmental Modelling and Software Society (iEMSs)*.

Facca, Chiara, Adriano Sfriso, and Pierfrancesco Ghetti. 2004. "Abbondanza E Diversità Del Fitoplancton E Delle Diatomee Bentoniche in Laguna Di Venezia." *Biologia Ambientale* 18(2):19–24.

Fan, Min and Hideaki Shibata. 2015. "Simulation of Watershed Hydrology and Stream Water Quality under Land Use and Climate Change Scenarios in Teshio River Watershed, Northern Japan." *Ecological Indicators* 50:79–89. Retrieved (http://linkinghub.elsevier.com/retrieve/pii/S1470160X14005263).

Ferguson, R. M. 2010. "A Vast Machine: Computer Models, Climate Data, and the Politics of

Global Warming." *Choice: Current Reviews for Academic Libraries* 48(2):324.

Ferrari, G., C. Badetti, and S. Ciavatta. 2004. "Real-Time Monitoring of the Venice Lagoon." *Sea Technology* 45(8):22–26.

FitzHugh, T. W. and D. S. Mackay. 2000. "Impacts of Input Parameter Spatial Aggregation on an Agricultural Nonpoint Source Pollution Model." *Journal of Hydrology* 236(1–2):35–53.

Flato, Gregory M. 2011. "Earth System Models: An Overview." *Wiley Interdisciplinary Reviews: Climate Change* 2(6):783–800.

Flint, Lorraine E. and Alan L. Flint. 2012. "Downscaling Future Climate Scenarios to Fine Scales for Hydrologic and Ecological Modeling and Analysis." *Ecological Processes* 1(1):2. Retrieved (http://ecologicalprocesses.springeropen.com/articles/10.1186/2192-1709-1-2).

Foley, Jonathan a et al. 2005. "Global Consequences of Land Use." *Science (New York, N.Y.)* 309(5734):570–74. Retrieved (http://www.ncbi.nlm.nih.gov/pubmed/16040698).

Follett, R. F., C. E. Stewart, E. G. Pruessner, and J. M. Kimble. 2012. "Effects of Climate Change on Soil Carbon and Nitrogen Storage in the US Great Plains." *Journal of Soil and Water Conservation* 67(5):331–42. Retrieved (http://www.jswconline.org/cgi/doi/10.2489/jswc.67.5.331).

Ford, James D. et al. 2010. "Case Study and Analogue Methodologies in Climate Change Vulnerability Research." *Wiley Interdisciplinary Reviews: Climate Change* 1(3):374–92. Retrieved (http://doi.wiley.com/10.1002/wcc.48).

Fowler, Hayley J., S. Blenkinsop, and C. Tebaldi. 2007. "Linking Climate Change Modelling to Impacts Studies: Recent Advances in Downscaling Techniques for Hydrological Modelling." *International Journal of Climatology* 27(12):1547–78.

Garg, V., S. P. Aggarwal, B. R. Nikam, and P. K. Thakur. 2013. "Hypothetical Scenario–based Impact Assessment of Climate Change on Runoff Potential of a Basin." *ISH Journal of Hydraulic Engineering* 19(3):244–49. Retrieved (http://www.tandfonline.com/doi/abs/10.1080/09715010.2013.804673).

GEOHAB. 2001. *Global Ecology and Oceanography of Harmful Algal Blooms, Harmful Algal Blooms in Eutrophic Systems.*

Giupponi, Carlo, Arianna Azzellino, Roberta Salvetti, Paolo Parati, and Marta Carpani. 2012. "Water Quality Assessment in the Venice Lagoon Watershed with Multiple Modelling Approaches." *Proceedings - 2012 International Congress on Environmental Modelling and Software* 1–8.

Glibert, Patricia M. et al. 2014. "Vulnerability of Coastal Ecosystems to Changes in Harmful Algal Bloom Distribution in Response to Climate Change: Projections Based on Model Analysis." *Global Change Biology* 20(12):3845–58. Retrieved (http://doi.wiley.com/10.1111/gcb.12662).

Graham, L.Phil, Johan Andréasson, and Bengt Carlsson. 2007. "Assessing Climate Change Impacts on Hydrology from an Ensemble of Regional Climate Models, Model Scales and Linking Methods – a Case Study on the Lule River Basin." *Climatic Change* 81(S1):293–307. Retrieved (http://link.springer.com/10.1007/s10584-006-9215-2).

Green, Timothy R. et al. 2011. "Beneath the Surface of Global Change: Impacts of Climate Change on Groundwater." *Journal of Hydrology* 405(3–4):532–60. Retrieved (http://linkinghub.elsevier.com/retrieve/pii/S0022169411002988).

Guerzoni, S. and D. Tagliapietra. 2006. *Atlante Della Laguna. Venezia Tra Terra E Mare*. 2nd ed. Venezia: Marsilio Editori.

Guse, Björn et al. 2015. "Eco-Hydrologic Model Cascades: Simulating Land Use and Climate Change Impacts on Hydrology, Hydraulics and Habitats for Fish and Macroinvertebrates." *Science of The Total Environment* 533:542–56. Retrieved (http://linkinghub.elsevier.com/retrieve/pii/S0048969715301364).

Haddeland, Ingjerd et al. 2014. "Global Water Resources Affected by Human Interventions and Climate Change." *Proceedings of the National Academy of Sciences* 111(9):3251–56. Retrieved (http://www.pnas.org/lookup/doi/10.1073/pnas.1222475110).

Haerter, J. O., S. Hagemann, C. Moseley, and C. Piani. 2011. "Climate Model Bias Correction and the Role of Timescales." *Hydrology and Earth System Sciences* 15(3):1065–79.

Harley, Christopher D. G. et al. 2006. "The Impacts of Climate Change in Coastal Marine Systems." *Ecology Letters* 9(2):228–41.

Harley, Christopher D. G. et al. 2006. "The Impacts of Climate Change in Coastal Marine

Systems." *Ecology Letters* 9(2):228–41. Retrieved (http://doi.wiley.com/10.1111/j.1461-0248.2005.00871.x).

Harris, G. P. 1986. *Phytoplankton Ecology: Structure, Function and Fluctuation*. London: Chapman and Hall.

Hartmann, D. L., a. M. G. K. Tank, and M. Rusticucci. 2013. "IPCC Fifth Assessment Report, Climatie Change 2013: The Physical Science Basis." *Ipcc* AR5(January 2014):31–39.

Heino, Jani, Raimo Virkkala, and Heikki Toivonen. 2009. "Climate Change and Freshwater Biodiversity: Detected Patterns, Future Trends and Adaptations in Northern Regions." *Biological Reviews* 84(1):39–54. Retrieved (http://doi.wiley.com/10.1111/j.1469-185X.2008.00060.x).

Hernandez-Farinas, T. et al. 2014. "Temporal Changes in the Phytoplankton Community along the French Coast of the Eastern English Channel and the Southern Bight of the North Sea." *ICES Journal of Marine Science* 71(4):821–33. Retrieved (https://academic.oup.com/icesjms/article-lookup/doi/10.1093/icesjms/fst192).

Herring, Stephanie C., Martin P. Hoerling, James P. Kossin, Thomas C. Peterson, and Peter A. Stott. 2015. "Introduction to Explaining Extreme Events of 2014 from a Climate Perspective." *Bulletin of the American Meteorological Society* 96(12):S1–4. Retrieved (http://journals.ametsoc.org/doi/10.1175/BAMS-D-15-00157.1).

Ho, Jeff C. and Anna M. Michalak. 2015. "Challenges in Tracking Harmful Algal Blooms: A Synthesis of Evidence from Lake Erie." *Journal of Great Lakes Research* 41(2):317–25. Retrieved (http://linkinghub.elsevier.com/retrieve/pii/S0380133015000027).

Hoegh-Guldberg, O. and J. F. Bruno. 2010. "The Impact of Climate Change on the World's Marine Ecosystems." *Science* 328(5985):1523–28. Retrieved (http://www.sciencemag.org/cgi/doi/10.1126/science.1189930).

Hole, Lars and Magnuz Engardt. 2008. "Climate Change Impact on Atmospheric Nitrogen Deposition in Northwestern Europe: A Model Study." *Ambio* 37(1):9–17.

Hoover, Carie, Tony Pitcher, and Villy Christensen. 2013. "Effects of Hunting, Fishing and Climate Change on the Hudson Bay Marine Ecosystem: II. Ecosystem Model Future Projections." *Ecological Modelling* 264:143–56. Retrieved

(http://linkinghub.elsevier.com/retrieve/pii/S0304380013000379).

Howarth, Robert W. and Roxanne Marino. 2006. "Nitrogen as the Limiting Nutrient for Eutrophication in Coastal Marine Ecosystems: Evolving Views over Three Decades." *Limnology and Oceanography* 51(1part2):364–76. Retrieved (http://doi.wiley.com/10.4319/lo.2006.51.1_part_2.0364).

Howden, S. M. et al. 2007. "Adapting Agriculture to Climate Change." *Proceedings of the National Academy of Sciences* 104(50):19691–96. Retrieved (http://www.pnas.org/cgi/doi/10.1073/pnas.0701890104).

Hunter-Cevera, K. R. et al. 2016. "Physiological and Ecological Drivers of Early Spring Blooms of a Coastal Phytoplankter." *Science* 354(6310):326–29. Retrieved (http://www.sciencemag.org/cgi/doi/10.1126/science.aaf8536).

Huttunen, Inese et al. 2015. "Effects of Climate Change and Agricultural Adaptation on Nutrient Loading from Finnish Catchments to the Baltic Sea." *Science of the Total Environment* 529:168–81.

IPCC. 2000. "IPCC Special Report on Emissions Scenarios." *Change* 599:599. Retrieved (http://www.grida.no/climate/ipcc/emission/).

IPCC. 2002. "Climate Change and Biodiversity - IPCC Technical Paper V." *Group* 24:77.

IPCC. 2013. *Climate Change 2013: The Physical Science Basis. Contribution of Working Group I to the Fifth Assessment Report of the Intergovernmental Panel on Climate Change*.

IPCC. 2014a. *Climate Change 2014: Impacts, Adaptation, and Vulnerability*. Cambridge, United Kingdom and New York, NY, USA.

IPCC. 2014b. "Summary for Policymakers." *Climate Change 2014: Impacts, Adaptation and Vulnerability - Contributions of the Working Group II to the Fifth Assessment Report* 1–32.

IPCC-TGICA. 2007. "General Guidelines on the Use of Scenario Data for Climate Impact and Adaptation Assessment." *Finnish Environment Institute* 312(June):66. Retrieved (http://www.citeulike.org/group/14742/article/8861417).

Jacob, Daniela et al. 2014. "EURO-CORDEX: New High-Resolution Climate Change Projections for European Impact Research." *Regional Environmental Change* 14(2):563–78.

Jeppesen, Erik et al. 2005. "Lake Responses to Reduced Nutrient Loading - An Analysis of

Contemporary Long-Term Data from 35 Case Studies." *Freshwater Biology* 50(10):1747–71.

Jeppesen, Erik et al. 2009. "Climate Change Effects on Runoff, Catchment Phosphorus Loading and Lake Ecological State, and Potential Adaptations." *Journal of Environmental Quality* 38(5):1930–41. Retrieved (http://dx.doi.org/10.2134/jeq2008.0113).

Joye, S., D. de Beer, and P. L. M. Cook. 2009. "Biogeochemical Dynamics of Coastal Tidal Flats in Coastal Wetlands - an Integrated Ecosystem Approach." P. 941 in *Coastal Wetlands: An inegrated ecosystem approach*, edited by G. Petrillo, E. Wolanski, D. R. Cahoon, and M. M. Brinson. New York: Elsevier.

Junge, C. O. 1966. "Depth Distributions for Quadratic Surfaces and Other Configurations." Pp. 257–65 in *Hydrobiological Studies*, edited by J. Hrbácek. Prague: Academia.

Justić, Dubravko, Nancy N. Rabalais, and R.Eugene Turner. 2005. "Coupling between Climate Variability and Coastal Eutrophication: Evidence and Outlook for the Northern Gulf of Mexico." *Journal of Sea Research* 54(1):25–35. Retrieved (http://linkinghub.elsevier.com/retrieve/pii/S1385110105000110).

Kanter, David R., Xin Zhang, Denise L. Mauzerall, Sergey Malyshev, and Elena Shevliakova. 2016. "The Importance of Climate Change and Nitrogen Use Efficiency for Future Nitrous Oxide Emissions from Agriculture." *Environmental Research Letters* 11(9):94003. Retrieved March 1, 2017 (http://stacks.iop.org/1748-9326/11/i=9/a=094003?key=crossref.6e9746d94d6a61ff777d0aa79d4a1a6c).

Karl, T. R. 2003. "Modern Global Climate Change." *Science* 302(5651):1719–23. Retrieved (http://www.sciencemag.org/cgi/doi/10.1126/science.1090228).

Khan, Shfaqat a et al. 2014. "Sustained Mass Loss of the Northeast Greenland Ice Sheet Triggered by Regional Warming." *Nature Clim. Change* 4(4):292–99. Retrieved (http://dx.doi.org/10.1038/nclimate2161%5Cn10.1038/nclimate2161%5Cnhttp://www.nature.com/nclimate/journal/v4/n4/abs/nclimate2161.html#supplementary-information).

Kiesel, Jens, Daniel Hering, Britta Schmalz, and Nicola Fohrer. 2009. "A Transdisciplinary Approach for Modelling Macroinvertebrate Habitats in Lowland Streams." Pp. 24–33 in

Ecohydrology of Surface and Groundwater Dependent Systems: Concepts, Methods and Recent Developments, vol. 328.

Kim, Soojun, Huiseong Noh, Jaewon Jung, Hwandon Jun, and Hung Soo Kim. 2016. "Assessment of the Impacts of Global Climate Change and Regional Water Projects on Streamflow Characteristics in the Geum River Basin in Korea." *Water (Switzerland)* 8(3).

Kirschbaum, Miko U. F. 1995. "The Temperature Dependence of Soil Organic Matter Decomposition, and the Effect of Global Warming on Soil Organic C Storage." *Soil Biology and Biochemistry* 27(6):753–60.

Laniak, Gerard F. et al. 2013. "Integrated Environmental Modeling: A Vision and Roadmap for the Future." *Environmental Modelling & Software* 39:3–23. Retrieved (http://linkinghub.elsevier.com/retrieve/pii/S1364815212002381).

Lassen, Majbritt Kjeldahl, Kathryn Dewar Nielsen, Katherine Richardson, Kristine Garde, and Louise Schlüter. 2010. "The Effects of Temperature Increases on a Temperate Phytoplankton Community — A Mesocosm Climate Change Scenario." *Journal of Experimental Marine Biology and Ecology* 383(1):79–88. Retrieved (http://linkinghub.elsevier.com/retrieve/pii/S002209810900450X).

Legates, David R. and Gregory J. McCabe. 1999. "Evaluating the Use of 'goodness-of-Fit' Measures in Hydrologic and Hydroclimatic Model Validation." *Water Resources Research* 35(1):233–41. Retrieved (http://doi.wiley.com/10.1029/1998WR900018).

Lenderink, G., a. Buishand, and W. van Deursen. 2007. "Estimates of Future Discharges of the River Rhine Using Two Scenario Methodologies: Direct versus Delta Approach." *Hydrology and Earth System Sciences* 11(3):1145–59.

Leta, Olkeba Tolessa, Aly I. El-Kadi, Henrietta Dulai, and Kariem A. Ghazal. 2016. "Assessment of Climate Change Impacts on Water Balance Components of Heeia Watershed in Hawaii." *Journal of Hydrology: Regional Studies* 8:182–97. Retrieved (http://linkinghub.elsevier.com/retrieve/pii/S2214581816301215).

Littell, Jeremy S., Donald McKenzie, Becky K. Kerns, Samuel Cushman, and Charles G. Shaw. 2011. "Managing Uncertainty in Climate-Driven Ecological Models to Inform Adaptation to Climate Change." *Ecosphere* 2(9):art102. Retrieved

(http://doi.wiley.com/10.1890/ES11-00114.1).

Liu, Yuqiong and Hoshin V. Gupta. 2007. "Uncertainty in Hydrologic Modeling: Toward an Integrated Data Assimilation Framework." *Water Resources Research* 43(7):n/a-n/a. Retrieved (http://doi.wiley.com/10.1029/2006WR005756).

Lloret, Javier, Arnaldo Marín, and Lázaro Marín-Guirao. 2008. "Is Coastal Lagoon Eutrophication Likely to Be Aggravated by Global Climate Change?" *Estuarine, Coastal and Shelf Science* 78(2):403–12. Retrieved (http://linkinghub.elsevier.com/retrieve/pii/S0272771408000097).

Lovato, Tomas, Alexey Androsov, Dmitry Romanenkov, and Angelo Rubino. 2010. "The Tidal and Wind Induced Hydrodynamics of the Composite System Adriatic Sea/Lagoon of Venice." *Continental Shelf Research* 30(6):692–706. Retrieved (http://linkinghub.elsevier.com/retrieve/pii/S0278434310000142).

Ludwig, Fulco and Senthold Asseng. 2006. "Climate Change Impacts on Wheat Production in a Mediterranean Environment in Western Australia." *Agricultural Systems* 90(1–3):159–79. Retrieved (http://linkinghub.elsevier.com/retrieve/pii/S0308521X05002659).

Magistrato alle Acque di Venezia (MAV). 1999. *Mappatura Dei Fondali Lagunari*.

Malone, Thomas C. et al. 1996. "Scales of Nutrient-Limited Phytoplankton Productivity in Chesapeake Bay." *Estuaries* 19(2):371–85.

Markensten, Hampus, Karen Moore, and Irina Persson. 2010. "Simulated Lake Phytoplankton Composition Shifts toward Cyanobacteria Dominance in a Future Warmer Climate." *Ecological Applications* 20(3):752–67. Retrieved (http://doi.wiley.com/10.1890/08-2109.1).

Maslin, Mark. 2013. "Cascading Uncertainty in Climate Change Models and Its Implications for Policy." *The Geographical Journal* 179(3):264–71. Retrieved (http://doi.wiley.com/10.1111/j.1475-4959.2012.00494.x).

Maslowski, Wieslaw, Jaclyn Clement Kinney, Matthew Higgins, and Andrew Roberts. 2012. "The Future of Arctic Sea Ice." *Annual Review of Earth and Planetary Sciences* 40(1):625–54.

MAV and CVN. 2002. *Attività Di Monitoraggio Ambientale Della Laguna Di Venezia: MELa1*.

Mechoso, C. R. and A. Arakawa. 2015. “NUMERICAL MODELS | General Circulation Models.” Pp. 153–60 in *Encyclopedia of Atmospheric Sciences*. Elsevier. Retrieved (http://linkinghub.elsevier.com/retrieve/pii/B9780123822253001572).

Meinshausen, Malte et al. 2011. “The RCP Greenhouse Gas Concentrations and Their Extensions from 1765 to 2300.” *Climatic Change* 109(1–2):213–41. Retrieved (http://link.springer.com/10.1007/s10584-011-0156-z).

Molinaroli, E. 2006. “Sedimenti Superficiali: La Classificazione Granulometrica.” Pp. 20–21 in *Atlante della Laguna*. Venezia: Marsilio Editori.

Mooij, W. M., J. H. Janse, L. N. De Senerpont Domis, S. Hülsmann, and B. W. Ibelings. 2007. “Predicting the Effect of Climate Change on Temperate Shallow Lakes with the Ecosystem Model PCLake.” Pp. 443–54 in *Hydrobiologia*, vol. 584.

Mooij, W. M., L. N. De Senerpont Domis, and J. H. Janse. 2009. “Linking Species- and Ecosystem-Level Impacts of Climate Change in Lakes with a Complex and a Minimal Model.” *Ecological Modelling* 220(21):3011–20. Retrieved (http://linkinghub.elsevier.com/retrieve/pii/S0304380009000921).

Mooij, Wolf M. et al. 2010. “Challenges and Opportunities for Integrating Lake Ecosystem Modelling Approaches.” *Aquatic Ecology* 44(3):633–67. Retrieved (http://link.springer.com/10.1007/s10452-010-9339-3).

Moriasi, D. N. et al. 2007. “Model Evaluation Guidelines for Systematic Quantification of Accuracy in Watershed Simulations.” *Transactions of the ASABE* 50(3):885–900. Retrieved (http://swat.tamu.edu/media/1312/moriasimodeleval.pdf).

Moss, R. H. et al. 2010. “The next Generation of Scenarios for Climate Change Research and Assessment.” *Nature* 463(7282):747–56. Retrieved (http://www.scopus.com/record/display.url?eid=2-s2.0-76749096338&origin=inward&txGid=CwkSAJPyATm2B6yoCS28rHm:11).

Moustache, Antoine Marie. 2017. “Adaptation to Impacts of Climate Change on the Food and Nutrition Security Status of a Small Island Developing State:” Pp. 919–44 in *Natural Resources Management: Concepts, Methodologies, Tools, and Applications*, edited by I. R. Management Association. IGI Global. Retrieved (http://services.igi-

global.com/resolvedoi/resolve.aspx?doi=10.4018/978-1-5225-0803-8).

Najafi, Mohammad Reza and Hamid Moradkhani. 2015. "Multi-Model Ensemble Analysis of Runoff Extremes for Climate Change Impact Assessments." *Journal of Hydrology* 525:352–61. Retrieved (http://linkinghub.elsevier.com/retrieve/pii/S0022169415002164).

Nakicenovic, N. and R. Swart. 2000. *IPCC Special Report on Emissions Scenarios (SRES)*. Retrieved (http://www7.nationalacademies.org/HDGC/SRES_Presentation_by_Nebojsa_Nakicenovic.pdf).

Nash, J. E. and J. V. Sutcliffe. 1970. "River Flow Forecasting through Conceptual Models Part I - A Discussion of Principles." *Journal of Hydrology* 10(3):282–90.

Neitsch, S. .., J. .. Arnold, J. .. Kiniry, and J. .. Williams. 2011. "Soil & Water Assessment Tool Theoretical Documentation Version 2009." *Texas Water Resources Institute* 1–647.

Nicks, A. D. 1974. "Stochastic Generation of the Occurrence, Pattern and Location of Maximum Amount of Daily Rainfall." Pp. 154–71 in *Proc. Symp. Statistical Hydrology*. Tucson, AZ.

NOAA. 2016. "State of the Climate: Global Analysis for Annual 2015, Published Online January 2016." Retrieved September 28, 2016 (http://www.ncdc.noaa.gov/sotc/global/201513).

North, Gerald R., Robert F. Cahalan, and James A. Coakley. 1981. "Energy Balance Climate Models." *Reviews of Geophysics* 19(1):91–121.

Noyes, Pamela D. et al. 2009. "The Toxicology of Climate Change: Environmental Contaminants in a Warming World." *Environment International* 35(6):971–86.

Ockenden, M. C. et al. 2016. "Changing Climate and Nutrient Transfers: Evidence from High Temporal Resolution Concentration-Flow Dynamics in Headwater Catchments." *The Science of the total environment* 548–549:325–39. Retrieved February 24, 2016 (http://www.sciencedirect.com/science/article/pii/S0048969715312420).

van Oldenborgh, Geert Jan et al. 2009. "Western Europe Is Warming Much Faster than Expected." *Climate of the Past* 5:1–12. Retrieved (http://arxiv.org/abs/0806.0715).

Paerl, H. W. and D. Justic. 2011. "Primary Producers: Phytoplankton Ecology and Trophic Dynamics in Coastal Waters." Pp. 23–42 in *Treatise on Estuarine and Coastal Science* –

Vol. 6: Trophic Relationships of Coastal and Estuarine Ecosystems.

Paerl, Hans W. 2006. "Assessing and Managing Nutrient-Enhanced Eutrophication in Estuarine and Coastal Waters: Interactive Effects of Human and Climatic Perturbations." *Ecological Engineering* 26(1):40–54. Retrieved (http://linkinghub.elsevier.com/retrieve/pii/S0925857405001928).

Paerl, Hans W. and Jef Huisman. 2008. "Blooms like It Hot." *Science (New York, N.Y.)* 320(5872):57–58.

Paerl, Hans W., Michael A. Mallin, Cindy A. Donahue, Malia Go, and Benjamin L. Peierls. 1995. *Nitrogen Loading Sources and Eutrophication of the Neuse River Estuary, North Carolina: Direct and Indirect Roles of Atmospheric Deposition*.

Paerl, Hans W. and Valerie J. Paul. 2012. "Climate Change: Links to Global Expansion of Harmful Cyanobacteria." *Water Research* 46(5):1349–63. Retrieved (http://linkinghub.elsevier.com/retrieve/pii/S0043135411004386).

Park, R. A. and J. S. Clough. 2009. *AQUATOX - Volume 2: Technical Documentation*.

Park, Richard A., Jonathan S. Clough, and Marjorie Coombs Wellman. 2008. "AQUATOX: Modeling Environmental Fate and Ecological Effects in Aquatic Ecosystems." *Ecological Modelling* 213(1):1–15.

Parkinson, Claire L. and Josefino C. Comiso. 2013. "On the 2012 Record Low Arctic Sea Ice Cover: Combined Impact of Preconditioning and an August Storm." *Geophysical Research Letters* 40(7):1356–61. Retrieved (http://doi.wiley.com/10.1002/grl.50349).

Parodi, Elisa R. and Sonia Barría De Cao. 2002. "Benthic Microalgal Communities in the Inner Part of the Bahia Blanca Estuary (Argentina): A Preliminary Qualitative Study." *Oceanologica Acta* 25(5):279–84.

Pielke Sr., R. A. 2005. "ATMOSPHERIC SCIENCE: Land Use and Climate Change." *Science* 310(5754):1625–26. Retrieved (http://www.sciencemag.org/cgi/doi/10.1126/science.1120529).

Pörtner, Hans O. and Rainer Knust. 2007. "Climate Change Affects Marine Fishes through the Oxygen Limitation of Thermal Tolerance." *Science* 315(5808):95–97. Retrieved (http://www.sciencemag.org/content/315/5808/95.abstract%5Cnhttp://www.ncbi.nlm.

nih.gov/pubmed/17204649).

Prosinger, J., D. Suhardimand, and M. Giordano. 2015. “Linking Climate Change Discourse with Climate Change Policy in the Mekong: The Case of Lao PDR.” in *Climate change and agricultural water management in Developing Countries*, edited by C. T. Hoanh, R. Johnston, and V. Smakhtin. Wallingford: CABI. Retrieved (http://www.cabi.org/cabebooks/ebook/20153417459).

Rabalais, Nancy N., R.Eugene Turner, Robert J. Díaz, and Dubravko Justić. 2009. “Global Change and Eutrophication of Coastal Waters.” *ICES Journal of Marine Science* 66(7):1528–37.

Redfield, A. 1934. “On the Proportions of Organic Derivatives in Sea Water and Their Relation to the Composition of Plankton.” Pp. 177–92 in *Daniel, R.J. (ed. James Johnstone Memorial Volume)*. University Press of Liverpool.

Regione Veneto. 2014. *Disciplinari Di Produzione Integrata (Tecniche Agronomiche)*.

Riahi, Keywan et al. 2011. “RCP 8.5-A Scenario of Comparatively High Greenhouse Gas Emissions.” *Climatic Change* 109(1):33–57.

Robbins, L. L., M. E. Hansen, J. A. Kleypas, and S. C. Meylan. 2010. *A User-Friendly Seawater Carbon Calculator*.

Rodrigues, Marta, Anabela Oliveira, Henrique Queiroga, Vanda Brotas, and André Bustorff Fortunato. 2015. “Modelling the Effects of Climate Change in Estuarine Ecosystems with Coupled Hydrodynamic and Biogeochemical Models.” Pp. 271–88 in. Retrieved (http://linkinghub.elsevier.com/retrieve/pii/B9780444635365000120).

Rummukainen, Markku. 2010. “State-of-the-Art with Regional Climate Models.” *Wiley Interdisciplinary Reviews: Climate Change* 1(1):82–96.

Sachindra, D. A., F. Huang, A. Barton, and B. J. C. Perera. 2014. “Statistical Downscaling of General Circulation Model Outputs to Precipitation-Part 2: Bias-Correction and Future Projections.” *International Journal of Climatology* 34(11):3282–3303. Retrieved (http://doi.wiley.com/10.1002/joc.3915).

Salvetti, Roberta et al. 2008. “Modelling the Point and Non-Point Nitrogen Loads to the Venice Lagoon (Italy): The Application of Water Quality Models to the Dese-Zero Basin.” *Desalination* 226(1–3):81–88.

SAMARAS, Achilleas G. and Christopher G. KOUTITAS. 2014. “Modeling the Impact of Climate Change on Sediment Transport and Morphology in Coupled Watershed-Coast Systems: A Case Study Using an Integrated Approach.” *International Journal of Sediment Research* 29(3):304–15. Retrieved (http://linkinghub.elsevier.com/retrieve/pii/S1001627914600469).

Schiedek, Doris, Brita Sundelin, James W. Readman, and Robie W. Macdonald. 2007. “Interactions between Climate Change and Contaminants.” *Marine Pollution Bulletin* 54(12):1845–56.

Schlabing, D., M. A. Frassl, M. M. Eder, K. Rinke, and A. Bárdossy. 2014. “Use of a Weather Generator for Simulating Climate Change Effects on Ecosystems: A Case Study on Lake Constance.” *Environmental Modelling & Software* 61:326–38. Retrieved (http://linkinghub.elsevier.com/retrieve/pii/S1364815214002059).

Schloss, I. R. et al. 2014. “On the Phytoplankton Bloom in Coastal Waters of Southern King George Island (Antarctica) in January 2010: An Exceptional Feature?” *Limnology and Oceanography* 59(1):195–210. Retrieved (http://doi.wiley.com/10.4319/lo.2014.59.1.0195).

Schramm, Harold L., Michael S. Cox, Todd E. Tietjen, and Andrew W. Ezell. 2009. “Nutrient Dynamics in the Lower Mississippi River Floodplain: Comparing Present and Historic Hydrologic Conditions.” *Wetlands* 29(2):476–87.

Scoccimarro, Enrico et al. 2011. “Effects of Tropical Cyclones on Ocean Heat Transport in a High-Resolution Coupled General Circulation Model.” *Journal of Climate* 24(16):4368–84.

Sellami, Haykel, Sihem Benabdallah, Isabelle La Jeunesse, and Marnik Vanclooster. 2016. “Quantifying Hydrological Responses of Small Mediterranean Catchments under Climate Change Projections.” *Science of the Total Environment* 543:924–36.

Servizio Acque Interne. 2008. *Le Acque Sotterranee Della Pianura Veneta - I Risultati Del Progetto SAMPAS. Technical Report*. Padova, PD, Italy.

Sfriso, A., B. Pavoni, A. Marcomini, and A. A. Orio. 1988. “Annual Variations of Nutrients in the Lagoon of Venice.” *Marine Pollution Bulletin* 19(2):54–60. Retrieved (http://linkinghub.elsevier.com/retrieve/pii/0025326X88907801).

Smith, J. B. et al. 2009. "Assessing Dangerous Climate Change through an Update of the Intergovernmental Panel on Climate Change (IPCC) 'reasons for Concern.'" *Proceedings of the National Academy of Sciences* 106(11):4133–37. Retrieved (http://www.pnas.org/cgi/doi/10.1073/pnas.0812355106).

Stahl, Ralph G. et al. 2013. "The Influence of Global Climate Change on the Scientific Foundations and Applications of Environmental Toxicology and Chemistry: Introduction to a SETAC International Workshop." *Environmental toxicology and chemistry / SETAC* 32(1):13–19. Retrieved (http://www.pubmedcentral.nih.gov/articlerender.fcgi?artid=3601432&tool=pmcentrez&rendertype=abstract).

Steele-Dunne, Susan et al. 2008. "The Impacts of Climate Change on Hydrology in Ireland." *Journal of Hydrology* 356(1–2):28–45. Retrieved (http://linkinghub.elsevier.com/retrieve/pii/S0022169408001546).

Sterk, Ankie, Jack Schijven, Ana Maria de Roda Husman, and Ton de Nijs. 2016. "Effect of Climate Change on Runoff of Campylobacter and Cryptosporidium from Land to Surface Water." *Water Research* 95:90–102. Retrieved (http://linkinghub.elsevier.com/retrieve/pii/S0043135416301324).

Taner, Mehmet Ümit, James N. Carleton, and Marjorie Wellman. 2011. "Integrated Model Projections of Climate Change Impacts on a North American Lake." *Ecological Modelling* 222(18):3380–93. Retrieved (http://linkinghub.elsevier.com/retrieve/pii/S030438001100398X).

Tassinari, G. 1976. *Manuale Dell'argonomo*. HOEPLI.

Teutschbein, Claudia and Jan Seibert. 2012. "Bias Correction of Regional Climate Model Simulations for Hydrological Climate-Change Impact Studies: Review and Evaluation of Different Methods." *Journal of Hydrology* 456–457:12–29.

Thomson, Allison M. et al. 2011. "RCP4.5: A Pathway for Stabilization of Radiative Forcing by 2100." *Climatic Change* 109(1):77–94.

Thornton, Philip K., Polly J. Ericksen, Mario Herrero, and Andrew J. Challinor. 2014. "Climate Variability and Vulnerability to Climate Change: A Review." *Global Change Biology*

20(11):3313–28. Retrieved (http://doi.wiley.com/10.1111/gcb.12581).

Tilman, D., C. Balzer, J. Hill, and B. L. Befort. 2011. "Global Food Demand and the Sustainable Intensification of Agriculture." *Proceedings of the National Academy of Sciences* 108(50):20260–64. Retrieved (http://www.pnas.org/cgi/doi/10.1073/pnas.1116437108).

Di Toro, D. M. 2001. *Sediment Flux Modeling*. Wiley-Interscience.

Trinh, T., K. Ishida, M. L. Kavvas, A. Ercan, and K. Carr. 2017. "Assessment of 21st Century Drought Conditions at Shasta Dam Based on Dynamically Projected Water Supply Conditions by a Regional Climate Model Coupled with a Physically-Based Hydrology Model." *Science of The Total Environment*. Retrieved (http://linkinghub.elsevier.com/retrieve/pii/S0048969717302231).

Trolle, Dennis, David P. Hamilton, Conrad A. Pilditch, Ian C. Duggan, and Erik Jeppesen. 2011. "Predicting the Effects of Climate Change on Trophic Status of Three Morphologically Varying Lakes: Implications for Lake Restoration and Management." *Environmental Modelling & Software* 26(4):354–70. Retrieved (http://linkinghub.elsevier.com/retrieve/pii/S1364815210002562).

UNEP. 2006. *Marine and Coastal Ecosystems and Human Well-Being: A Synthesis Report Based on the Findings of the Millennium Ecosystem Assessment*. Retrieved (http://www.vliz.be/imisdocs/publications/120064.pdf).

USGS. 2012. *Load Estimator (LOADEST): A Fortran Program for Estimating Constituent Loads in Streams and Rivers*.

Villani, Veronica, Luigi Cattaneo, Alessandra Lucia Zollo, and Paola Mercogliano. 2015. "Climate Data Processing with GIS Support: Description of Bias Correction and Temporal Downscaling Tools Implemented in Clime Software." *CMCC Research Papers* (RP0262).

Vohland, Katrin, Sven Rannow, and Judith Stagl. 2014. "Climate Change Impact Modelling Cascade – Benefits and Limitations for Conservation Management." Pp. 63–76 in. Retrieved (http://link.springer.com/10.1007/978-94-007-7960-0_5).

van Vuuren, Detlef P. et al. 2011. "The Representative Concentration Pathways: An Overview." *Climatic Change* 109(1–2):5–31. Retrieved (http://link.springer.com/10.1007/s10584-011-0148-z).

Wakelin, Sarah L., Yuri Artioli, Momme Butenschön, J.Icarus Allen, and Jason T. Holt. 2015. "Modelling the Combined Impacts of Climate Change and Direct Anthropogenic Drivers on the Ecosystem of the Northwest European Continental Shelf." *Journal of Marine Systems* 152:51–63. Retrieved (http://linkinghub.elsevier.com/retrieve/pii/S092479631500130X).

Ward, J. H. 1963. "Heirarchical Grouping to Optimize an Objective Function." *Journal of American Statistics Association* 58:236–44.

Watson, Reg A. et al. 2013. "Ecosystem Model of Tasmanian Waters Explores Impacts of Climate-Change Induced Changes in Primary Productivity." *Ecological Modelling* 264:115–29. Retrieved (http://linkinghub.elsevier.com/retrieve/pii/S0304380012002281).

Webster, Mort et al. 2003. "Uncertainty Analysis of Climate Change and Policy Response." *Climatic Change* 61(3):295–320. Retrieved (http://link.springer.com/10.1023/B:CLIM.0000004564.09961.9f).

Weisse, Thomas, Birgit Gröschl, and Victoria Bergkemper. 2016. "Phytoplankton Response to Short-Term Temperature and Nutrient Changes." *Limnologica - Ecology and Management of Inland Waters* 59:78–89. Retrieved (http://linkinghub.elsevier.com/retrieve/pii/S0075951116300251).

Wells, Mark L. et al. 2015. "Harmful Algal Blooms and Climate Change: Learning from the Past and Present to Forecast the Future." *Harmful Algae* 49:68–93. Retrieved (http://linkinghub.elsevier.com/retrieve/pii/S1568988315300615).

Whitehead, P. G., R. L. Wilby, R. W. Battarbee, M. Kernan, and a. J. Wade. 2009. "A Review of the Potential Impacts of Climate Change on Surface Water Quality." *Hydrological Sciences Journal* 54(1):101–23.

Wiens, J. A., D. Stralberg, D. Jongsomjit, C. A. Howell, and M. A. Snyder. 2009. "Niches, Models, and Climate Change: Assessing the Assumptions and Uncertainties." *Proceedings of the National Academy of Sciences* 106(Supplement_2):19729–36. Retrieved (http://www.pnas.org/cgi/doi/10.1073/pnas.0901639106).

Wilby, R. L. et al. 2006. "Integrated Modelling of Climate Change Impacts on Water Resources

and Quality in a Lowland Catchment: River Kennet, UK." *Journal of Hydrology* 330(1–2):204–20.

Wilby, Robert L. and Suraje Dessai. 2010. "Robust Adaptation to Climate Change." *Weather* 65(7):180–85. Retrieved (http://doi.wiley.com/10.1002/wea.543).

Wilcke and L. Bärring. 2016. "Selecting Regional Climate Scenarios for Impact Modelling Studies." *Environmental Modelling and Software* 78:191–201.

Williams, J. R. 1969. "Flood Routing with Variable Travel Time or Variable Storage Coefficients." *Transactions of the ASAE* 12(1):100–103. Retrieved (http://0-elibrary.asabe.org.library.unl.edu/azdez.asp?AID=38772&t=2).

Xu, C. Y. 1999. "From GCMs to River Flow: A Review of Downscaling Methods and Hydrologic Modelling Approaches." *Progress in Physical Geography* 23(2):229–49. Retrieved (http://ppg.sagepub.com/cgi/doi/10.1177/030913339902300204).

Zhang, Jinlun. 2005. "Warming of the Arctic Ice-Ocean System Is Faster than the Global Average since the 1960s." *Geophysical Research Letters* 32(19):1–4.

Zirino, Alberto et al. 2014. "Salinity and Its Variability in the Lagoon of Venice, 2000–2009." *Advances in Oceanography and Limnology* 5(1):41–59. Retrieved (http://www.tandfonline.com/doi/abs/10.1080/19475721.2014.900113).

Zirino, Alberto et al. 2016a. "Nitrogen to Phosphorus Ratio in the Venice (Italy) Lagoon (2001–2010) and Its Relation to Macroalgae." *Marine Chemistry* 180:33–41. Retrieved (http://linkinghub.elsevier.com/retrieve/pii/S0304420316300020).

Zirino, Alberto et al. 2016b. "Nitrogen to Phosphorus Ratio in the Venice (Italy) Lagoon (2001–2010) and Its Relation to Macroalgae." *Marine Chemistry* 180:33–41. Retrieved (http://linkinghub.elsevier.com/retrieve/pii/S0304420316300020).

Zobeck, Ted M. and R.Scott Van Pelt. 2006. "Wind-Induced Dust Generation and Transport Mechanics on a Bare Agricultural Field." *Journal of Hazardous Materials* 132(1 SPEC. ISS.):26–38.

Zouiten, Hala, César Álvarez Díaz, Andrés García Gómez, José Antonio Revilla Cortezón, and Javier García Alba. 2013. "An Advanced Tool for Eutrophication Modeling in Coastal Lagoons: Application to the Victoria Lagoon in the North of Spain." *Ecological Modelling*

265:99–113. Retrieved (http://linkinghub.elsevier.com/retrieve/pii/S0304380013002937).

Zuliani, Aleardo, Luca Zaggia, Flaviano Collavini, and Roberto Zonta. 2005. “Freshwater Discharge from the Drainage Basin to the Venice Lagoon (Italy).” *Environment International* 31(7 SPEC. ISS.):929–38.